

© 2018

MARIE R SOUTHERLAND

ALL RIGHTS RESERVED

SYNTHESIS AND BIOLOGICAL EVALUATION OF IMIDAZOLIUM SALTS AS ANTI-
CANCER AGENTS

A Dissertation

Presented to

The Graduate Faculty of The University of Akron

In Partial Fulfillment

of the Requirements for the Degree

Doctor of Philosophy

Marie R. Southerland

May 2018

SYNTHESIS, AND BIOLOGICAL EVALUATION OF IMIDAZOLIUM SALTS AS ANTI-
CANCER AGENTS

Marie R. Southerland

Dissertation

Approved:

Advisor
Dr. Wiley J. Youngs

Committee Member
Dr. Claire A. Tessier

Committee Member
Dr. Sailaja Paruchuri

Committee Member
Dr. Leah P. Shriver

Committee Member
Dr. Chrys Wesdemiotis

Accepted:

Department Chair
Dr. Christopher J. Ziegler

Dean of the College
Dr. John Green

Dean of the Graduate School
Dr. Chad Midha

Date

ABSTRACT

Imidazolium salts are a group of compounds that have received attention in literature for their ability to inhibit the growth of cancer cells. However, there is a limited amount of information known about how imidazolium salts actually go about killing cancer cells. As more knowledge is gained in this area, more effective imidazolium salt derivatives can be made.

Chapter I provides a literature review of N-heterocyclic carbene complexes and the importance of their precursor ligand imidazolium salts in regard to anti-cancer and antimicrobial activity.

Contained in Chapter II is a study of lead imidazolium salt compounds and looks at the mode of cell death induced in cancer cells. The Annexin V assay has been utilized to distinguish between the process of apoptosis and necrosis that is caused by the lead imidazolium salts. Results show that the majority of imidazolium salts promote an apoptotic mode of cell death, although this is dependent upon substituents on the imidazole core. Apoptosis was further confirmed using the JC-1 assay to evaluate depolarization of the mitochondrial membrane potential. Furthermore, DNA has been excluded as the potential cellular target of imidazolium salts after studies of potential interactions with calf thymus DNA. Finally, the use of

excipients such as 2-hydroxypropyl- β -cyclodextrin to solubilize lipophilic compounds is explored.

Chapter III presents the *in vivo* toxicity evaluation of select imidazolium salts. Results show that two of the tested compounds were received well. Weight recovery was apparent and animals were able to receive multiple injections at 20 mg/kg. The other compounds tested had varying degrees of success, with most animals dying before the study could be completed.

Chapter IV provides preliminary data of a new class of imidazolium salts that contain triphenylphosphonium groups. Newly synthesized compounds were determined to have anti-cancer potential.

Chapter V describes the *in vitro* evaluation of a fluorescent imidazolium salt. Not only does this imidazolium salt have potent anti-cancer activity, but it also can be visualized in cells using fluorescence microscopy. Finally, Chapter VI provides concluding remarks and the future outlook of imidazolium salts as anti-cancer agents.

DEDICATION

I would like to dedicate this dissertation to my mom. Thank you for everything you have given me and for always believing in me. None of this would have been possible without you.

ACKNOWLEDGEMENTS

I first must thank my advisor, Dr. Wiley J. Youngs. You have been an amazing advisor and a wonderful friend throughout my five years at Akron. There have been countless laughs, quotes and jokes that I will always remember and that have made being in your lab so much fun. Thank you for letting me be creative and for letting me dream up compounds with you. My most favorite times these last few years have been the whole group just sitting in your office imagining and drawing up new compounds on the board that we wanted to make. I could not have picked a better lab to join. I must also thank you for teaching me racquetball and of course the ever-popular Settlers of Catan, even if it was annoying when you bugged me to play Catan instead of getting work done. I have truly enjoyed the time I have spent working for you and I know that no boss I have from here on out will ever compare.

I would also like to thank my co-advisor, Dr. Claire A. Tessier. You have always been there for me and I can never thank you enough for your help and support. I have learned so much from you and I can't tell you how much I love getting your "light reading" emails. It means so much that you always take time to share articles, videos, and stories that you know I am interested in. You have also given me one of the most important gifts of graduate school in the constant supply of Dubble Bubble gum. I will never be able to buy it without thinking of you!

Thank you also to Dr. Matthew J. Panzner. After all you have done for me, thank you just does not seem like enough. You have been a constant source of knowledge and support for my entire five years at Akron. Somehow you always knew when I needed encouragement on tough days and I can't thank you enough for that. I had so much fun being your TA for advanced lab and I would not trade in that experience for anything in the world. You have taught me so much about how to be an effective teacher and I will always take that with me in my future endeavors. I also want to thank you for letting me hang around when you were fixing instrumentation. I have always loved learning about how things work and you were always willing to teach me. You are an amazing person and a great friend and I would not be where I am without you.

I would also like to thank my committee members. You have all made me strive to do the best that I can and have always been there to help if I needed guidance. I truly appreciate all you have done to help me along here at Akron.

Thank you also to my wonderful family. I know it has not always been easy to deal with me during this stressful time but you all still love me anyway. Thank you for your constant love and support because none of this would have been possible without you.

Finally, I would like to thank all of the graduate students of the Youngs and Tessier groups as well as my fellow classmates here at Akron. I have learned so much from each and every one of you. Your friendships have made this experience in graduate school so much fun and I never in my life thought I would find a group of friends as wonderful as you all are. Thank you to our daily lunch crew as well. We

talk about anything and everything and those breaks in the middle of the day to joke around and relax have made graduate school so much fun. From games of Settlers to playing racquetball, from movie nights to the many conversations we all have about research, you have all been an important part of this experience.

TABLE OF CONTENTS

	Page
LIST OF TABLES	xiii
LIST OF FIGURES	xiv
LIST OF CHARTS	xix
LIST OF EQUATIONS	xxiii
CHAPTER	
1. MEDICINAL APPLICATIONS OF TRANSITION-METAL N-HETEROCYCLIC CARBENE COMPLEXES AND LIGAND PRECURSOR IMIDAZOLIUM SALTS.....	1
1.1. Introduction.....	1
1.2. General Synthesis and Biological Assays.....	5
1.3. Mono-Nuclear Imidazole NHC Complexes.....	12
1.4. Di-Nuclear imidazole NHC Complexes.....	51
1.5. Mono-Nuclear Benzimidazole NHC Complexes.....	58
1.6. Di-Nuclear Benzimidazole NHC Complexes.....	78
1.7. Other Compounds.....	81
1.8. Imidazolium Salts.....	95
1.9. Conclusion.....	129
II <i>IN VITRO</i> EVALUATION OF IMIDAZOLIUM SALTS AS ANTI-CANCER AGENTS.....	132
2.1. Introduction.....	132
2.2 Results and Discussion.....	135

2.3. Conclusion and Future Outlook.....	169
2.4. Acknowledgements.....	170
2.5. Materials and Methods.....	171
III <i>IN VIVO</i> TOXICITY STUDIES OF SELECT IMIDAZOLIUM SALTS.....	183
3.1. Introduction.....	183
3.2. Results and Discussion.....	185
3.3. Conclusion and Future Outlook.....	198
3.4. Acknowledgements.....	200
3.5. Materials and Methods.....	200
IV SYNTHESIS AND <i>IN VITRO</i> EVALUATION OF MITOCHONDRIAL TARGETING IMIDAZOLIUM SALTS.....	203
4.1. Introduction.....	203
4.2. Preliminary Results and Discussion.....	205
4.3. Conclusion and Future Outlook.....	212
4.4. Acknowledgements.....	213
4.5. Materials and Methods.....	213
V <i>IN VITRO</i> EVALUATION OF A FLUORESCENT IMIDAZOLIUM SALT.....	218
5.1. Introduction.....	218
5.2. Preliminary Results and Discussion.....	219
5.3. Conclusion and Future Outlook.....	224
5.4. Acknowledgements.....	225
5.5. Materials and Methods.....	225
VI CONCLUDING REMARKS.....	229
REFERENCES.....	235

APPENDICES.....	246
APPENDIX A. APPROVAL FOR ANIMAL USE.....	247
APPENDIX B. ABBREVIATIONS AND ACRONYMS.....	248

LIST OF TABLES

Table	Page
Table II-1. IC ₅₀ values of compounds II 1 – II 5 in either 1% DMSO/water or a 10% (w/v) HPCD solution.....	141
Table II-2. Growth percent values for NSCLC cell lines treated with II 1 – II 5 in the NCI DTP 60 human tumor cell line one-dose assay.....	144
Table II-3. GI ₅₀ , TGI, and LC ₅₀ values for NSCLC cell lines treated with II 1 – II 5 in the NCI DTP 60 human tumor cell line one-dose assay. All values are presented in μM concentrations.....	145
Table III-1. IC ₅₀ values of compounds II 3 , II 5 , III 1 , and III 2	186
Table IV-1. IC ₅₀ values of IV 1 and IV 2 solubilized in pure water.....	211
Table V-1. IC ₅₀ values of compound V 1 in a 1% DMSO/water solution.....	222

LIST OF FIGURES

Figure	Page
Figure I-1. Structure of YM155, I 336	98
Figure I-2. Structure of I 337 , a heteroaryl ethylene imidazolium salt that is inactive against the MCF7 human breast cancer cell line.....	99
Figure I-3. Structure of 2-Phenylbenzofuran Substituted Imidazole.....	102
Figure II-1. Structures of compounds II 1–II 5	135
Figure II-2. Thermal ellipsoid plot of the cationic portion of II 2 with thermal ellipsoids drawn at 50 % probability. Hydrogen atoms, carbon labels and the bromide anion have been removed for clarity.....	138
Figure II-3. Thermal ellipsoid plot of II 3 with thermal ellipsoids drawn at 50% probability. Hydrogen atoms and carbon labels have been removed for clarity.....	139
Figure II-4. Thermal ellipsoid plot of II 5 with thermal ellipsoids drawn at 50% probability. Hydrogen atoms and bromide anion have been removed for clarity.....	139
Figure II-5. H460 cells grown in 6-well plates. Merged images of Annexin V (green), propidium iodide (red), and normal transmitted light image. Images captured using an EVOS fl Digital Inverted Microscope with the 10x objective (A and B), and the 20x objective (C-E). A: Control cells grown in the presence of 10% FBS supplemented RPMI-1640 media. B: Cells grown in the presence of 40µM cisplatin. Note that the presence of green fluorescence indicates early stage apoptosis. H460 cells grown in the presence of 40µM II 1 for a period of (C) 1 hour, (D) 3 hours, and (E) 6 hours. Note the presence of early stage apoptotic cells comparable to the 6 hour cisplatin treatment at 1 hour, late stage apoptotic cells showing blebbing at 3 hours, and dead, end stage apoptotic cells at 6 hours.....	148

- Figure II-6. H460 cells grown in 6-well plates. Merged images of Annexin V (green), propidium iodide (red), and normal transmitted light image. Images captured using an EVOS fl Digital Inverted Microscope with the 20x objective. Blebbing was observed after 3 hour treatment with **II 1** at 40 μ M.....149
- Figure II-7. H460 cells grown in 6-well plates. Merged images of Annexin V (green), propidium iodide (red), and normal transmitted light image. Images captured using an EVOS fl Digital Inverted Microscope with the 10x and the 20x objectives. A: Control cells grown in the presence of 10% FBS supplemented RPMI-1640 media. B: Cells grown in the presence of 40 μ M cisplatin. Note that the presence of green fluorescence indicates early stage apoptosis. H460 cells grown in the presence of 40 μ M **II 2** for a period of (C) 1 hour, (D) 3 hours, and (E) 6 hours. Note the presence of early stage apoptotic cells at 6 hours.....150
- Figure II-8. H460 cells grown in 6-well plates. Merged images of Annexin V (green), propidium iodide (red), and normal transmitted light image. Images captured using an EVOS fl Digital Inverted Microscope. A: DMSO Control cells. B: Cells grown in the presence of 40 μ M cisplatin for 14 h. Note that the presence of green fluorescence indicates early stage apoptosis. H460 cells grown in the presence of 40 μ M **II 2** for a period of (C) 8 hours, (D) 10 hours, (E) 12 hours, and (F) 14 hours.....151
- Figure II-9. H460 cells grown in 6-well plates. Merged images of Annexin V (green), propidium iodide (red). Images captured using an EVOS fl Digital Inverted Microscope with the 20x objective. Blebbing was observed after 12 hour treatment with **II 2** at 40 μ M. All images were taken at the 12 hour time point, unless otherwise noted.....152
- Figure II-10. Images of the Annexin V assay on H460 cells grown in 6-well plates using compound **II 3** in 1% DMSO aqueous solution as the compound treatment. All images taken using a 20x objective unless otherwise stated. Images are presented as a merged image of the normal transmitted light, green fluorescence and red fluorescence figures. (A) DMSO control, 12 hours. (B) Cisplatin control, 12 hours. (C) **II 3**, 1 hour. (D) **II 3**, 3 hours. (E) **II 3**, 6 hours, 10x objective. (F) **II 3**, 12 hours, 10x objective. (A-D) Scale bars equal 200 μ m; (E and F) Scale bars equal 400 μ m.....154
- Figure II-11. Images of the Annexin V assay on H460 cells grown in 6-well plates using compound **II 3** in 1% DMSO aqueous solution as the compound treatment. All images taken using a 20x objective. Images are presented as a merged image of the green fluorescence and red fluorescence figures, omitting the normal transmitted light image for blebbing clarity. All images taken at the 3 hour time point.....155

Figure II-12. Images of the Annexin V assay on H460 cells grown in 6-well plates using compound **II 3** in 10% by weight HPCD aqueous solution as the compound treatment. All images taken using a 20x objective. Images are presented as a merged image of the normal transmitted light, green fluorescence and red fluorescence figures. (A) HPCD control, 20 hours. (B) Cisplatin control, 20 hours. (C) **II 3**, 12 hours. (D) **II 3**, 14 hours. (E) **II 3**, 17 hours. (F) **II 3**, 20 hours. Scale bars equal 200 μm156

Figure II-13. Images of the Annexin V assay on H460 cells grown in 6-well plates using compound **II 3** in 10% by weight HPCD aqueous solution as the compound treatment. All images taken using a 20x objective. Images are presented as a merged image of the green fluorescence and red fluorescence figures, omitting the normal transmitted light image for blebbing clarity. Images A–C were taken at the 14 hour time point and D-F were taken at the 17 hour time point.....157

Figure II-14. Images of the Annexin V assay on H460 cells grown in 6-well plates using compound **II 5** in 20% (w/v) HPCD aqueous solution as the compound treatment. All images were taken using a 10x objective. Images are presented as a merged image of the normal transmitted light, green fluorescence and red fluorescence figures. (A) HPCD control, 20 hours. (B) Compound **II 5**, 14 hours. (C) Compound **II 5**, 20 hours. Scale bars equal 400 μm159

Figure II-15. Images of the Annexin V assay on H460 cells grown in 6-well plates using compound **II 5** in 20% (w/v) HPCD aqueous solution as the compound treatment. All images were taken using a 20x objective. Images are presented as a merged image of the green fluorescence and red fluorescence figures, omitting the normal transmitted light image for blebbing clarity. Images A-C were taken at the 20 hour time point, D-E were taken at the 17 hour time point, F-G were taken at the 14 hour time point, and images H-I were taken at the 12 hour time point.....160

Figure II-16. Images of the Annexin V assay on H460 cells grown in 6-well plates using **II 4** dissolved in a 1% DMSO aqueous solution as the compound treatment. All images were taken using a 20x objective. Images are presented as a merged image of the normal transmitted light, green fluorescence and red fluorescence figures. (A) Media control, 12 hours. (B) DMSO control, 12 hours. (C) Cisplatin control, 12 hours. (D) Compound **II 4**, 1 hour. (E) Compound **II 4**, 3 hours. (F) Compound **II 4**, 6 hours. (G) Compound **II 4**, 12 hours. Scale bars equal 200 μm161

Figure II-17. Images of the Annexin V assay on H460 cells grown in 6-well plates using **II 4** dissolved in a 1% DMSO aqueous solution as the compound treatment. All images were taken using a 20x objective. Images are presented

as a merged image of the normal transmitted light, green fluorescence and red fluorescence figures. (A) Compound II 4 , 1 hour. (B) Compound II 4 , 12 hours. Scale bars equal 200 μm	162
Figure II-18. Image depicting the comparison of compound II 4 versus compound II 5 treated cells. (Row A) H460 blebbing cells after treatment with compound II 5 (normal transmitted light image omitted for blebbing clarity). (Row B) H460 cells after treatment with compound II 4	162
Figure II-19. Viscosity plot of compound II 3 using CT-DNA relative to controls....	164
Figure II-20. Plot of FID measurements of compound II 3 using CT-DNA relative to controls.....	165
Figure II-21. Structure of JC-1.....	166
Figure II-22. Images of the JC-1 assay on H460 cells grown in 35 mm glass bottom dishes using compounds II 1 and II 3 at 40 μM in a 1% DMSO aqueous solution as the compound treatment. All images were taken using a 100x objective. Images are presented as a merged image of the normal transmitted light, green fluorescence, blue fluorescence, and red fluorescence figures (merged columns) or the red fluorescence alone (J-aggregates columns) at the specified time frames. Scale bars equal 50 μM	167
Figure II-23. Images of the JC-1 assay on H460 cells grown in 35 mm glass bottom dishes using compound II 3 at 20 μM in a 1% DMSO aqueous solution as the compound treatment. All images were taken using a 100x objective. Images are presented as the individual a merged image of the normal transmitted light, green fluorescence, blue fluorescence, and red fluorescence figures (merged columns) or the red fluorescence alone (J-aggregates columns) at the specified time frames. Scale bars equal 50 μM	168
Figure III-1. Structures of lead imidazolium salts, II 3 , II 5 , III 1 , and III 2 , tested for <i>in vivo</i> cytotoxicity. Compounds II 3 and II 5 have been previously tested in chapter II.....	185
Figure III-2. Kaplan Meier curve of mice treated with imidazolium salts.....	188
Figure III-3. Graph of the average weight gain percent for mice treated with II 3 as compared to HPCD control mice. Black data point markers indicate days of injection, with all mice being injected on day 1.....	190
Figure III-4. Graph of the average weight gain percent for mice treated with II 5 as compared to HPCD control mice. Black data point markers indicate days of injection, with all mice being injected on day 1.....	192

Figure III-5. Graph of the average weight gain percent for mice treated with III 1 as compared to HPCD control mice. Black data point markers indicate days of injection, with all mice being injected on day 1.....	194
Figure III-6. Graph of the average weight gain percent for mice treated with III 2 as compared to HPCD control mice. Black data point markers indicate days of injection, with all mice being injected on day 1.....	195
Figure III-7. Comparison of the average weight gain percent of all tested imidazolium salt compounds and controls.....	198
Figure IV-1. Thermal ellipsoid plot of IV 1 with thermal ellipsoids drawn to 50% probability. Hydrogen and carbons labels and solvent molecules have been removed for clarity.....	208
Figure IV-2. Thermal ellipsoid plot of IV 2 with thermal ellipsoids drawn to 50% probability. Hydrogens, carbon labels and solvent molecules have been removed for clarity.....	209
Figure V-1. Structure of V 1	220
Figure V-2. Thermal ellipsoid plot of IV 2 with thermal ellipsoids drawn to 50% probability. Hydrogens, carbon labels and solvent molecules have been removed for clarity.....	220
Figure V-3. Fluorescence spectrum of V 1 (excitation wavelength : 456 nm).....	221
Figure V-4. H460 cells stained with V 1 and imaged at the 30 minute and 2 hour time point.....	223
Figure V-5. H460 cells stained with V 1 at the 2 hour time point. Images depict both the green and red fluorescence of V 1	224

LIST OF CHARTS

Chart	Page
Chart I-1. Structures of Amide and Ester Functionalized Carbene Complexes and the Corresponding Imidazolium Salt Precursors.....	13
Chart I-2. Structures of Triazine Functionalized Carbene Complexes and the Corresponding Imidazolium Salt Precursors.....	16
Chart I-3. Structures of Triazole Functionalized Carbene Complexes.....	17
Chart I-4. Structures of Gold(I) Carbene Complexes I 23 and I 24	19
Chart I-5. Structures of 1-Thio- β -d-glucopyranosido (I 27) and Tetra-O-acetyl-1-thio- β -d-glucopyranosido (I 28) Functionalized Gold(I) Carbene Complexes and the Corresponding Imidazolium Salt (I 25) and Gold(I) Chloride (I 26) Precursors.....	20
Chart I-6. Structures of Titanocene Functionalized Gold(I) Carbene Complexes I 33- I 36 and the Corresponding Hmba Precursors I 29- I 32	23
Chart I-7. Structures of Propargyloxybenzene Linked Imidazolium Salts I 37- I 38 and Consequent Gold(I) Carbene Complex I 39	24
Chart I-8. Structures of Imidazolium Salts I 40- I 46 and Consequent Gold(I) Carbene Complexes I 47- I 54	27
Chart I-9. Structures of Bidentate Ru(II) Carbene Complexes I 55 and I 56	28
Chart I-10. Structures of 4,5-Diphenyl Substituted Imidazolylidene Ruthenium (II) and Gold(I) Carbene Complexes.....	30
Chart I-11. Structures of 4,5-Diphenyl Substituted Imidazolylidene Silver(I) Carbene Complexes I 73- I 77 and an Imidazolium Salt Precursor I 72	32
Chart I-12. Structures of 4,5-Diphenyl Substituted Imidazolylidene Silver(I) Carbene Complexes and the Corresponding Imidazolium Salt Precursors.....	33
Chart I-13. Structures of 4,5-Diphenyl Substituted Imidazolylidene Copper(I) Carbene Complexes I 100- I 108 and the Benzimidazolylidene NHC, I 109 ..	35

Chart I-14. Structures of 4,5-Diphenyl Substituted Imidazolylidene Gold(I) Carbene Complexes with Thiolates and Psuedo Halide Ligands.....	36
Chart I-15. Structures of Bidentate Imidazolylidene Platinum(II) Carbene Complexes I 116- I 124	38
Chart I-16. Structures of Imidazolylidene Platinum(II) Carbene Complexes I 125- I 137	40
Chart I-17. Structures of Imidazolylidene Platinum(II) Carbene Complexes with Metal Bound PDA Ligands and Corresponding Precursors.....	43
Chart I-18. Structures of Imidazolylidene Platinum(II) Carbene Complexes with Metal Bound Amine Ligands.....	46
Chart I-19. Structures of Platinum(IV) Carbene Complexes with Metal Bound Amine and Halide Ligands.....	48
Chart I-20. Structures of Platinum(II) Carbene Complexes with Metal Bound Ammines and Targeting Group Functionalized Imidazolylidenes.....	50
Chart I-21. Structures of Di-nuclear Imidazolylidene Silver(I) Carbene Complexes with Xylyl Linkers.....	52
Chart I-22. Structures of Di-nuclear Imidazolylidene Silver(I) Carbene Complexes and Mono-nuclear Silver(I) NHC, I 179	53
Chart I-23. Structures of Di-nuclear Imidazolylidene Gold(I) Carbene Complexes I 180- I 183	54
Chart I-24. Structures of Di-nuclear Imidazolylidene Silver(I) and Gold(I) Carbene Complexes and the Corresponding Imidazolium Salt Precursors.....	56
Chart I-25. Structures of Di-nuclear Silver(I) and Gold(I) Carbene and Bis-Carbene Complexes.....	58
Chart I-26. Structures of Tetrachloroimidazolylidene and Dichloroimidazolylidine Silver(I) Carbene Complexes.....	59
Chart I-27. Structures of Benzimidazolylidene Silver(I) Carbene Complexes and the Corresponding Imidazolium Salts.....	60
Chart I-28. Structures of Benzimidazolylidene Silver(I) Carbene Complexes I 207- I 216	62
Chart I-29. Structures of Benzimidazolylidene Silver(I) Carbene Complexes I 217- I 223	63
Chart I-30. Structures of Benzimidazolylidene Silver(I) Carbene Complexes and the Corresponding Imidazolium Salt Precursors.....	65

Chart I-31. Structures of Benzimidazolylidene Silver(I) Carbene Complexes I 237- I 243	66
Chart I-32. Structures of Benzimidazolylidene Silver(I) Carbene Complexes I 244- I 250	68
Chart I-33. Structures of N-methyldioxane and N-propylphthalimide Functionalized Benzimidazolylidene Silver(I) Carbene Complexes I 251- I 255	69
Chart I-34. Structures of Silver(I) Bis-Carbene Complexes and the Benzimidazolium Salt Precursor.....	71
Chart I-35. Structures of Mono-Nuclear and Di-Nuclear Silver(I) Bis-Carbene Complexes and the Benzimidazolium Salt Precursors.....	73
Chart I-36. Structures of Silver(I) Bis-Carbene Complexes and the Corresponding Benzimidazolium Salt Precursors.....	74
Chart I-37. Structures of Gold(I) Bis-Carbene Complexes I 282- I 287	76
Chart I-38. Structures of Palladium(II) Carbene Complexes and the Corresponding Benzimidazolium Salt Precursors.....	77
Chart I-39. Structures of Di-Nuclear Silver(I) Bis-Carbene Complexes and the Bis-Imidazolium Salt Precursors.....	79
Chart I-40. Structures of Di-Nuclear Silver(I) Bis-Carbene Complexes I 305 and I 306	80
Chart I-41. Structures of Pyridine Wing-tip Functionalized Gold(I) Carbene Complexes.....	82
Chart I-42. Structures of Tridentate Bis-Imidazolylidine Ruthenium(II) Carbene Complexes.....	83
Chart I-43. Structures of Xanthine Derived Platinum(II) Carbene Complexes (I 312- I 313) and Xanthine Coordination Complexes (I 314- I 315).....	85
Chart I-44. Structures of Quinone Functionalized Imidazolylidene Gold(I) Carbene Complexes and Bis-Carbene Complex, I 320	88
Chart I-45. Structures of Porphyrine Imidazolylidene Gold(I) Carbene Complexes and the Imidazolium Salt Precursor, I 321	90
Chart I-46. Structures of Triazolylidene Metal Carbene Complexes and the Corresponding Imidazolium Salt Precursor.....	92
Chart I-47. Structures of Triazolylidene Silver(I) and Gold(I) Carbene.....	94
Chart I-48. Structures of Triazolylidene Gold(I) Carbene Complexes I 331- I 333 ...	95

Chart I-49. Structure of the first imidazolium salts evaluated for anti-cancer properties, Lepidiline A and Lepidiline B.....	97
Chart I-50. Structures of Benzofuran Functionalized Imidazolium Salts.....	100
Chart I-51. Structures of 2-Phenylbenzofuran Functionalized Imidazolium Salts...	101
Chart I-52. Structures of 2-Benzylbenzofuran Functionalized Imidazolium Salts...	103
Chart I-53. Structures of 2-Benzylbenzofuran Substituted Imidazolium Salts.....	105
Chart I-54. Structures of 2-Methylbenzofuran Functionalized Imidazolium Salts...	107
Chart I-55. Structures of Dibenzo[b,d]furan Functionalized Imidazolium Salts.....	109
Chart I-56. Structures of Benzodifuran Functionalized Imidazolium Salts.....	111
Chart I-57. Structures of 1-(indol-3-yl)methyl Functionalized Imidazolium Salts..	113
Chart I-58. Structures of Indolene Functionalized Imidazolium Salts.....	115
Chart I-59. Structures of Fluorene Functionalized Imidazolium Salts.....	116
Chart I-60. Structures of Carbazole Functionalized Imidazolium Salts.....	118
Chart I-61. Structures of Tetrahydro- β -carboline Imidazolium Salts.....	120
Chart I-62. Structures of Naphthalene Functionalized Imidazolium Salts.....	122
Chart I-63. Structures of Modified Imidazolium Salts I 708- I 715	124
Chart I-64. Structures of 4,5-Diphenyl Imidazolium Salts.....	125
Chart I-65. Structures of Functionlized Benzimidazolium Salts.....	127
Chart I-66. Structures of 2-Alkyl Imidazolium Salts.....	129

LIST OF EQUATIONS

Equation	Page
Equation I-1. Average resonance form of an imidazolium salt with the numbering scheme that is used throughout the review.....	3
Equation I-2: General Synthesis of Transition-Metal NHC Complexes and the Corresponding Imidazolium Salt Ligand Precursors.....	7
Equation II-1. Synthesis of compounds II 1–II 5	135
Equation IV-1. Synthesis of compound IV 1	206
Equation IV-2. Synthesis of compound IV 2	207

CHAPTER I
MEDICINAL APPLICATIONS OF TRANSITION-METAL N-HETEROCYCLIC CARBENE
COMPLEXES AND LIGAND PRECURSOR IMIDAZOLIUM SALTS

“Reproduced in part with permission from [Southerland, M. R.; Stromyer, M. L.; DeBord, M. A.; Johnson, N. A.; Tessier, C. A.; Youngs, W. J. (Manuscript in Progress)]

1.1. Introduction

N-Heterocyclic carbenes (NHCs) have become an important family of compounds in the scientific literature. The first synthetic report of NHCs occurred in 1968 by Wanzlick¹ and Öfele.² The field was further strengthened and established by Bertrand and co-workers in 1988 when they published studies on the first carbene utilizing phosphorus and silicon for stability.³ Three years later, Arduengo reported the first NHC that was isolated and structurally characterized by X-ray crystallography, the final stepping stone that opened the door for a vast field of chemistry that is still to this day giving rise to new compounds that have a wide variety of applications.⁴

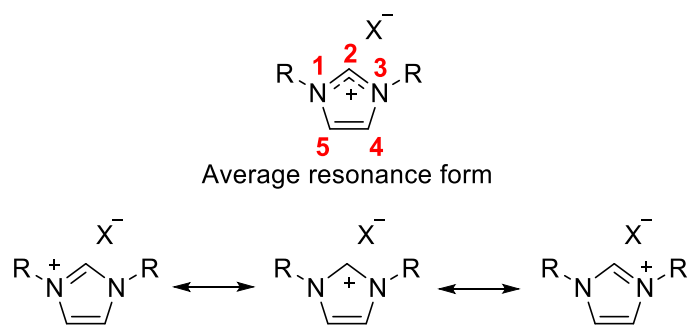
NHC complexes have been utilized in many areas such as organometallic materials and olefin metathesis as well as in medicinal chemistry as antimicrobial

and anti-cancer compounds.⁵ They can bind to hard and soft metals, a property that enhances their ability to act as a delivery system for a wide variety of metals.⁶ One of the earliest reports of medicinal NHC complexes came in 1996 by Çetinkaya et al., where they describe the antimicrobial activity of rhodium(I) and ruthenium(II) carbenes.⁷ NHC complexes have been widely studied for their use as antimicrobial agents and their success in this area has depended largely on their ability to deliver a metal cation into biological systems. Transition metals, such as silver, gold, and copper, have low to moderate toxicities to humans but great potential for killing microorganisms.^{8,9} However, metals have not just been used solely in medicinal chemistry for the purpose of antimicrobials. After the discovery by Rosenberg et al. of cisplatin¹⁰⁻¹², the world of metal chemotherapeutics has grown exponentially, with the number of new derivatives rapidly increasing.¹³⁻¹⁵ Thus the shift of NHC complexes into the genre of metal-based chemotherapeutics was inevitable due to their synthetic versatility and success in delivery of a wide variety of metals. Early work in both of these areas by Youngs and coworkers on silver(I) and gold(I) NHC complexes is an example of the success of these compounds for both antimicrobial and anti-cancer applications.¹⁶⁻²²

However, by delivering the metal in the form of an NHC complex, an imidazolium salt also is generated, in most cases. With two different species being released it is important to distinguish between activity that can be attributed to the metal or to the imidazolium salt. Imidazolium salts are products of the alkylation of both nitrogen atoms of an imidazole ring. The imidazole structure is ubiquitously found in nature, most notably as part of the essential amino acid histidine²³ and the signaling

molecule histamine.²⁴ An example of a generic imidazolium salt is shown in Equation I-1, which depicts the average resonance form and general numbering scheme of an imidazolium salt as it will be used in this review. An imidazolium salt, as with any other salt, consists of a cation and anion pair. The cation is of utmost importance when discerning the anti-cancer properties that will be discussed. However, research has been performed to understand the role of the anion and its effects on activity and solubility as well.

Equation I-1. Average resonance form of an imidazolium salt with the numbering scheme that is used throughout the review.



Imidazolium salts can be easily and readily synthesized to be highly functionalized at any positions of the imidazole ring. However, they are most easily substituted and modified at the N¹ and N³ positions. The most common route is to alkylate both nitrogen atoms on an imidazole core in subsequent steps.²⁵ This approach can be used to synthesize both symmetric²⁶ and asymmetric^{27,28} imidazolium salts. They can also be synthesized by cyclization of diamine intermediates, produced from the reaction of primary amines with glyoxal. However, this synthetic route limits the products to symmetrical imidazolium salts and is less commonly used.^{29,30} With the wide variety of synthetically achievable

imidazolium salts, the ability to fine-tune them for use as NHC complexes is endless. Some imidazolium salt precursors were designed to be innocuous, such as the xanthine derivatives made by Youngs and coworkers.³¹⁻³³ This would ensure that the delivery of the NHC metal would result in activity caused only by the metal of choice. However, as the field has grown, modifications to the imidazole core have led to the development of imidazolium salts that can also exhibit biological activity.³⁴ Therefore, with new derivatives being constantly made, it has become increasingly important to learn about both the imidazolium salt precursors and the NHC complexes.

This review will focus on recently published literature (within the last few years from 2012-2017) outlining newly synthesized NHC complexes that also study, specifically, their anti-cancer and antimicrobial properties. This review focuses on transition metals that include silver, gold, copper, ruthenium, platinum and palladium. Research articles that note differences in activity between the ligand precursors and NHC complexes will be discussed as outlined by the authors. Where applicable, the structure activity relationship (SAR) will also be discussed. Furthermore, recent literature in the field of imidazolium salts will be examined due to their importance in the consideration of NHC complexes and their medicinal applications. With the multitude of literature available on ionic liquids they will not be discussed in this review. However, interested readers are directed to a review article by Egorova et al., outlining the biological activity and medicinal applications of ionic liquids.³⁵

There are two main purposes and goals of this review article. First, we would like to give interested scientists the information necessary to begin research in the area of NHC complexes. Outlining general synthetic approaches as well as biological activity will serve as an introduction into the recent directions of this field and will give the tools necessary for individuals to begin work in the field. The second purpose of this review is to outline the trends in biological activity as related to structure for those new to the field and for those who are experts. In order to make new compounds that have the potential for use as medicinal therapeutics, the biological activity of the already synthesized derivatives should serve as a guide. For readers interested in more information on NHC complexes, we direct you to several reviews that have been published.^{5,21,22,36-40}

1.2. General Synthesis and Biological Assays

The synthesis of NHC complexes begins with the synthesis of the imidazolium salt precursors. In general the imidazole cores are commercially available or generated through many synthetic routes. Substituents at all positions of the imidazolium ring contribute to the overall properties of the corresponding NHC. Various functional groups can be chosen to alter solubility and stability of the metal ligand bond, which in turn both affect the biological activity of the NHC complexes. However, in general, the nitrogen atoms of the imidazole core are substituted by alkylation with various alkyl and aryl halides. The resulting imidazolium salts are metalated through various techniques including free carbene formation, metal base reactions, and transmetalation (Equation I-2).⁴¹

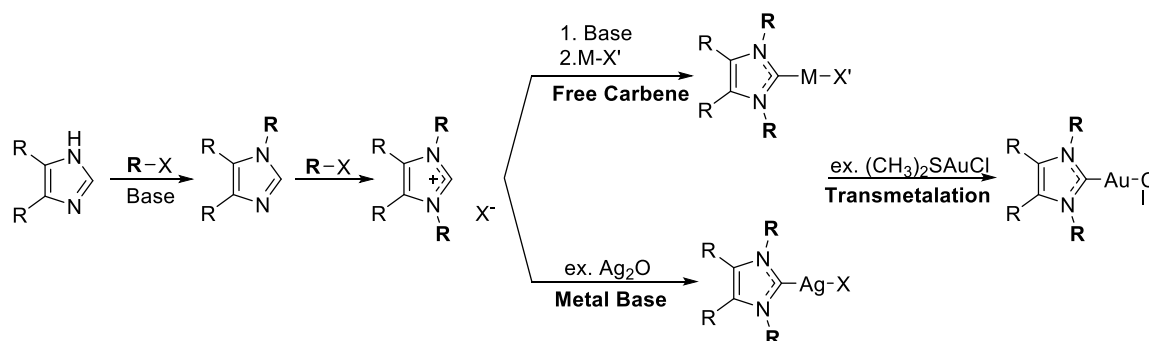
The free carbene synthetic route is generally a two-step process. Ideally under inert atmosphere, an imidazolium salt is treated with a base and then reacted with a metal salt. The base deprotonates the imidazole to form the free carbene, which will coordinate to the metal forming the metal-NHC complex.⁴¹ Throughout current literature for medicinal NHC complexes this technique can be used for the synthesis of a myriad of metal complexes, for example copper(I) carbene complexes are synthesized by free carbene formation and subsequent reaction with tetrakis(acetonitrile)copper(I) halide. This is not the only example of this technique, as it is used to form other metal-NHC complexes such as gold, silver, platinum, palladium, and ruthenium complexes.⁴²

Another common NHC synthetic route is the metal base technique. This reaction is a concerted reaction synthesis, which includes a dual reagent, for example silver oxide or silver acetate, which deprotonates the imidazolium salt and promotes metalation concurrently. Silver bases are the most common for this reaction type due to quantitative yields of the NHC complex and the ability to transmetalate to other metals.²¹

Transmetalation is the final synthetic route that will be discussed. Commonly a silver NHC complex is used as a transmetalation precursor because of the weak silver to carbene bond. These silver complexes are reacted with a transmetalation reagent, which will displace the silver. This process is driven by the formation of stable silver halide salts that are insoluble in common solvents. Examples of two common transmetalation reagents are chlorodimethylsulfide

gold(I) which is used to obtain gold(I) complexes, or dichloro-(p-cymene) ruthenium(II) to transmetalate to ruthenium(II) complexes.^{21,38}

Equation I-2: General Synthesis of Transition-Metal NHC Complexes and the Corresponding Imidazolium Salt Ligand Precursors



In a review that discusses multiple types of compounds, it is important to distinguish and define terms. NHCs, as outlined above, are N-heterocyclic carbenes, defined as neutral compounds containing a lone pair on a carbon atom. Metals are able to bind to the carbene lone pair through σ -donation and by a small extent through π -back-donation.^{21,22} The compound formed by this bond of the carbene to the metal is called an NHC complex. The carbenes are formed by different methods outlined above, but often begin as imidazolium salts. The carbene itself is the ligand of the NHC complex. Therefore, imidazolium salts are the ligand precursors for NHC complexes.

The major methods of determining a compounds biological activity are the MTT/MTS assays, broth or agar dilution, and Kirby-Bauer disc diffusion. The former is used to screen for anti-tumor activity whereas the other two methods are to screen for activity against microbes. The data gained from these studies is evaluated in multiple ways that will be described and defined in this section. The broth and agar dilution methods are the more popular methods by which to determine a

compounds minimum inhibitory concentration (MIC) value, defined as the lowest concentration of a compound that visibly inhibits growth of a microorganism after overnight incubation.⁴³ The compound to be tested is incorporated into either broth or agar, which can then be diluted to various concentrations. The microorganism is then introduced to the broth or agar and incubated under ideal conditions. MIC values are often presented in units of $\mu\text{g}/\text{mL}$. A lower MIC value indicates higher antimicrobial activity. The Kirby-Bauer disc diffusion method involves a disc made of filter paper that is saturated with the compound in question and placed on an agar plate containing the microorganism that is to be tested.⁴³ The zone of inhibition is the area around the disc that is cleared of all bacteria or fungi, with the clearance occurring due to diffusion of the test compound from the disc to the agar, preventing the growth of the microorganism. This zone of inhibition is measured in millimeters. A larger zone of inhibition indicates better antimicrobial activity of the tested compound while a smaller zone of inhibition indicates less activity.

Assays to determine anti-cancer activity rely on the reduction of tetrazolium salts, either intracellularly (MTT) or extracellularly (MTS and XTT), into colored formazan products that are either soluble in cell culture media (MTS and XTT) or detergents and other solvents (MTT).⁴⁴ The level of formazan formation can be measured in a high-throughput method by use of a plate reader to measure absorbance, typically in a 96-well plate format. Results are presented as an IC_{50} value or the concentration of a compound that inhibits a specific activity by 50% as compared to control cells. In the case of this review, the activity is cell proliferation

therefore IC₅₀ values and GI₅₀ values give similar information. The use of either IC₅₀ or GI₅₀ is dependent here upon the term used by the original authors.

While the MTT assay is a relatively high-throughput method for determining the anti-cancer activity of a library of compounds, it does not give any information about how the tested compounds induce cell death. To distinguish between the process of apoptosis (programmed cell death) and necrosis (cell death caused by trauma), other studies need to be incorporated, such as the Annexin V assay, JC-1 assay, Western blot analysis and cell morphology studies by microscopy. Programmed cell death can occur through two different signaling cascades, either the intrinsic pathway or the extrinsic pathway. The intrinsic pathway is considered to be mediated by mitochondria inside the cell while the extrinsic pathway occurs through a ligand-receptor interaction at the outside of the membrane which activates a signal cascade that leads to cell death. In both cases, caspases play an important role.⁴⁵ Caspases are proteases, specifically cysteinyl aspartate-specific proteases, a description that explains the derivation of their name. Caspases begin as a single chain procaspase that is cleaved to form the active complex.⁴⁶ The two types of caspases are the initiator caspases (caspase-8, -9, and -10) and the executioner caspases (caspase-3, -6, and -7), which directly cause the cell to undergo apoptosis.^{45,46}

In order for the caspase cascade to be activated through the intrinsic pathway, cytochrome c needs to be released. This is facilitated by a number of factors that increase the permeability of the outer mitochondrial membrane, which is facilitated by the Bcl-2 protein Bax as well as oxidation of cardiolipin (CL).^{45,47} CL

is important for keeping cytochrome c at the inner mitochondrial membrane during normal cellular function to participate in the electron transport chain. Upon cellular stress and production of reactive oxygen species (ROS), cardiolipin is oxidized, releasing its hold on cytochrome c. It is postulated that CL is translocated to the outer mitochondrial membrane where it binds to tBid, promoting the formation of pores by Bax.⁴⁷ The release of cytochrome c begins the caspase cascade, which results in apoptosis. Regulation of Ca²⁺ is also an important factor in health and death of cells by apoptosis.⁴⁸

Since delocalized lipophilic cations (DLCs), such as imidazolium salts, are able to target the mitochondria of cells, it is increasingly important to study the effects that anti-cancer imidazolium salts have on mitochondria.⁴⁹ However, there are many steps in the apoptosis cascade that imidazolium salts could be affecting. In order to study the mechanism of action of imidazolium salts, a systematic approach needs to be taken. First, it is important to determine whether tested compounds are killing cancer cells through the process of apoptosis or necrosis. Those that induce a necrotic cell death cause general trauma to cancer cells through a variety of methods and would cause an inflammatory response when translated to *in vivo* studies due to the release of cellular components to the extracellular space. This inflammatory response can be beneficial in that it would target the host's immune system to the tumor. However, damage to normal tissue can also occur as well as the production of cytokines that can lead to metastasis. Compounds that kill cancer cells through apoptosis eliminate the possibility for an inflammatory response due to the generation of apoptotic bodies.^{45,46} The process of how the apoptotic cascade begins

and progresses can be studied through various methods, leading to more information regarding the mechanism of action of imidazolium salts that cause apoptosis. Release of cytochrome c, ATP production, mitochondrial membrane potential, ROS production, interaction with CL, decrease in superoxide dismutase (SOD) or catalase activity are among the many studies that can be completed to begin determining how imidazolium salts disrupt cancer cells.

While many microorganisms and cancer cell lines are similarly tested in the research articles contained within this review, it is difficult to directly compare the results from one paper to another. Therefore, comparing MIC or IC₅₀ values between research groups may not accurately reflect biological activity trends that would be seen if each compound was tested in the same lab or with the same reference compounds. Varying environmental conditions and protocols, among other things, can contribute to this. Therefore, this review focuses solely on the comparison of compounds that were studied within their respective research group. MIC, IC₅₀, and GI₅₀ values that are said to be lower reflect a higher level of biological activity of that particular compound or group of compounds. Likewise, those values that are said to be higher reflect a decrease in biological activity. In contrast, a larger zone of inhibition measurement value in millimeters for the disc diffusion method reflects an increase in biological activity while a smaller value corresponds to a decrease in biological activity. While the numbers cannot be compared directly, structure activity relationship (SAR) trends will be discussed as well as comparisons to control compounds where applicable. Standard deviations are also presented if determined by the authors.

1.3. Mono-Nuclear Imidazole NHC Complexes

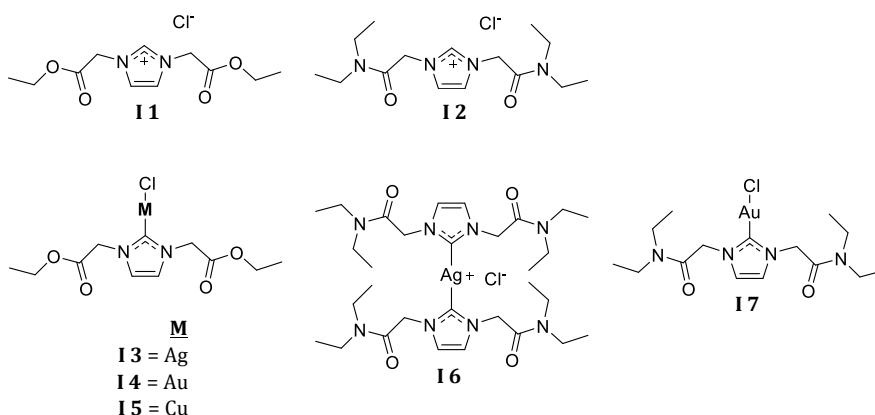
1.3.1. Biologically Active Silver and Gold NHC Complexes Incorporating Nitrogen Containing Substituents

Pellei, et al. have reported the synthesis of novel imidazol-2-ylidene metal complexes for the treatment of cancer utilizing all three of the previously mentioned NHC metalation techniques (Chart I-1).⁵⁰ The first was the silver base technique by reacting silver(I) oxide with 1,3-bis(2-ethoxy-2-oxoethyl)imidazol-3-ium chloride (**I 1**) or 1,3-bis(2-(diethylamino)-2-oxoethyl)imidazol-3-ium chloride (**I 2**) to form the ester (**I 3**) or amide (**I 6**) functionalized NHC. The ester complex formed a single carbene NHC whereas the amide functionalized NHC promoted the formation of the bis-carbene. The second technique used was formation of the free carbene via the reaction of the imidazolium salt with lithium bis(trimethylsilyl)amide and copper(I) chloride to afford the copper(I) NHC complex (**I 5**). Finally to synthesize the gold complexes (**I 4**, **I 7**), the silver NHC complexes previously mentioned were transmetalated to gold via the reaction with chloro(dimethylsulfide) gold(I). Additionally, when the amide functionalized bis-carbene silver complex is transmetalated to gold with 2 equivalents of chloro(dimethylsulfide) gold(I), the formation of the mono-carbene predominates.

These complexes were tested against the cancer cell lines A549 (lung), HCT-15 (colon), MCF-7 (breast), and A375 (melanoma) using the MTT assay. The IC₅₀ values were not determined for the copper complex due to its instability in media. The precursor ligands, **I 1** and **I 2**, did not exhibit significant cytotoxicity overall. The silver complexes, **I 3** and **I 6**, were found to be more effective than the gold

complexes, **I 4** and **I 7**. However, even the silver compounds were not as active as cisplatin. Based on the IC₅₀ values (A375 = 24.46 ± 2.81 μM; A549 = 16.23 ± 2.31 μM; HCT-15 = 14.11 ± 2.11 μM; MCF-7 = 15.31 ± 3.44 μM), compound **I 6** was determined to be the lead compound. Compound **I 6** was also found to have a higher IC₅₀ value against non-cancerous HEK293 cells as compared to cisplatin (77.36 ± 3.95 μM and 19.56 ± 3.47 μM, respectively). TrxR inhibition was also tested *in vitro* and it was found that the gold and silver complexes were able to inhibit TrxR function. At 90 nM, both were able to decrease activity by about 80%, leading the authors to believe this to be the cellular target. The IC₅₀ values for compound **I 6** for the cell line 2008, human ovarian cancer, versus C13*, a cisplatin resistant ovarian cancer cell line, were similar to each other (14.22 ± 2.82 μM and 12.33 ± 3.62 μM, respectively) in contrast to cisplatin which displayed values of 2.24 ± 1.32 μM for 2008 and 22.54 ± 2.16 μM for C13*. These values indicate that not only can complexes like **I 6** act as anti-cancer agents, they can elude the normal resistance mechanisms that cells utilize against cisplatin.

Chart I-1. Structures of Amide and Ester Functionalized Carbene Complexes and the Corresponding Imidazolium Salt Precursors

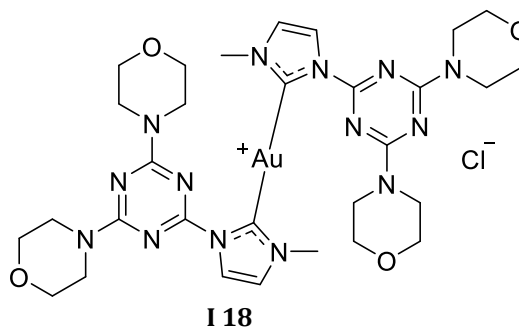
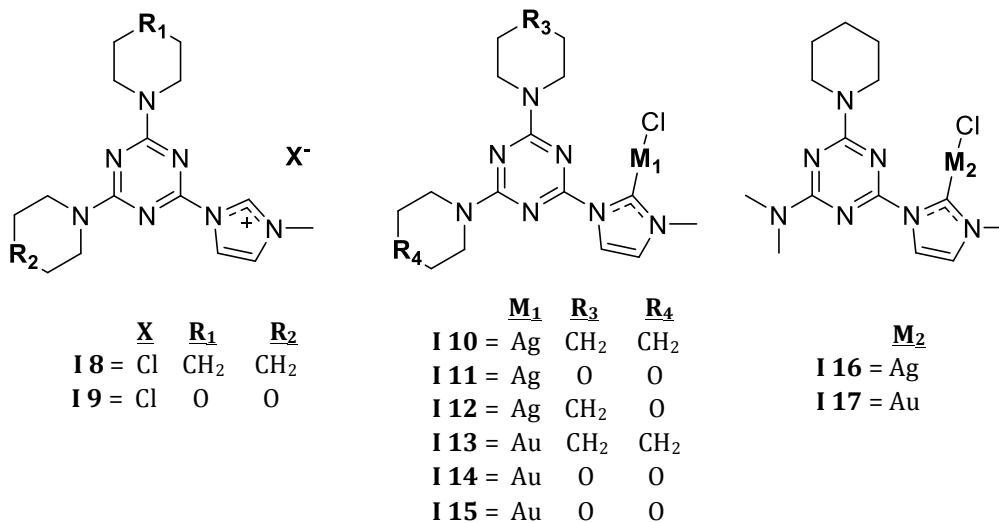


Other novel NHC complexes utilizing silver and gold were also synthesized and tested for antimicrobial activity by Almaloti et al. (Chart I-2).⁵¹ The starting imidazolium salts were alkylated with cyanuric chloride that was converted into triazine chloride with piperidine or morpholine substituents. These species were then used as the alkylating agents to substitute onto 1-methylimidazole. The imidazolium salts **I 8** and **I 9** were metalated with silver via the silver base route or metalated with gold(I) via transmetalation or the free carbene synthesis. The mono-imidazolium salts were reacted with silver(I) oxide in chloroform, yielding silver chloride NHC complexes **I 10- I 12**. To achieve the gold(I) NHC complexes (**I 13- I 15**) two synthetic schemes were used. The first route was the transmetalation from a silver NHC using chloro(tetrahydrothiophene)gold(I). The second route was formation of the free carbene using sodium acetate to deprotonate the C₂ proton of the imidazolium salt and an addition of the gold salt chloro(tetrahydrothiophene)gold(I). Adjusting the stoichiometry of the metalation reactions to form the gold NHC complexes resulted in the formation of the mono-carbene (**I 14**) and bis-carbene (**I 18**) complexes for the morpholine substituted aminotriazines. The transmetalation from silver to gold with a concentration of the starting NHC complex equivalent to the gold salt resulted in a 54:46 ratio of mono-carbene to bis-carbene, whereas the formation of the free carbene and metalation by the gold salt primarily formed the mono-carbene with a 91:9 ratio. When the starting silver carbene was in excess by 2 equivalents, the resulting gold bis-carbene formed with a 67:33 ratio. It can be deduced that transmetalation from silver to gold for the dimorpholine substituted aminotriazines favored bis-carbene formation.

Alternatively, use of the free carbene route of the gold NHC favored the mono-carbene formation. In addition to the mono-imidazolium salts, the bis-imidazolium salts were metalated with silver (**I 16**) and gold (**I 17**). The bis-imidazolium salts were reacted with silver(I) oxide or sodium acetate and chloro(tetrahydrothiophene)gold. It was discovered that the reaction solvent was key in formation of the carbene. When the reaction was attempted in chloroform, no reaction occurred. Upon running the reactions in methanol in the presence of silver(I)oxide, methanol deprotonates and substitutes the aminotriazine driving off 1-methylimidazole. If DMF is utilized as the solvent, loss of 1-methylimidazole still occurs and dimethylamine from hydrolyzed DMF substitutes onto the triazine ring.

The precursors **I 8** and **I 9**, as well as the complexes **I 10** and **I 11** were tested against four bacteria (MRSA NCTC 13277, *S. aureus* NCTC 6571, *P. aeruginosa* NCTC 10662, and *Proteus mirabilis* NCTC 11938) as well as the fungal organism *Candida albicans* ATCC 90028 by agar diffusion assays. The Gram-positive strains (MRSA and *S. aureus*) were significantly more inhibited when treated with **I 10** and **I 11**. Compound **I 11** was more active against MRSA. The Gram-negative bacteria were not significantly inhibited by either compound but moderate antifungal activity for both was found. The imidazolium precursors were also tested. Compound **I 8** was active against all the strains except for *P. mirabilis*, demonstrating that both the precursors and NHC complexes exhibit antimicrobial activity.

Chart I-2. Structures of Triazine Functionalized Carbene Complexes and the Corresponding Imidazolium Salt Precursors

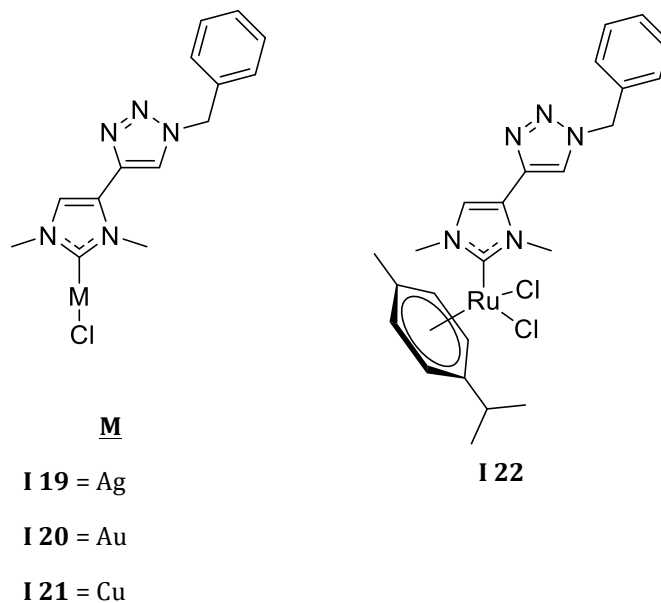


Similar to Almaloti et al., Monticelli et al. report the synthesis of NHC complexes functionalized with other N-heterocycles (Chart I-3).⁵² To form the NHC, the precursor imidazolium salt was first synthesized. First 5-[(trimethylsilyl)ethynyl]-1-methylimidazole was deprotected with potassium carbonate to form 5-ethynyl-1-methylimidazole. Using a copper catalyzed alkyne-azide cycloaddition reaction between the alkyne and benzyl azide, the benzyl triazole substituent was formed. From this, an imidazolium salt was synthesized via methylation of the imidazole. Methyl iodide was not reactive enough to alkylate the nitrogen of the triazole, selectively producing the methylated imidazole. The imidazolium salt precursor was then metalated to the silver(I) NHC (**I 19**) using

silver(I) oxide. Complex **I 19** was transmetalated to the gold (**I 20**), copper (**I 21**), or ruthenium (**I 22**) complex.

Only the most stable complexes, **I 19**, **I 20** and **I 22**, were tested for activity against the cancer cell lines HCT-116 (human colorectal adenocarcinoma), MCF-7 (breast cancer), and PC3 (prostate cancer) by the MTS assay. The compound with the highest activity, even higher than cisplatin, was the silver NHC **I 19**, with IC_{50} values of $0.3 \pm 0.1 \mu\text{M}$ (PC3), $1.38 \pm 0.36 \mu\text{M}$ (HCT-116), and $2.0 \pm 0.2 \mu\text{M}$ (MCF-7). The gold complex, **I 20**, had values between 6-7 μM for all cell lines tested. The ruthenium complex was the least active (HCT-116: $40 \pm 1 \mu\text{M}$ and PC3: $25 \pm 2 \mu\text{M}$), despite having a relatively high activity against the MCF-7 cell line ($11.6 \pm 0.5 \mu\text{M}$). The authors note that introduction of the triazole substituent actually increases the activity of gold and ruthenium complexes whereas it hinders the activity of silver complexes, as compared to previous reports.

Chart I-3. Structures of Triazole Functionalized Carbene Complexes



1.3.2. Gold Mono-Nuclear Imidazole NHC Complexes

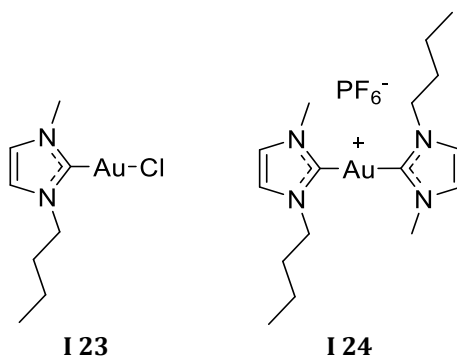
Gabbiani and coworkers reported the synthesis of strictly gold(I) NHC complexes for the application of anti-cancer materials (Chart I-4).⁵³ These NHC complexes were synthesized via metalation of 1-butyl-3-methylimidazole with silver(I) oxide. After the silver NHC complex formed, chloro(dimethylsulfide) gold(I) was added to yield the gold chloride complex (**I 23**). When the anion was exchanged with PF₆⁻, the resulting complex was the bis-carbene (**I 24**). Uniquely, the imidazolium salt was finely tuned as the authors state that lipophilicity can increase selectivity for malignant tissue.

Cell lines used to study compounds **I 23** and **I 24** were A2780/S and A2780/R ovarian cancer cell lines, which are sensitive and resistant to cisplatin, respectively. Both compounds displayed IC₅₀ values in the low micromolar range for both cell lines tested. They also were both found to be more efficacious against the resistant cell line than cisplatin (IC₅₀ = 0.68 ± 0.07 μM for **I 23**; 0.75 ± 0.05 μM for **I 24**; 23.24 ± 0.75 μM for cisplatin). These results were for treatment at 72 hours. However, treatment for only 24 hours showed a remarkable increase in IC₅₀ values, for the gold complexes and cisplatin, establishing that these gold carbene compounds require longer treatment times for full efficacy. This data also suggests that these complexes can kill cancer cells through a different mechanism than cisplatin.

In order to study how these compounds react with proteins, ESI-MS was used in conjunction with UV-Vis spectrophotometry. Results suggest that cytochrome c and HEWL do not form adducts with the gold complexes. However, Atox-1, a copper

chaperone protein containing the CXXC motif, does form adducts. This indicates that certain proteins have a much higher affinity for gold.

Chart I-4. Structures of Gold(I) Carbene Complexes **I 23** and **I 24**



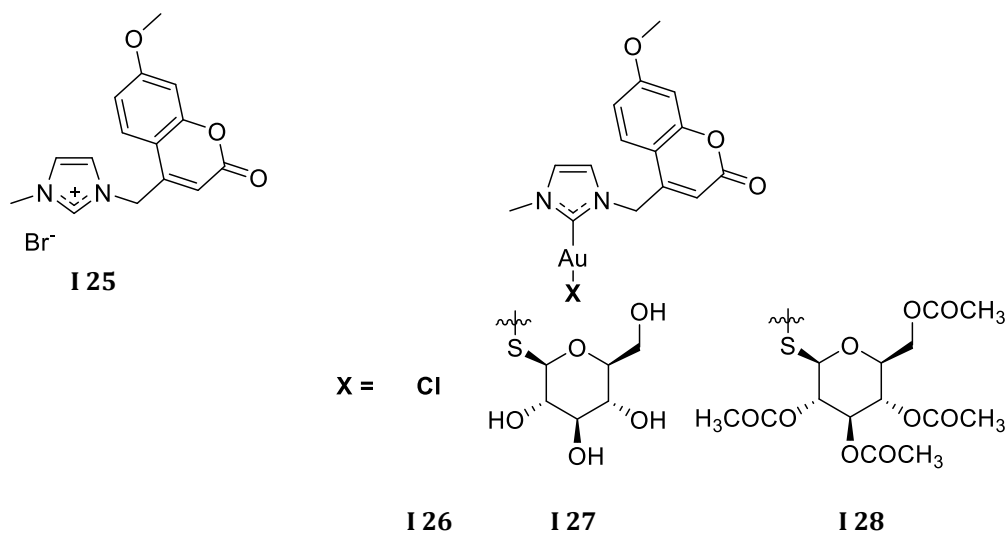
In 2014, the Bertrand group reported novel gold(I) NHC complexes synthesized via metalation of 1-methyl-3-((2-oxochromen-4-yl)methyl)imidazolium bromide (Chart I-5).⁵⁴ This imidazolium salt precursor (**I 25**) was synthesized via standard alkylation procedures. The imidazolium salt was first metalated by silver(I) oxide to form the silver NHC complex. This silver complex was transmetalated to the gold(I)chloride NHC (**I 26**) by the reaction with chloro(tetrahydrothiophene)gold(I). Additionally, the chloro ligands were exchanged with 1-thio- β -d-glucopyranosido (**I 27**) and the tetra-O-acetyl-1-thio- β -d-glucopyranosido (**I 28**) substituted gold NHC complexes. These glucopyranoside ligands are believed to increase cytotoxicity as well as increase cellular uptake.

An MTT assay was used to evaluate efficacy of compounds **I 25- I 28** on ovarian cancer A2780, breast cancer MCF-7, human lung cancer A549, and normal human embryonic kidney HEK-293T cell lines. All compounds were less effective than cisplatin ($1.9 \pm 0.6 \mu\text{M}$ for A2780, $8.0 \pm 0.5 \mu\text{M}$ for A549, $20.0 \pm 3.1 \mu\text{M}$ for MCF-

7, and $11.0 \pm 2.9 \mu\text{M}$ for HEK-293T) with the exception of **I 28** on the MCF-7 cell line, which was found to have an IC_{50} value of $11.6 \pm 0.8 \mu\text{M}$. Since TrxR is a known target for gold containing compounds *in vitro*, TrxR studies were completed against rat TrxR. None of the gold complexes were as efficient as auranofin; however, they did inhibit both TrxR1 and TrxR2 to an extent.

Bertrand et al. also studied if the inhibition of TrxR was the cause of the observed anti-proliferative activity. To do this, A2780 cells were treated with $10 \mu\text{M}$ of **I 28** and enzyme activity was evaluated after 48 hours. TrxR activity was inhibited by approximately 30% and glutathione reductase was activated, which the authors explain is a normal stress response for cells when TrxR is inhibited. In addition, fluorescence microscopy was used to evaluate the uptake of **I 28** in A2780 cells. Co-localization with propidium iodide indicated that **I 28** was targeted to the nucleus.

Chart I-5. Structures of 1-Thio- β -d-glucopyranosido (**I 27**) and Tetra-O-acetyl-1-thio- β -d-glucopyranosido (**I 28**) Functionalized Gold(I) Carbene Complexes and the Corresponding Imidazolium Salt (**I 25**) and Gold(I) Chloride (**I 26**) Precursors



The work reported by Contel and coworkers in 2016 also discusses the formation of gold(I) NHC complexes, but instead bound to titanocenes via a 4-mercaptobenzoic acid (Hmba) linker (Chart I-6).⁵⁵ The gold(I) chloride NHC precursors were synthesized via previously discussed procedures. To produce the Hmba linker off of the metal center (**I 29- I 32**), the gold NHC complexes were reacted with H₂mha under basic conditions. Once the Hmba ligand complexes were synthesized, addition of [(η⁵-C₅H₅)₂TiMe₂] resulted in the bimetallic titanocene-gold complexes (**I 33- I 36**) via coordination of the acetate to the titanium metal center.

Compound activity was determined using the PrestoBlue Cell Viability assay. Cell lines that were used include prostate cancer cells PC3 and DU-145, renal cancer Caki-1, colon cancer DLD1, breast cancer MDA-MB-231 and human embryonic kidney HEK-293T cell lines. Compounds that are considered to be heterometallic (i.e. they have both gold and titanium; **I 33- I 36**) were more toxic than the monometallic gold compounds (**I 29- I 32**) in all of the cell lines tested, with the exception of MDA-MB-231 in which only the control, titanocene Y, exhibited cytotoxic activity. Consistently, compound **I 33** had the lowest IC₅₀ values, making it the most active of the heterometallic complexes (9.8 ± 2.2 μM for PC3, 11.8 ± 3.0 μM for DU-145, 21.0 ± 1.9 μM for Caki-1, and 13.9 ± 1.7 μM for DLD1). The heterometallic complexes also exhibited selectivity for cancer cells versus the non-cancerous cell line HEK-293T with all IC₅₀ values being 58.8 ± 6.7 μM or higher.

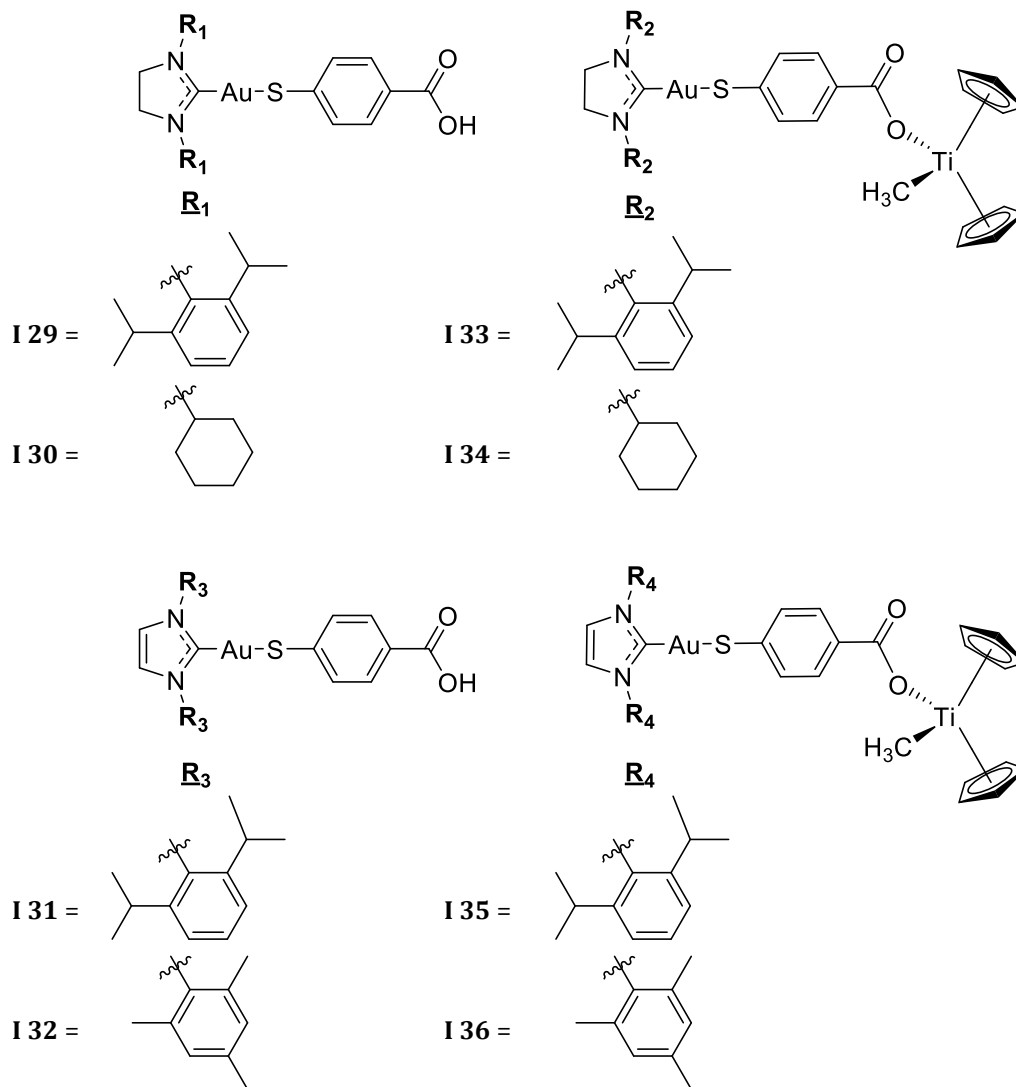
ICP-MS was employed to determine intracellular amounts of gold and titanium after treatment with **I 33**. Research showed that the ratio of titanium to gold was very close, indicating that either the complex is stable in cells or uptake of

both metals occurs in a close ratio. Tests also showed that complexes **I 29**, **I 31**, **I 33**, and **I 35** induced apoptosis in renal and prostate cancer cell lines; however, the IC₅₀ value for **I 29** and **I 31**, as discussed above, were higher.

A scratch assay was used with PC3 cells to determine if the heterometallic complexes could inhibit cell migration. Complexes **I 33** and **I 35** showed the lowest percentage of invasion as compared to controls and the gold complexes with 42% and 33%, respectively. The 0.1% DMSO control treated cells invaded 88% of the scratched area after treatment. These results indicate that **I 33** and **I 35** have the ability to exert antimigratory effects on PC3 cells.

Gel electrophoresis studies on plasmid pBR322 DNA were used to evaluate the interaction of the complexes with DNA where a decrease in mobility of the plasmid indicates binding of the metals/drug to DNA. Complexes **I 33** and **I 35** did not show significant interaction with the plasmid DNA. Inhibition of TrxR was also studied in PC3 cells. After 24 hours at a concentration of 5 μ M, **I 33** and **I 35** were found to have inhibition percentages of 61% and 76%, respectively, while **I 29** and **I 31** had inhibitions of only 30% and 36%, respectively, at a concentration of 30 μ M. Overall, all of these studies indicate that the inclusion of the titanium portion of the molecule increases anti-cancer activity. However, no SAR was determined in regards to the NHC complexes.

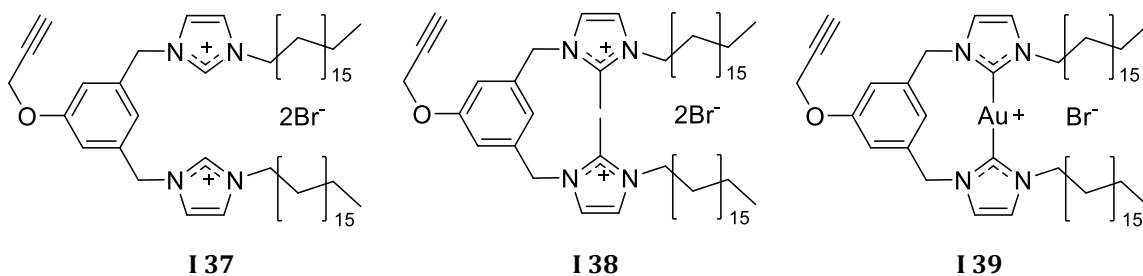
Chart I-6. Structures of Titanocene Functionalized Gold(I) Carbene Complexes **I 33- I 36** and the Corresponding Hmba Precursors **I 29- I 32**



The synthesis of a highly lipophilic gold(I) NHC was reported by Rodrigues et al. (Chart I-7).⁵⁶ The imidazolium salt precursor (**I 37**) was produced via the reaction of two equivalents of 1-octadecylimidazole with 1,3-bis(bromomethyl)-5-propargyloxybenzene (DBMPB). This substituent promoted the formation of the bisimidazolium salt, which once metalated with chloro(dimethylsulfide) gold(I) under basic conditions formed the bis-carbene (**I 39**).

HT-29 colon adenocarcinoma and MDA-MB-231 breast adenocarcinoma cell lines were used to determine the cytotoxicity of the tested compounds. The ligand precursors alone exhibited moderate IC_{50} values (**I 37**: $7.4 \pm 0.6 \mu\text{M}$ HT-29 and $12.1 \pm 2.4 \mu\text{M}$ MDA-MB-231; **I 38**: $6.3 \pm 1.5 \mu\text{M}$ HT-29 and $9.4 \pm 1.0 \mu\text{M}$ MDA-MB-231). Due to the limited solubility of **I 39**, it could only be tested at concentrations equal to or below $10 \mu\text{M}$. Its IC_{50} value against HT-29 was found to be $>10 \mu\text{M}$ and $7.3 \pm 0.9 \mu\text{M}$ for MDA-MB-231. The nanoparticles made from the imidazolium salts **I 37** and **I 38**, known as **I 37-AuNP** and **I 38-AuNP**, were also tested at a concentration of $0.0044 \mu\text{M}$, which corresponds to a $16 \mu\text{M}$ concentration of the imidazolium salt. However, no activity was detected at this concentration. This shows that the free imidazolium salt versus those in the nanoparticles have different activities. The authors suggest that the imidazolium salts alone have higher toxicity because they can better interact with cells.

Chart I-7. Structures of Propargyloxybenzene Linked Imidazolium Salts **I 37**- **I 38** and Consequent Gold(I) Carbene Complex **I 39**



Ott and co-workers have also reported the synthesis of novel gold(I) NHC complexes and their biological activity (Chart I-8).⁵⁷ These complexes were synthesized by metalation of the precursor benzimidazolium (**I 40** and **I 41**),

imidazolium (**I 42** and **I 43**), and phenylimidazolium (**I 44- I 46**) salts. The metalation was performed following standard procedures by reacting the imidazolium salts with silver(I) oxide and then transmetalation to Au(I) complexes (**I 47- I 54**) with chlorodimethylsulfide gold(I).

Crystal violet staining was used to determine each compounds IC₅₀ value against cancer cell lines such as HT-29, MCF-7, MDA-MB-231 and the normal cell line RC-124 (human kidney cells). Compounds **I 47- I 54** had moderate IC₅₀ values ranging from 4-17 μM. There was no selectivity observed for cancer cells versus normal cells for any of the compounds tested and auranofin had higher activities than all compounds tested. The imidazolium salts, **I 40- I 46**, showed no cytotoxic activity (IC₅₀ >100 μM) for all cell lines. Compounds **I 52- I 54** were found to have the highest activity against all of the cell lines tested, with IC₅₀ values ranging from 4.46 ± 0.04 μM to 8.13 ± 0.60 μM.

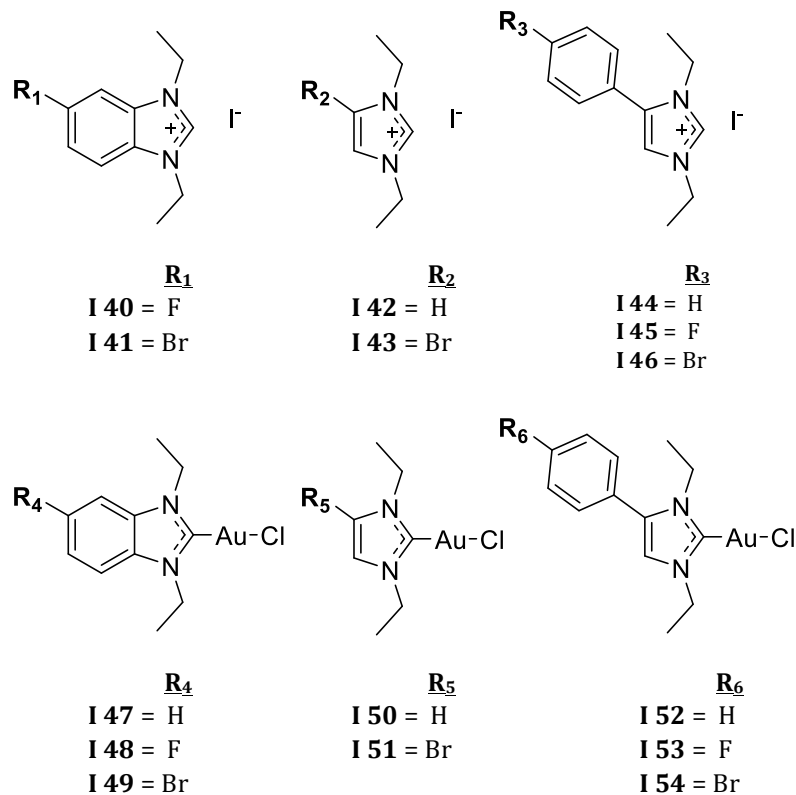
Protein binding and cellular accumulation was studied for **I 52- I 54**. Fetal calf serum gave protein binding values of >80% and albumin gave values of 100% for the compounds tested. HR-CS AAS was used to determine the amount of gold taken up by MCF-7 cells after treatment with 12.0 μM of **I 52- I 54**. In serum-containing medium, **I 52** was shown to have a higher uptake than **I 53** and **I 54**, leading the authors to believe that the halides of **I 53** and **I 54** promote protein binding while **I 52** is more directed towards cellular uptake. The same trend was seen when testing **I 50** and **I 51** where the bromine-containing compound **I 51** had less accumulation. When using serum-free medium the cellular uptake of **I 53** and **I 54** was significantly increased, but still below that of **I 52**.

Compound **I 51** was further studied for its effect on leukemia cells that are drug-resistant, specifically daunorubicin-resistant Nalm-6 (Nalm-6 DNR) and vincristine-resistant Nalm-6 (Nalm-6 VCR). These resistant cell lines overexpress P-glycoprotein, a known drug efflux pump. Compound **I 51** killed cells through an apoptotic mode of cell death. When evaluated for intracellular gold content after treatment with **I 51**, all cell lines (the two resistant and normal wild type Nalm-6) had comparable gold levels and higher concentrations of intracellular gold corresponding with an induction of apoptosis. This indicates that P-glycoprotein or another efflux transporter does not efflux **I 51** out of the cell.

Antibacterial efficacy of **I 47- I 54** were tested against the ESKAPE panel, a collection of pathogens that continue growing to be resistant to traditional antibiotics. This panel includes Gram-negative strains (*A. baumannii*, *E. cloacae*, *E. coli*, *K. pneumoniae*, *P. aeruginosa*) and Gram-positive strains (*E. faecium* and *S. aureus*). Gram-negative strains were less affected by the compounds than the Gram-positive strains. Specifically *E. faecium* and the *S. aureus* strains had MIC values in the low micromolar range for all compounds tested. Compound **I 51** was found to have the highest toxicity with MIC values of 3.12 μM for *E. faecium* and 0.64 μM for both *S. aureus* strains, activities higher than those of auranofin.

Mamalian and bacterial TrxR were used to evaluate whether compounds **I 47- I 54** were effective in inhibiting TrxR function. The compounds were better at inhibiting the mammalian form and **I 48**, **I 49**, and **I 51** were the most pronounced in this preference. The authors suggest that halogens present in the NHC scaffold increase inhibition of mammalian TrxR, but not bacterial TrxR.

Chart I-8. Structures of Imidazolium Salts **I 40- I 46** and Consequent Gold(I) Carbene Complexes **I 47- I 54**

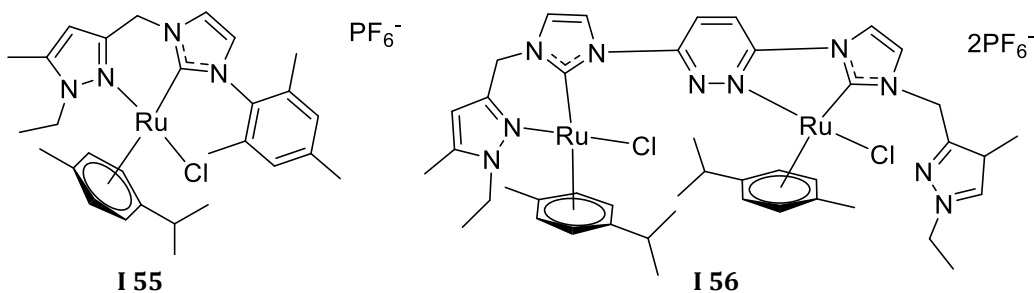


1.3.3. Ruthenium Mono-Nuclear Imidazole NHC Complexes

Chen et al. have developed a novel set of ruthenium(II) NHC complexes via metalation of pyrazole substituted imidazolium salt precursors (Chart I-9).⁵⁸ These precursors are synthesized by multi-step reactions, first of which is the alkylation of 5-methylpyrazole-3-carboxylate. The pyrazole carboxylate group is reduced with LiAlH_4 and the resulting alcohol is chlorinated via SOCl_2 addition. This starting material is used to alkylate 1-mesitylimidazole and pyridazine linked bis-imidazoles. The resulting imidazolium salts are metalated to silver NHC complexes and transmetalated to the ruthenium(II) complexes (**I 55, I 56**).

An MTT assay was used to evaluate these compounds against cancer cell lines including Bcap-37 (breast cancer), LoVo (colon cancer), SCG7901 (gastric cancer), and SCG7901-R (cisplatin-resistant gastric cancer). From the assay it was determined that **I 55** had comparable or higher activity than cisplatin with IC_{50} values of $11.2 \pm 0.8 \mu\text{M}$ (Bcap-37), $9.2 \pm 0.5 \mu\text{M}$ (LoVo), and $2.9 \pm 0.5 \mu\text{M}$ (SCG7901) for **I 55** and IC_{50} values of $8.5 \pm 0.9 \mu\text{M}$ (Bcap-37), $4.1 \pm 0.2 \mu\text{M}$ (LoVo), and $10.5 \pm 0.6 \mu\text{M}$ (SCG7901) for cisplatin. The authors attribute the increase of activity for **I 55** versus **I 56** to increased lipophilicity of substituents. Against the cisplatin resistant gastric cancer cell line, SCG7901-R, **I 55** displayed much higher activity than cisplatin ($5.8 \pm 0.4 \mu\text{M}$ and $83.1 \pm 0.4 \mu\text{M}$, respectively) indicating that ruthenium can combat the typical resistant mechanisms of this cell type. Cellular morphology of LoVo cells was observed after treatment with **I 55**. Cell shrinkage, rounding, and clearance were all apparent, indicating the process of apoptosis. A migration assay was also completed and it was determined that **I 55** decreased the migration percentage relative to control cells from 36% to 8.5%.

Chart I-9. Structures of Bidentate Ru(II) Carbene Complexes **I 55** and **I 56**



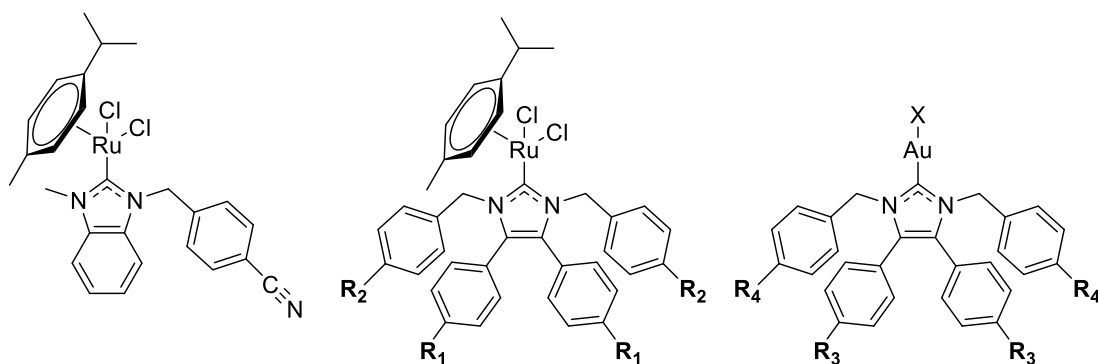
1.3.4. Biologically Active 4,5-Diphenyl Imidazolylidene NHC Complexes

In 2013, Tacke and coworkers reported that benzimidazol-2-ylidene and 4,5-diphenyl imidazol-2-ylidene NHC complexes utilizing ruthenium(II) or gold(I) can be synthesized (Chart I-10).⁵⁹ To form the imidazolium salt precursor, imidazoles were alkylated with various benzyl substituents. Once the precursors were achieved, metalation occurred via the silver base, silver(I) oxide. These reactions yielded silver halide mono-carbene complexes. The silver carbenes were then utilized as transmetalation reagents and were reacted with dichloro-(p-cymene) ruthenium(II) dimer and chloro(dimethylsulfide) gold(I) to form the ruthenium(II) complexes (**I 57- I 62**) and gold(I) complexes (**I 63- I 65**), respectively. The further functionalization of the gold NHC complex was achieved via ligand exchange with silver(I) acetate to form the gold acetate NHC complexes (**I 66- I 68**) or reaction with (2',3',4',6'- tetra-O-acetyl- β -D-glucopyranosyl-1-thiolate) to form the gold thiolate complexes (**I 69- I 71**).

MTT assay values against the Caki-1 cell line showed that the ruthenium complexes did not exhibit higher activity than cisplatin (3.3 μ M). However, in testing against the MCF-7 cell line much higher activity was observed. Compounds **I 60- I 62** even exhibited higher activity than cisplatin. Compound **I 60** had a marked increase in IC₅₀ value for Caki-1 cells (170 \pm 20 μ M) versus MCF-7 cells (7.1 \pm 1.2 μ M). Varying groups on the substituents, such as replacing the isopropyl group of **I 60** with the methoxy groups in **I 61** in the para position of the phenyl ring, showed a 3-fold increase when tested on the MCF-7 cell line.

The authors note several conclusions from this data. First is that the substituents on the imidazole of the NHC can have a major influence on the activity of the complex. Second is that there must be two different mechanisms of cell death for the two different cell lines that gives rise to the variable IC₅₀ values. With the exception of complexes **I 64** and **I 68**, the gold compounds showed higher activity against MCF-7 than Caki-1. Overall, complexes **I 69- I 71** had greater than or equal activity compared to the corresponding NHC-Au(I)Cl complex (**I 63- I 65**) and increased activity than the corresponding NHC-Au(I)OAc compounds (**I 66- I 68**) against both cell lines, with a few exceptions. The authors note that the lower IC₅₀ values for **I 69- I 71** is most likely due to enhanced solubility and cellular uptake of this series.

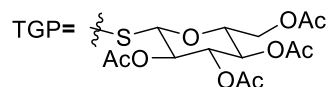
Chart I-10. Structures of 4,5-Diphenyl Substituted Imidazolylidene Ruthenium (II) and Gold(I) Carbene Complexes



I 57

	<u>R₁</u>	<u>R₂</u>
I 58 =	H	H
I 59 =	CH ₃	CH ₃
I 60 =	CH(CH ₃) ₂	CH ₃
I 61 =	OCH ₃	CH ₃
I 62 =	CH(CH ₃) ₂	OCH ₃

	<u>R₁</u>	<u>R₂</u>	<u>X</u>
I 63 =	H	H	Cl
I 64 =	CH ₃	CH ₃	Cl
I 65 =	CH(CH ₃) ₂	CH ₃	Cl
I 66 =	OCH ₃	CH ₃	COOCH ₃
I 67 =	CH(CH ₃) ₂	OCH ₃	COOCH ₃
I 68 =	CH(CH ₃) ₂	OCH ₃	COOCH ₃
I 69 =	H	H	TGP
I 70 =	CH ₃	CH ₃	TGP
I 71 =	CH(CH ₃) ₂	OCH ₃	TGP



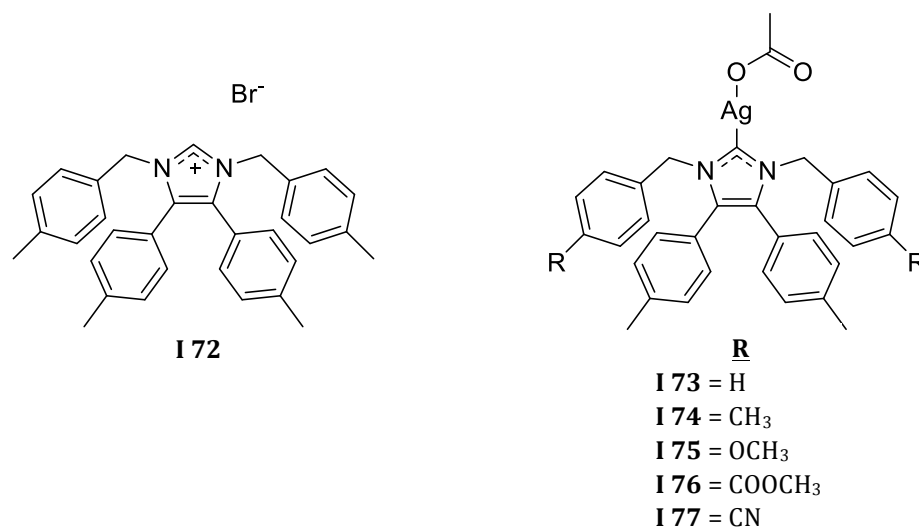
Also in 2013, Tacke and coworkers reported that 4,5-bis-(4-methylphenyl) substituted imidazol-2-ylidene NHC complexes can have biological activity (Chart I-11).⁶⁰ The imidazolium salt precursors were synthesized by previously described techniques.⁵⁹ Once the precursors were synthesized, researchers proceeded with metalation via silver(I) acetate. These reactions yielded silver acetate mono-carbene complexes (**I 73- I 77**).

The synthesized compounds were tested for both anti-cancer and antibacterial activity. Using the MTT assay on Caki-1 renal cancer cells line and MCF-7 breast cancer cells, the anti-cancer activity for synthesized compounds was evaluated. The compounds displayed variable IC_{50} values, showing that the substituents on the benzyl ring have different effects on the cytotoxic activity. The most effective compound was found to be **I 74**, with an IC_{50} values of $0.51 \pm 0.07 \mu\text{M}$ and $1.4 \pm 0.1 \mu\text{M}$ against Caki-1 and MCF-7, respectively. The replacement of the methyl groups at the para position of the benzyl ring in **I 74** with hydrogens, as in **I 73**, provided a marked change in activity, with **I 73** having activities of $3.6 \pm 1.0 \mu\text{M}$ and $2.3 \pm 0.4 \mu\text{M}$ in Caki-1 and MCF-7 respectively. The precursor **I 72** was also tested to determine its activity. With an IC_{50} value of $4.8 \pm 0.3 \mu\text{M}$ against Caki-1, the precursor shows cytotoxicity but is much more effective when combined with the effects of silver acetate, as in **I 74**.

Antibacterial activity was also assessed using the Kirby-Bauer disc diffusion method. An area of clearance of 0 mm was considered no activity while 1-3 mm was low, 4-7 mm was medium and greater than or equal to 8 mm was considered high activity. No activity was observed for **I 74**, **I 76** or **I 77** while medium activity was

observed from **I 75** against *S. aureus*. The highest activity was found for compound **I 73**, which had 7 mm of clearance for both *E. coli* and *S. aureus*. However, the authors note that there was no improvement in antibacterial activity when comparing to the other lead compounds previously synthesized.

Chart I-11. Structures of 4,5-Diphenyl Substituted Imidazolydene Silver(I) Carbene Complexes **I 73- I 77** and an Imidazolium Salt Precursor **I 72**



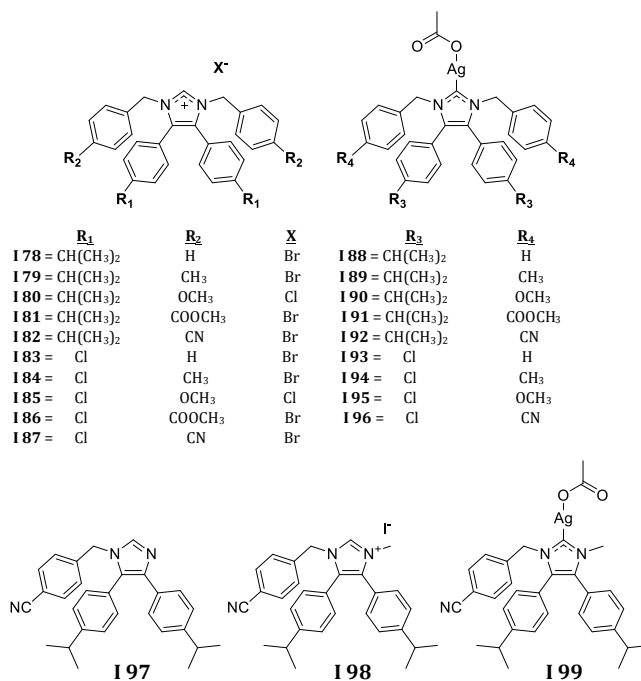
Continuing in 2014, Tacke and coworkers report the synthesis of 4,5-diphenylimidazoles with isopropyl and chloro substituents at the para position of the diphenylimidazole moieties (Chart I-12).⁶¹ Synthesis of these imidazolium salts (**I 78- I 87**, **I 97** and **I 98**) and NHC complexes (**I 88- I 96** and **I 99**) was adapted from the previously described work.⁵⁹

The Kirby-Bauer disc diffusion method was used to evaluate the antibacterial efficacy of the imidazolium salts (**I 78- I 87**, **I 97** and **I 98**) and their NHC complexes (**I 88- I 96** and **I 99**). The two strains tested were Gram-positive *S. aureus* and Gram-negative *E. coli*. Almost no antibacterial activity could be detected for **I 79- I 82** or **I 89- I 92**. Imidazolium salts **I 78**, **I 83- I 87**, and **I 98** had low to medium activity

(clearance area of 4-5 mm) against *S. aureus* but more variable activity (clearance area of 1-5 mm) against *E. coli*. Precursor compounds **I 83- I 87**, and NHC complexes **I 88** and **I 99** were found to have the highest activity against *S. aureus* (4-7 mm). The authors note that none of the synthesized compounds have an increase in activity compared to the group's previous lead compound, indicating that the modifications made do not significantly increase antibacterial activity.

An MTT assay was utilized to determine if these compounds had any anti-cancer activity against MCF-7 and Caki-1 cell lines. Compound **I 89**, which was found to have no antibacterial activity, was found to have the best anti-cancer activity with IC₅₀ values of 2.1 ± 0.8 μM and 4.6 ± 0.1 μM against MCF-7 and Caki-1, respectively. However, **I 89** had lower activity than cisplatin (3.3 μM) against the Caki-1 cell line.

Chart I-12. Structures of 4,5-Diphenyl Substituted Imidazolydene Silver(I) Carbene Complexes and the Corresponding Imidazolium Salt Precursors

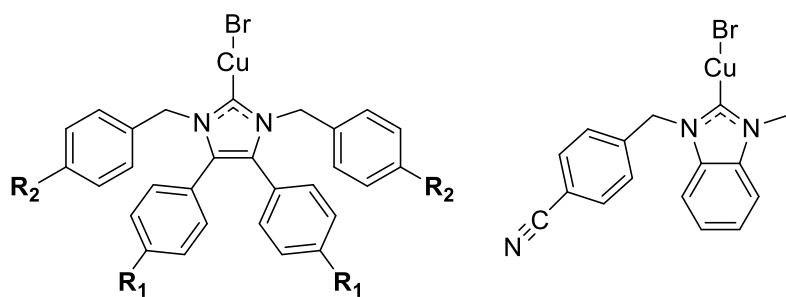


Tacke and coworkers have also reported the synthesis of copper(I) NHC complexes for anti-cancer applications (Chart I-13).⁶² The para substituted bis(benzyl)-4,5-diphenylimidazolium salts were metalated to the silver bromide NHC complex. From this, 1.1 equivalents of bromo(dimethylsulfide) copper(I) were reacted with the silver NHC complex to form the transmetalated copper(I) complexes (**I 100-108**). In addition, the asymmetric NHC complex (**I 109**) was synthesized via the use of 1-(4-cyanobenzyl)-3-methyl-benzimidazolium salt under the same reaction conditions as the 4,5-diphenylimidazolylidene NHC complexes mentioned previously.⁵⁹

The synthesized compounds were tested against the renal cancer cell line Caki-1 and breast cancer cell line MCF-7. The IC₅₀ values were highly variable for both families of compounds, indicating that the substituents in the para position of the benzyl ring have a significant effect on activity. While both families of compounds displayed activity (**I 100- I 104** for MCF-7 = 3.8 ± 0.9, 7.4 ± 2.4, 0.60 ± 0.09, 13 ± 4 and 42 ± 7 μM, Caki-1 = 5.6 ± 0.9, 3.3 ± 0.6, 0.65 ± 0.08, 18 ± 3 and 126 ± 10 μM; **I 105- I 109** for MCF-7 = 17 ± 2, 21 ± 3, 26 ± 5, 68 ± 7 and 61 ± 10 μM, Caki-1 = 17 ± 2, 19 ± 1, 18 ± 1, 47 ± 3 and 134 ± 16 μM), **I 102** was identified as the copper complex with the highest anti-cancer activity against both cell lines (Caki-1 = 0.65 ± 0.08 μM; MCF-7 = 0.60 ± 0.09 μM). The previously made silver derivative of this complex (**I 90**) can be directly compared to the copper analogue **I 102**. The copper complex had a significant increase in activity over the silver complex (Caki-1 = 5.5 ± 0.6 μM; MCF-7 = 3.4 ± 0.6 μM). The copper complex also had higher activity than cisplatin, which displayed values of 3.3 ± 0.2 μM and 10.4 ± 0.2 μM against Caki-1

and MCF-7, respectively. The authors suggest that the metal and the substituents all play an important role in the biological activity of these NHC complexes, as witnessed by the data in this study. Also, the combination of metal and ligand precursor cannot be used to predict the activity of the same ligand precursor with a different metal counterpart. Overall, compound **I 102** proved to be the lead compound in this series.

Chart I-13. Structures of 4,5-Diphenyl Substituted Imidazolydene Copper(I) Carbene Complexes **I 100- I 108** and the Benzimidazolydene NHC, **I 109**



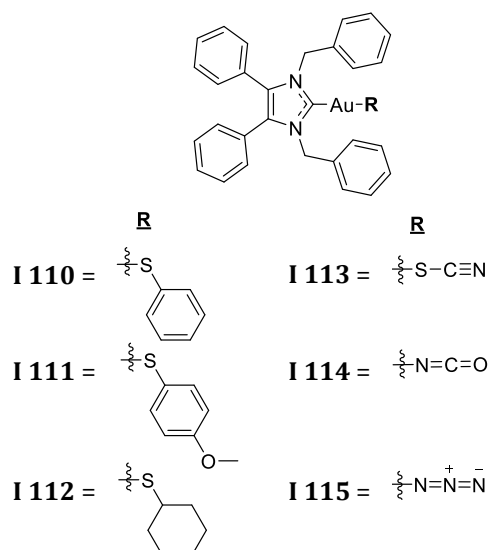
	R₁	R₂
I 100	= CH(CH ₃) ₂	H
I 101	= CH(CH ₃) ₂	CH ₃
I 102	= CH(CH ₃) ₂	OCH ₃
I 103	= CH(CH ₃) ₂	COOCH ₃
I 104	= CH(CH ₃) ₂	CN
I 105	= H	H
I 106	= CH ₃	CH ₃
I 107	= OCH ₃	CH ₃
I 108	= Cl	OCH ₃

Recently in 2017, Tacke and coworkers have also published the synthesis of six novel gold(I) NHC complexes with varying ligands substituted at the metal center (Chart I-14).⁶³ The standard gold halide NHC complexes were synthesized via previously discussed methods. To functionalize the gold centers, the authors utilized techniques to exchange halide ligands with thiolates (**I 110- I 112**) and pseudo halide ligands such as isocyanate (**I 114**). To prepare the thiolate

complexes, the precursor NHC complex was reacted with a thiol in the presence of base. The formed thiolate can then exchange with the halide. In addition to thiolates, Tacke and coworkers use the term pseudo halides as representation of thiocyanate (**I 113**), isocyanate (**I 114**), and azide (**I 115**) ligands. These complexes are formed via the reaction of the gold chloride NHC complex with the potassium or sodium salt of the ligand. These syntheses resulted in the formation of six novel gold(I) NHC complexes.

The pseudohalides and thiolates were tested on the NCI 60-cell line test with a concentration of 10 μM for **I 110**- **I 115**. Compounds **I 112**, **I 113**, and **I 115** showed the highest activity with 99%, 94% and 93% average growth inhibitions, respectively. These three compounds were then used in the five-dose experiment. Compound **I 113** was found to have an average GI_{50} value of 0.47 μM , which was more active than **I 112** and **I 115** by a factor of four, making **I 113** the most active compound of the series.

Chart I-14. Structures of 4,5-Diphenyl Substituted Imidazolylidene Gold(I) Carbene Complexes with Thiolates and Pseudo Halide Ligands



1.3.5. Platinum Mono-Nuclear Imidazole NHC Complexes

Novel platinum(II) bis-NHC complexes (**I 116- I 124**) were synthesized by Chi-Ming Che and coworkers by reacting 2-phenylpyridine, benzoquinoline, and 2-(thiophen-2-yl)pyridine platinum salts with three bis-imidazolium salt precursors, synthesized via standard procedures, under basic conditions (Chart I-15).⁶⁴ This technique utilizes the formation of the free carbene first followed by coordination of the platinum metal.

The conjugated ligands coordinated to the platinum metal promotes luminescent properties. It was reported the metal to ligand charge transfer bands in these systems have emissions ranging from 486-517 nm for the 2-phenylpyridine (**I 116- I 118**) complexes, 476-517 nm for the benzoquinoline complexes (**I 119- I 121**), and 562-605 nm for tge 2-(thiophen-2-yl)pyridine complexes (**I 122- I 124**) in degassed CH₂Cl₂.

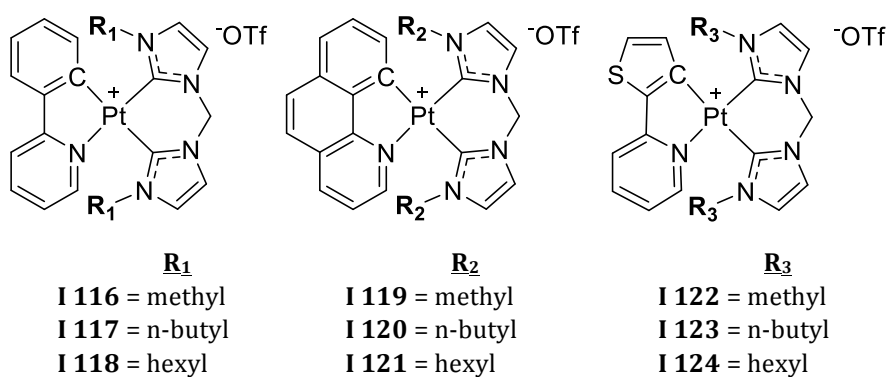
Compound **I 118** was tested for its affinity to DNA along with BSA and it was determined that the platinum(II) complex had a higher affinity for BSA, going against the normal DNA target that is often seen with the platinum NHC complexes. Fluorescence microscopy was utilized to determine the cellular location of **I 118** after treatment of HeLa cells. Green emission was seen in the cytoplasm after 10 minutes of 5 μ M concentration treatment. Co-localization studies were also done with **I 118** on HeLa cells, which showed that the only specific cellular location where **I 118** could be found was the endoplasmic reticulum.

The MTT assay was then used to determine if the Pt(II) complexes displayed any cytotoxic activity. Cell lines tested include HeLa (cervical cancer), HONE1 and

SUNE1 (nasopharyngeal carcinoma), MCF-7 (breast cancer), HepG2 (hepatocellular carcinoma), HCC827 and H1975 (lung carcinoma) and MIHA (non-tumorigenic liver cell line). Compound **I 118** had the highest activity with a range of IC₅₀ values from 0.45-1.59 μM. Some of the complexes even exhibited selectivity for cancer cells versus the non-cancerous cell line. HeLa cells were also tested for ER stress markers and treatment with **I 118** up-regulated PERK, eIF2α, and CHOP. Apoptosis was determined to be the mode of cell death after it was observed that caspase-3, -7, -9 and PARP were cleaved. Disruption of mitochondria was observed via the JC-1 assay with mitochondrial swelling also being apparent.

Compounds **I 122- I 124** were tested for their photo-toxicity in cancer cells which showed that there was a significant decrease of 5.6-33.1 fold for cells treated under light versus in the dark while also exhibiting a moderate selectivity for cancer cells (1.63-9.82 μM for cancer cell lines and 31.3 μM for the MIHA cell line).

Chart I-15. Structures of Bidentate Imidazolylidene Platinum(II) Carbene Complexes **I 116- I 124**



In 2015, Chi-Ming Che and co-workers synthesized new NHC complexes by reacting 6-phenyl-2,2'-bipyridine, 2,2':6',2''-terpyridine, 1,3-di(pyridin-2-

yl)benzene, or 3,3'-(pyridine-2,6-diylbis(1H-benzo[d]imidazole-2,1-diyl))bis(propene-1-sulfonate) ligated platinum salts with various imidazolium salts under basic conditions (Chart I-16).⁶⁵ The synthesis of these NHC complexes (**I 125- I 137**) used a modification of a procedure by Che and co-workers.⁶⁴

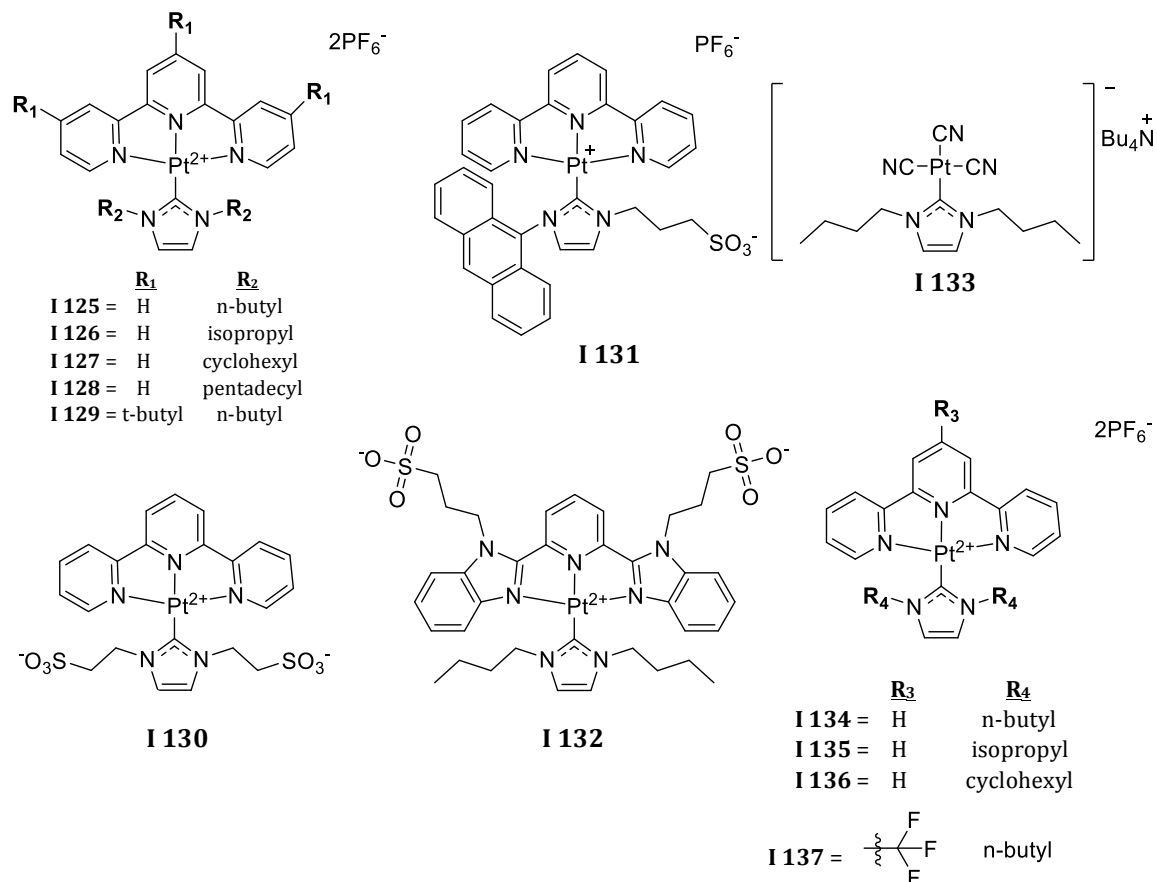
Luminescent properties of the conjugated ligands are enhanced by coordination to the platinum metal. It was reported the metal to ligand charge transfer bands in these systems have emissions ranging from 460-577 nm depending on the ligands attached to the platinum metal. Additionally, the terpyridal complex **I 125**, as well as the di(pyridin-2-yl)benzene complex **I 134**, can be reacted with cyanide anions to displace any pyridine coordination, which quenches emission. These complexes can then be used to determine cellular localization or cyanide detection based on emission quenching.

The MTT assay was used to evaluate the Pt(II) complexes against HeLa cells. Complexes **I 134- I 137** were tested and compared to cisplatin, which revealed that **I 136** had the highest activity ($IC_{50} = 0.46 \mu\text{M}$) followed by **I 137** ($IC_{50} = 1.70 \mu\text{M}$), **I 134** ($IC_{50} = 2.45 \mu\text{M}$), and **I 135** ($IC_{50} = 3.00 \mu\text{M}$). Authors attribute an increase in activity to an increase in lipophilicity of the alkyl groups substituted on the imidazolium salt. Complexes **I 125- I 128** and **I 130- I 132** had significantly decreased activity with IC_{50} values $>50 \mu\text{M}$ with the exception of **I 128**, that had an IC_{50} value of $16.4 \mu\text{M}$.

The fluorescence emission of these compounds affords the ability to visualize cellular localization via fluorescence microscopy. HeLa cells treated with **I 136** had accumulation in the mitochondria. This was also observed for cells treated with **I**

134. Co-localization studies with **I 134** or **I 136** and MitoTracker revealed a disruption of mitochondria rather than accumulation. Thus mitochondrial membrane potential was tested via the JC-1 assay, which based on the fluorescent emission can give insight into mitochondrial dysfunction. Control HeLa cells exhibited the usual orange fluorescence of mitochondria while treatment with **I 136** at 2 μM for 1 hour caused depolarization of the mitochondrial membrane potential and thus only green fluorescence was observed. The conclusion based on these observations was that **I 136** could disrupt mitochondria and lead to cell death.

Chart I-16. Structures of Imidazolylidene Platinum(II) Carbene Complexes **I 125- I 137**



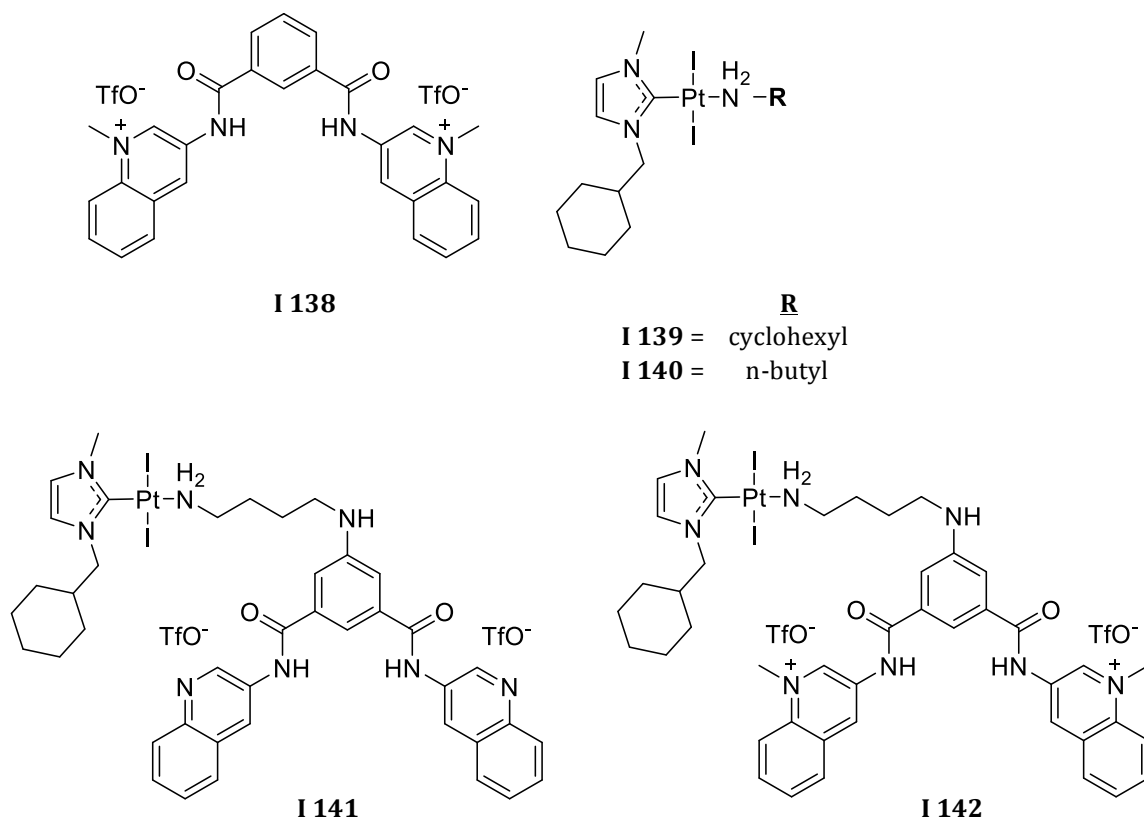
Betzer et al. reports the conjugation of anti-cancer platinum complexes to bisquinolinium pyridodicarboxamide (PDA) groups which target telomeres and oncogenes (Chart I-17).⁶⁶ These complexes were synthesized through a series of multi-step reactions. The first step was synthesis of the platinum NHC complex via the reaction of 1-(cyclohexylmethyl)-3-methylimidazolium bromide with platinum(0)-1,3-divinyl-1,1,3,3-tetramethyldisiloxane (dvtms) under basic conditions. To obtain **I 139- I 142**, the Pt(0) complex was oxidized to Pt(II) by addition of I₂. To attach the PDA molecule, the chlorine substituent on the pyridine ring underwent N-arylation to produce the amine linker. The amine then displaces a dvtms ligand to form **I 141**, and quinolines of PDA are protonated via methyltriflate to form the platinum(II) NHC PDA complex (**I 142**).

DNA drug targeting is extremely important in cancer treatments today. However, targeting DNA has largely been uncontrolled and random. To combat this random nature, secondary structure targeting has become of interest, specifically the DNA quadruplex called G4-DNA formed by the folding of guanine-repeat sequences. These elements have been seen in oncogenes and telomeres. They regulate transcription and replication by stopping the normal function of proteins like helicases. Small molecules have the ability to target quadruplexes meaning that specific targeting of drugs is a possibility for treatment.

The G4-FID assay is a test used to evaluate if a specific drug is able to bind to quadruplex structures while comparing that to a duplex control. This study measures binding by the displacement of thiazole orange and the DC₅₀ value obtained from the experiment corresponds to the concentration of compound that

displaces 50% of the thiazole orange. The binding of **I 142** was directly compared to **I 139** and **I 138**. Alone, **I 138** was found to have all DC_{50} values of $<1 \mu\text{M}$ for all quadruplex structures tested, which is considered medium to high affinity. Complex **I 142** was able to bind two of the quadruplex oligonucleotides with medium to high affinity ($DC_{50} 1 \mu\text{M}$) while it had only a weak affinity for the other two tested ($DC_{50} \geq 1\mu\text{M}$). This indicates that the affinity of **I 142** is decreased as compared to **I 138** but that it does not lose all of its binding ability being conjugated to the NHC. Authors note that steric hindrance of the **I 142** compound could be the reason that binding is different between quadruplexes. Selectivity for quadruplex versus duplex DNA was maintained. The *in vitro* cytotoxicities of **I 139**, **I 142**, and **I 141** were also evaluated against two ovarian cancer cell lines, A2780 and A2780cis, which are sensitive or resistant to cisplatin, respectively. Complex **I 139** had the lowest IC_{50} values of $0.5 \mu\text{M}$ and $0.8 \mu\text{M}$ for A2780 and A2780cis, respectively. Complex **I 142** had increased IC_{50} values of $8 \mu\text{M}$ (A2780) and $15 \mu\text{M}$ (A2780cis) indicating that addition of the PDC compound hindered anti-cancer activity. However, as compared to the IC_{50} value for **I 138** against A2780 cells of $15 \mu\text{M}$, it is clear that the combination of **I 138** with **I 139** (making compound **I 142**) is better for anti-cancer activity.

Chart I-17. Structures of Imidazolylidene Platinum(II) Carbene Complexes with Metal Bound PDA Ligands and Corresponding Precursors



Bellemin-Lapponnaz and co-workers have also published a recent study in 2016 reporting the synthesis of novel platinum(II) NHC complexes (Chart I-18).⁶⁷ The first family of compounds include platinum(II) NHC coordination polymers. The precursor complex $\text{trans}[(\text{NHC})\text{PtI}_2(\text{pyridine})]$ was synthesized via standard procedures. The complex then underwent ligand exchange from pyridine to other amines such as aminoethanol (**I 143**), ethylenediamine (**I 144**), diethylene triamine (**I 145**), and linear polyethylenimine (PEI) (**I 146- I 148**). PEI, which is commonly used as a transfection agent and proposed to increase potency, was incorporated

with platinum complexes by varying platinum concentrations, ranging from one platinum complex per 10-30 ethylenediamine monomer units.

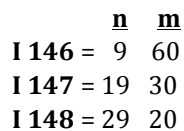
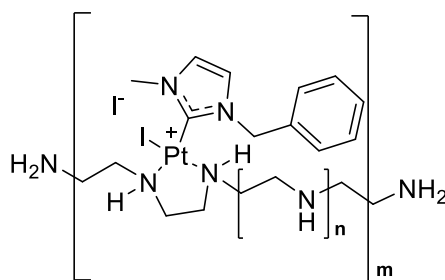
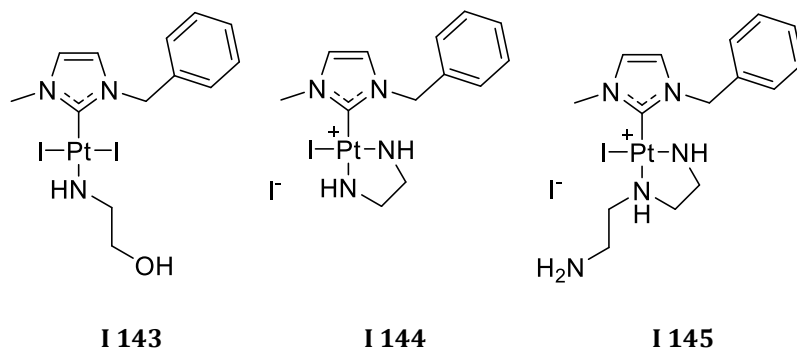
Cancer cell lines used to evaluate the anti-cancer activity of these complexes were HCT-116 (human colorectal adenocarcinoma), U87 (human glioblastoma), PC3 (human prostate adenocarcinoma), and TC1 (murine lung carcinoma). The non-cancerous cell line 3T3 (murine fibroblast) was also tested. The MTS assay was utilized to determine cell viability after 24 hours of treatment, with cisplatin and oxaliplatin as the controls. The neutral NHC platinum complex **I 143** had IC₅₀ values ranging from 28 ± 3.5 μM (TC1) to 38 ± 2.4 μM (3T3; non-cancerous cell line) whereas the cationic compounds **I 144** and **I 145** did not display any activity (>100 μM). Compound **I 143** was found to have increased activity when compared to cisplatin (>100 μM for U87, HCT-116, and TC1, 39 ± 1.4 μM for PC3 and 13 ± 0.1 μM for the non-cancerous 3T3 line) and comparable activity to oxaliplatin (ranging from 15 ± 0.1 μM for the non-cancerous 3T3 line to 35.5 ± 6 μM for HCT-116). The conjugates (NHC-Pt-PEI) displayed even higher activity (1.8 ± 0.1 μM to 27 ± 1.0 μM), and were more effective than PEI on its own (47 ± 4.2 μM to >100 μM). Cytotoxicity of the conjugates was found to be inversely correlated to the Pt/polymer unit ratio (i.e. a decrease in Pt/PEI unit ratio resulted in an increase in toxicity). Complex **I 148** was found to be more toxic than cisplatin and oxaliplatin when compared at the same platinum concentration. Stability studies showed no change in activity *in vitro* while keeping the conjugate **I 148** in ethanol for 3 months at 4°C and there was also no UV-Vis change after several days under physiological conditions. This indicates that linear PEI can increase the activity of NHC-Pt

complexes. The authors believe this could be due to multivalency effects or that PEI can protect the Pt metal from side reactions with other molecules that would be less desirable.

Complex **I 148** was further tested for apoptosis on HCT-116 cells using Hoechst 33342 and Annexin V. At concentrations greater than 20 μM , apoptosis was induced and was at a higher level as compared to oxaliplatin. An *in vivo* study was also conducted using **I 148** on an HCT-116 tumor xenograft mouse model. The final solution of the drug contained 10% ethanol. Tumor volume inhibition was observed (80% inhibition) in mice that were treated with 10 mg/kg by intraperitoneal (ip) injection every 48 hours. Oxaliplatin was used at 2 mg/kg, so that the Pt metal concentration was the same as the **I 148** mice, but this dose did not have as great of an effect.

ICP-MS was used to test intracellular concentration versus extracellular concentration of platinum. Researchers found that the concentration inside cells is 2.5 times higher for the NHC-Pt-PEI complexes than for oxaliplatin. This was also done with subcellular fractions to determine cellular localization. It was found that 57% of the oxaliplatin was located in the nucleus and 3.5% was located in the mitochondria while **I 148** was found in ratios of 16% in the nucleus and 20% in the mitochondria. Studies also showed that while oxaliplatin and cisplatin did not have cytotoxicity against HCT-116 cells deficient in p53, **I 148** was able to induce cell death.

Chart I-18. Structures of Imidazolylidene Platinum(II) Carbene Complexes with Metal Bound Amine Ligands



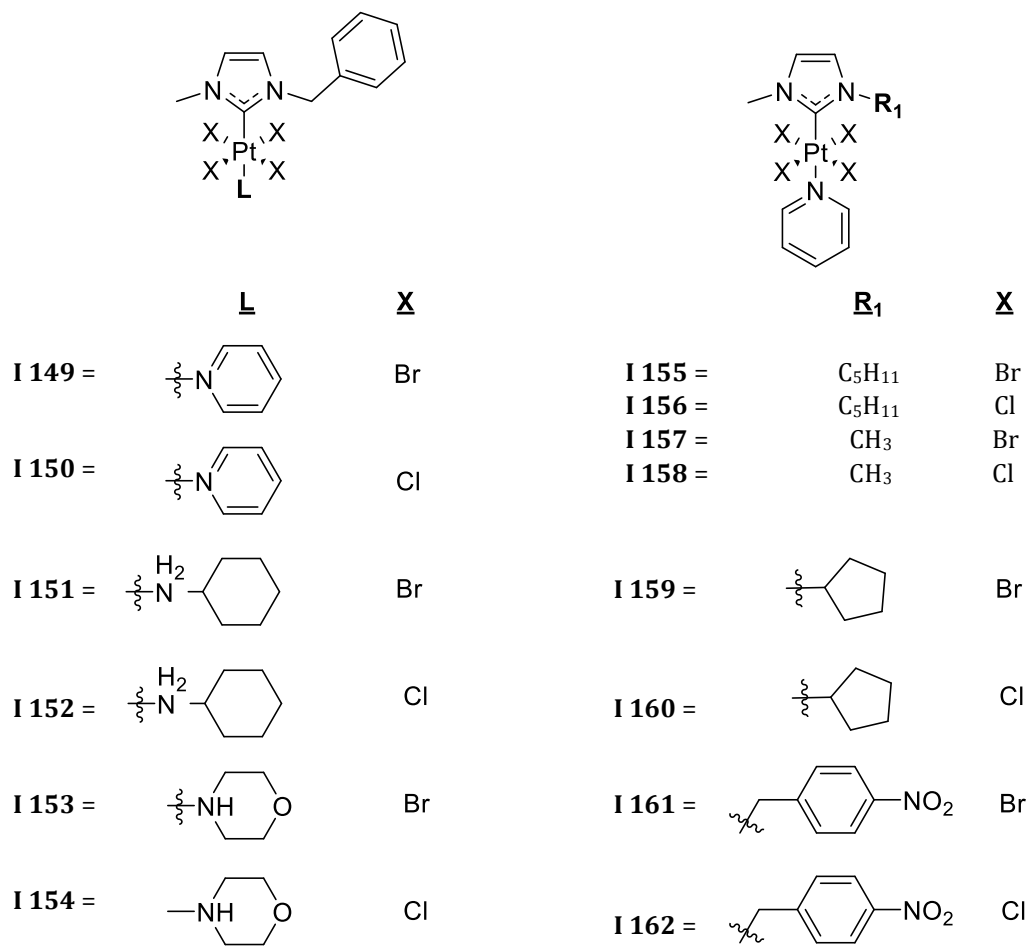
Platinum(IV) NHC complexes with antitumor properties were described in 2016 by Bellemin-Lapponnaz and co-workers.⁶⁸ To form the complexes, the platinum(II) NHC was formed via standard reaction procedures summarized previously. To oxidize to the Pt(IV) complexes, two equivalents of Br₂ or PhICl₂ was reacted with the Pt(II) precursor. This reaction resulted in an oxidation of the platinum metal to form the trans-octahedral complexes (**I 149- I 150, I 155- I 162**). Additionally the non-halide ligands such as pyridine can be exchanged to other amines by addition of cyclohexylamine (**I 151** and **I 152**) or morpholine (**I 153** and **I 154**).

An MTS assay was used with three cell lines, MCF-7 (breast cancer), HCT-116 (colon cancer), and PC3 (human prostate cancer), to determine cytotoxicity. All Pt(IV) complexes had moderate activities as compared to cisplatin, with a few exceptions. Chloride complexes (**I 150**, **I 152**, **I 154**, **I 156**, **I 158**, **I 160**, and **I 162**) were more effective than the bromide complexes (**I 149**, **I 151**, **I 153**, **I 155**, **I 157**, **I 159**, and **I 161**) overall with IC₅₀ values ranging from 0.5 ± 0.09 μM to 1.7 ± 0.6 μM for chloride derivatives and 2.1 ± 0.5 μM to 14 ± 2 μM for bromide complexes. Complexes **I 155** and **I 156** were tested for their ability to induce apoptosis in HCT-116 p53 KO cells, which were oxaliplatin resistant. Both **I 155** and **I 156** induced apoptosis, indicating that they can overcome the oxaliplatin resistance mechanism(s). Pt(II) complexes were shown to be much less active than Pt(IV) complexes by their anti-proliferative test with values of 63 ± 5 μM to >100 μM for the DMSO tested adducts. Studies showed that in pure DMSO at high concentrations at room temperature the bromide platinum(IV) complexes were reduced to platinum(II) within half a day while the chloride complexes took one month for complete conversion. However, no conversion was observable when testing the concentrations that were used for the *in vitro* studies but addition of glutathione accelerated the reduction.

Complexes **I 155** and **I 156** were further studied for their effect on mitochondria, specifically production of reactive oxygen species (ROS). The Pt(IV) complexes produced more ROS than oxaliplatin with more ROS production at higher concentrations. The same general trend is seen with **I 155** and **I 156** while testing for mitochondrial respiratory activity. These tests were performed using flow

cytometry with mitoSOX and mitoTracker dye, respectively. Authors suggest that the results of biological activity correspond to the stability of the complexes.

Chart I-19. Structures of Platinum(IV) Carbene Complexes with Metal Bound Amine and Halide Ligands



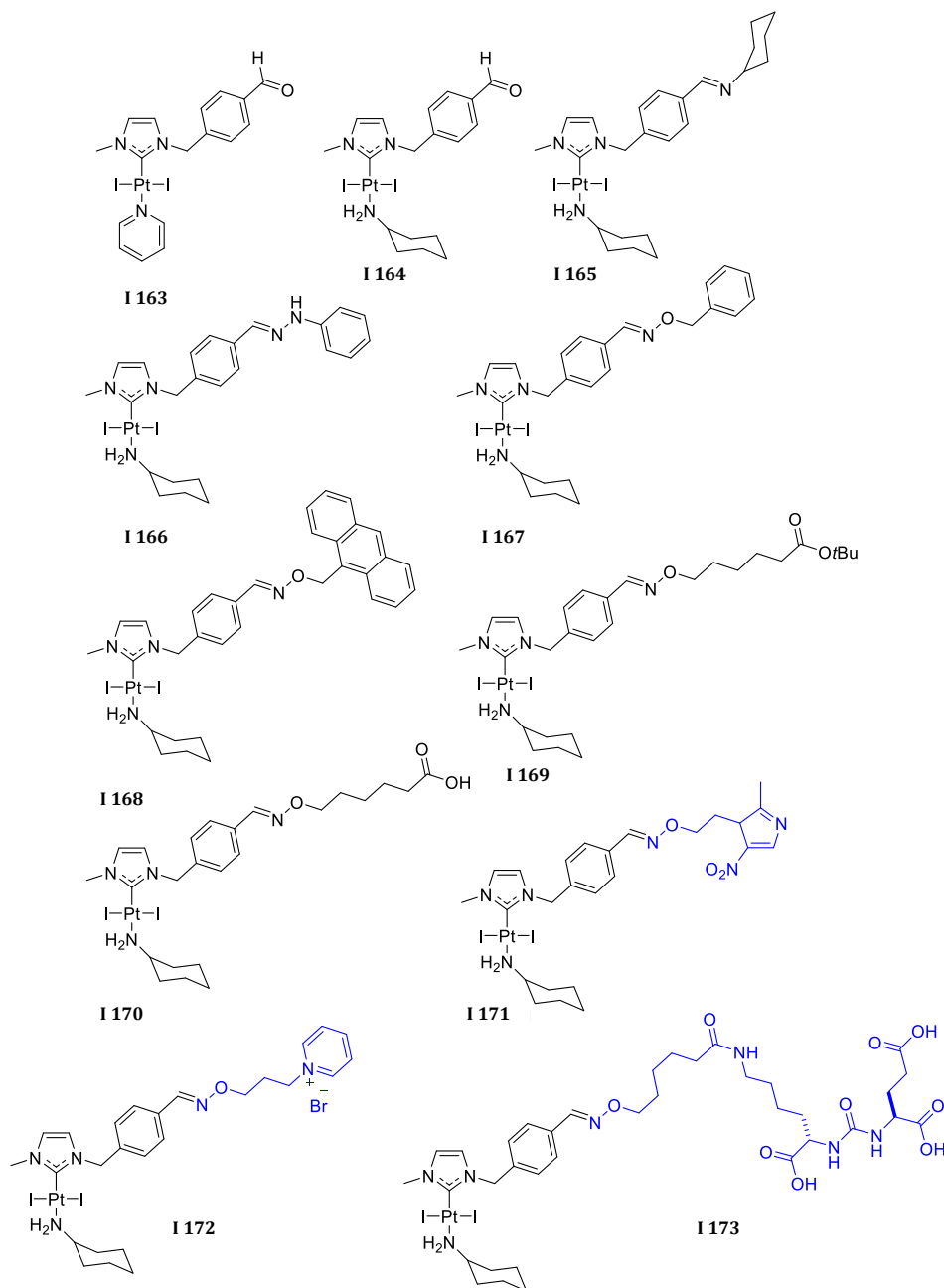
Bellemin-Lapponaz and coworkers have also reported platinum(II) complexes containing targeting moieties (Chart I-20).⁶⁹ The work presents an alternative synthesis as the targeting ligands were attached post NHC formation. The researchers synthesized platinum(II) NHC complexes with benzaldehyde functionalized imidazolium salts. Once the NHC was formed, imine coupling reactions were utilized to attach cyclohexylamine groups to the imidazol-2-ylidene

portion of the complex (**I 165**). This ultimately was unstable as the imine hydrolyses in water. To remedy this issue, they explored hydrazone (**I 166**) and oxime couplings to form water stable bonds. It was determined that only oximes were relatively stable. The platinum(II) NHC complexes were then reacted with various hydroxylamine ligands (**I 167- I 170**) as well as targeting moieties (**I 171- I 173**) with hydroxylamine substituents, with the purpose of an anti-cancer targeting complex. The platinum (II) targeting complexes were functionalized with hypoxic cell (**I 171**), cartilaginous cell (**I 172**), and prostate cell (**I 173**) targeting moieties highlighted in blue in Chart I-20.

The Pt(II) NHC complexes in Chart I-20 were evaluated for cytotoxic properties against four cancer cell lines (HCT-116 colon cancer, MCF-7 breast cancer, PC3 prostate adenocarcinoma, and SKOV3 ovarian cancer) and two non-cancer cell lines (MRC5 human fetus lung cells and EPC endothelial progenitor cells). Complexes **I 163** and **I 164**, containing an aldehyde group attached to the benzyl substituent, displayed high activities with IC₅₀ values for all six cell lines tested of less than 2 μM, for complex **I 163**, and less than 1.1 μM for complex **I 164**. Complex **I 167**, with a benzyl hydroxylamine group, had even higher activity with IC₅₀ values of less than 0.4 μM for all cell lines tested. Similar to values for complexes **I 163** and **I 164**, complex **I 169**, containing the 6-(aminoxy)hexanoate, displayed IC₅₀ values of less than 1.7 μM for all cell lines. A wide range of activities were seen for complex **I 171** based on the variable IC₅₀ values of 0.11 ± 0.01 μM to 5.13 ± 0.24 μM, indicating that this compound containing the metronidazole derivative is efficacious but to a greater extent against certain cell lines. Lower activities were seen for

complexes **I 172** and **I 173**, despite addition of the targeting moieties, which is believed to be due to issues in crossing the cell membrane. For the most active compounds there is no observable selectivity for cancer cells versus non-cancer cells.

Chart I-20. Structures of Platinum(II) Carbene Complexes with Metal Bound Amines and Targeting Group Functionalized Imidazolylidenes



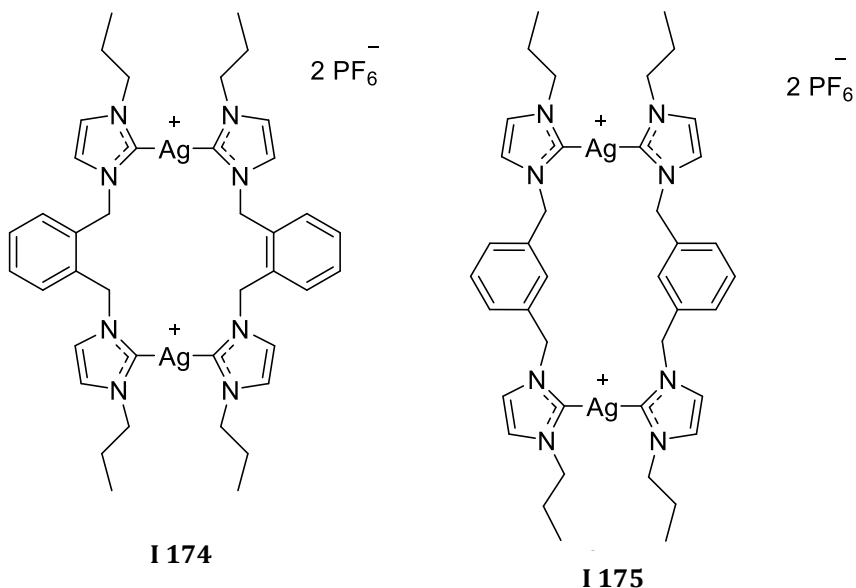
1.4. Di-Nuclear Imidazole NHC Complexes

1.4.1. Silver Bis-Imidazole Di-Nuclear NHC Complexes

Haque et al. report the synthesis of dinuclear silver(I) NHC complexes with ortho and meta xylyl linkers (Chart I-21).⁷⁰ The imidazolium salts were synthesized via standard alkylation of N-propylimidazole with 1,2-bis(bromomethyl)benzene or 1,3-bis(bromomethyl)benzene. The imidazolium salts were then metalated via the silver base technique using silver(I) oxide, to form the cyclic di-nuclear silver NHC complexes (**I 174**- **I 175**). The bromide anions were exchanged with PF₆⁻ anions for purification purposes.

The MTT assay was used to evaluate the activity of **I 174** and **I 175** against HCT-116 colon cancer and MCF-7 breast cancer cell lines. The bis-imidazole precursors were found to have no activity (>200 μM) against the HCT-116 cell line and little to no activity against MCF-7 (158- >200 μM). The silver compounds showed significant activity with IC₅₀ values of 5.6- 20.3 μM for HCT-116 and 1.12- 6.38 μM for MCF-7. Complex **I 175**, which contained the meta-xylyl bridge, had higher activity than **I 174**, with the ortho-xylyl bridge, with IC₅₀ values of 5.6 μM and 1.12 μM for HCT-166 and MCF-7 and values of 20.3 μM and 6.38 μM for HCT-116 and MCF-7, respectively. The authors suggest that lipophilicity of the complex enhances the ability to deliver silver cations into the cell so they can exert their antiproliferative effects.

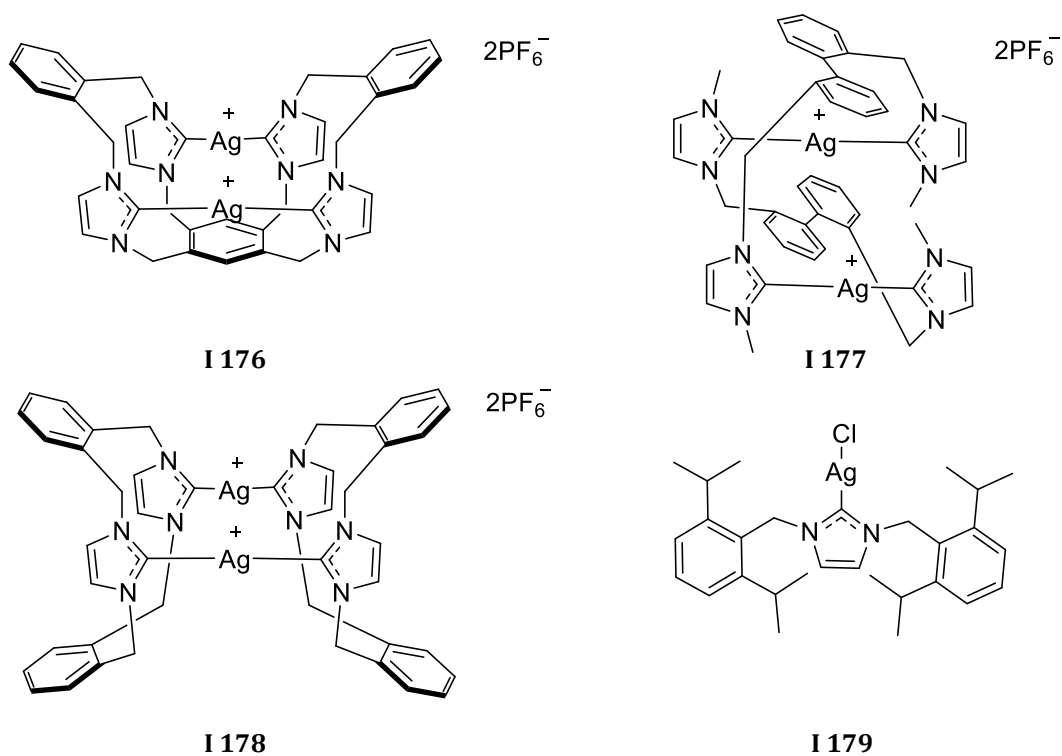
Chart I-21. Structures of Di-nuclear Imidazolydene Silver(I) Carbene Complexes with Xylyl Linkers



Four novel silver NHC complexes were synthesized via silver base metalation by Sakamoto et al. in 2016 (Chart I-22).⁷¹ Three of these complexes formed di-nuclear silver species (**I 176- I 178**) and one was a silver chloride salt (**I 179**). The imidazolium precursors were synthesized via standard alkylation procedures, but some were synthesized to form ring species. Two compounds synthesized were the tetrakis-imidazolium salt, bridged by two o-xylene groups and a tetrakis(methyl)benzyl substituent. Other precursors synthesized were a cyclic bis-imidazolium salt with o-xylene moieties as the linking substituent, a biphenyl linked bis-imidazolium salt, and a single imidazolium salt bis(di-isopropylbenzyl)imidazolium chloride. The bis- and tetrakis-imidazolium salts underwent metathesis to form the hexafluorophosphate salts. This weakly coordinating anion was utilized to promote formation of dinuclear NHC complexes.

The antimicrobial activity of the synthesized complexes **I 176- I 179** was highly variable (15.7->1000 $\mu\text{g/mL}$), indicating that the synthesized structures have very different effects on activity. Compound **I 176**, with a planar linker, had the highest activity of all the compounds tested, with MIC values ranging from 15.7-125 $\mu\text{g/mL}$.

Chart I-22. Structures of Di-nuclear Imidazolylidene Silver(I) Carbene Complexes and Mono-nuclear Silver(I) NHC, **I 179**



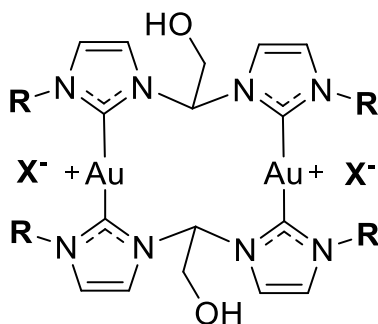
1.4.2. Gold Bis-Imidazole Di-Nuclear NHC Complexes

Rieb et al. reports the synthesis of dinuclear gold(I) NHC complexes with varying N-substituents on the imidazole ring (Chart I-23).⁷² They compared the change in anti-cancer activity by altering the N-substituents from methyl to an isopropyl or mesityl group. To form the imidazolium salt 1-alkyl imidazole was

reacted with 2,2-dichloroethan-1-ol via a standard imidazolium salt synthesis. The bis-imidazolium salt was then metalated with silver(I) oxide to form the dinuclear complex. For purification purposes, the chloride salt underwent a metathesis reaction to exchange the anion to PF₆⁻ or BPh₄⁻. The silver NHC complexes then were transmetalated via the addition of chloro(dimethylsulfide)gold(I) or chloro(tetrahydrothiophene)gold(I) (**I 180- I 183**).

The gold complexes were tested for their anti-cancer properties against A549 lung cancer cells and HepG2 liver cancer cells. The lead compound was found to be **I 183**, which displayed IC₅₀ values of 42.2 ± 2.2 μM and 14.9 ± 0.9 μM against A549 and HepG2, respectively. The only other compound that showed activity was **I 180**, which displayed an IC₅₀ value of 69.4 ± 6.2 μM against HepG2 and no activity against A549.

Chart I-23. Structures of Di-nuclear Imidazolylidene Gold(I) Carbene Complexes **I 180- I 183**



<u>R</u>	<u>X</u>
I 180 = methyl	PF ₆
I 181 = isopropyl	PF ₆
I 182 = isopropyl	BPh ₄
I 183 = mesityl	PF ₆

1.4.3. Gold and Silver Di-Nuclear Imidazole NHC Complexes

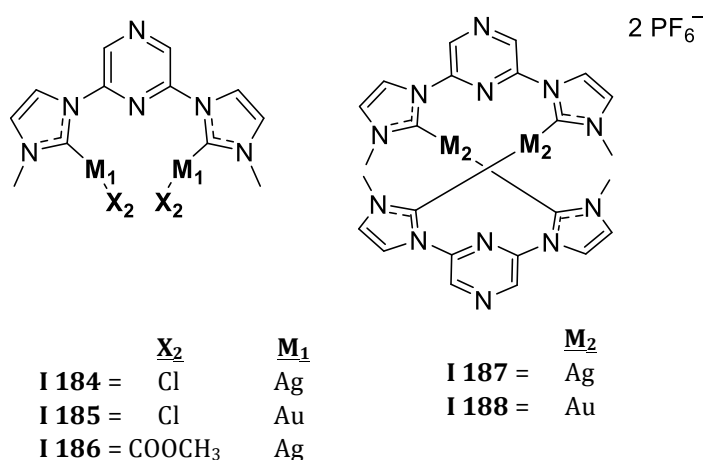
Proligand imidazolium salts and bis-cationic imidazolium salts were synthesized by Roymahapatra et al. via alkylation of imidazole with 1-methyl-3-pyrimidinechloride and 2,6-bis-[1-methylimidazol-2-yl]pyrazinechloride, respectively (Chart I-24).⁷³ Proligands were metalated with silver to form the NHC complexes. Depending on the anion, different connectivity could be achieved. A chloride salt resulted in the formation of the mono-nuclear silver(I) NHC **I 184**. With the anion exchanged to a weakly coordinating PF₆⁻, the metalation resulted in a di-nuclear silver(I) NHC between two proligands (**I 187**). From the silver(I) NHC complexes, transmetalation can occur to form the gold conjugates **I 185** and **I 188**.

MIC values were evaluated on the Gram-positive strains *S. mutans* and *S. epidermis* as well as the Gram-negative strains *P. aeruginosa* and *E. coli*. Precursor imidazolium salt ligands were tested against the strains and compared to the NHC complexes. The ligand precursor with the best activity had an MIC value of 256 µg/mL against all four strains. However, complexes **I 184- I 186** and **I 187- I 188** exhibited better activity with MIC values ranging from 2-8 µg/mL and 16-32 µg/mL, respectively. Specifically, **I 185**, the gold NHC complex, performed better against Gram-positive (MIC = 2 µg/mL) and Gram-negative bacteria (MIC = 4 µg/mL) than **I 184** (Gram-positive MIC = 4 µg/mL; Gram-negative MIC = 8 µg/mL). Compounds **I 184** (Ag NHC) and **I 185** (Au NHC) were identified to have the highest activity and were further tested against clinical isolates that are resistant to several antibiotics. MIC values ranging from 2-8 µg/mL were found for **I 184** and **I 185**, while traditional antibiotics ranged from 16-128 µg/mL indicating that these NHC

complexes are able to overcome some of the antibiotic resistant mechanisms of these clinical isolates. These two compounds were also able to disturb biofilm formation of certain bacterial strains, a common defense mechanism of bacteria.

SEM was also used to determine effect of **I 185** on bacterial cell walls of *B. subtilis*, *S. epidermidis*, and *P. aeruginosa*. Images show a change in morphology and integrity of the cell wall. The authors postulate that the stability of the gold-NHC bond can cause the changes in observed activity.

Chart I-24. Structures of Di-nuclear Imidazolylidene Silver(I) and Gold(I) Carbene Complexes and the Corresponding Imidazolium Salt Precursors



In 2013, four bisimidazol-2-ylidene metal NHC complexes were synthesized via silver base technique and transmetallation to gold complexes (Chart I-25).⁷⁴ The bisimidazolium salts were synthesized by standard alkylation procedures to afford 1-(2-methylallyl)imidazole linked with dibromo-p-xylene. To make the silver bromide (**I 189**) and gold bromide (**I 190**) monocarbene complexes, the previously mentioned imidazolium salt was reacted with excess silver(I) oxide, and transmetallated with chloro(dimethylsulfide)gold(I). To achieve the biscarbene complexes **I 191** and **I**

192, the bromide anions of the starting bisimidazolium salt were exchanged with PF_6^- anions. These weakly coordinating anions allowed the bis-carbene di-nuclear species to be formed under the metalation reaction conditions.

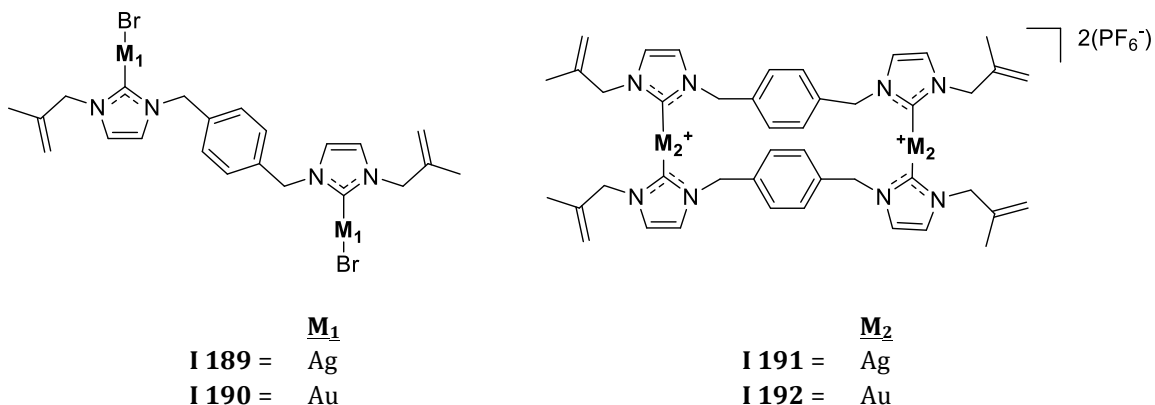
Compounds were tested against Gram-positive, Gram-negative, and fungal cell lines, with all strains having resistance to common treatments. Overall, complexes **I 189** and **I 190** displayed higher activities (0.97-3.90 μM) than those of **I 191** and **I 192** (all values = 125 μM). Complex **I 190** had a significant activity against *P. aeruginosa* and *A. fumigatus* with MIC values of 0.97 μM . Of importance is also the ability to destroy biofilms created as a defense mechanism by certain organisms. Complexes **I 189** and **I 190** were tested for this ability and it was determined that the gold complex, **I 190**, was 3-10 fold more active than the silver complex or traditional antibiotics.

SEM was used to study morphological changes of the cell membrane. *P. aeruginosa* and *C. albicans* were both treated with **I 190** and changes were noticed after 1 hour, indicating to the authors that the mechanism of action of **I 190** may have to do with interaction with the membrane. In order to test the toxicity of **I 190**, it was administered on a goat eye as a drop six times per day. After 2 days, for a total of 12 treatments, **I 190** had a low toxicity (the pigment and lens remained normal). This led the authors to the conclusion that **I 190** could be effective at controlling keratitis.

The authors suggest the mechanism of action is due to cell membrane disruption. The variability in activity between **I 189** and **I 190** is attributed to the stability of the metal-NHC bond. The gold-NHC bond is more stable than the silver-

NHC bond, making **I 189** more reactive and better able to interact with other molecules.

Chart I-25. Structures of Di-nuclear Silver(I) and Gold(I) Carbene and Bis-Carbene Complexes



1.5. Mono-Nuclear Benzimidazole NHC Complexes

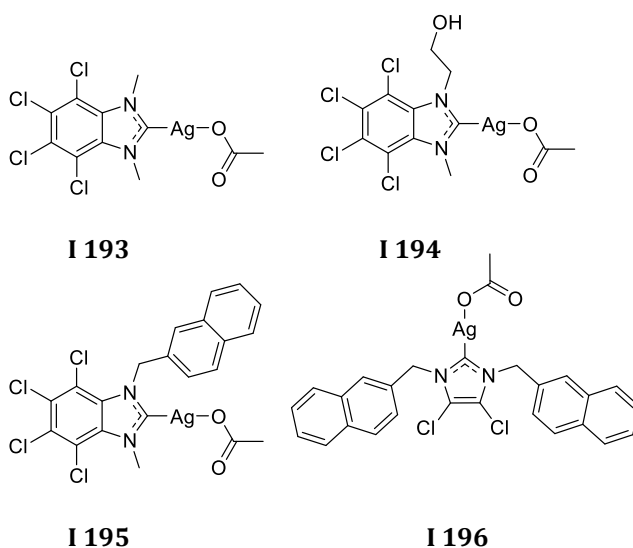
1.5.1. 4,5,6,7-Tetrachlorobenzimidazolium Silver NHC Complexes

Novel silver NHC complexes were synthesized from various substituted 4,5,6,7-tetrachlorobenzimidazolium salts by Youngs and coworkers (Chart I-26).⁷⁵ The imidazolium salts were metalated using the silver base technique through addition of silver acetate. Three NHC complexes were synthesized from 1-methyl-4,5,6,7-tetrachlorobenzimidazole, the first being the methyl substituent off of the nitrogen (**I 193**), the second with a hydroxyethyl (**I 194**), and lastly the 2-methylnaphthalene (**I 195**).

Complexes **I 193**, **I 194**, and **I 195** were tested against a wide variety of organisms. When testing these complexes against the J53 strain of *E. coli*, MIC values were 0.5 µg/mL for **I 193** and **I 194** while **I 195** had a value of 2 µg/mL. However,

when the J53 strain with the pMG101 silver resistant plasmid was tested, MIC values increased to >20, 8, and 10 $\mu\text{g/mL}$ for **I 193**, **I 194** and **I 195**, respectively. This indicates that silver is important for the observed activity and that the substituents on the ligand can affect activity as well. Minimum bactericidal concentrations (MBCs) for each complex were also determined. MBCs for all silver complexes were $\leq 6 \mu\text{g/mL}$, with the exception of the silver resistant J53 strain. Complex **I 195** was the only compound that was bactericidal against the J53+pMG101 strain as well as being the only compound to incorporate the methylnaphthalene substituent. This can be compared to a previously synthesized compound **I 196**, which has methynaphthyl groups off of both nitrogens and is also effective against J53+pMG101, displaying the utility of this substituent. This research shows the importance of the imidazolium salt to the activity of NHC complexes.

Chart I-26. Structures of Tetrachloroimidazolylidene and Dichloroimidazolylidine Silver(I) Carbene Complexes

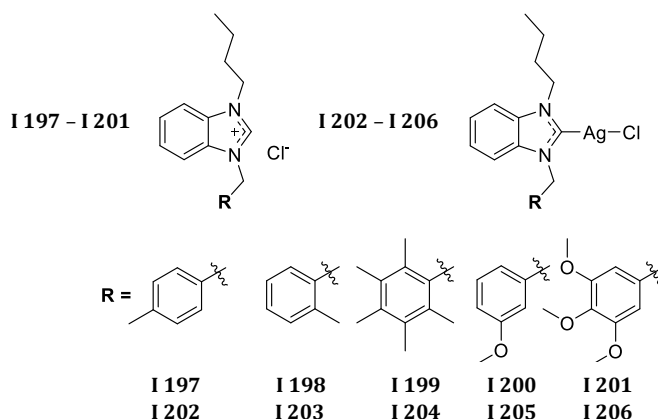


1.5.2. Silver Halide Mono-Nuclear Benzimidazole NHC Complexes

Özdemir and coworkers have published the synthesis of novel asymmetric imidazolium salts containing a silver halide NHC (Chart I-27).⁷⁶ In 2012, a number of compounds were synthesized by alkylating 1-butylbenzimidazole with benzyl chloride comprised of varying substituents on the aromatic ring (**I 197- I 201**). This collection of imidazolium salts were then metalated with silver(I) oxide to form the silver chloride NHC complexes (**I 202- I 206**).

The silver complexes **I 202- I 206** were shown to be more effective against Gram-positive and Gram-negative bacteria as well as fungi as compared to the benzimidazolium precursors **I 197- I 201**, which had the lowest MIC value of 100 µg/mL for **I 197- I 199** against the fungal strains. However, none of the compounds reached the level of the control drugs. The most promising compound was found to be **I 202**, which displayed MIC values between 25 – 50 µg/mL against all the strains tested (*E. coli*, *S. aureus*, *E. faecalis*, *P. aeruginosa*, *C. albicans*, *C. tropicalis*) as compared to the control compounds (ampicillin, ciprofloxacin and fluconazole), which had values equal to or lower than 3.12 µg/mL.

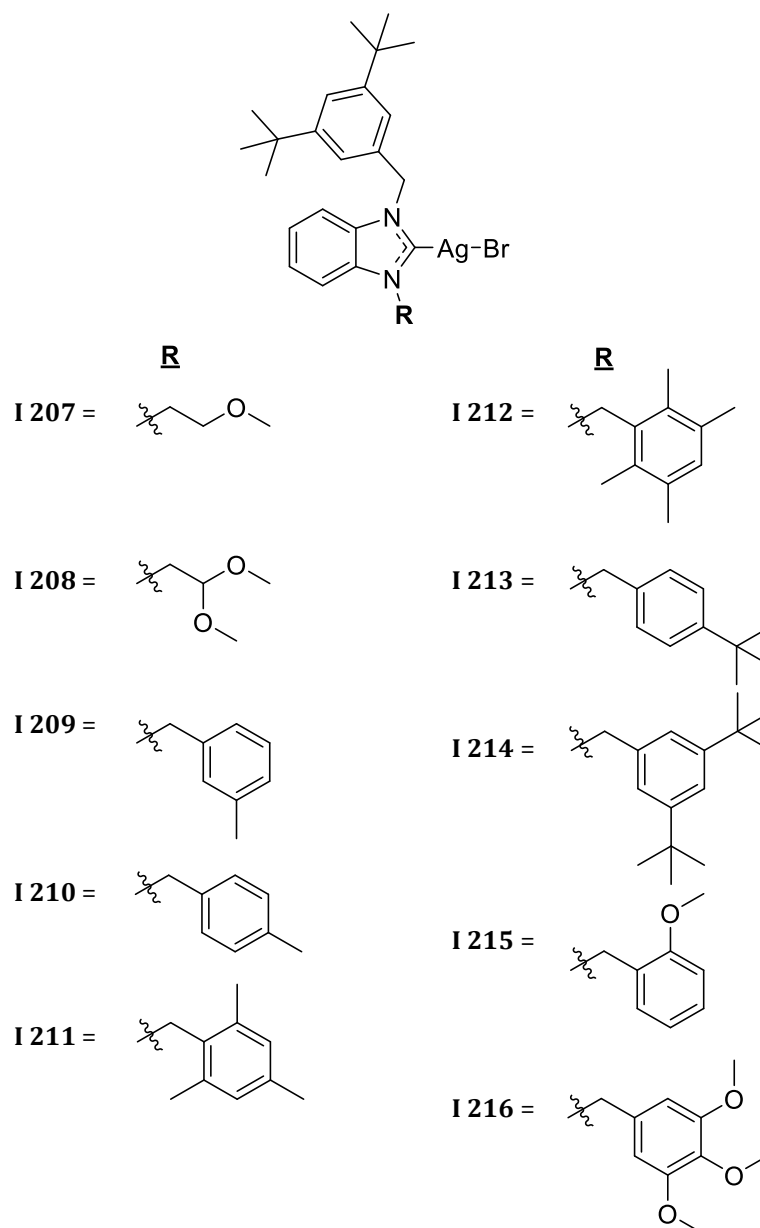
Chart I-27. Structures of Benzimidazolylidene Silver(I) Carbene Complexes and the Corresponding Imidazolium Salts



In 2017, Özdemir and coworkers also published ten silver NHC complexes with bulky 3,5-di-tert-butyl benzyl substituents on the imidazole ring (Chart I-28).⁷⁷ The imidazolium salts were synthesized by the alkylation of 1-(3,5-di-tert-butylbenzyl)benzimidazole with various alkyl bromides under a standard procedure. The imidazolium salts were then metalated using silver(I) oxide to form NHC complexes **I 207- I 216**.

MIC values were determined and the silver complexes showed varying rates of antibacterial activity against both Gram-positive and Gram-negative bacteria, with **I 214** being the most promising compound (MIC = 6.25 µg/mL for *E. coli*, *P. aeruginosa*, *S. aureus*, and *E. faecalis*). MIC values were also tested against the fungal strains *C. albicans* and *C. tropicalis*, with **I 213** and **I 214** displaying the highest activity with MIC values of 6.25 µg/mL on each cell line for both compounds. As with other studies, the authors concluded that the substituents on the nitrogen atoms of the benzimidazole, give rise to compounds with different levels of activity. Electron-donating and bulky groups contributed to higher antimicrobial activity.

Chart I-28. Structures of Benzimidazolylidene Silver(I) Carbene Complexes **I 207- I 216**

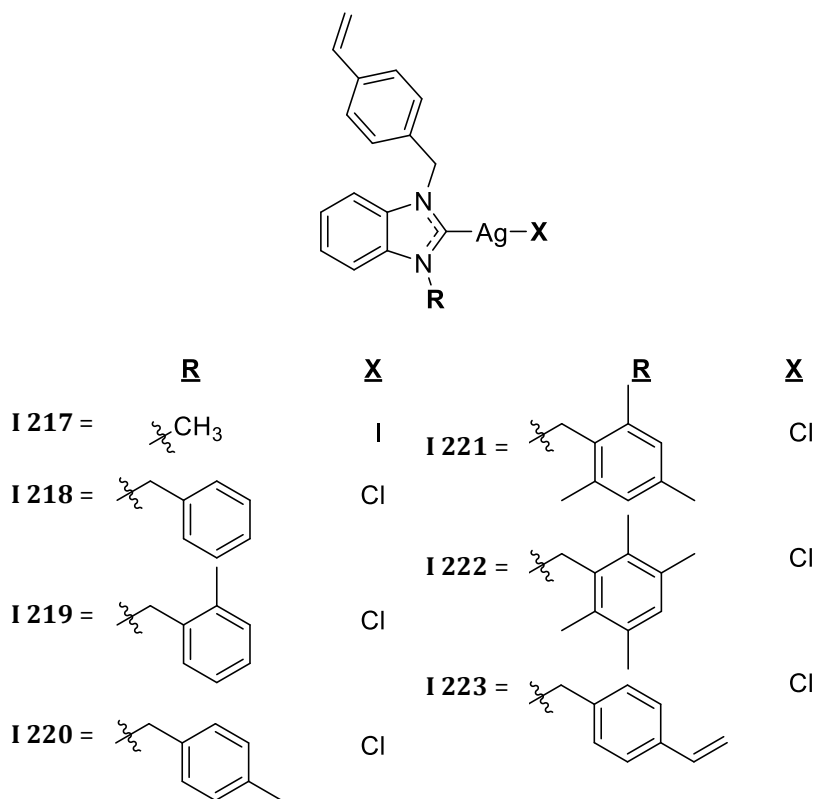


Gök et al. have also contributed significantly to the class of silver halide complexes of benzimidazole-based NHC complexes.⁷⁸ In 2014, novel benzimidazolium salts were synthesized and metalated with silver(I) oxide to form the NHC complex (Chart I-29). These imidazolium salts were synthesized under standard procedures via alkylation of the benzimidazole with alkyl halides. To

prepare the silver halide NHC complexes (**I 217- I 223**), the imidazolium salts were metalated with silver(I) oxide.

Complexes **I 218**, **I 221**, and **I 222** exhibited moderate activity against all bacteria and fungi with a range of MIC values from 25-50 $\mu\text{g/mL}$. None of the compounds were as effective as ampicillin, ciprofloxacin, or fluconazole. However, it is clear from the range of MIC values that different substituents on the nitrogen atoms play an important role in changing the activity.

Chart I-29. Structures of Benzimidazolylidene Silver(I) Carbene Complexes **I 217- I 223**

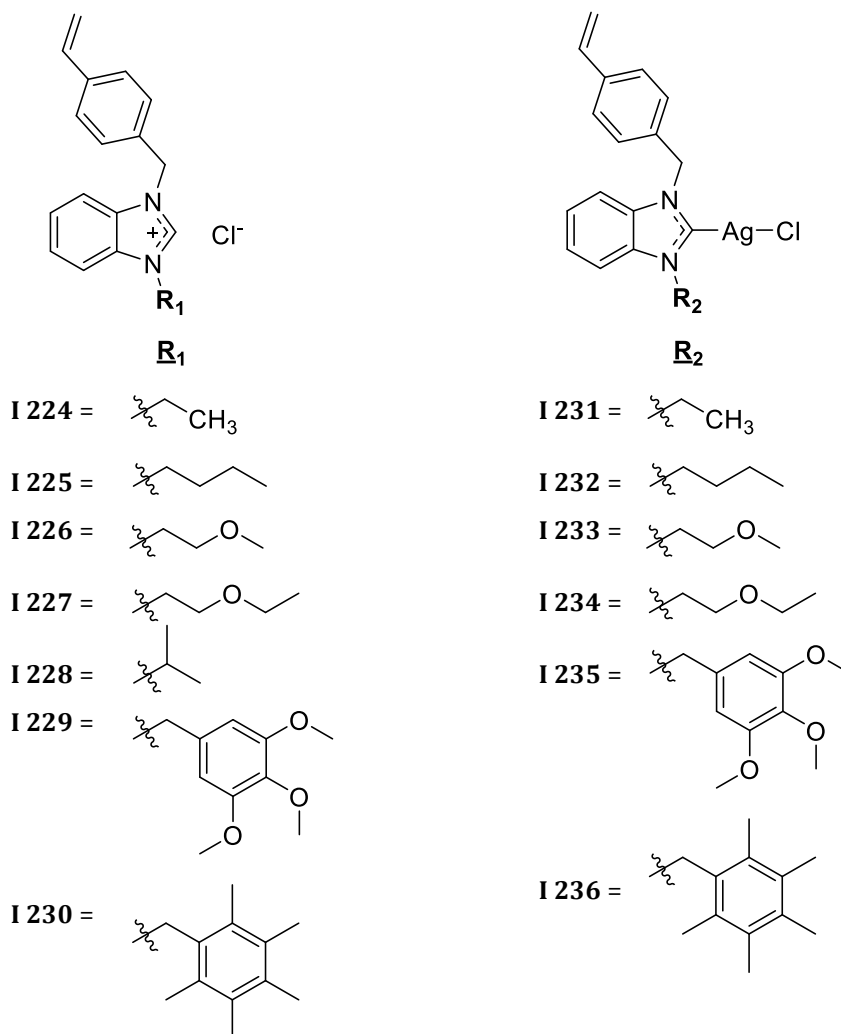


In 2016, Gök et al. synthesized a second set of substituted benzimidazolium salts that were metalated with silver(I) to form the NHC complexes (Chart I-30).⁷⁹

These benzimidazolium salts (**I 224- I 230**) were synthesized and metallated with silver(I) oxide under standard procedures to produce complexes **I 231- I 236**.

Strains used to test these compounds using the agar-well diffusion method include the Gram-positive strains *B. subtilis*, *L. monocytogenes* and *S. aureus*; Gram-negative strains include *E. coli*, *K. pneumonia*, *P. mirabilis*, *P. aeruginosa*, *S. typhimurium*, and *Y. enterocolitica*; and a yeast strain *C. albicans*. Both the benzimidazole salts (**I 224- I 230**) and silver complexes (**I 231- I 236**), demonstrated good antimicrobial activity against the tested microorganisms. The silver complexes displayed higher zones of inhibition than the benzimidazolium salts. Compound **I 230** showed the highest activity of the salts. Silver complexes were better antifungals than the salts, displaying a 12-15 mm inhibition versus 7-10 mm zones of inhibition for the benzimidazolium salts. However, none of the compounds at 10 mg/mL were able to reach the inhibition zone of tetracycline at the same concentration (16-27 mm).

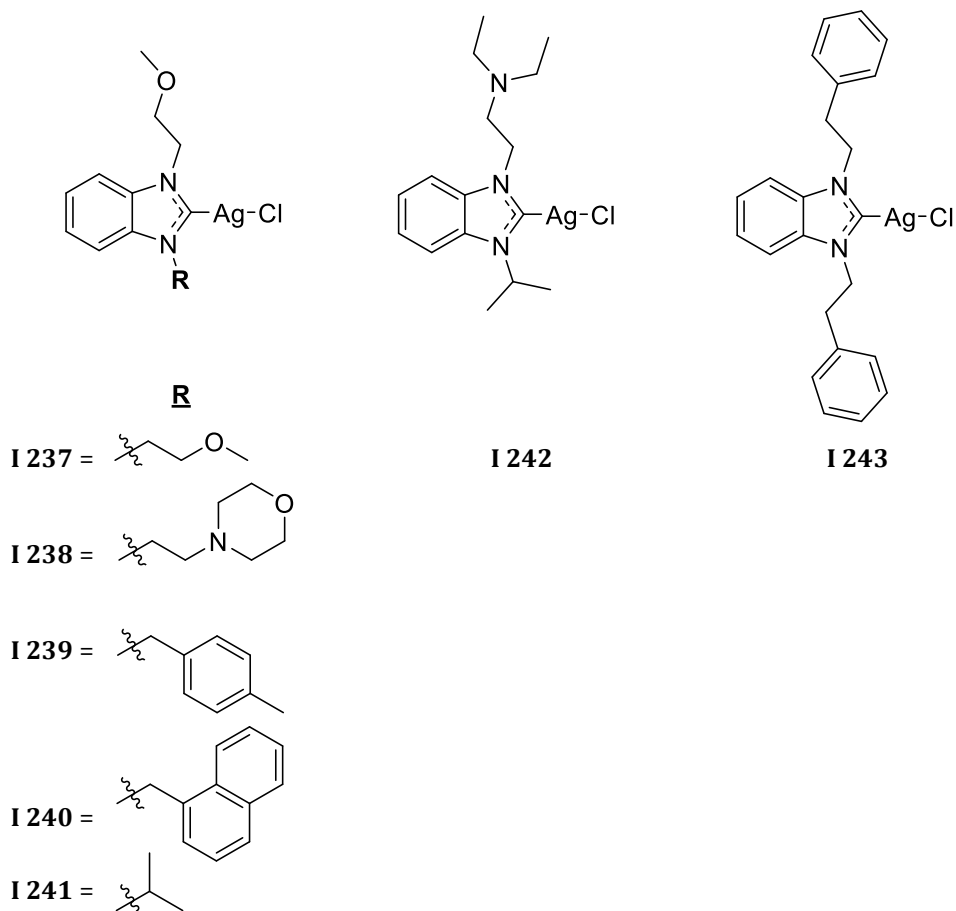
Chart I-30. Structures of Benzimidazolylidene Silver(I) Carbene Complexes and the Corresponding Imidazolium Salt Precursors



Seven benzimidazol-2-ylidene silver(I) NHC complexes (**I 237- I 243**) were synthesized via silver base metalation method by reacting the benzimidazolium salts with silver(I) carbonate (Chart I-31).⁸⁰ The benzimidazolium salts precursors were synthesized under standard reaction procedures to alkylate the nitrogen atoms.

Antimicrobial efficacy of these compounds were determined by MIC testing against *E. coli*, *S. aureus*, *E. faecalis*, *P. aeruginosa*, as well as the fungal strains *C. albicans* and *C. tropicalis*. While all silver complexes showed activity within the tested range (50-200 $\mu\text{g/mL}$), the compound with the highest activity was found to be **I 237**, which had an MIC value of 50 $\mu\text{g/mL}$ for all bacteria and fungi tested. The most effective complex against the fungi alone was **I 239**, with MIC values of between 12.5-25 $\mu\text{g/mL}$. In contrast, complex **I 239** had MIC values of 100 $\mu\text{g/mL}$ for the bacterial strains. This shows that the substituents on the nitrogen atoms can alter the activity for different organisms.

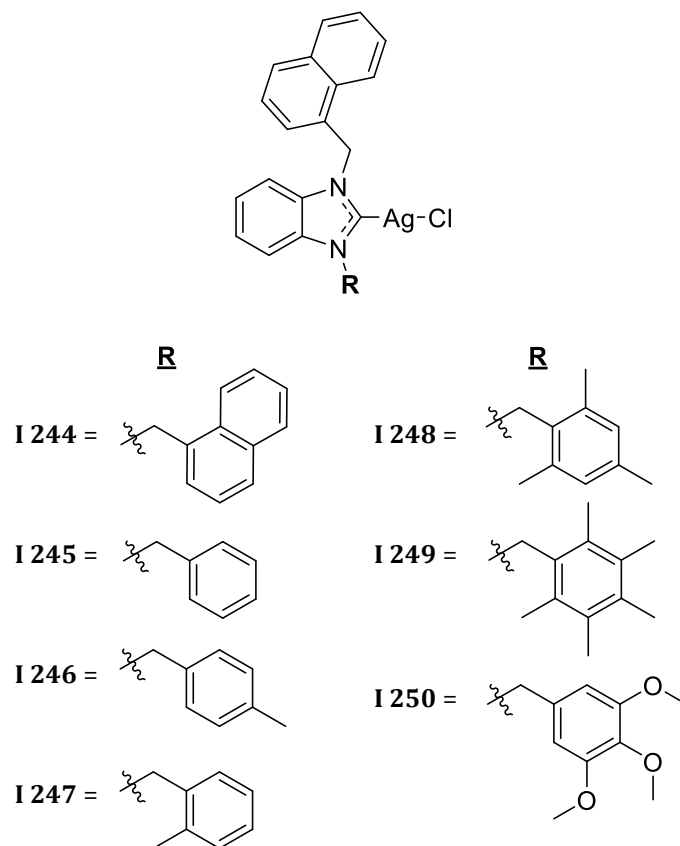
Chart I-31. Structures of Benzimidazolylidene Silver(I) Carbene Complexes **I 237**- **I 243**



The reaction of silver(I) oxide with alkyl substituted benzimidazolium salts gave the benzimidazolylidene silver(I) carbene complexes in Chart I-32.⁸¹ These salts all have 1-methylnaphthalene substituents with varying alkyl substituents on the other nitrogen position. Through addition of silver(I) oxide the mono-carbene chloride complexes (**I 244- I 250**) were formed.

Complexes were tested against *P. aeruginosa*, *E. coli*, *S. aureus*, *E. faecalis*, *C. albicans*, and *C. tropicalis* to determine their MIC values. Compounds **I 245- I 249** displayed high activity against Gram-positive bacteria with MIC values ranging from 6.25-25 µg/mL. They were less effective against Gram-negative bacteria with values ranging from 100-200 µg/mL. Compound **I 250** displayed the least amount of activity against the bacteria and the fungi tested. Compound **I 247** had the highest activity against the fungi with values of 6.25 µg/mL against both strains. Compounds **I 244- I 249** were all effective against the fungi tested with MIC values ranging from 6.25-12.5 µg/mL. Overall, **I 245** displayed the highest activity against Gram-positive bacteria and **I 247** was the most effective against the fungi.

Chart I-32. Structures of Benzimidazolylidene Silver(I) Carbene Complexes **I 244- I 250**

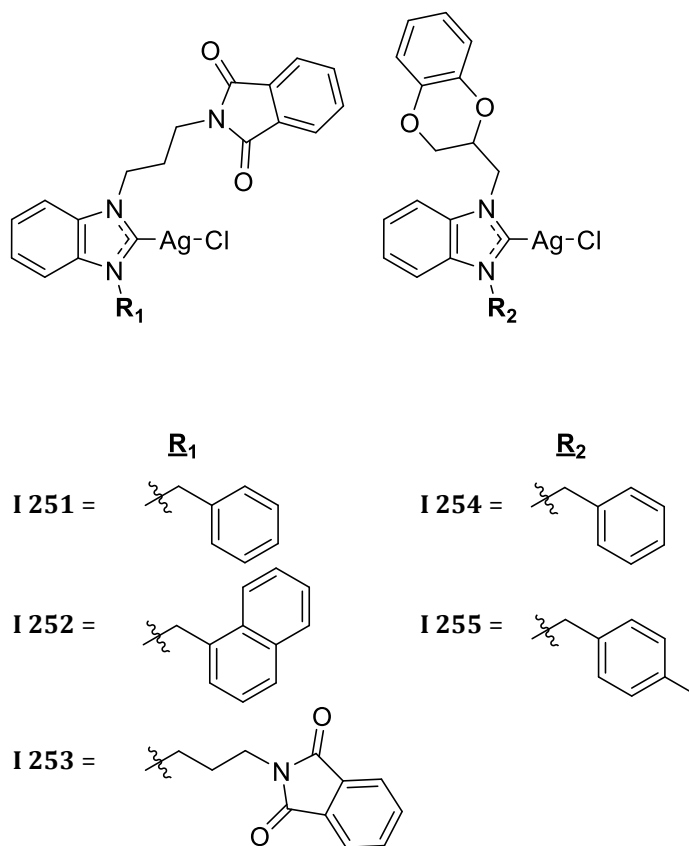


Sari et al. report the synthesis of benzimidazol-2-ylidene silver(I) NHC complexes from N-methyldioxane and N-propylphthalimide substituted benzimidazolium salts (Chart I-33).⁸² The salts were metalated with silver(I) oxide via the silver base technique to form the silver(I) chloride carbene complexes (**I 251- I 255**).

The agar dilution procedure was used to determine MIC's on bacterial strains (*E. coli*, *P. aeruginosa*, *S.aureus*, and *E. faecalis*) and broth dilution was used for the yeast strains (*C. albicans* and *C. tropicalis*). All of the compounds tested had had higher MIC values than the antibiotic controls, but overall compounds **I 252** (MIC =

25 µg/mL for yeast strains and 50 µg/mL for Gram-positive and Gram-negative strains) and **I 255** (MIC = 50 µg/mL for yeast strains and Gram-negative bacteria and 100 µg/mL for Gram-positive bacteria) had the highest activity. Compounds **I 251** and **I 253** displayed MIC values of 200 µg/mL for all strains tested, while compound **I 254** had MIC values of 100 µg/mL for all strains tested. The benzodioxane group of **I 254** versus the propyl phthalimide group of **I 251** may contribute to the higher activity of **I 254**. Complex **I 252** contained a naphthalene-1-ylmethyl group which, based on previous reports, contributed to a higher antimicrobial activity, a trend seen in this work as well.

Chart I-33. Structures of N-methyldioxane and N-propylphthalimide Functionalized Benzimidazolylidene Silver(I) Carbene Complexes **I 251- I 255**



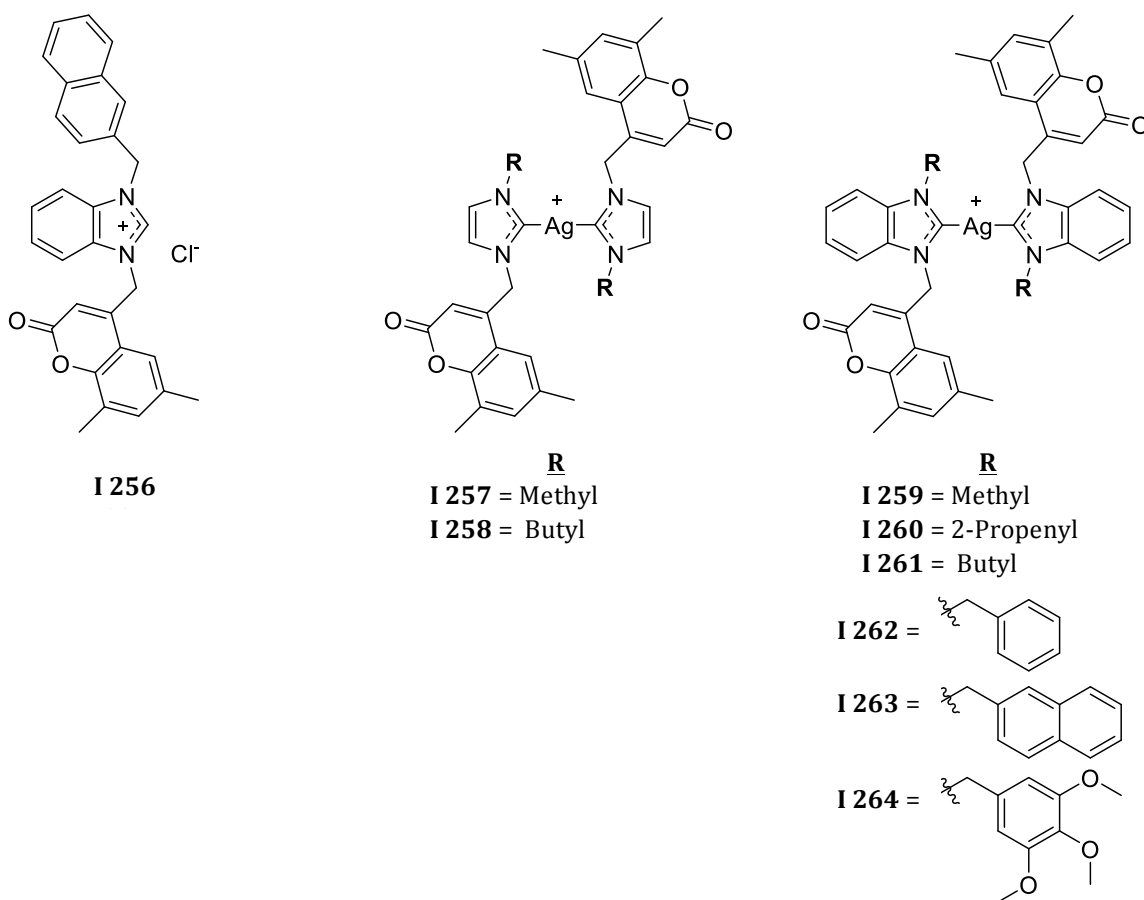
1.5.3. Coumarin Substituted Silver Benzimidazole NHC Complexes

Novel imidazol-2-ylidene silver(I) NHC complexes (**I 257- I 258**) as well as benzimidazol-2-ylidene silver(I) NHC complexes (**I 259- I 264**) were synthesized by the silver base method (Chart I-34).⁸³ The starting imidazolium salts were synthesized by reacting alkyl chlorides with 1-(4-methylene-6,8-dimethyl-2H-chromen-2-one)imidazole and 1-(4-methylene-6,8-dimethyl-2H-chromen-2-one)benzimidazole. These imidazolium salts were metalated with a half molar equivalent of silver(I) oxide to drive the formation of the bis-carbene complexes. The purpose of the coumarin substituent on the imidazole ring was to generate a dual drug complex, because coumarins can be anti-inflammatory as well as antibacterial.

MIC values were determined for both the ligand precursors and the silver complexes in Chart I-34. Gram-positive strains included *S. aureus* and *E. faecalis*, Gram-negative strains included *E. coli* and *P. aeruginosa* and fungal strains included *C. albicans* and *C. tropicalis*. Overall, all compounds exhibited cytotoxic activity at different levels. The silver complexes were more active than their ligand precursors alone. Compound **I 256** was found to be the imidazolium salt with the highest activity (25 µg/mL against both Gram-positive strains and both fungal strains and 400 µg/mL against Gram-negative strains) and is also the most lipophilic. All other imidazolium salts had values of 200 µg/mL or greater against the tested bacteria and fungi. Compound **I 256** showed higher inhibition, at 25 µg/mL, than seven of the silver complexes, with the exception of **I 263**, the corresponding silver complex of **I 256**, against the Gram-positive bacteria. Other notable compounds include **I**

262, which showed good inhibition (25 µg/mL) against the fungi strains and activity against *E. coli* with an MIC of 50 µg/mL. These results indicate that lipophilicity is important for activity.

Chart I-34. Structures of Silver(I) Bis-Carbene Complexes and the Benzimidazolium Salt Precursor



1.5.4. Silver Bis-Benzimidazole NHC Complexes

Haque et al. report novel silver NHC complexes for biological activity toward bacteria and cancer cells (Chart I-35).⁸⁴ Three benzimidazole-2-ylidene NHC complexes were synthesized via the metalation of benzyl and m-xylene substituted benzimidazolium hexafluorophosphate salts with silver(I) oxide. This reaction

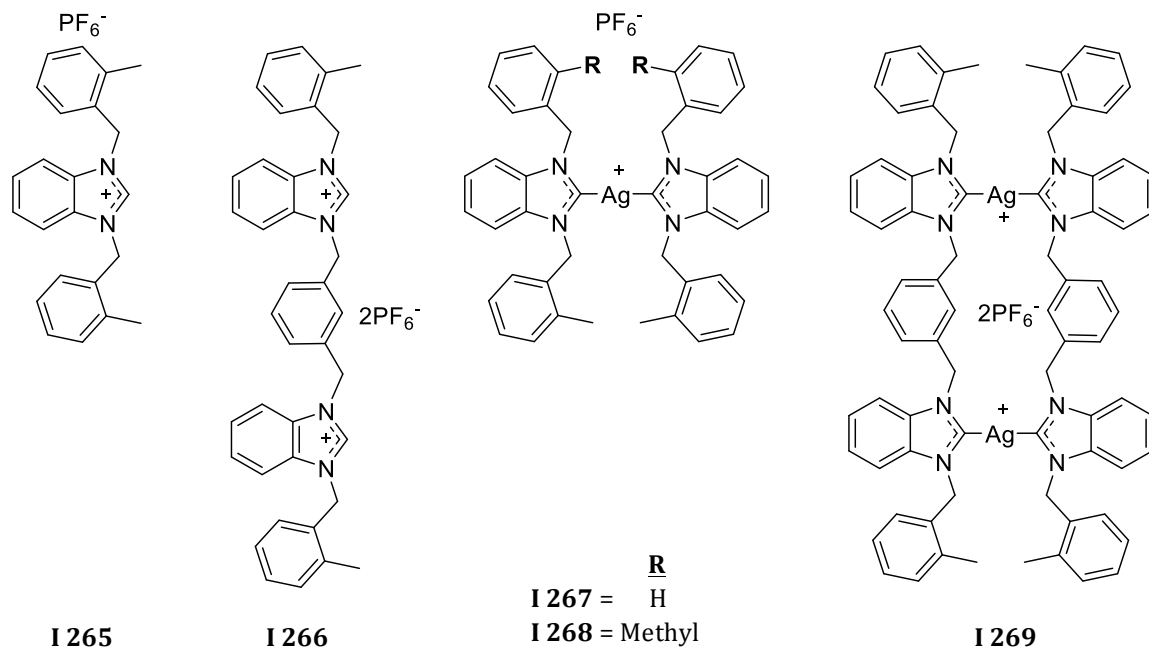
yielded bis-carbenes (**I 267** and **I 268**) for the mono-imidazolium salts and the dinuclear silver carbene (**I 269**) for the m-xylyl linked bis-imidazolium salt.

Antibacterial activity was tested against *E. coli* (Gram-negative) and *B. subtilis* (Gram-positive) and ampicillin was used as a standard. The mononuclear silver complexes **I 267** and **I 268** showed values of 16 ± 1 mm and 26 ± 1 mm against *E. coli*, respectively. Authors state that increased lipophilicity of **I 268** is the likely reason for a larger zone of inhibition. The binuclear complex, **I 269**, displayed less activity with an inhibition zone of 9 ± 1 mm, which is believed to be because of the slower release rate of the ligand. Benzimidazolium salts also displayed no activity against *B. subtilis* whereas the complexes **I 267**- **I 269** had a decreased activity, with inhibition values of 10 ± 1 mm, 16 ± 0 mm, and 16 ± 0 mm, respectively. MIC and MBC studies also showed low to moderate activity against the same strains, with values between 1.0-2.0 mg/mL for compounds **I 267**- **I 269** and no activity for the benzimidazolium salts.

Anti-cancer studies were also performed for the compounds in Chart I-35 using HCT-116 (human derived colorectal cancer) and HT29 (colorectal adenocarcinoma) cancer cells. The benzimidazolium salts exhibited lower anti-cancer activity as compared to the silver complexes. However, salts **I 265** (8.7 ± 0.8 μ M for HT29) and **I 266** (4.8 ± 0.6 μ M for HCT-116) showed higher activity in some cases than the standard, 5-fluorouracil (5.2 ± 0.3 μ M for HCT-116 and 10.0 ± 0.8 μ M for HT29). Overall, the silver complexes displayed higher activity against the cancer cell lines but with varying activity profiles against the two cell lines, suggesting the mechanism of action may be different in each cell line. For instance, complex **I 269**

displayed an IC_{50} value of $103.0 \pm 2.3 \mu M$ for HT29 and an IC_{50} value of $1.20 \pm 0.3 \mu M$ for HCT-116. This indicates that HCT-116 cells are more vulnerable to the silver carbene complexes.

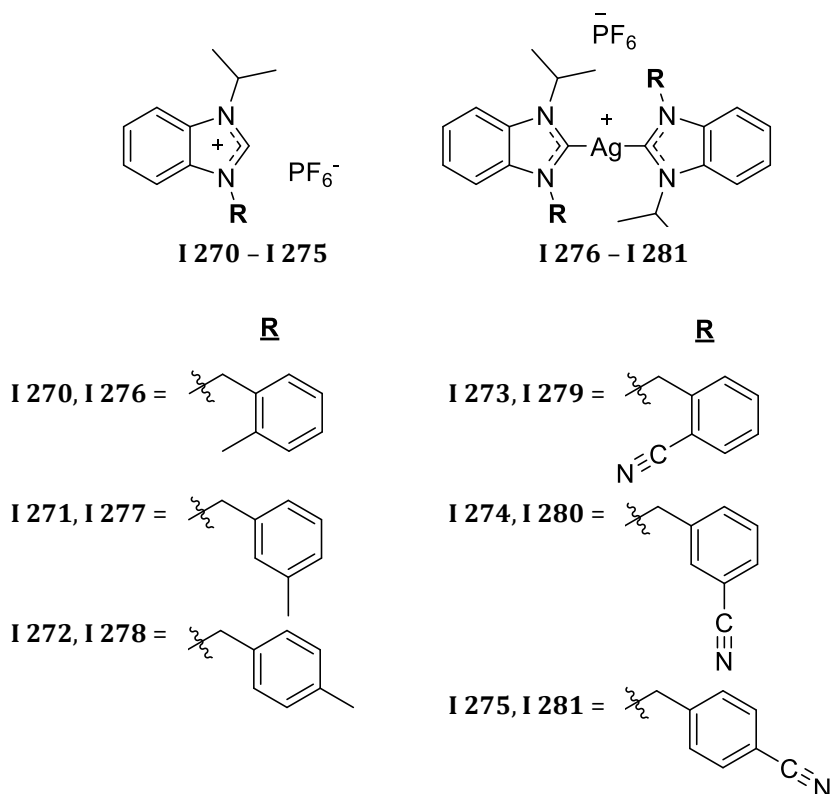
Chart I-35. Structures of Mono-Nuclear and Di-Nuclear Silver(I) Bis-Carbene Complexes and the Benzimidazolium Salt Precursors



Haque et al. also reported in 2016 the synthesis of six novel silver NHC complexes from various benzimidazolium salts derived from 1-isopropylbenzimidazole (Chart I-36).⁸⁵ The 1-isopropylbenzimidazole was alkylated with various aromatic substituents ranging from benzyl to benzonitriles. These imidazolium salts (**I 270- I 275**) undergo anion exchange via a metathesis reaction with potassium hexafluorophosphate. Then the compounds were metalated using silver(I) oxide to afford the final bis-NHC complexes (**I 276- I 281**).

The disc diffusion method was used to test the benzimidazole salts **I 270- I 275** and the silver complexes **I 276- I 281** against *E. coli* and *S. aureus*. No inhibition zone was seen for the benzimidazole compounds. Compound **I 278** showed the highest activity against *E. coli* (13 ± 1 mm at the highest concentration) while compound **I 276** showed the highest activity against *S. aureus* (14 ± 1 mm at the highest concentration). However, none of the complexes could surpass the inhibition caused by ampicillin.

Chart I-36. Structures of Silver(I) Bis-Carbene Complexes and the Corresponding Benzimidazolium Salt Precursors



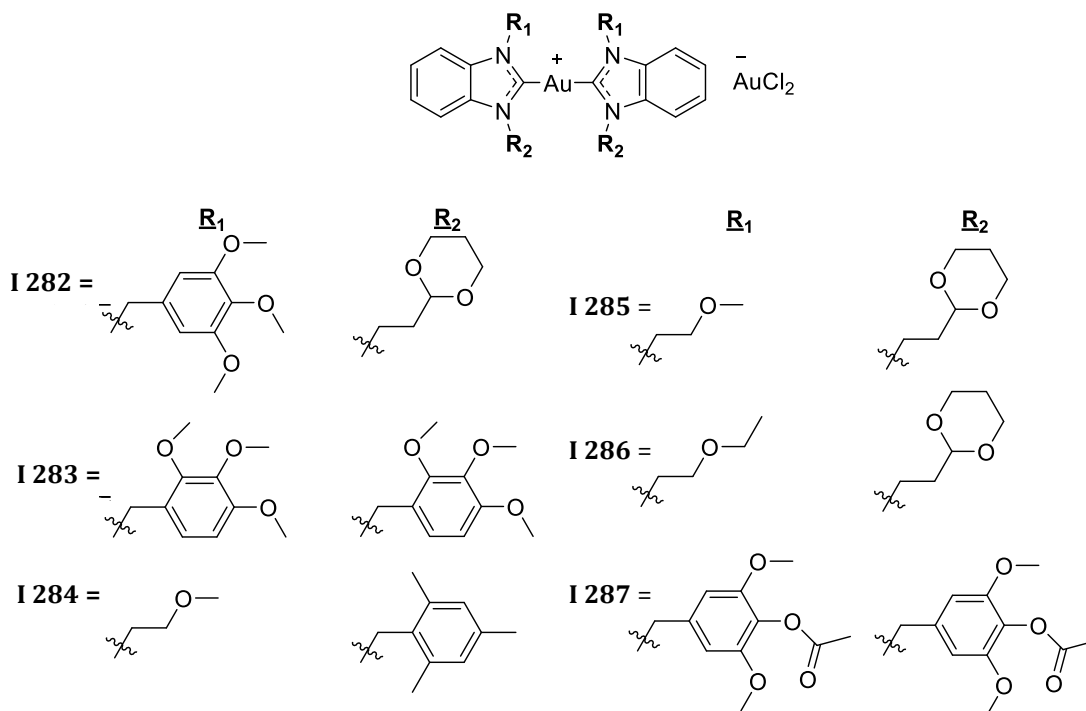
1.5.5. Gold and Palladium Mono-Nuclear Benzimidazole NHC Complexes

Various benzimidazolium salts were synthesized and metalated with gold(I) (Chart I-37).⁸⁶ These imidazolium salts were synthesized under standard

procedures via alkylation of the benzimidazole with alkyl halides. To prepare the bis-carbene gold(I) NHC complexes (**I 282**- **I 287**), the imidazolium salts were metalated with silver(I) oxide and then transmetalated with 0.5 equivalents of chloro(triphenylphosphine)gold(I).

The compounds in Chart I-37 were tested for antimicrobial activity. Gram-positive bacteria used were *S. aureus*, *E. faecalis* and Gram-negative bacteria used were *E. coli* and *P. aeruginosa*. They also tested against *C. albicans* and *C. tropicalis*. All values are reported as an MIC. Compound **I 282** had values ranging from 100-400 µg/mL for all strains tested and was the least active of the series. Complexes **I 283** and **I 284** had values of 12.5 µg/mL against *S. aureus* and the two fungal strains and activity values of 100 µg/mL against *E. coli* and differed in their values for *E. faecalis* (12.5 µg/mL for **I 283**, and 25 µg/mL for **I 284**) and *P. aeruginosa* (50 µg/mL for **I 283**, and 100 µg/mL for **I 284**). Complex **I 285** displayed values of 50 µg/mL for all strains except *E. coli* and *P. aeruginosa* in which the activity was 100 µg/mL. Against *E. faecalis* and *P. aeruginosa*, **I 286** and **I 287** had values of 100 µg/mL while **I 286** had values of 25 µg/mL and **I 287** had values of 50 µg/mL for the remaining strains tested. This data shows that the antimicrobial activity of these compounds is highly variable. This indicates that the ligand that the gold is bound to is important for overall activity. None of the compounds had lower MIC values than those of ampicillin, ciprofloxacin or fluconazole that were tested alongside the complexes (all values equal to or less than 3.12 µg/mL).

Chart I-37. Structures of Gold(I) Bis-Carbene Complexes **I 282- I 287**

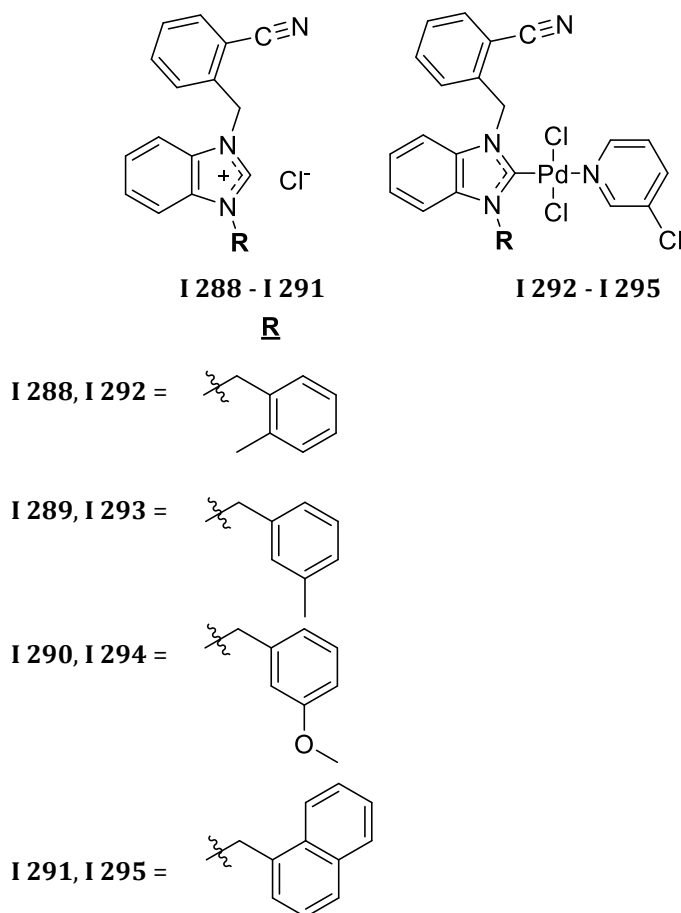


Akkoç et al. have developed palladium NHC complexes with 3-chloropyridine ligands (Chart I-38).⁸⁷ These complexes were synthesized via the reaction of various imidazolium salts with palladium(II) chloride, 3-chloropyridine, and potassium carbonate, the latter reagent serving to deprotonate the imidazolium salts. The imidazolium salt precursors (**I 288- I 291**) were synthesized from the reaction of 1-(methylbenzimidazole)benzimidazole with various aryl halides. To achieve the square planar palladium(II) complexes (**I 292- I 295**), 3-chloropyridine was added to serve as a ligand to the metal center.

An MTT assay was used to determine the compounds IC₅₀ values against cancer cell lines DLD-1 and MDA-MB-231 and a non-cancerous cell line, HEK-293T. Benzimidazoles (**I 288** = 38.95 ± 4.8->200 μM; **I 289** = 53.29 ± 3.7- 139.3 ± 3.4 μM; **I 290** = 57.2 ± 5.6- 161.46 ± 6.5 μM; and **I 291** = 5.630 ± 3.5- 48.58 ± 4.42 μM) had

higher anti-cancer activity than the Pd-NHC complexes (**I 292- I 295**; >200 μM for DLD-1 and MDA-MB-231 and >100 μM for HEK-293T). Compounds **I 288- I 291** had cytotoxicities higher than that of cisplatin (5.68 ± 2.8 - $34.83 \pm 2.14 \mu\text{M}$) with the exception of **I 291** against the HEK-293T normal cell line ($5.630 \pm 3.5 \mu\text{M}$ for **I 291** versus $34.83 \pm 2.14 \mu\text{M}$ for cisplatin). Benzimidazoles **I 288- I 291** all had lower IC_{50} values against the normal cell line than the cancerous cell line. The complexes **I 292- I 295** did not have any discernable cytotoxicity at the concentrations tested.

Chart I-38. Structures of Palladium(II) Carbene Complexes and the Corresponding Benzimidazolium Salt Precursors



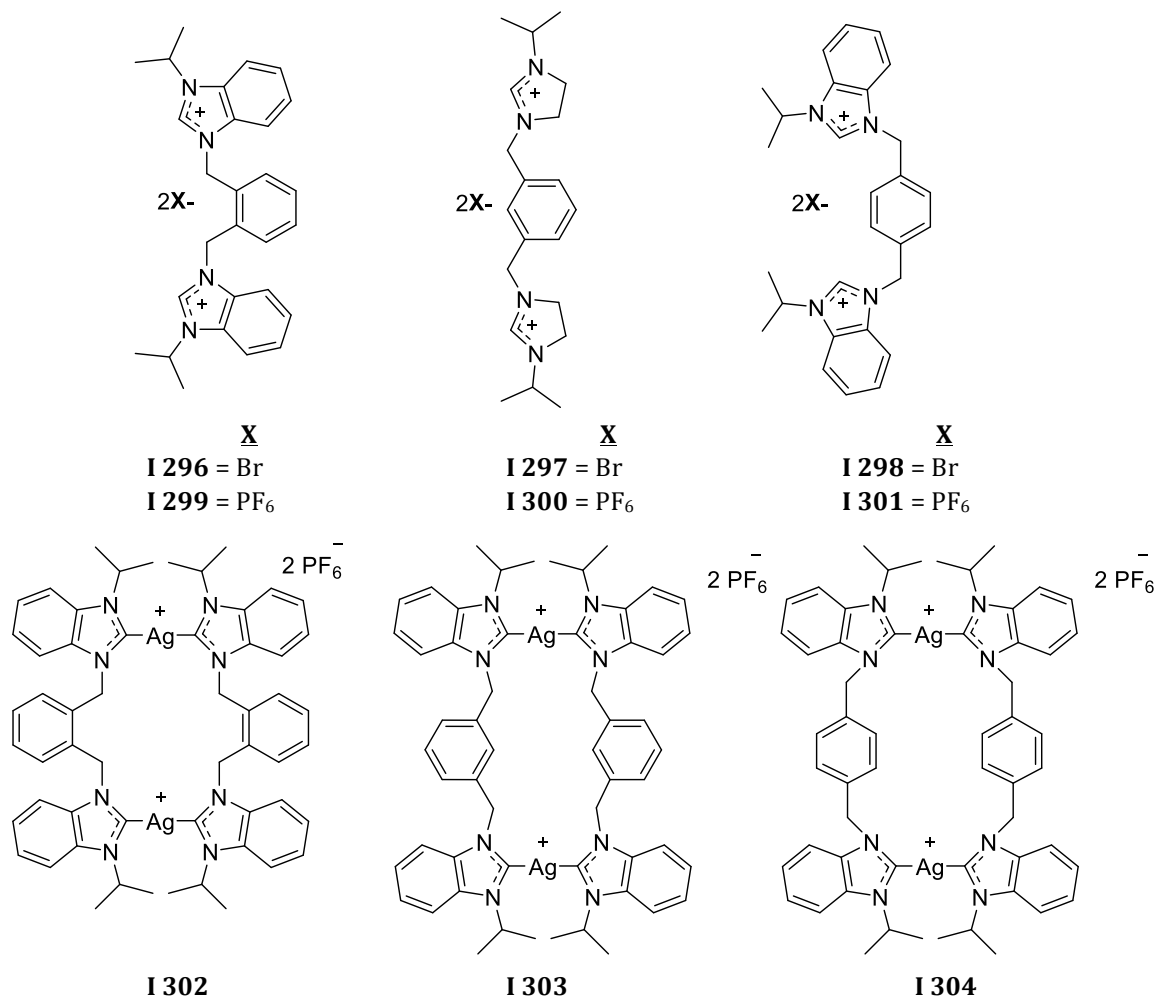
1.6. Di-Nuclear Benzimidazole NHC Complexes

1.6.1. Silver Di-Nuclear Bis-Benzimidazole NHC Complexes

Iqbal et al. report the synthesis of dinuclear silver(I) NHC complexes with ortho, para, and meta xylyl linkers (Chart I-39).⁸⁸ The imidazolium salts (**I 296- I 301**) were synthesized via standard alkylation of 1-isopropylbenzimidazole with xylyl bromide. The imidazolium salts were metalated with silver(I) oxide, to form the cyclic dinuclear silver NHC complexes **I 302- I 304**. The PF₆⁻ imidazolium salts were also used, but unlike previous work stating PF₆⁻ facilitates the bis-carbene formation, Iqbal and coworkers report PF₆⁻ anions are utilized for purification purposes.

For this study the MTT assay was utilized on HCT-116 cells to determine cytotoxicity. The bis-benzimidazolium salts with the bromide anion were found to be much more cytotoxic versus complexes with the PF₆⁻ anion (IC₅₀ values of >200 μM for **I 299- I 301**). The IC₅₀ values of the silver complexes **I 302- I 304** (43, 44.5, and 9.7 μM, respectively) were shown to be better in most cases than those of their benzimidazolium salts alone (85, 0.2, and 157.52 μM for **I 296- I 298**, respectively). Microscopic studies also point to apoptosis as the cell death pathway. Authors suggest that lipophilicity plays a large role in the efficacy of these compounds and that inclusion of silver also increases activity. It was also suggested that **I 304** had the highest cytotoxicity because it has the largest cavity, being the para-xylyl linked complex, which increases the NHC ring exposure.

Chart I-39. Structures of Di-Nuclear Silver(I) Bis-Carbene Complexes and the Bis-Imidazolium Salt Precursors



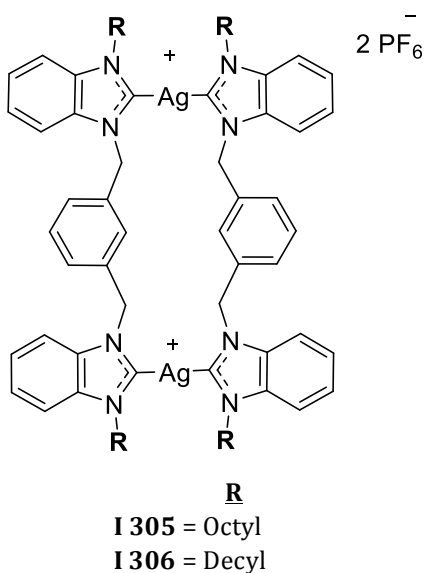
The work continued by Asif et al. pertains to meta substituted xylene linked benzimidazolium salts and their silver metalated NHC counterparts (Chart I-40).⁸⁹ The synthesis has been adapted from Iqbal et al.⁸⁸ to increase lipophilicity with octyl (**I 305**) and decyl (**I 306**) substituents on the imidazole nitrogen atoms.

Cell lines used include HCT-116 (colorectal carcinoma), HT-29 (colorectal adenocarcinoma), MCF-7 (breast cancer), MDA-MB-231 (breast cancer), PANC-1 (pancreatic cancer), SH-SH5Y (neuroblastoma), U-937 (malignant monocytes), and

3T3 L1 (normal mouse fibroblasts). Compounds were tested by the MTT assay. Silver complex **I 306** (decyl) was found to be more cytotoxic than **I 305** (octyl). A selectivity index was calculated showing that **I 306** was toxic towards HCT-116, U-937 and PANC-1 cancer cells. Morphological studies show less changes to the normal cell line by **I 305** and **I 306**. HCT-116 was the chosen cell line for further studies.

Using Rhodamine 123, compound **I 306** decreased the fluorescent signal indicating mitochondrial membrane damage and activation of apoptosis. Furthermore, an increase in Hoechst 33258 fluorescence was seen in a similar study, also indicating membrane permeability during apoptosis. Using cell migration and colony formation assays, the anti-metastatic nature of **I 306** was revealed. These results indicate that an increase in lipophilicity, such as a change from octyl to decyl, can increase cytotoxic activity.

Chart I-40. Structures of Di-Nuclear Silver(I) Bis-Carbene Complexes **I 305** and **I 306**



1.7. Other Compounds

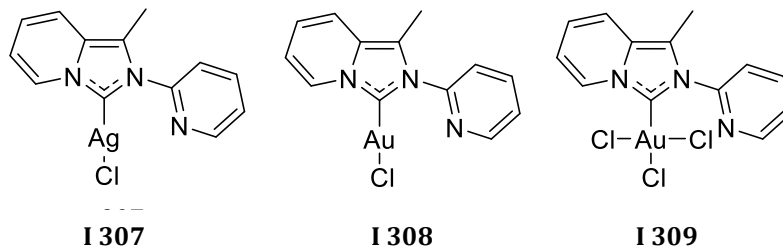
1.7.1. Annelated NHC Complexes with Pyridine Wingtip Substituents

Bielawski and coworkers report the synthesis and biological testing of annelated NHC complexes with pyridine wingtip substituents (Chart I-41).⁹⁰ To form these silver chloride NHC complexes, 1-methyl-2-pyridin-2-ylimidazo[1,5- α]pyridin-4-ylum chloride was reacted with 0.5 equivalents of silver(I) oxide to afford the silver chloride NHC complex (**I 307**). Then transmetalation from the silver(I) NHC (**I 307**) to gold(I) (**I 308**) occurred via reaction with Au(SMe₂)Cl. In order to obtain the gold(III) complex (**I 309**), a disproportionation reaction was used, by adding excess Au(SMe₂)Cl to the previously mentioned gold(I) complex (**I 308**). These syntheses result in the silver(I) (**I 307**), gold(I) (**I 308**), and gold(III) (**I 309**) NHC complexes shown in Chart I-41.

An MTT assay was used to determine the IC₅₀ values of compounds **I 307- I 309** on HepG2, HCT-116, A549, and MCF-7 cell lines. Overall, the gold(I) complex **I 308** (IC₅₀ = 4.91 ± 3.6 μM for HepG2; 5.08 ± 3.8 μM for HCT-116; 5.23 ± 2.96 μM for A549; 5.18 ± 1.35 μM for MCF-7) had slightly higher activity than the silver(I) complex **I 307** (IC₅₀ = 7.57 ± 4.06 μM for HepG2; 5.67 ± 2.29 μM for HCT-116; 6.23 ± 1.49 μM for A549; 6.42 ± 0.78 μM for MCF-7) or the gold(III) complex **I 309** (IC₅₀ = 7.01 ± 1.65 μM for HepG2; 5.98 ± 2.17 μM for HCT-116; 6.56 ± 1.42 μM for A549; 4.96 ± 1.43 μM for MCF-7), which the authors believe is related to lipophilicity and presence of chloride ligands. Complex **I 308** also displayed comparable activity to cisplatin (IC₅₀ = 4.31 ± 1.10 μM for HepG2; 4.89 ± 2.29 μM for HCT-116; 6.12 ± 3.67 μM for A549; 4.42 ± 1.02 μM for MCF-7). It was also suggested that the decreased

activity of **I 309** is due to reduction of Au(III) to Au(I) by thiols. Complex **I 308** exhibited an apoptotic mode of cell death in HepG2 cells via DAPI and Annexin V staining. Further studies showed that complex **I 308** may lead to cell cycle arrest in the G2/M phase and also increases ROS generation in HepG2 cells. Complex **I 308** was also shown to affect the expression of apoptotic proteins such as an increase in Bax, decrease of Bcl-2, increased cytosolic cytochrome c and increased PARP cleavage. Therefore, it was concluded that **I 308** causes cell death via a mitochondrial pathway.

Chart I-41. Structures of Pyridine Wing-tip Functionalized Gold(I) Carbene Complexes



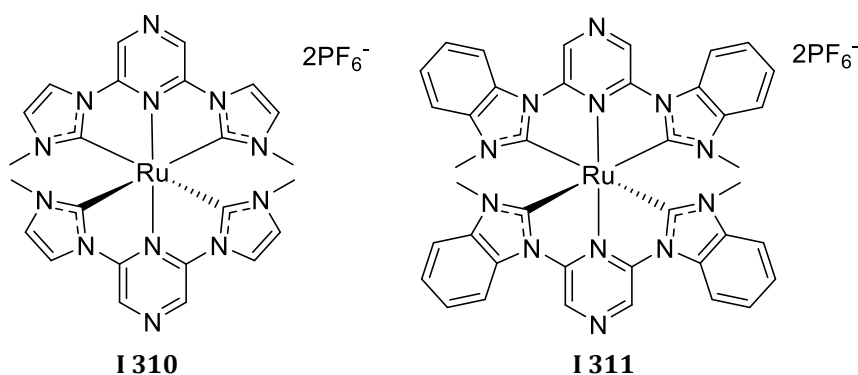
1.7.2. Octahedral Ruthenium(II) Tridentate NHC Complexes

Roymahapatra et al. have synthesized tridentate imidazolium precursor ligands for the formation of ruthenium(II) NHC octahedral complexes (**I 310** and **I 311**; Chart I-42).⁹¹ The tridentate ligands were formed via alkylation of 1-methylimidazole and 1-methylbenzimidazole with the 2,6-dichloropyrazine. The bis-imidazolium salts were then metalated with RuCl₃ and the chloride anion was exchanged with PF₆⁻ for ease of purification.

An MTT assay was used to test cytotoxicity of complexes **I 310** and **I 311** against human colon carcinoma (HCT15) and human epidermoid cancer cells

(Hep2). Overall, complex **I 310** had higher anti-cancer activities than complex **I 311**, with a 3 to 4 fold increase in activity. Complex **I 310** displayed IC_{50} values of $22.70 \pm 1.3 \mu\text{M}$ and $18.46 \pm 2.3 \mu\text{M}$ while complex **I 311** had values of $82.2 \pm 4.6 \mu\text{M}$ and $61.8 \pm 3.3 \mu\text{M}$ against HCT15 and Hep2, respectively. Gel electrophoresis of supercoiled plasmid DNA after treatment with complex **I 310** showed that **I 310** could aggregate and also nick the supercoiled DNA. CD spectroscopy also indicates an interaction between **I 310** and CT DNA. Complex **I 310** was also shown to contribute to cell cycle arrest in the G0-G1 phase in HCT15 cells. Complex **I 310** also exhibited better antibacterial and antifungal activity than complex **I 311** with IC_{50} values ranging from 8-16 μM for **I 310** and 64-256 μM for **I 311**. SEM images indicated that **I 310** could interact with and damage the cell wall of *C. albicans*. This led the authors to conclude that damage to the cell wall may be the primary mechanism of action for complex **I 310**.

Chart I-42. Structures of Tridentate Bis-Imidazolylidene Ruthenium(II) Carbene Complexes



1.7.3. Terpyridal Platinum(II) Xanthine NHC Complexes

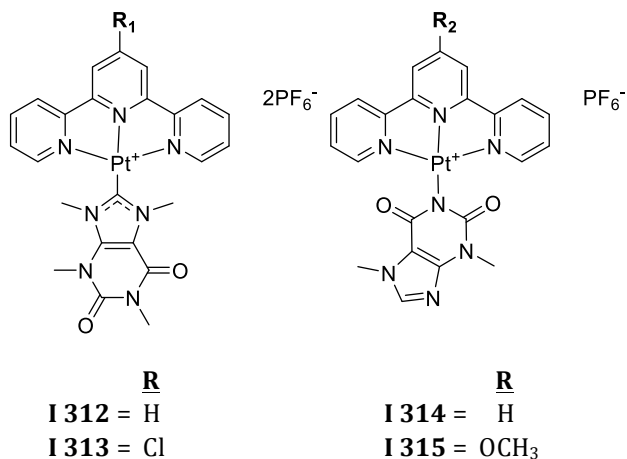
Ott and coworkers report the synthesis of methylated caffeine based platinum(II) NHC complexes with the application as anti-cancer materials (Chart I-43).⁹² The platinum(II) coordination precursors were synthesized first via displacement of a chloride ligand with a dimethyl sulfoxide molecule off of the chloro(2,2':6',2''-terpyridine)platinum(II) chloride complexes. The platinum(II) precursors were then reacted with silver trifluoromethanesulfonate to exchange the halide ligands to triflates. Upon halide ligand exchange, the platinum complexes were reacted with 1,3,7,9-tetramethylxanthinium salt under basic conditions to afford the platinum(II) NHC complexes (**I 312** and **I 313**). The NHC salt complexes then underwent a metathesis reaction to exchange anions to PF₆⁻. Additionally theobromine platinum(II) coordination complexes **I 314** and **I 315** were synthesized for a comparison between the activity of non-NHC complexes and NHC complexes **I 312** and **I 313**.

The crystal violet assay was used to determine *in vitro* toxicities against MCF-7, MDA-MB-231, and HT-29 cancer cell lines. Compounds **I 314** and **I 315** did not display significant activity. The carbene complexes exhibited high activity with a range of IC₅₀ values between 0.24-0.83 μM in contrast to the other analogues that had no observable activity. Platinum complexes **I 312** and **I 313** also displayed higher activity than cisplatin. Further studies were completed, in particular comparing **I 312** and **I 314**, to determine how the effect of the coordination placement of the xanthine ligand can alter activity.

MCF-7 cells were treated with **I 312**- **I 315** at various concentrations to evaluate morphological changes via light microscopy. The changes observed indicate that the MCF-7 cells were undergoing differentiation-like changes. However, the authors note that further studies would need to be completed to confirm this. Changes occurred dependent on the compound concentration, which was much lower for **I 312** and **I 313** (1.6 μM and 3.1 μM , respectively) than it was for **I 314** and **I 315** (400 μM for both compounds).

A tube-formation assay was used to study the potential for these compounds to have anti-angiogenic effects. All compounds were found to inhibit tube-formation. The authors also note that TrxR inhibition was studied for compounds **I 312** and **I 314**, however there was not enough inhibition to say that this is the primary mechanism of action of these platinum complexes. The authors note that both the double positive charge and coordination mode of complexes **I 312** and **I 313** show an increased activity and give important insight into the structure activity relationship of these compounds.

Chart I-43. Structures of Xanthine Derived Platinum(II) Carbene Complexes (**I 312**- **I 313**) and Xanthine Coordination Complexes (**I 314**- **I 315**)



1.7.4. Naphthoquinone Gold(I) NHC Complexes

Sessler, Arumugam, Arambula and coworkers report the synthesis of 1,4-naphthoquinone gold(I) NHC complexes as anti-cancer compounds (Chart I-44).⁹³ The naphthoquinone imidazolium salt (**I 319**) was synthesized via a literature procedure. The quinone species was N,N functionalized with mesityl substituents and then metalated via silver(I) oxide to produce the silver NHC complex. Depending on concentration of silver(I) oxide multiple complexes formed ranging from bis-carbenes to mono-carbenes. The gold complexes (**I 316- I 318**) were achieved through transmetallation of the silver NHC complexes using chloro(tetrahydrothiophene)gold(I). Interestingly, this naphthoquinone core is similar to that seen in the structure of YM155, an imidazolium salt that went through clinical trials. YM155 will be discussed in detail in the imidazolium salt portion of this review. The well known chemotherapeutic Doxorubicin also contains a quinone group.

Compounds were tested using the MTT assay on A549 cells and compared to the control complex **I 320**. The most active compounds were found to be **I 316** and **I 317** with IC_{50} values of $0.073 \pm 0.016 \mu\text{M}$ and $0.075 \pm 0.013 \mu\text{M}$, respectively. Although compound **I 318** displayed an IC_{50} value of $12.06 \pm 0.18 \mu\text{M}$, it was considered inactive due to the fact that it was more than 150x less active than **I 316**. The imidazolium salt **I 319** also had high activity with an IC_{50} value of $0.994 \pm 0.12 \mu\text{M}$.

ICP-MS was used to determine the concentration of gold levels inside the cell. A549 cells were treated with either **I 316**, **I 318**, **I 320**, or auranofin and tested via

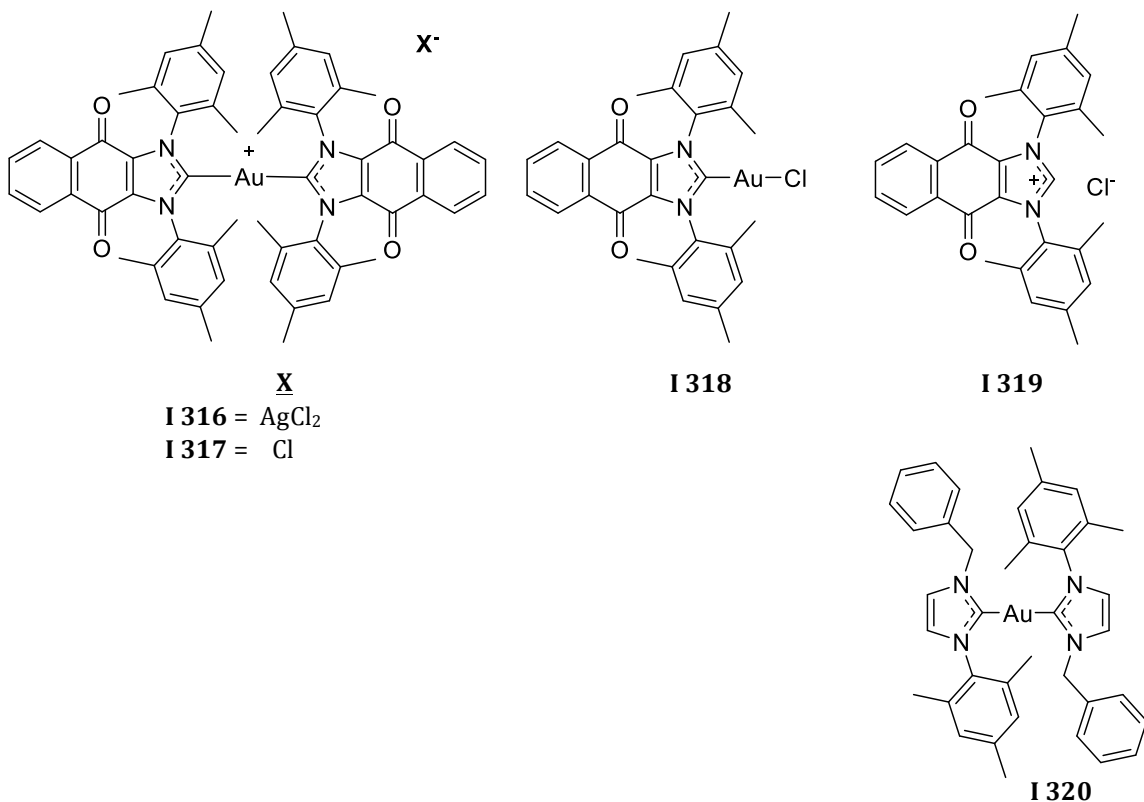
ICP-MS. Intracellular levels of gold for auranofin were 2-5 fold higher than found for cells treated with **I 316**. The neutral compound **I 318** did not show any intracellular gold, with complexes **I 316** and **I 320** showing similar results. ICP-MS was also used to detect free gold in samples of fetal bovine serum (FBS) that were treated with **I 316**, **I 318**, or auranofin. Free gold decreased over time in samples with auranofin, similar to what was observed for **I 318**. However, complex **I 316** displayed minimal changes in the free gold concentration. This lead the authors to believe that complex **I 316** has an alternative way to enter the cell as compared to auranofin and that the differences in binding of gold between **I 316** and **I 318** contribute to the difference in efficacy.

Using flow cytometry to study ROS production indicated that complex **I 316** induced increase in ROS production inside the cell. Confocal microscopy was used to determine the locale of ROS, which was found to be the mitochondria. In addition, to determine the ability to inhibit TrxR, a colorimetric experiment to monitor the reduction of lipoate was employed. In A549 cells, complex **I 316**, auranofin and **I 319+ I 320** showed an inhibition of TrxR at low concentrations. The authors proposed, based on this work, that **I 316** could act as an inhibitor of TrxR. Apoptosis was also studied for complex **I 316** and it was found that **I 316** could induce apoptosis in A549 cells, utilizing flow cytometry with Annexin V/PI staining.

Complex **I 316** was also tested for toxicity in zebrafish, finding that the maximum tolerated dose (MTD) of **I 316** was 0.5 μM . Zebrafish were then inoculated with CM-Dil A549 cells and treated with complex **I 316** for one day. Those treated with complex **I 316** showed green fluorescence from acridine orange

indicating cancer cell apoptosis. Authors determined that complex **I 316** enters cells better than the neutral complex **I 318**.

Chart I-44. Structures of Quinone Functionalized Imidazolylidene Gold(I) Carbene Complexes and Bis-Carbene Complex, **I 320**



1.7.5. Protoporphyrine Gold(I) NHC Complexes

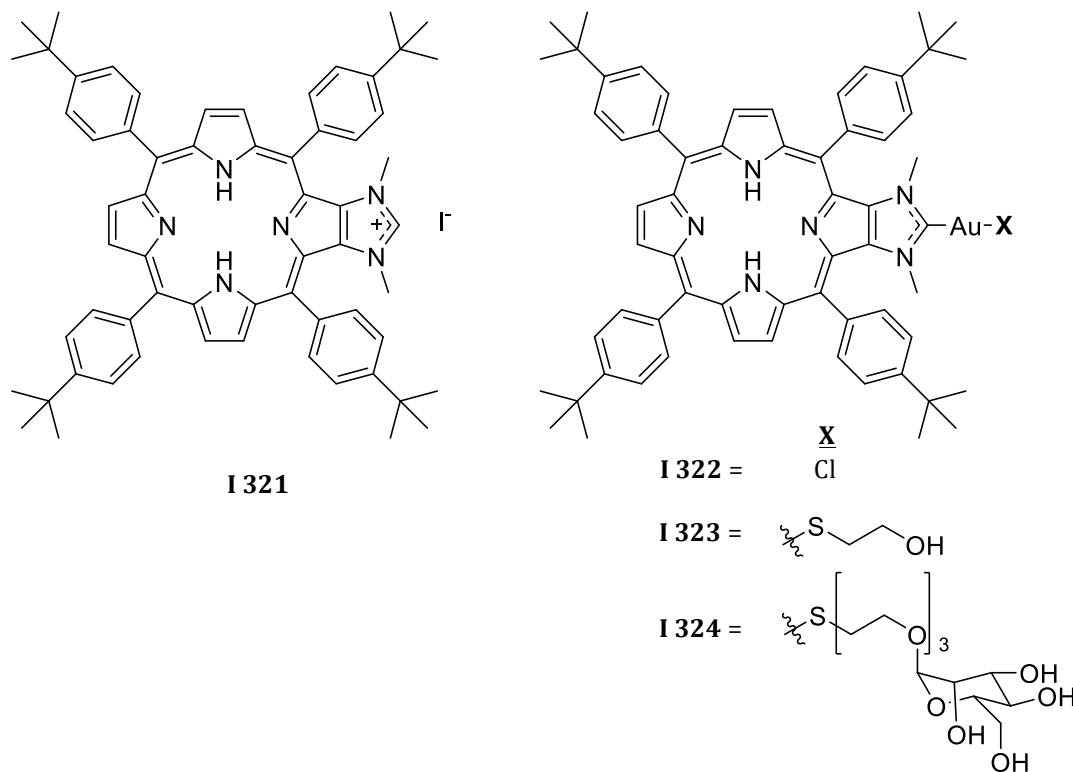
Richeter and co-workers synthesized a protoporphyrin conjugated imidazolium salt (**I 321**) and a nickel porphyrin conjugated imidazolium salt with the purpose of forming gold(I) NHC conjugated complexes for photodynamic therapy (Chart I-45).⁹⁴ The nickel and proto-porphyrin NHC complexes were synthesized via standard literature procedure. The imidazolium salt precursors were metalated using silver(I) oxide then transmetalated to gold(I) with chloro(tetrahydrothiophene)gold(I). In order to obtain the metal free

protoporphyrin, the zinc porphyrin Au(I) NHC complex was reacted with trifluoroacetic acid. The chloride NHC complexes of the protoporphyrin complex (**I 322**) was then substituted with mercaptoethanol (**I 323**) or mannose (**I 324**) by deprotonation of the thiol with potassium-t-butoxide. In addition to the thiol protoporphyrins the nickel complexes were also substituted with mercaptoethanol and mannose. The purpose of the mannose moiety is to increase solubility as well as help target cancer cells. Once these complexes were synthesized, the photodynamic activity via detection of singlet oxygen when photo-irradiated was tested. It was determined that the generation of singlet oxygen drives the loss of the mannose ligand by cleaving the weak Au-S bond. The nickel complex is stable and does not have a loss of the mannose ligand or generation of singlet oxygen. This is believed to be due to the nickel metal preventing the singlet to triplet transition, which is necessary for singlet oxygen production. For this reason, only the anti-cancer properties of complexes **I 322- I 324** were able to be tested.

An MTT assay was used on MCF-7 cells that were treated with the photosensitizer compounds either in the dark or irradiated with 405 nm light for 10 minutes. None of the compounds, **I 321**, **I 322**, **I 323**, or **I 324**, displayed any activity when left in the dark with less than 5% cell death at a concentration of 5 μ M. This indicates that the gold NHC moiety does not have any cytotoxic activity at the concentrations tested. Complex **I 324** showed a 37% cell death upon irradiation while concurrently having no activity in the dark. At a concentration of 10 μ M **I 324** showed 100% cell death when irradiated. When combined with mannose, **I 324** showed no significant cell death however, in the absence of mannose 33% cell death

was observed. This indicated that the mannose receptors are integral for **I 324** involvement in cancer cell death.

Chart I-45. Structures of Porphyrine Imidazolylidene Gold(I) Carbene Complexes and the Imidazolium Salt Precursor, **I 321**



1.7.6. Triazole Containing NHC Complexes

Pellei et al. report the synthesis of bis-1,4-(p-nitrobenzyl) triazol-5-ylidene silver, gold, and copper metal NHC complexes (Chart I-46).⁹⁵ The starting triazolium salt (**I 325**) was synthesized under similar procedures to that of imidazolium salts, in that it underwent alkylation with aryl or alkyl halides. The silver(I) bromide NHC complex (**I 326**) was obtained by the reaction of the triazolium salt with silver(I) oxide. From the silver complex **I 326**, transmetalation was performed via (CH₃)₂SAuCl in methylene chloride to yield the gold(I) bromide complex (**I 327**). To

produce the copper(I) NHC (**I 328**) the triazolium salt was reacted with copper(I) oxide through the metal base reaction pathway.

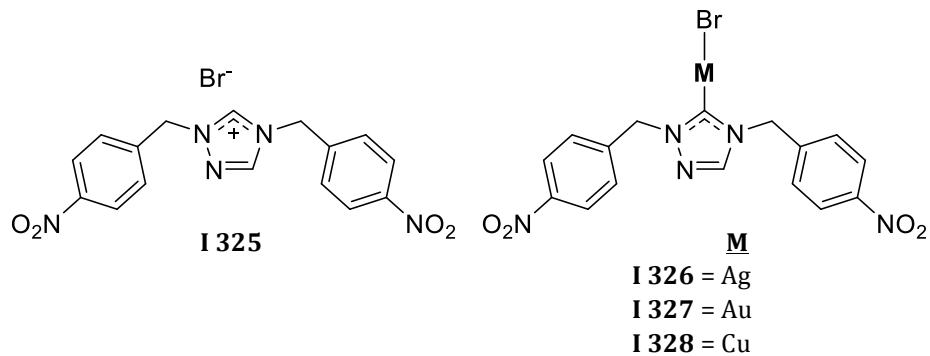
Cell lines used in this study include cervical cancer A431, colon cancer HCT-15, pancreatic cancer BxPC3, lung cancer A549, breast cancer MCF-7, cisplatin-sensitive ovarian cancer 2008, cisplatin-resistant ovarian adenocarcinoma C13*, melanoma A375, and osteosarcoma U-2 OS. The normal cell line HEK293 (human embryonic kidney cells) were tested as well. Cytotoxicity was determined by the MTT assay. The precursor ligand, compound **I 325**, was found to be completely ineffective against all of the cell lines tested with IC_{50} values of $>100 \mu\text{M}$. The copper complex **I 328** was found to have IC_{50} values (ranging from $0.48 \pm 0.39 - 7.27 \pm 3.15 \mu\text{M}$ for the cancer cell lines and a value of $7.75 \pm 2.08 \mu\text{M}$ for the normal line HEK293) that were 3-fold lower than the silver complex, **I 326** ($4.56 \pm 2.06 - 19.62 \pm 1.77 \mu\text{M}$ for the cancer cell lines and $18.75 \pm 3.36 \mu\text{M}$ for the normal cell line HEK293), and 8-fold lower than the gold complex, **I 327** ($19.25 \pm 2.15 - 53.13 \pm 3.03 \mu\text{M}$ for the cancer cell lines and $29.84 \pm 4.29 \mu\text{M}$ for the normal cell line HEK293). In some cases, the copper complex also displayed higher activity than cisplatin ($1.64 \pm 0.51 - 24.46 \pm 3.03 \mu\text{M}$ for the cancer cell lines and $19.75 \pm 2.29 \mu\text{M}$ for the normal cell line HEK293). Complex **I 326**, the silver NHC, was found to have higher activity than cisplatin for the HCT-15 cell line, while the gold complex was not shown to be more effective than cisplatin against any of the cell lines. The MTT data also indicates that NHC complexes can be effective in cisplatin resistant cell lines. Selectivity for cancer cells was observed in some cases for both the silver and copper NHC complexes.

Graphite furnace atomic absorption spectroscopy (GF-AAS) was used to evaluate intracellular accumulation of the NHC complexes. It was found that accumulation occurred was proportionally dependent on concentration and time. However, the copper complex (**I 328**) was found to have a 5-fold and 14-fold larger uptake compared to the silver (**I 326**) and gold complexes (**I 327**), respectively.

Lipophilicity of each complex was determined via an n-octanol/water partition test. This showed that the silver and copper complexes (**I 326** and **I 328**, respectively) had very similar Log P values while the gold complex was much more lipophilic. In this case, increased lipophilicity did not correlate to better activity, suggesting that transport may occur via active transport rather than passive diffusion.

TrxR inhibition was also studied. Both the silver (**I 326**) and gold (**I 327**) complexes inhibited mammalian TrxR1 but the copper complex did not affect its activity *in vitro*. The same trend was seen in A431 cells. Further studies showed an apoptotic mechanism of cell death via adjustment of the redox state of the cells.

Chart I-46. Structures of Triazolylidene Metal Carbene Complexes and the Corresponding Imidazolium Salt Precursor

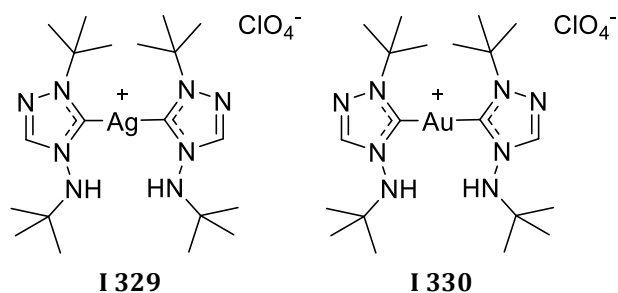


Ott and coworkers also reported the synthesis of novel triazolium silver(I) NHC complexes (Chart I-47).⁹⁶ The synthesis began with 1-t-butyl-4-(t-butylamino)-1,2,4-triazolium perchlorate being metalated via addition of silver(I)oxide. It was observed that the silver base technique did not form the NHC complex. In order to facilitate the reaction potassium carbonate or sodium carbonate must be added to the reaction mixture. The product formed from this reaction was the bis-carbene silver(I)complex (**I 329**), which forms primarily due to the weakly coordinating anion ClO_4^- having little interaction with silver(I) oxide. To produce the gold(I) NHC complex **I 330**, an equivalent of chloro(dimethylsulfide) gold(I) was reacted with complex **I 329**.

Two cancer cell lines were used in this study, HT-29 colon cancer cells and MDA-MB-231 breast cancer cells. Against both cell lines, gold complex **I 330** showed good IC_{50} values (HT-29 = $2.1 \pm 0.0 \mu\text{M}$; MDA-MB-231 = $1.0 \pm 0.0 \mu\text{M}$). The precursor ligand showed no activity. TrxR inhibition was also observed with an IC_{50} value of $1.2 \pm 0.6 \mu\text{M}$ via the DTNB reduction assay.

High-resolution continuum source atomic absorption spectroscopy (HR-CS AAS) was used to determine the concentration of gold taken in by HT-29 cells treated with **I 330** at various concentrations and time points. Authors concluded that **I 330** is taken up quickly by cells, due to the fact that intracellular concentrations at 1 hour and 4 hours were comparable with a decrease at 8 hours. Also, **I 330** was taken up by cells in an incredible amount compared to the medium, with a 45-fold increase of the intracellular concentration.

Chart I-47. Structures of Triazolylidene Silver(I) and Gold(I) Carbene

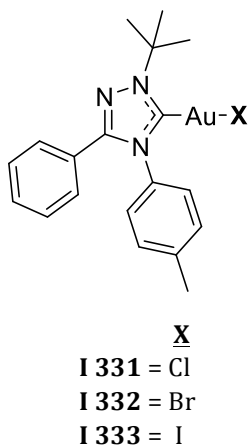


Turek and co-workers have also reported synthetic methods to produce gold(I) triazolium NHC complexes (Chart I-48).^{97,98} The syntheses of these complexes were investigated to determine if amino substituted triazoles would inhibit the linear structure of silver, copper, and gold NHC complexes. The NHC complexes that were tested for biological activity were the gold(I) complexes **I 331-I 333** and were produced via metalation of 1-tert-butyl-4-{2-[(dimethylamino)methyl]phenyl}-3-phenyl-4H-1,2,4-triazol-1-ium perchlorate by free carbene formation with addition of AuCl or transmetalation from the silver carbene with (SMe₂)AuCl. Additionally the halide ligand was exchanged using triorganotin(IV) halides where the halogen was a bromide or iodide.

Cytotoxicity of compounds was tested on HL-60 (promyelocytic leukemia), HepG2 (hepatocellular carcinoma), HeLa S3 (cervical carcinoma) and CCRF-CEM (T-lymphoblastic leukemia) cell lines using the XTT assay. All IC₅₀ values were in the low micromolar range for the compounds tested while the **I 333** gold complex displayed the least amount of activity. The authors note that if the difficulties in solubility are addressed, it is likely that the cytotoxicities will be increased.

It was also determined that all compounds tested could increase the number of apoptotic CCRF-CEM cells and that **I 332** was the best compound at inducing apoptosis. All compounds were able to increase the sub-G1 population of cells by 44-58%. In contrast, auranofin was shown in previous studies to cause cell cycle arrest in the G1 phase of treated MCF-7 cells. The authors note this is a good indication that the mechanism of the newly synthesized compounds may differ from that of auranofin.

Chart I-48. Structures of Triazolylidene Gold(I) Carbene Complexes **I 331- I 333**



1.8. Imidazolium Salts

1.8.1. Application of Imidazolium Salts

Imidazolium salts can be used for a variety of applications. One such application utilizes imidazolium salts as precursors to free and metal N-heterocyclic carbenes (NHCs).⁹⁹ Robert Grubb's shared the Nobel Prize in Chemistry in 2005 for his work on olefin metathesis that included his well-known ruthenium NHC second-

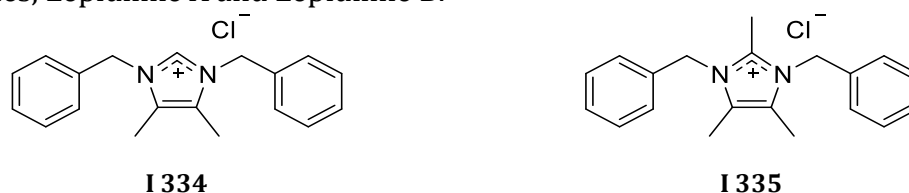
generation catalyst.¹⁰⁰ Arduengo also played a major role in carbene chemistry as he was the first to isolate and characterize by X-ray crystallography a free N-heterocyclic carbene, as mentioned previously.¹⁰¹ Another application of imidazolium salts deals with their ability to form ionic liquids which has allowed the field of ionic liquid imidazolium salts as green solvents to rapidly gain interest due to their unique properties.¹⁰² Finally, the medicinal potential of imidazolium salts has received an increasing amount of attention. While there are many fields in medicine that imidazolium salts can contribute to, such as antimicrobials,^{103,104} and anti-oxidants,¹⁰⁵ this portion will focus specifically on the role of imidazolium salts as anti-cancer agents.

1.8.2. Notable Historic Examples of Imidazolium Salts in Medicinal Chemistry

The first report of imidazolium salts with anti-cancer activity included **I 334** (Lepidiline A) and **I 335** (Lepidiline B) which were extracted from the roots of *Lepidium meyenii* (Chart I-49).¹⁰⁶ These two natural products were tested for their anti-cancer properties against a panel of human cancer cell lines including the A549 (lung carcinoma), UMUC3 (bladder carcinoma), HT-29 (colon adenocarcinoma), PC-3 (prostate adenocarcinoma), PACA2 (pancreatic adenocarcinoma), A4982LM (kidney carcinoma), MDA231 (breast carcinoma), and FDIGROV (ovarian carcinoma) cell lines. Compound **I 334** was only active against the FDIGROV cell line with an ED₅₀ value of 7.39 µg/mL; whereas **I 335** was effective against the UMUC3 (6.47 µg/mL), PACA2 (1.38 µg/mL), MDA231 (1.66 µg/mL), and FDIGROV (5.26 µg/mL) cell lines. Both compounds were inactive against the A549, HT-29, PC-3, and

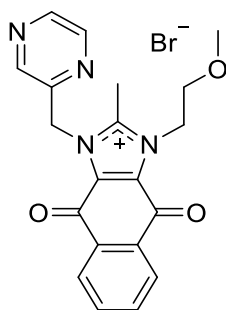
A4982LM cell lines. As is illustrated in Chart I-49, the only difference in structure between **I 334** and **I 335** is a methyl group substituted at the C² position for **I 335** versus a proton at the C² position for **I 334**. This slight difference in structure seems to make a substantial difference in the anti-proliferative effects of these compounds.

Chart I-49. Structure of the first imidazolium salts evaluated for anti-cancer properties, Lepidiline A and Lepidiline B.



YM155, **I 336** (Figure I-1), is the only imidazolium salt to enter clinical trials for the treatment of cancer thus far. The anti-tumor properties of this compound was first established when it was discovered to inhibit the protein survivin, which is a member of the family of proteins that inhibit apoptosis.¹⁰⁷ Survivin was found to be highly expressed in cancer cells with limited expression in most non-cancerous tissue.¹⁰⁸ Compound **I 336** was found to inhibit the promoter activity at low nanomolar ranges and induce apoptosis in human hormone-refractory prostate cancer cells *in vitro*.¹⁰⁷ In an orthotopic xenograft model of hormone-refractory prostate cancer, the PC-3 model, **I 336** was able to inhibit 80% of the growth of tumors when compared to control cells. In a phase I clinical trial, **I 336** could be safely administered without severe toxicities.¹⁰⁹ The results were favorable and suggested further exploration of **I 336**, including possible future use in combination with other chemotherapeutics. A phase II study with **I 336** used in combination with carboplatin or paclitaxel resulted in minimal response to the use of **I 336** in patients

with non-small cell lung cancer, but the drug was well tolerated. Although **I 336** was not effective in the treatment of non-small cell lung cancer (NSCLC) clinically, it could still have potential for other malignancies such as chondrosarcoma considering **I 336** was able to inhibit growth *in vitro* and it could safely be administered to patients in clinical trials.¹¹⁰

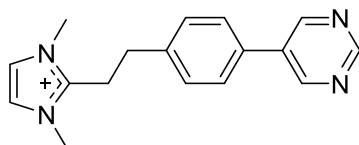


I 336

Figure I-1. Structure of YM155, **I 336**.

1.8.3. Recent Studies on the Medicinal Properties of Imidazolium Salts

In 2013, Barresi et al., published a series of heteroaryl ethylenes and evaluated their *in vitro* anti-cancer properties against the MCF7 cell line.¹¹¹ Only one compound from this series was an imidazolium salt, compound **I 337** (Figure I-2). Barresi used the computer modeling program, Volsurf+ to predict the chemotherapeutic potential of these compounds, and correctly predicted **I 337** to be inactive against the MCF-7 cell line. Results from the anti-tumor studies were reported as log GI₅₀ values, with **I 337** having a value greater than -4.00, meaning the actual value was above the range of concentrations tested in the experiment.



I 337

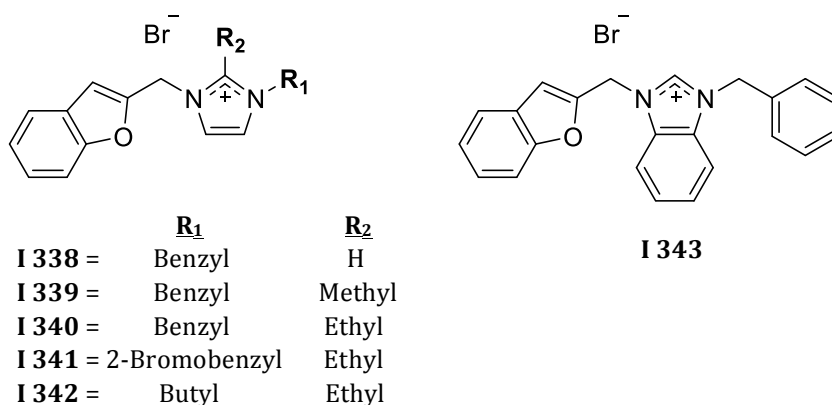
Figure I-2. Structure of **I 337**, a heteroaryl ethylene imidazolium salt that is inactive against the MCF7 human breast cancer cell line.

Zhang and Yang have been leaders in the field, publishing manuscripts on imidazolium salts with high anti-cancer activity for many years, specializing in hybrid imidazolium salts.^{28,112-125} The first report was in 2009 describing the synthesis and anti-cancer activity of phenacylimidazolium bromides,¹¹² which had previously received attention for use as oral hypoglycemic agents¹²⁶ and in the synthetic route to produce 3-substituted L-histidines.¹²⁷

Recently, following the first report of dihydrobenzofuran-imidazolium salt hybrid compounds with anti-cancer activity, a second report was published in 2012 focusing on modifying the imidazole core to create a SAR (Chart I-50).¹¹⁵ The anti-cancer properties of several imidazolium salts were evaluated against a panel of human cancer cell lines including Skov-3 (ovarian carcinoma), HL-60 (myeloid leukemia), and MCF-7 (breast carcinoma) by their IC₅₀ values. The group of imidazoles evaluated included compounds with imidazole, 2-methylimidazole, 2-ethylimidazole, or benzimidazole at the N³ position. Compound **I 343**, a benzimidazolium salt with a benzofuran substituent at the N¹ position and a benzyl substituent at the N³ position, was the most active (9.1 μg/mL or 21.6 μM) with over three-fold higher activity against the Skov-3 ovarian carcinoma cell line when compared to the other imidazolium salts (20.8 μg/mL or 65.6 μM for **I 338**). The

imidazolium, 2-methylimidazolium, and 2-ethylimidazolium salts had similar IC_{50} values against the Skov-3 cell line. Compound **I 343** was also the only active compound against the HL-60 and MCF-7 cell lines; whereas, the other imidazole derivatives were completely inactive at the highest concentration tested ($40 \mu\text{g mL}^{-1}$). Authors suggest that in this series of compounds, benzimidazolium salts have the highest activity and benzyl substituents at the N³ position were more active than 2-bromobenzyl and butyl substituents.

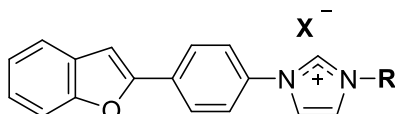
Chart I-50. Structures of Benzofuran Functionalized Imidazolium Salts



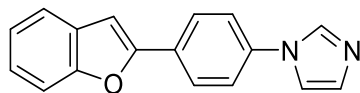
These benzofuran-substituted imidazolium salts were active and served as a starting point for the synthesis of novel compounds, including 2-phenylbenzofuran imidazolium salts.¹¹⁶ 2-Phenylbenzofuran based compounds found in the literature served as examples of natural product inhibitors of the hypoxia-inducible factor-1 protein, which can promote tumor growth under hypoxic conditions,¹²⁸ and breast carcinoma tumor growth inhibitors.¹²⁹ A second report in 2012 by Yang and Zhang reported the synthesis and *in vitro* anti-cancer properties of a series of 2-phenylbenzofuran-imidazolium salts (Chart I-51).¹¹⁶ This series of 2-

phenylbenzofuran derivatives was exposed to a panel of human tumor cell lines *in vitro* including SMMC-7721 (myeloid liver carcinoma), SW480 (colon carcinoma), MCF-7 (breast carcinoma), A549 (lung carcinoma), and HL-60 (leukemia) cells to determine their IC₅₀ values and create a SAR. Of note, the neutral imidazole, **I 355**, with a 2-phenylbenzofuran substituent at the N¹ position and no substituent at the N³ position was completely inactive, suggesting the positive charge of imidazolium salts is necessary for activity (Figure I-3). As seen previously, the phenacyl groups were more active than the benzyl or alkyl groups. Finally, of the phenacyl groups, the naphthylacyl, 4-bromophenylacyl, and 2'-phenyl-phenacyl groups had similar activities and were the most potent of the phenacyl groups at the N³ position.

Chart I-51. Structures of 2-Phenylbenzofuran Functionalized Imidazolium Salts



	<u>R</u>	<u>X</u>
I 344 =	Benzyl	Br
I 345 =	2-Bromobenzyl	Br
I 346 =	Allyl	Br
I 347 =	Butyl	I
I 348 =	Phenacyl	Br
I 349 =	4-Hydroxyphenacyl	Br
I 350 =	4-Methoxyphenacyl	Br
I 351 =	4-Fluorophenacyl	Br
I 352 =	4-Bromophenacyl	Br
I 353 =	Naphthylacyl	Br
I 354 =	2'-Phenyl-phenylacyl	Br



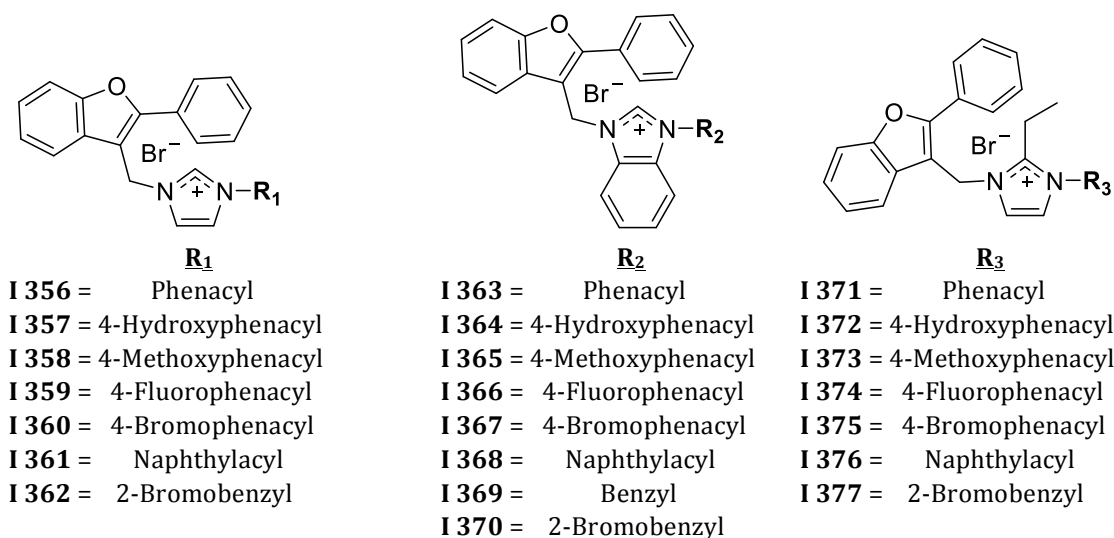
I 355

Figure I-3. Structure of 2-Phenylbenzofuran Substituted Imidazole.

A second report considering a series of imidazolium salt hybrid compounds with 2-phenylbenzofuran substituents was presented in 2013.¹¹⁹ However, the substituents were more specifically described as 2-phenyl-3-alkylbenzofurans and connected to the N¹ position of the imidazole ring by the benzofuran moiety versus attachment to the phenyl ring (Chart I-52). Motivation for this series of compounds came from the above mentioned 2-phenylbenzofuran derivatives and from the natural product ebenfuran III, isolated from *Onobrychis ebenoides*, which has *in vitro* anti-cancer activity against human breast cancer cells.¹³⁰ The 2-phenyl-3-alkylbenzofuran imidazolium salt hybrid compounds were exposed to a panel of human cancer cell lines *in vitro* including the HL-60 (leukemia), SMMC-7221 (myeloid liver carcinoma), A549 (lung carcinoma), MCF-7 (breast carcinoma), and SW480 (colon carcinoma) cell lines to determine their anti-cancer properties, which were reported as IC₅₀ values, and to determine a SAR. Several SARs were established from this large series of compounds. Several imidazole rings were compared with equivalent substituents at the N¹ and N³ position. Compounds that contained 2-ethylimidazole had the lowest IC₅₀ values. However, those with benzimidazole cores were also highly active and were comparable to the 2-ethylimidazole compounds. A new substituent was introduced at the N³ position, 2-bromobenzyl, which displayed the highest activity compared to all other substituents at that position. Compounds

with naphthylacyl substituents at the N³ position also displayed high activity, similar to previous reports. Compound **I 377** had the highest anti-cancer activity with IC₅₀ values ranging from 0.08 to 0.55 μM suggesting that the 2-bromobenzyl at the N³ position and 2-ethylimidazole are essential to the high activity seen in combination with the 2-phenyl-3-alkylbenzofuran substituent. The ability of **I 377** to inhibit the signaling of mTOR, the mammalian target of rapamycin which is involved in cell growth and proliferation,¹³¹ was evaluated using molecular docking studies. Compound **I 377** was able to dock with an upstream regulator of the mTOR signaling pathway, namely P13K_λ.

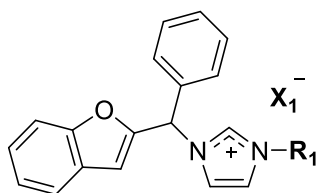
Chart I-52. Structures of 2-Benzylbenzofuran Functionalized Imidazolium Salts



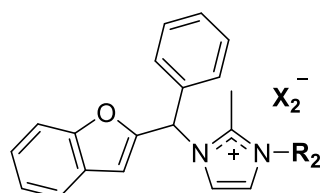
A report on the synthesis and cytotoxic activities of a series of compounds with modifications made to the benzofuran ligand was published in 2013. The report focused on the use of a 2-benzylbenzofuran substituent (Chart I-53).¹¹⁸ Motivation for this series of hybrid compounds came from a report of modified 2-

benzylbenzofuran compounds with cytotoxic activity.¹³² The series of N¹-substituted 2-benzylbenzofuran hybrid imidazolium salts includes different imidazole cores and different N³-substituted phenacyl ligands.¹¹⁸ The cytotoxic activities of this series was evaluated against a panel of human cancer cell lines *in vitro* including the HL-60 (leukemia), A549 (lung carcinoma), SW480 (colon carcinoma), MCF-7 (breast carcinoma), and SMMC-7721 (myeloid liver carcinoma) cell lines. Several derivatives displayed high anti-cancer activity, comparable to cisplatin. The results from the SAR study with this series of compounds suggested that the benzimidazole ring contributed to the most active compounds and, as described above, naphthylacyl and 4-methoxyphenacyl ligands at the N³ position produced the most active derivatives.

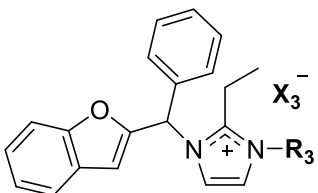
Chart I-53. Structures of 2-Benzylbenzofuran Substituted Imidazolium Salts



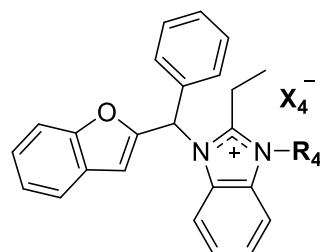
	<u>R₁</u>	<u>X₁</u>
I 378 =	Allyl	Br
I 379 =	Butyl	I
I 380 =	Benzyl	Br
I 381 =	4-Nitrobenzyl	Br
I 382 =	Phenacyl	Br
I 383 =	4-Fluorophenacyl	Br
I 384 =	4-Bromophenacyl	Br
I 385 =	4-Hydroxyphenacyl	Br
I 386 =	4-Methoxyphenacyl	Br
I 387 =	Naphthylacyl	Br



	<u>R₂</u>	<u>X₂</u>
I 388 =	Allyl	Br
I 389 =	Butyl	I
I 390 =	Benzyl	Br
I 391 =	Phenacyl	Br
I 392 =	4-Fluorophenacyl	Br
I 393 =	4-Bromophenacyl	Br
I 394 =	4-Hydroxyphenacyl	Br
I 395 =	4-Methoxyphenacyl	Br
I 396 =	Naphthylacyl	Br



	<u>R₃</u>	<u>X₃</u>
I 397 =	Allyl	Br
I 398 =	Butyl	I
I 399 =	Benzyl	Br
I 400 =	Phenacyl	Br
I 401 =	4-Fluorophenacyl	Br
I 402 =	4-Bromophenacyl	Br
I 403 =	4-Hydroxyphenacyl	Br
I 404 =	4-Methoxyphenacyl	Br
I 405 =	Naphthylacyl	Br



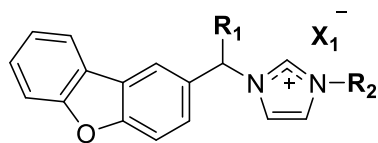
	<u>R₄</u>	<u>X₄</u>
I 406 =	Allyl	Br
I 407 =	Butyl	I
I 408 =	Benzyl	Br
I 409 =	4-Nitrobenzyl	Br
I 410 =	Phenacyl	Br
I 411 =	4-Fluorophenacyl	Br
I 412 =	4-Bromophenacyl	Br
I 413 =	4-Hydroxyphenacyl	Br
I 414 =	4-Methoxyphenacyl	Br
I 415 =	Naphthylacyl	Br

A study of a series of hybrid 2-alkylbenzofuran imidazolium salts derivatives was published in 2014.¹²² This series of hybrid compounds was modeled after the naturally occurring benzofuran compound denthyrsin, which had anti-cancer activity against leukemia, breast and cervical cancers.¹³³ This library of compounds included the 2-alkylbenzofuran attached to the N¹ position of various imidazole cores with acyl and alkyl substituents attached to the N³ position (Chart I-54).¹²²

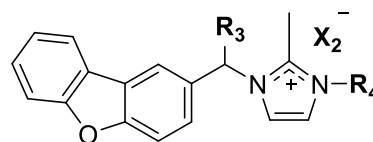
The *in vitro* anti-cancer properties of these 2-alkylbenzofuran derivatives were determined against the HL-60 (leukemia), SW480 (colon carcinoma), A549 (lung carcinoma), MCF-7 (breast carcinoma), and SMMC-7721 (myeloid liver carcinoma) cell lines and reported as IC₅₀ values in micromolar concentration. Although previous results suggested the benzimidazole core yields the highest anti-cancer properties, the 2-methylimidazole and 2-ethylimidazole derivatives with naphthylacyl and methoxyphenacyl substituents were the most active. For example, compounds **I 433** and **I 436** displayed high activity with IC₅₀ values of 0.78 μM (HL-60), 0.28 μM (SW480), 0.37 μM (A549), 1.44 μM (MCF-7), and 11.59 μM (SMMC-7721) and 1.04 μM (HL-60), 1.03 μM (SW480), 4.97 μM (A549), 1.09 μM (MCF-7), and 3.50 μM (SMMC-7721), respectively. The authors reported that collectively, the 2-alkylbenzofuran hybrids, when compared to the 2-phenylbenzofuran hybrids, had better anti-cancer properties against the SW480, A549, and MCF-7 cells lines and worse anti-cancer properties against the HL-60 and SMMC-7721 cell lines. The authors attributed the differences in activity to steric effects and charge distribution. It was suggested that these compounds would also be able to inhibit the mTOR pathway, considering **I 433** and **I 436** were able to dock with the PI3K λ protein using a molecular modeling approach, which is involved in the mTOR pathway.

(imidazole, 2-methylimidazole, and benzimidazole), either a phenyl or methyl substituent on the methylene group bridging the N¹ position of the imidazole to the dibenzo[b,d]furan ligand, and various phenacyl substituents at the N³ position.¹¹⁷ The *in vitro* anti-cancer properties of this series of compounds was evaluated against the human cancer cell lines HL-60 (leukemia), MCF-7 (breast carcinoma), A549 (lung carcinoma), SW480 (colon carcinoma), and SMMC-7221 (myeloid liver carcinoma). Compounds **I 461**, **I 470**, and **I 493** were found to be the most active with IC₅₀ values in the nanomolar range for the HL-60 cell line and less than 4 μM for all other cell lines. The SAR study from this series of compounds also suggested that the benzimidazole ring and naphthylacyl substituent at the N³ position were essential for the highest anti-cancer activity. Also, the phenyl group versus a methyl group bound to the bridging methylene of the dibenzo[b,d]furan ligand resulted in higher activity. Compound **I 493** was also shown to induce apoptosis in SMMC-72221 cells by the Annexin V-FITC/PI double-labeled cell cytometry experiment which may have been due to **I 493** causing cell cycle arrest at the G1 phase in the cell cycle.

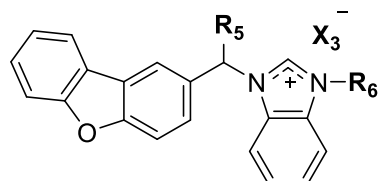
Chart I-55. Structures of Dibenzo[b,d]furan Functionalized Imidazolium Salts



<u>R₁</u>	<u>R₂</u>	<u>X₁</u>
I 446 = Methyl	Butyl	I
I 447 = Methyl	Benzyl	Br
I 448 = Methyl	Phenacyl	Br
I 449 = Methyl	4-Hydroxyphenacyl	Br
I 450 = Methyl	4-Methoxyphenacyl	Br
I 451 = Methyl	4-Bromophenacyl	Br
I 452 = Methyl	4-Fluorophenacyl	Br
I 453 = Methyl	Naphthylacyl	Br
I 454 = Phenyl	Butyl	I
I 455 = Phenyl	4-Nitrobenzyl	Br
I 456 = Phenyl	Phenacyl	Br
I 457 = Phenyl	4-Hydroxyphenacyl	Br
I 458 = Phenyl	4-Methoxyphenacyl	Br
I 459 = Phenyl	4-Bromophenacyl	Br
I 460 = Phenyl	4-Fluorophenacyl	Br
I 461 = Phenyl	2-Phenylphenacyl	Br
I 462 = Phenyl	Naphthylacyl	Br



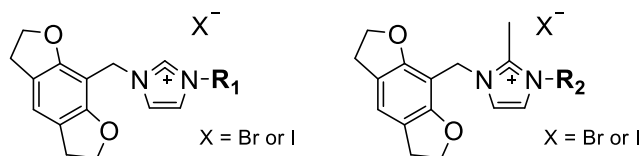
<u>R₃</u>	<u>R₄</u>	<u>X₂</u>
I 463 = Methyl	Butyl	I
I 464 = Methyl	4-Nitrobenzyl	Br
I 465 = Methyl	Phenacyl	Br
I 466 = Methyl	4-Hydroxyphenacyl	Br
I 467 = Methyl	4-Methoxyphenacyl	Br
I 468 = Methyl	4-Bromophenacyl	Br
I 469 = Methyl	4-Fluorophenacyl	Br
I 470 = Methyl	Naphthylacyl	Br
I 471 = Phenyl	Butyl	I
I 472 = Phenyl	4-Nitrobenzyl	Br
I 473 = Phenyl	4-Hydroxyphenacyl	Br
I 474 = Phenyl	4-Bromophenacyl	Br
I 475 = Phenyl	4-Fluorophenacyl	Br
I 476 = Phenyl	Naphthylacyl	Br



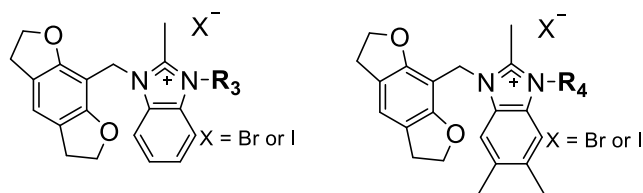
<u>R₅</u>	<u>R₆</u>	<u>X₃</u>
I 477 = Methyl	Butyl	I
I 478 = Methyl	4-Nitrobenzyl	Br
I 479 = Methyl	Phenacyl	Br
I 480 = Methyl	4-Hydroxyphenacyl	Br
I 481 = Methyl	4-Methoxyphenacyl	Br
I 482 = Methyl	4-Bromophenacyl	Br
I 483 = Methyl	4-Fluorophenacyl	Br
I 484 = Methyl	2-Phenylphenacyl	Br
I 485 = Methyl	Naphthylacyl	Br
I 486 = Phenyl	Butyl	I
I 487 = Phenyl	4-Nitrobenzyl	Br
I 488 = Phenyl	Phenacyl	Br
I 489 = Phenyl	4-Hydroxyphenacyl	Br
I 490 = Phenyl	4-Methoxyphenacyl	Br
I 491 = Phenyl	4-Bromophenacyl	Br
I 492 = Phenyl	4-Fluorophenacyl	Br
I 493 = Phenyl	Naphthylacyl	Br

A slight modification to the dibenzo[b,d]furan hybrid imidazolium salts was reported in 2014. The report focused on a library of 2,3,5,6-tetrahydrobenzo[1,2-b:4,5-b']difuran imidazolium salt hybrids (Chart I-56).¹²⁰ A novel tetrahydrobenzodifuran compound derived from *Cyperus rhizomes* with *in vitro* anti-cancer activity against human T-cell leukemia Jurkat cells¹³⁵ inspired this series of imidazolium salt hybrid compounds. This hybrid series consisted of the novel 2,3,5,6-tetrahydrobenzo[1,2-b:4,5-b']difuran ligand at the N¹ position of a variety of imidazole cores including imidazole, 2-methylimidazole, benzimidazole, and 5,6-dimethylbenzimidazole; and substituted benzyl substituents, substituted phenacyl substituents, and a new substituent, 2-naphthylmethyl, at the N³ position.¹²⁰ The *in vitro* anti-cancer properties of these hybrid imidazolium salts were evaluated against the HL-60 (myeloid leukemia), MCF-7 (breast carcinoma), SW480 (colon carcinoma), A549 (lung carcinoma), and SMMC-7721 (liver carcinoma) human cancer cell lines. Results from the *in vitro* studies against this panel of human cancer cell lines suggested the 5,6-dimethylbenzimidazole and the 2-naphthylmethyl substituent at the N³ position formed the most active compound, **I 525**, of the series. The IC₅₀ values were found to be 0.26 μM (HL-60), 0.20 μM (MCF-7), 0.26 μM (SW480), 0.83 μM (A549), and 1.81 μM (SMMC-7721). It was thought that **I 525** may also be able to inhibit the mTOR pathway considering it was shown to dock with the PI3K protein using a molecular modeling approach.

Chart I-56. Structures of Benzodifuran Functionalized Imidazolium Salts



<u>R₁</u>	<u>R₂</u>
I 494 = Benzyl	I 503 = Benzyl
I 495 = 4-Methylbenzyl	I 504 = 4-Methylbenzyl
I 496 = 4-Bromobenzyl	I 505 = 4-Bromobenzyl
I 497 = 4-Nitrobenzyl	I 506 = 4-Nitrobenzyl
I 498 = 2-Naphthylmethyl	I 507 = 2-Naphthylmethyl
I 499 = Phenacyl	I 508 = Phenacyl
I 500 = 4-Bromophenacyl	I 509 = 4-Bromophenacyl
I 501 = 4-Methoxyphenacyl	I 510 = 4-Methoxyphenacyl
I 502 = Naphthylacyl	I 511 = Naphthylacyl

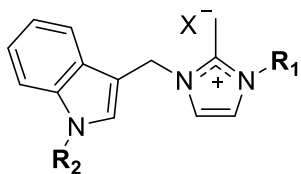


<u>R₃</u>	<u>R₄</u>
I 512 = Butyl	I 521 = Butyl
I 513 = Benzyl	I 522 = Benzyl
I 514 = 4-Methylbenzyl	I 523 = 4-Methylbenzyl
I 515 = 4-Bromobenzyl	I 524 = 4-Bromobenzyl
I 516 = 2-Naphthylmethyl	I 525 = 2-Naphthylmethyl
I 517 = Phenacyl	I 526 = Phenacyl
I 518 = 4-Bromophenacyl	I 527 = 4-Bromophenacyl
I 519 = 4-Methoxyphenacyl	I 528 = 4-Methoxyphenacyl
I 520 = Naphthylacyl	I 529 = Naphthylacyl

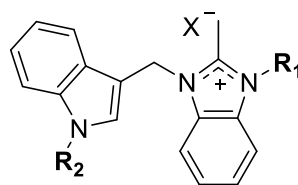
Another study in 2014 revealed a series of 1-(indol-3-yl)methyl hybrid imidazolium salts with anti-cancer properties.¹²¹ The 1-(indol-3-yl)methyl ligand was incorporated into the hybrid imidazolium salts because of indole-based compounds with high anti-cancer activity against lung cancer.¹³⁶ The series of hybrid imidazolium salts has the 1-(indol-3-yl)methyl ligand at the N¹ position; imidazole, 2-methylimidazole, benzimidazole, or a 5,6-dimethylbenzimidazole

imidazole core and various phenacyl groups at the N³ position (Chart I-57). The *in vitro* anti-cancer activity of these indole-based imidazolium salts were evaluated against the HL-60 (leukemia), SMMC-7721 (myeloid liver carcinoma), A549 (lung carcinoma), MCF-7 (breast carcinoma), and SW480 (colon carcinoma) human cancer cell lines. These indole compounds were not as active as the previously described benzodifuran derivatives. However, the most active compounds contained the 5,6-dimethylbenzimidazole and naphthylacyl substituent at the N³ position similar to previously described compounds. There was no difference in the observed activities between compounds only differing in structure by either the 'Ts' or 'Boc' substituent bound to the indole nitrogen. The most active compound was determined to be compound **I 556** containing a naphthylacyl-substituent and the 5,6-dimethylbenzimidazole core. Compound **I 556** was also able to induce apoptosis as determined by an Annexin V-FITC/PI double-labeled cell cytometry experiment with 48% apoptotic cells at 24 hours from 16 μ M compound exposure. With a slight increase in the percentage of cells in the S phase of the cell cycle in a cell cycle analysis assay, authors suggest that **I 556** may induce S phase arrest.¹²¹

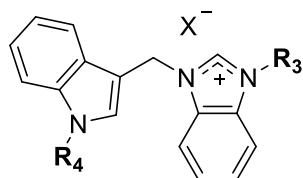
Chart I-57. Structures of 1-(indol-3-yl)methyl Functionalized Imidazolium Salts



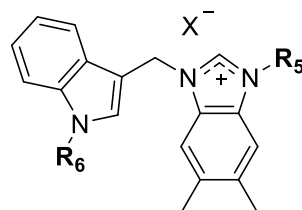
	<u>R₁</u>	<u>R₂</u>
I 530 =	Phenacyl	Ts
I 531 =	4-Hydroxyphenacyl	Ts
I 532 =	4-Methoxyphenacyl	Ts
I 533 =	4-Bromophenacyl	Ts
I 534 =	Naphthylacyl	Ts



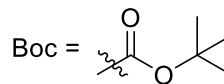
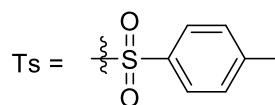
	<u>R₁</u>	<u>R₂</u>
I 535 =	Phenacyl	Ts
I 536 =	4-Hydroxyphenacyl	Ts
I 537 =	4-Methoxyphenacyl	Ts
I 538 =	4-Bromophenacyl	Ts
I 539 =	Naphthylacyl	Ts



	<u>R₃</u>	<u>R₄</u>
I 540 =	Phenacyl	Ts
I 541 =	4-Hydroxyphenacyl	Ts
I 542 =	4-Methoxyphenacyl	Ts
I 543 =	4-Bromophenacyl	Ts
I 544 =	Naphthylacyl	Ts
I 545 =	Phenacyl	Boc
I 546 =	4-Hydroxyphenacyl	Boc
I 547 =	4-Methoxyphenacyl	Boc
I 548 =	4-Bromophenacyl	Boc
I 549 =	Naphthylacyl	Boc



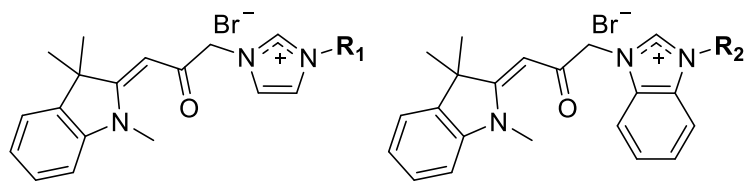
	<u>R₅</u>	<u>R₆</u>
I 550 =	Phenacyl	Ts
I 551 =	4-Hydroxyphenacyl	Ts
I 552 =	4-Methoxyphenacyl	Ts
I 553 =	4-Bromophenacyl	Ts
I 554 =	Naphthylacyl	Ts
I 555 =	4-Hydroxyphenacyl	Boc
I 556 =	Naphthylacyl	Boc



A report on a series of 2-substituted indoline hybrid imidazolium salts, related to the indole hybrid imidazolium salts discussed above, was published in 2015.¹²³ Compounds bearing a 2-substituted indoline moiety displayed anti-cancer activity against multiple cancer cell types *in vitro* including breast, colon, lung, and renal cancers.^{137,138} These compounds served as inspiration to incorporate indoline moieties into hybrid imidazolium salts as potential chemotherapeutics. The series of

indoline substituted imidazolium salts including the 2-substituted indoline at the N¹ position of the imidazole also included numerous imidazole cores (imidazole, benzimidazole, 2-methylbenzimidazole, and 5,6-dimethylbenzimidazole) and phenacyl or alkyl substituents at the N³ position of the imidazole core (Chart I-58). The *in vitro* anti-cancer properties of this series of hybrids was evaluated against a panel of human cancer cell lines including the HL-60 (myeloid leukemia), A549 (lung carcinoma), SMMC-7721 (liver carcinoma), MCF-7 (breast carcinoma), and SW480 (colon carcinoma) cell lines. The cytotoxic activities of numerous derivatives were very high and comparable to other hybrid imidazolium salts. The most active compounds of this series contained a substituted benzimidazole ring (2-methylbenzimidazole or 4,5-dimethylbenzimidazole) and a naphthylacyl or 2-naphthylmethyl substituent at the N³ position. Compound **I 574**, comprised of a 2-methylbenzimidazole and naphthylacyl group at the N³ position displayed the best cytotoxic activity with IC₅₀ values of 0.24 μM (HL-60), 0.98 μM (A549), 1.09 μM (SMMC-7721), 1.13 μM (MCF-7), and 1.18 μM (SW480). Compound **I 574** was shown to induce apoptosis in a higher percentage of cells than negative control cells in a dose-dependent manner after 48 hours using the Annexin V-FITC/PI double-labeled cell cytometry experiment.

Chart I-58. Structures of Indolene Functionalized Imidazolium Salts

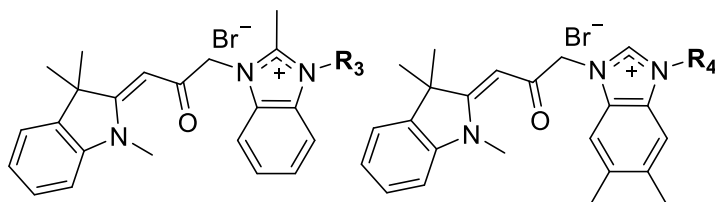


R₁

I 557 = 2-Bromobenzyl
I 558 = Phenacyl
I 559 = 4-Bromophenacyl
I 560 = 4-Methoxyphenacyl
I 561 = Naphthylacyl

R₂

I 562 = 4-Methylbenzyl
I 563 = 2-Bromobenzyl
I 564 = 2-Naphthylmethyl
I 565 = Phenacyl
I 566 = 4-Bromophenacyl
I 567 = Naphthylacyl



R₃

I 568 = 4-Methylbenzyl
I 569 = 2-Bromobenzyl
I 570 = 2-Naphthylmethyl
I 571 = Phenacyl
I 572 = 4-Bromophenacyl
I 573 = 4-Methoxyphenacyl
I 574 = Naphthylacyl

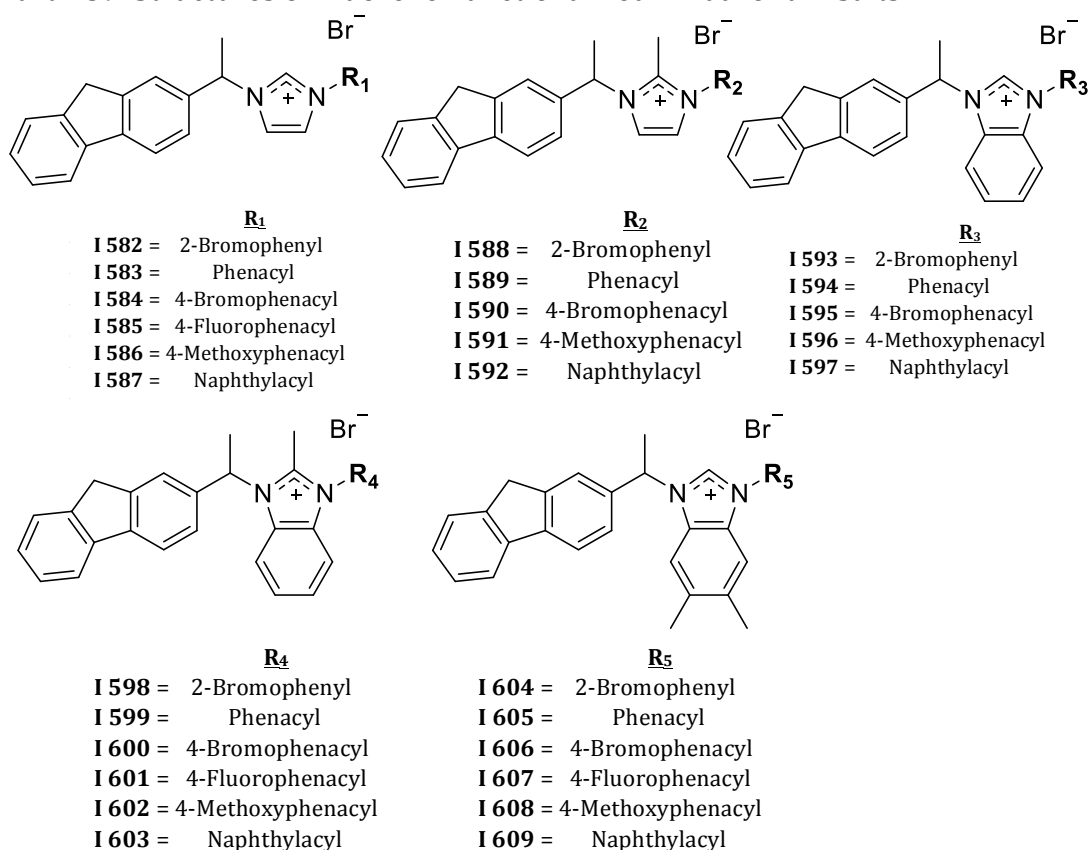
R₄

I 575 = 4-Methylbenzyl
I 576 = 2-Bromobenzyl
I 577 = 2-Naphthylmethyl
I 578 = Phenacyl
I 579 = 4-Bromophenacyl
I 580 = 4-Methoxyphenacyl
I 581 = Naphthylacyl

A modification to the dibenzo[b,d]furan ligand discussed above came in the form of a fluorene ligand in a series of hybrid imidazolium salts with a 3-substituted fluorene ligand incorporated at the N¹ position of the imidazolium salts (Chart I-59).¹²⁵ Several compounds with the fluorene ligand, such as the natural peptide Ixorapeptide, isolated from *Ixora cocinea*,¹³⁹ have *in vitro* anti-cancer activity against liver, breast, and colon cancer cells.¹⁴⁰ These compounds encouraged the synthesis of this new hybrid series of imidazolium salts that utilize various imidazoles (imidazole, 2-methylimidazole, benzimidazole, 2-methylbenzimidazole, and 5,6-dimethylbenzimidazole) and various phenacyl or alkyl groups at the N³ position in addition to the fluorene substituent at the N¹ position.¹²⁵ The *in vitro* anti-

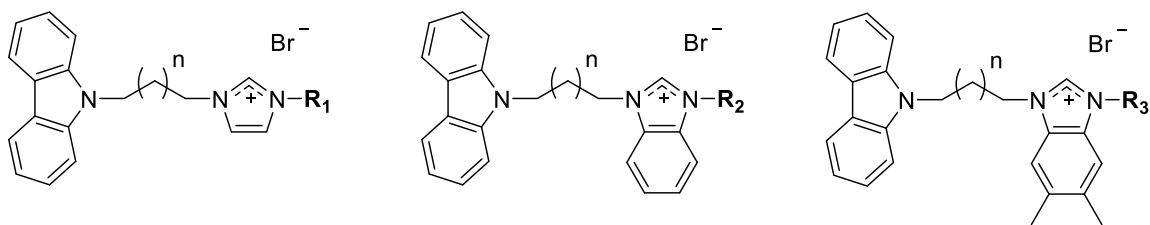
proliferative effects of this hybrid series of compounds was evaluated against several human tumor cell lines including the HL-60 (myeloid leukemia), SMCC7721 (liver carcinoma), A549 (lung carcinoma), MCF-7 (breast carcinoma), and SW480 (colon carcinoma) cell lines. Results suggested that the substituted benzimidazoles (2-methylbenzimidazole and 4,5-dimethylbenzimidazole) and the naphthylacyl and 4-methoxyphenacyl ligands at the N³ position formed the most potent derivatives of the compounds tested. Compounds **I 596**, **I 603**, and **I 608** were also exposed to normal lung epithelial cells, the BEAS-2B cell line, to determine their toxicity to healthy tissue. Only compound **I 596** displayed any appreciable difference in the IC₅₀ value when compared to the cancerous cell line A549 (16.26 μM for BEAS-2B and 2.58 μM for A549).

Chart I-59. Structures of Fluorene Functionalized Imidazolium Salts



A study of a series of hybrid imidazolium salts with carbazole ligands, a similar structure to the dibenzo[b,d]furan and fluorene moiety, at the N¹ position of the imidazole ring was published in 2015 (Chart I-60).¹²⁴ Motivation for this series of compounds came from natural product compounds containing the carbazole ligand isolated from the roots of *Clausena harmandiana*.¹⁴¹ Each compound in this hybrid series contained a carbazole moiety linked to the N¹ position of the imidazole ring by a three, four, or five carbon chain; an imidazole, benzimidazole, or 5,6-dimethylbenzimidazole; and a phenacyl or alkyl substituent at the N³ position.¹²⁴ The *in vitro* cytotoxic activities of each carbazole-imidazolium salt was evaluated against several human cancer cell lines including the HL-60 (myeloid leukemia), SMMC-7721 (liver carcinoma), A549 (lung cancer), MCF-7 (breast cancer), and the SW480 (colon cancer) cell lines to create a SAR. Compounds with the 5,6-dimethylbenzimidazole and either a 2-bromobenzyl or naphthylacyl substituent at the N³ position were the most active. Compound **I 657** was the most active with IC₅₀ values of 0.51 μM (HL-60), 1.40 μM (MCF-7), 2.38 μM (SMMC-7721), 2.48 μM (SW480), and 3.12 μM (A549). Compound **I 657** was also shown to induce apoptosis at a significantly higher rate than negative control in a dose-dependent manner and cause G2/M phase cell cycle arrest.

Chart I-60. Structures of Carbazole Functionalized Imidazolium Salts

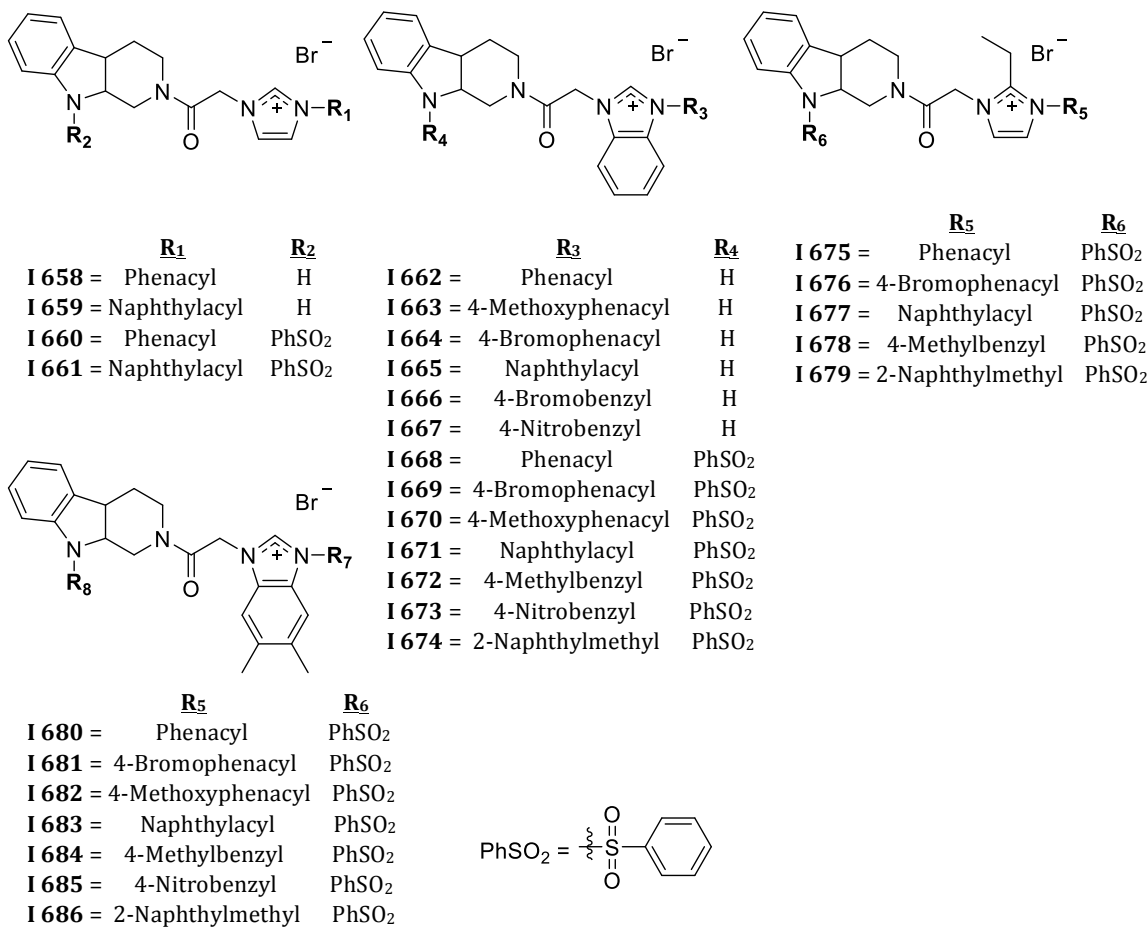


<u>n</u>	<u>R₁</u>	<u>n</u>	<u>R₂</u>	<u>n</u>	<u>R₃</u>
I 610 = 1	Phenacyl	I 625 = 1	Phenacyl	I 643 = 1	Naphthylacyl
I 611 = 1	4-Methoxyphenacyl	I 626 = 1	4-Methoxyphenacyl	I 644 = 1	4-Methoxyphenacyl
I 612 = 1	Naphthylacyl	I 627 = 1	Naphthylacyl	I 645 = 1	4-Methylbenzyl
I 613 = 1	4-Bromophenacyl	I 628 = 1	4-Bromobenzyl	I 646 = 2	Naphthylacyl
I 614 = 1	4-Bromobenzyl	I 629 = 1	4-Methylbenzyl	I 647 = 2	4-Methoxyphenacyl
I 615 = 1	4-Methylbenzyl	I 630 = 1	2-Bromobenzyl	I 648 = 3	4-Bromophenacyl
I 616 = 2	Naphthylacyl	I 631 = 2	Naphthylacyl	I 649 = 3	Phenacyl
I 617 = 2	4-Methoxyphenacyl	I 632 = 2	4-Methoxyphenacyl	I 650 = 3	2-Bromobenzyl
I 618 = 2	4-Bromophenacyl	I 633 = 2	4-Bromophenacyl	I 651 = 3	4-Methylbenzyl
I 619 = 2	Phenacyl	I 634 = 2	Phenacyl	I 652 = 3	Phenacyl
I 620 = 2	4-Methylbenzyl	I 635 = 2	4-Methylbenzyl	I 653 = 3	4-Methoxyphenacyl
I 621 = 2	2-Bromobenzyl	I 636 = 2	2-Bromobenzyl	I 654 = 3	Naphthylacyl
I 622 = 3	4-Methoxyphenacyl	I 637 = 3	Phenacyl	I 655 = 3	4-Bromophenacyl
I 623 = 3	Naphthylacyl	I 638 = 3	4-Methoxyphenacyl	I 656 = 3	4-Methylbenzyl
I 624 = 3	4-Methylbenzyl	I 639 = 3	Naphthylacyl	I 657 = 3	2-Bromobenzyl
		I 640 = 3	4-Bromophenacyl		
		I 641 = 3	4-Methylbenzyl		
		I 642 = 3	2-Bromobenzyl		

A study on a series of hybrid tetrahydro- β -carboline-imiazolium salts was published in 2016.²⁸ These compounds were modeled from those that contain the tetrahydro- β -carboline moiety and were shown to have anti-cancer activity in the literature.¹⁴² The structures of compounds in this hybrid series entails the tetrahydro- β -carboline moiety linked to the N¹ position of the imidazole ring by a ethylacyl group and alkyl or phenacyl groups at the N³ position with either an imidazole, benzimidazole, 2-ethylimidazole, or 5,6-dimethylbenzimidazole at the core (Chart I-61). The *in vitro* anti-cancer properties were evaluated against a panel of human cancer cell lines including the HL-60 (myeloid leukemia), SMMC-7721 (liver carcinoma), A549 (lung carcinoma), MCF-7 (breast carcinoma), and SW480

(colon carcinoma) cell lines. The most active compounds of this series were those substituted with the 5,6-dimethylbenzimidazole ring and either a 2-naphthylmethyl or naphthyl substituent at the N³ position as with compound **I 686**, whose IC₅₀ values were 2.61 μM (HL-60), 14.15 μM (A549), 17.13 μM (SMMC-7721), 2.79 μM (MCF-7), and 9.46 μM (SW480). These values are higher, suggesting the compound is less active, than the previously published hybrid imidazolium salts with different substituents at the N¹ position. However, **I 686** had an IC₅₀ of >40 μM against the normal lung epithelial cell line BEAS-2B, compared to 17.13 μM for the cancerous A549 cell line, suggesting the compound may exhibit selective cytotoxicity towards cancerous tissue. Compound **I 686** was also shown to induce apoptosis at a significantly higher rate, in a dose-dependent manner, than cells treated with no drug and caused cell cycle arrest at the G1 phase.

Chart I-61. Structures of Tetrahydro- β -carboline Imidazolium Salts

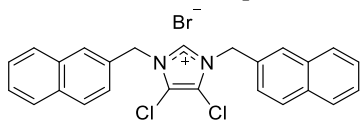


Youngs and coworkers began investigating the antimicrobial and anti-tumor properties of imidazolium salts because they are the ligand precursors and eventual degradation products of NHC complexes.^{17,143-147} However, it was quickly discovered that the anti-tumor properties were largely due to the imidazolium salt and not the NHC complex.²⁵ It was suggested that the *in vitro* anti-cancer properties of imidazolium salts against several non-small cell lung cancer (NSCLC) cell lines was highly dependent on the substituents at the N¹ and N³ positions of the imidazole ring and chemical modifications could be made to the C⁴ and/or C⁵ positions

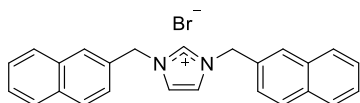
without altering the anti-proliferative effects (Chart I-62).²⁶ N,N'-bis(naphthylmethyl)imidazolium salts were found to be the most active of the derivatives studied. Imidazolium salts with one naphthylmethyl substituent and one alkyl chain at the N¹ and N³ positions, respectively, had variable activities. Compounds with alkyl chains of n = 5 or less carbons had moderate to poor activity while those with alkyl chains of n = 6 or more carbon atoms had high anti-cancer activity, with IC₅₀ values in the low micro-molar range. This study supports the data previously published by Malhotra's NCI-60 human tumor cell line screen on the effects lipophilicity plays on the anti-cancer properties of ionic liquids.¹⁴⁸ Exchanging one naphthylmethyl group for a benzyl group reduced the activity significantly; whereas, exchanging both naphthylmethyl groups for benzyl groups resulted in an inactive compound. Changing the linking moiety joining the imidazole ring to the naphthalene substituent from a methyl to ethyl group seemed to have little effect on the anti-cancer properties of the compound, just as altering the connectivity from the 2-position to the 1-position of the naphthalene ring had little effect on the activity. Although these naphthylmethyl substituted imidazolium salts had potent anti-cancer activity against NSCLC, they were limited in their clinical potential by poor aqueous solubility. The final modification to the N¹ position was adding a nitrogen heteroatom to the naphthalene ring in the form of a quinoline substituent to increase aqueous solubility, which also had minimal effects on the anti-cancer properties, but again, the compounds suffered from insufficient solubility for systemic administration. Direct comparisons were made to N,N'-bis(naphthylmethyl)imidazolium salts with differing groups at the C⁴(C⁵) positions

including protons, chlorides, and a benzimidazolium salt. These three derivatives (**I 687- I 689**) had comparable anti-cancer properties suggesting this could be a position for chemical modification to add solubilizing and/or targeting groups.

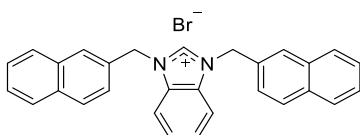
Chart I-62. Structures of Naphthalene Functionalized Imidazolium Salts



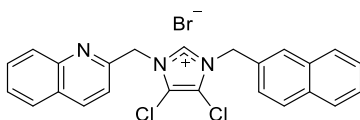
I 687



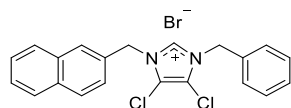
I 688



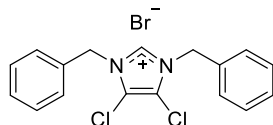
I 689



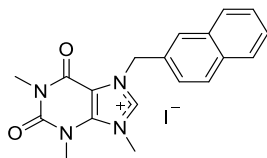
I 690



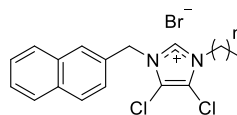
I 691



I 692



I 693



I 694: n = 1

I 695: n = 2

I 696: n = 3

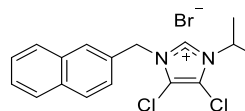
I 697: n = 4

I 698: n = 5

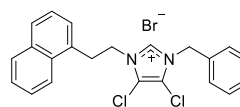
I 699: n = 6

I 700: n = 8

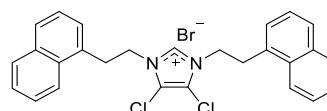
I 701: n = 11



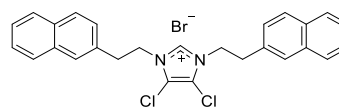
I 702



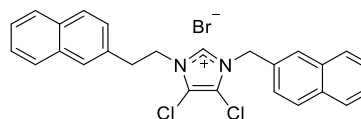
I 703



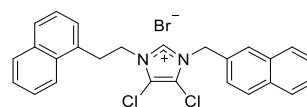
I 704



I 705



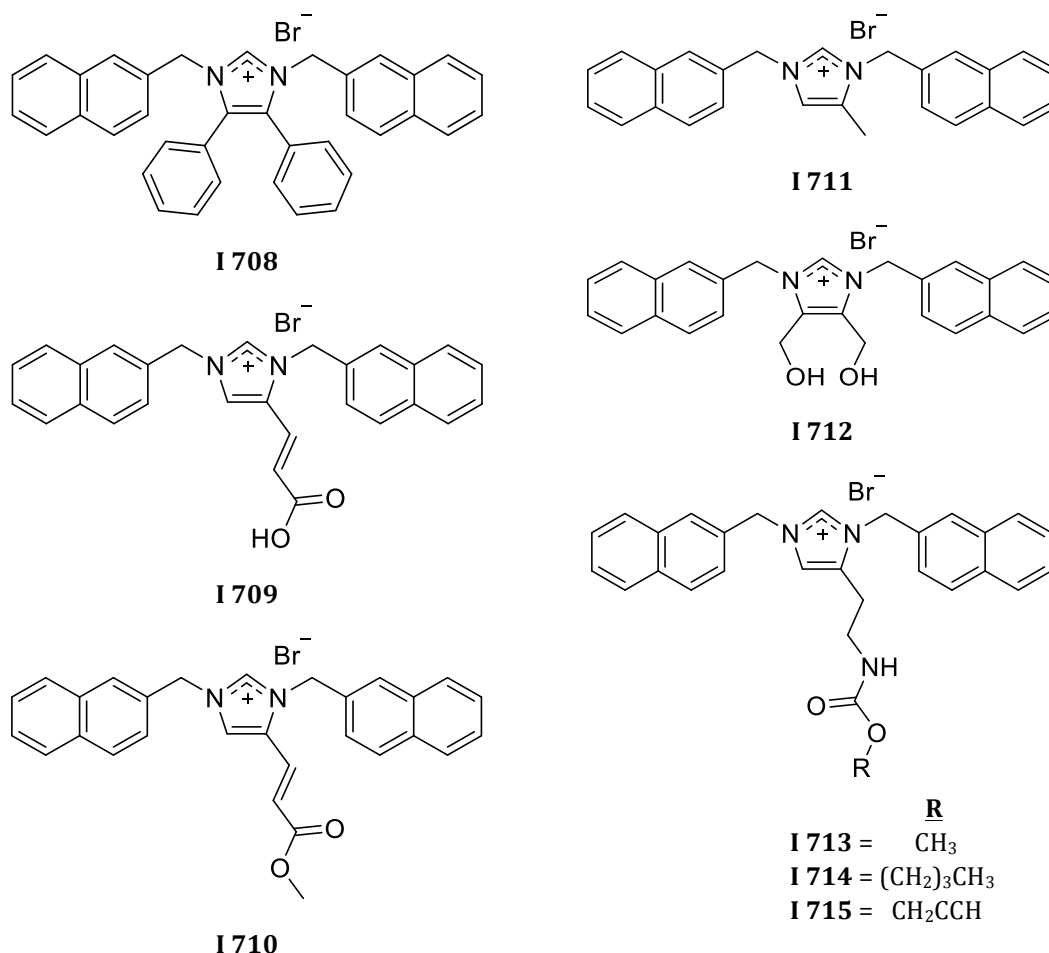
I 706



I 707

The Youngs groups further explored chemical modifications at the N¹(N³) and C⁴(C⁵) positions to create a SAR with various hydrophilic and lipophilic substituents at each of these positions (Chart I-63).¹⁴⁹ The anti-cancer properties of eight imidazolium salts with naphthylmethyl substituents at the N¹(N³) positions and a variety of lipophilic and hydrophilic substituents at the C⁴(C⁵) positions were evaluated. These modifications included methyl, hydroxymethyl, carbamate, carboxylic acid, ester, and phenyl substituents. The C⁴(C⁵)-phenyl substituted derivative, **I 708**, was the most active with IC₅₀ values of 3 μM (NCI-H460), <1 μM (NCI-H1975), and 2 μM (HCC827), closely followed in activity by the lipophilic derivative **I 711** with a methyl substituent at the C⁴ position. Compound **I 711** had IC₅₀ values of 3 μM (NCI-H460), 3 μM (NCI-H1975), and 4 μM (HCC827) against the select panel of NSCLC cell lines. The more hydrophilic carboxylic acid and hydroxymethyl derived compounds, **I 709** and **I 712** respectively, had the lowest anti-cancer activity of the series, with all values being above the highest tested concentration of 30 μM, with the exception of **I 712** having an IC₅₀ value of 11 μM against the NCI-H1975 line. The histamine derived imidazolium salts (**I 713**, **I 714**, **I 715**) and ester moiety, **I 710**, had moderate activities suggesting that certain groups could be used to increase solubility without hindering the anti-cancer properties whereas other functional groups were too detrimental to the activity. Compound **I 708** and **I 711** were also tested by the NCI's DTP in the NCI-60 human tumor cell line screen, revealing both compounds had high anti-cancer activity in the one- and five-dose assay against the nine NSCLC cell line tested.

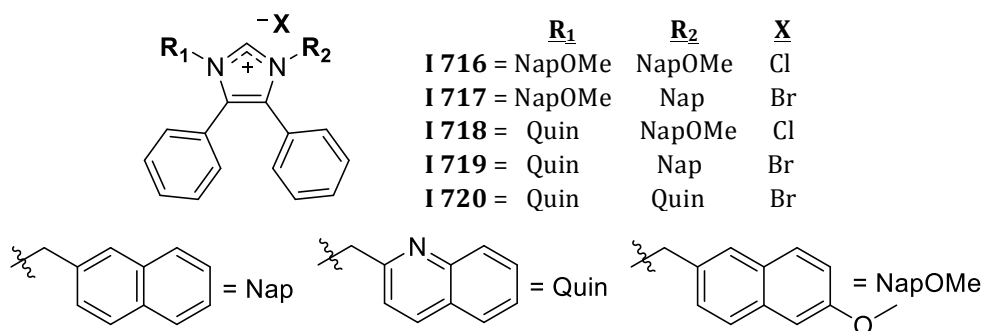
Chart I-63. Structures of Modified Imidazolium Salts **I 708- I 715**



Considering **I 708** was highly active against the NSCLC cell lines tested, this was further modified at the N¹(N³) positions in an attempt to increase aqueous solubility and maintain the high anti-cancer activity (Chart I-64).¹⁴⁹ Compounds **I 716- I 720** were strategically synthesized with planar aromatic groups similar to the naphthalene moiety, such as quinoline and 6-methoxy-naphthalene substituents, that included heteroatoms to increase the aqueous solubility. These five derivatives, with various combinations of these three planar, bicyclic ring systems were synthesized and tested for their anti-cancer properties against NSCLC. All of these

derivatives had IC₅₀ values of 3 μM or less against the three NSCLC cell lines tested (NCI-H460, NCI-H1975, and HCC927). Noticeable differences in solubility were not observed for any of these derivatives because the solubilities were still extremely poor (< 0.5 mg/mL).

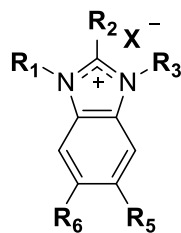
Chart I-64. Structures of 4,5-Diphenyl Imidazolium Salts



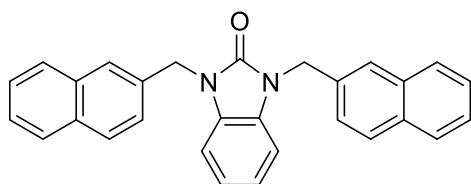
Considering the high anti-cancer activity of the lipophilic 4,5-diphenylimidazolium salt derivatives, the Youngs group published a report on a series of benzimidazolium salts in 2016 (Chart 65).¹⁵⁰ The *in vitro* anti-cancer properties of these benzimidazolium salts were evaluated against a panel of non-small cell lung cancer cell lines. This series of benzimidazolium salts had a variety of lipophilic and hydrophilic functional groups at the N¹ and N³ positions as well as the C², C⁵, and C⁶ positions. A SAR was established from combining the anti-cancer properties and structures of each benzimidazolium salt. Results from this study suggested that the most lipophilic compounds possessed the highest anti-cancer activity. However, as with other derivatives, these lipophilic compounds displayed poor aqueous solubility. Certain hydrophilic functional groups deactivate the compounds, such as carboxylic acids, whereas mildly hydrophilic substituents such

as quinolylmethyl groups at the N¹ and/or N³ positions and ethers at the C², C⁵, and/or C⁶ positions increased the aqueous solubility without having a drastic impact on the anti-proliferative properties. Two N¹/N³-naphthylmethyl substituted neutral benzimidazoles, **I 748** and **I 749**, were also tested for their anti-cancer properties and found to be inactive against the lung cancer cells lines in the study. This suggested that the positive charge of the benzimidazolium salt is necessary for high anti-cancer activity, in addition to the details provided above. The NCI's DTP also found **I 721**, **I 724**, **I 731**, **I 734**, **I 735**, and **I 745** to be active in the 60-human tumor cell line one-dose assay screen. Compound **I 745** was administered to C57BL/6 mice in a preliminary *in vivo* toxicity study. Although the compound was toxic at the tested dose, the study provided information for future toxicity trials and lung xenograft models.

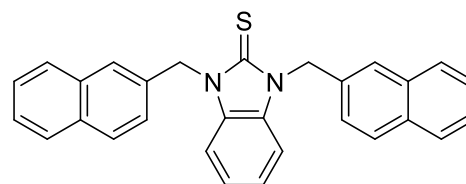
Chart I-65. Structures of Functionized Benzimidazolium Salts



<u>R₁</u>	<u>R₂</u>	<u>R₃</u>	<u>R₅</u>	<u>R₆</u>	<u>X</u>
I 721 = Nap	H	Nap	H	H	Br
I 722 = Nap	H	Nap	OCH ₃	H	Br
I 723 = Nap	H	Nap	CO ₂ CH ₃	H	Br
I 724 = Nap	H	Nap	CH ₃	CH ₃	Br
I 725 = Nap	H	Nap	CO ₂ CH ₃	CO ₂ CH ₃	Br
I 726 = Nap	H	Nap	CO ₂ CH ₂ Nap	H	Br
I 727 = Nap	H	Nap	CO ₂ H	CO ₂ H	Cl
I 728 = Nap	H	Nap	CO ₂ H	H	Br
I 729 = Nap	CH ₂ CO ₂ CH ₃	Nap	H	H	Br
I 730 = Nap	(CH ₂) ₂ CO ₂ CH ₃	Nap	H	H	Br
I 731 = Nap	CH ₃	Nap	H	H	Br
I 732 = Nap	(CH ₂) ₂ CO ₂ H	Nap	H	H	Cl
I 733 = Nap	CH ₂ CH ₃	Nap	H	H	Br
I 734 = Nap	(CH ₂) ₂ CH ₃	Nap	H	H	Br
I 735 = Nap	(CH ₂) ₃ CH ₃	Nap	H	H	Br
I 736 = Nap	(CH ₂) ₆ CH ₃	Nap	H	H	Br
I 737 = Nap	(CH ₂) ₂ OCH ₃	Nap	H	H	Br
I 738 = Nap	(CH ₂) ₃ OH	Nap	H	H	Br
I 739 = Quin	(CH ₂) ₃ OH	Nap	H	H	Br
I 740 = Quin	(CH ₂) ₃ OH	Quin	H	H	Cl
I 741 = Quin	H	Quin	H	H	Cl
I 742 = Quin	CH ₃	Quin	H	H	Cl
I 743 = Quin	H	Quin	CH ₃	CH ₃	Cl
I 744 = Nap	O(CH ₂ CH ₂ O) ₂ CH ₃	Nap	H	H	Br
I 745 = Quin	O(CH ₂ CH ₂ O) ₂ CH ₃	Nap	H	H	Br
I 746 = Quin	O(CH ₂ CH ₂ O) ₂ CH ₃	Quin	H	H	Cl
I 747 = Nap	O(CH ₂ CH ₂ O) ₂ CH ₃	Nap	CH ₃	CH ₃	Br



I 748



I 749

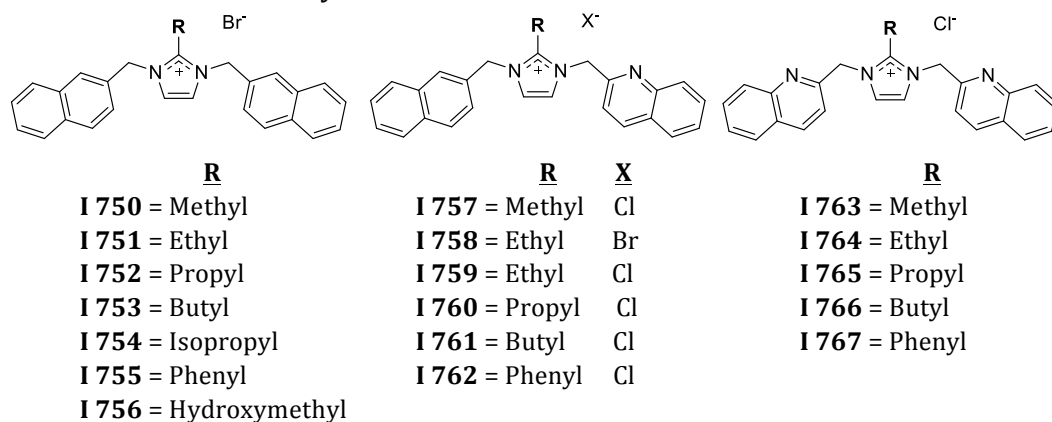
Additionally, Youngs and co-workers most recent work entails the synthesis and investigation of the biological activity of 2-alkyl substituted imidazolium salts (Chart I-66).^{151,152} The salts were synthesized by standard alkylation procedures of

2-alkyl imidazole with 2-(bromomethyl)naphthalene or 2-(chloromethyl)quinoline. These compounds were tested against several NSCLC cancer cell lines (NCI-H460, NCI-H1975, HCC827 and A549) as well as a variety being tested through the National Cancer Institute's Developmental Therapeutics Program (NCI DTP) in their NCI-60 human tumor cell line screen. Compound **I 755** had IC₅₀ values in the range of 2-4 μM showing that a bulky substituent in the C² position did not decrease activity. In order to increase aqueous solubility, a hydroxymethyl group was put in the C² position, giving compound **I 756**. Activity was significantly decreased (7->30 μM) while solubility was not greatly enhanced. A quinoline group was also introduced to impart some solubility (**I 757- I 762**) and was found to not significantly change the anti-cancer activity. The different anions of **I 758** and **I 759** also did not change activity but solubility was increase for the chloride derivative. Overall, an increase in lipophilicity was associated with higher anti-cancer activity but limited aqueous solubility, supported by results from the NCI-60 human tumor cell line screen.

The bis-naphthalene compounds (**I 750- I 754**), also suffered from limited water solubilities. Thus, the excipient 2-hydroxypropyl-β-cyclodextrin was employed to increase solubility. Compounds **I 750- I 754** were tested via an MTT assay in both the presence and absence of the cyclodextrin. Results showed that the use of the excipient did not drastically change anti-cancer activity. The NCI-60 cell line screen also exhibited potent anti-cancer activity for the tested compounds. The same general trend was seen that an increase in lipophilicity increased the activity.

Further biological studies were completed using the Annexin V and JC-1 assays. Annexin V after treatment with **I 751** showed an apoptotic mode of cell death. After DNA was determined to not be the cellular target, the JC-1 assay was used to evaluate mitochondrial disruption. It was found that **I 751** could disrupt the mitochondrial membrane potential at very early time points. This confirms the process of apoptosis and indicates that mitochondria could be the cellular target.

Chart I-66. Structures of 2-Alkyl Imidazolium Salts



1.9. Conclusion

Throughout this review of recent literature regarding the medicinal applications of NHC complexes, there are a few overwhelming similarities. What seems to be one of the most promising similarities is that many of the complexes tested have been shown to be able to elude the typical resistance mechanisms that cancer cells utilize, a property that exhibits the great potential for NHC complexes in medicine. Activity is greatly affected by the substituents on the precursor imidazolium salt. In fact, research has overwhelmingly shown that an increase in lipophilicity will contribute to an increase in activity. However, this can also affect the aqueous solubility of a complex. A delicate balance must be struck between

lipophilicity, for better activity, and aqueous solubility, for ease of medicinal administration. Choice of the anion is also important to both solubility and activity. Luckily, the possibilities of functionalizing ligands with various substituents are endless and thus activity can be fine-tuned. Also of note, some complexes can display antibacterial activity but no anti-cancer activity and vice versa, while some display both. This shows that NHC complexes have a wide range of applications in medicinal chemistry. Of further importance, is that imidazolium salts are able to exhibit biological activity, particularly showing anti-cancer properties while their neutral analogs show no activity. Therefore, it has become increasingly important for researchers to test both the imidazolium salt precursors as well as the NHC complexes side-by-side to obtain more information. The overwhelming pattern of the imidazolium salts is the same as that observed for the NHC complexes, increasing lipophilicity increases the biological activity.

However, there are some challenges to this field of study. One limitation of this area deals with the side effects that could potentially arise. Chemotherapeutics, such as doxorubicin, can have severe effects such as cardiotoxicity, damage to the heart muscle. While the mechanism of doxorubicin toxicity for cancer cells deals with DNA damage, the effects on cardiomyocytes are due to the reduction of doxorubicin in mitochondria producing reactive oxygen species. This is observed in cardiomyocytes due to the high amount of mitochondria present, and this can cause heart failure for patients treated with doxorubicin. These effects are seen with anthracycline containing chemotherapeutics such as doxorubicin and daunorubicin.¹⁵³ This effect pertains to NHC complexes and imidazolium salts due to

the fact that imidazolium salts are compounds that can be classified as delocalized lipophilic cations (DLCs). DLCs are known to target the mitochondria of cells due to the mitochondrial membrane potential, causing cations to be attracted to the inner matrix.¹⁵⁴ If the degradation products of NHC complexes, namely the resulting imidazolium salt, are able to target the mitochondria, cardiotoxicity could cause a serious issue if reactive oxygen species are produced. This leads to the second limitation, being the limited knowledge of the mechanism of action for both imidazolium salts and the corresponding NHC complexes. While there have been important developments in the mechanisms of particular metals, the release of an imidazolium salt that can also exhibit activity is not something that can be ignored. A better understanding of the mechanism of action of all parts of an NHC complex is of utmost importance for moving forward with research. This information can aid in the progression of already synthesized compounds with great potential but could also guide the synthesis of new complexes that have even better activity. It is clear that NHC complexes and imidazolium salts have a promising future in antimicrobial and anti-cancer drug development.

CHAPTER II

IN VITRO EVALUATION OF IMIDAZOLIUM SALTS AS ANTI-CANCER AGENTS

“Reproduced in part with permission from [Wright, B. D.; Deblock, M. C.; Wagers, P. O.; Duah, E.; Robishaw, N. K.; Shelton, K. L.; Southerland, M. R.; DeBord, M. A.; Kersten, K. M.; McDonald, L. J.; Stiel, J. A.; Panzner, M. J.; Tessier, C. A.; Paruchuri, S.; Youngs, W. J. *Med. Chem. Res.* **2015**, *24* (7), 2838–2861.]

[DeBord, M. A.; Southerland, M. R.; Wagers, P. O.; Tiemann, K. M.; Robishaw, N. K.; Whiddon, K. T.; Konopka, M. C.; Tessier, C. A.; Shriver, L. P.; Paruchuri, S.; Hunstad, D. A.; Panzner, M. J.; Youngs, W. J. *Bioorganic Med. Chem. Lett.* **2017**, *27* (4), 764–775.]

[Shelton, K. L.; DeBord, M. A.; Wagers, P. O.; Southerland, M. R.; Taraboletti, A.; Robishaw, N. K.; Jackson, D. P.; Tosanovic, R.; Kofron, W. G.; Tessier, C. A.; Paruchuri, S.; Shriver, L. P.; Panzner, M. J.; Youngs, W. J. *Tetrahedron* **2016**, 1–15.]”

2.1. Introduction

Cancer is one of the leading causes of death in the United States today, preceded only by heart disease. The American Cancer Society expects 1.7 million cancer diagnoses in 2018, excluding basal and squamous cell skin cancers. It is also estimated that over 600,000 Americans in 2018 are expected to die from cancer,

which equates to roughly 1,670 deaths per day. It is estimated that prostate cancer and breast cancer for men and women, respectively, will have the highest percentage of diagnosed cases, followed in both instances by lung cancer. However, it is estimated that around 25% of estimated cancer deaths will be due to lung cancer in 2018 for both men and women, leaving lung cancer to account for more deaths than any other cancer. Research in the area of increasing the survival of those with cancer has allowed the 5-year survival rate of other leading cancers, such as breast cancer, to increase significantly with current survival rates being 90% for breast cancer. However, for lung cancer, the 5-year survival rate has increased marginally with an 18% 5-year survival rate today. One major issue in the treatment of lung cancer is that it can go largely unnoticed until the cancer is at an advanced stage, leading to difficulty in treatment. While determining more efficient methods to diagnose lung cancer would be beneficial, it is also important to develop new ways that are more effective for the treatment of lung cancer, as even the 16% of lung cancer cases that are diagnosed at a localized stage have a 5-year survival rate of only 56%.¹⁵⁵

Currently, lung cancer is treated by a combination of surgery, radiation and chemotherapy, depending on the stage and type of lung cancer present. Lung cancer is divided into two categories, small cell and non-small cell with the latter accounting for 84% of the diagnosed cases.¹⁵⁵ Cisplatin is a first line treatment for lung cancer but there are issues that arise from the use of cisplatin. Oftentimes cancer cells have an intrinsic or develop an acquired resistance to drugs such as cisplatin. Also, the negative effects of platinum toxicity lead to unwanted side effects

such as ototoxicity or nephrotoxicity.¹⁵⁵⁻¹⁵⁸ Recent literature has shown that imidazolium salts are a class of organic compounds that have a promising ability to stop the proliferation of non-small cell lung cancer cells (NSCLCs), the most common type of lung cancer.^{26,149-152} Originally finding use as N-heterocyclic carbene precursor ligands, imidazolium salts have found their own application in medicinal chemistry as potential chemotherapeutics. Unfortunately, there is a limited amount of information known about how imidazolium salts kill cancer cells. As more knowledge is gained about the anti-proliferative effect of imidazolium salts, the synthesis of new, more effective compounds can be completed.

Lead compounds that have been previously outlined by the Youngs lab include compounds **II 1- II 5** (Figure II-1).^{26,149,151} These compounds were identified as lead compounds by the MTT assay. While the MTT assay is useful for the rapid testing of a large library of compounds, it gives no information about how the cancer cells are killed. For further information, other assays must be incorporated. This chapter focuses on the *in vitro* evaluation of imidazolium salts by the MTT assay, Annexin V assay and the JC-1 assay. Furthermore, DNA studies will be presented in order to evaluate whether or not imidazolium salts have the ability to interact with DNA.

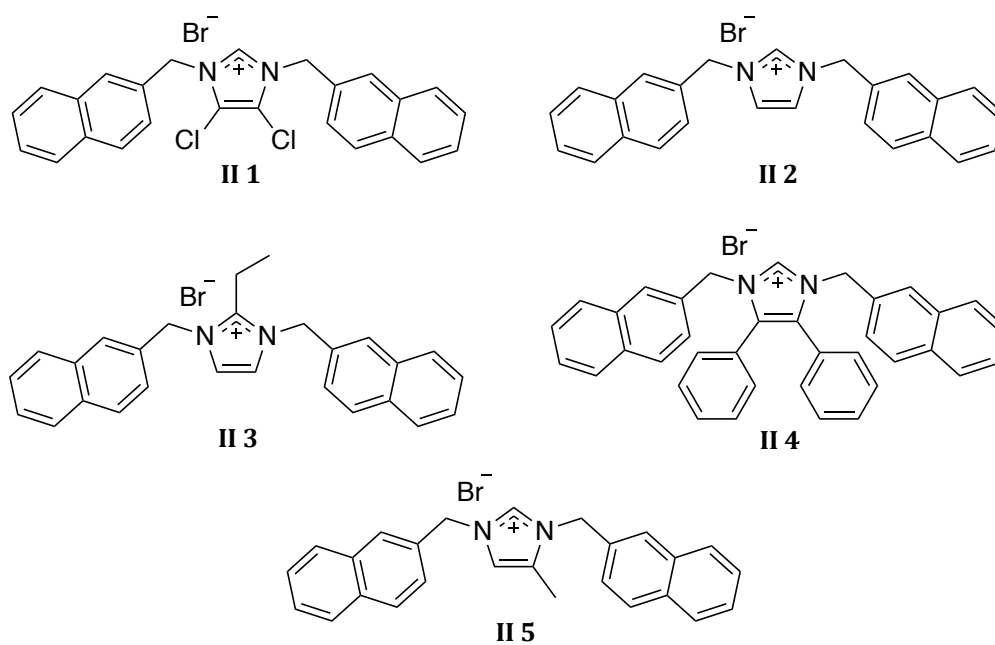
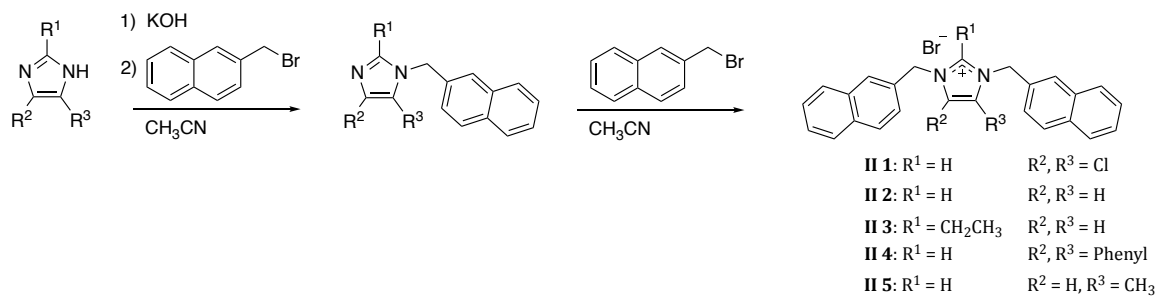


Figure II-1. Structures of compounds **II 1–II 5**.

2.2. Results and Discussion

2.2.1. General Synthesis

Compounds **II 1–II 5** have been synthesized based on previously published procedures.^{26,149,151,159} The general synthesis of these imidazolium salts is outlined in Equation II-1.



Equation II-1. Synthesis of compounds **II 1–II 5**.

Briefly, 4,5-dichloroimidazole was deprotonated with a slight excess of potassium hydroxide at reflux for 1 h. 2-(Bromomethyl)naphthalene was then added and after 2.5 h of stirring, a precipitate (presumed to be potassium bromide) was removed by vacuum filtration. Another equivalent of 2-(bromomethyl)naphthalene was then added to the filtrate which was allowed to stir at reflux for 1.5 h. The product, **II 1**, was isolated by vacuum filtration.¹⁵⁹

Compound **II 2** was produced by the same reaction with the starting material being imidazole rather than 4,5-dichloroimidazole. Imidazole was stirred at reflux for 0.5 h with a slight excess of potassium hydroxide. 2-(Bromomethyl)naphthalene was introduced in two separate additions in refluxing acetonitrile. The first addition was refluxed for 2.5 h before the precipitate (presumed to be potassium bromide) was removed by vacuum filtration. Subsequently the second addition of 2-(bromomethyl)naphthalene was added and refluxed for 1 h. A white solid, **II 2**, was isolated after volatiles were removed and the resulting oil was extracted with hot water. Compound **II 2** was precipitated from the cooled water layers and isolated by filtration.

The starting imidazole for compound **II 3**, 2-ethylimidazole, was deprotonated with a slight excess of potassium hydroxide followed by addition of 2-(bromomethyl)naphthalene. The mixture was refluxed overnight, which resulted in formation of a white precipitate (presumed to be potassium bromide) that was removed by filtration. 2-(Bromomethyl)naphthalene was added to the filtrate and the mixture was refluxed overnight. Compound **II 3** precipitated after the addition of diethyl ether to the reaction mixture and was washed with diethyl ether to

remove any excess 2- (bromomethyl)naphthalene. The final product was recrystallized from ethanol.

Compound **II 4** was prepared by stirring 4,5-diphenylimidazole with a slight excess of potassium hydroxide for 0.5 h to which was added one equivalent of 2-(bromomethyl)naphthalene in refluxing acetonitrile overnight. Removal of the generated precipitate (presumed to be potassium bromide) and the addition of one equivalent of the 2-(bromomethyl)naphthalene in refluxing acetonitrile overnight produced compound **II 4** which was removed by filtration and washed in diethyl ether.

Compound **II 5** was prepared by deprotonating the starting material, 4-methylimidazole, with potassium hydroxide and subsequently adding 2-(bromomethyl)naphthalene which was refluxed. The resulting precipitate was removed by filtration and a second equivalent of 2-(bromomethyl)naphthalene was added to the refluxing mixture to generate **II 5**. Crystals suitable for single crystal X-ray diffraction were obtained by slow evaporation of a concentrated solution of **II 5** in acetonitrile.

Compounds **II 1** – **II 5** were characterized by ^1H and ^{13}C NMR spectroscopy, mass spectrometry and melting point determination. Structures of **II 2**, **II 3**, and **II 5** were determined by single-crystal X-ray diffraction (Figures II-2 - II-4). In the ^1H NMR spectra, the chemical shifts of the methylene linkers bridging the imidazole ring and the naphthalene rings were used as evidence for the formation of the imidazolium salts. The chemical shift of the methylene linker in the desired imidazolium salts ranged from 5.61 ppm to 5.71 ppm. The second naphthylation

was indicated by a downfield shift of the mono-naphthylated intermediate due to the deshielding effect of the cationic imidazolium ring. Where applicable, the C²-H imidazolium proton signal was also an indicator of the formation of the desired products as the range (9.50 ppm to 9.79 ppm) was also shifted downfield by the deshielding effect of the cationic imidazolium ring. The ¹³C NMR spectra were consistent with the proposed structures. Additionally, ESI mass spectrometry in the positive mode was performed on the imidazolium salts, and the identity of each product was strongly supported by the presence of the corresponding [M-Br]⁺ fragment in its spectrum.

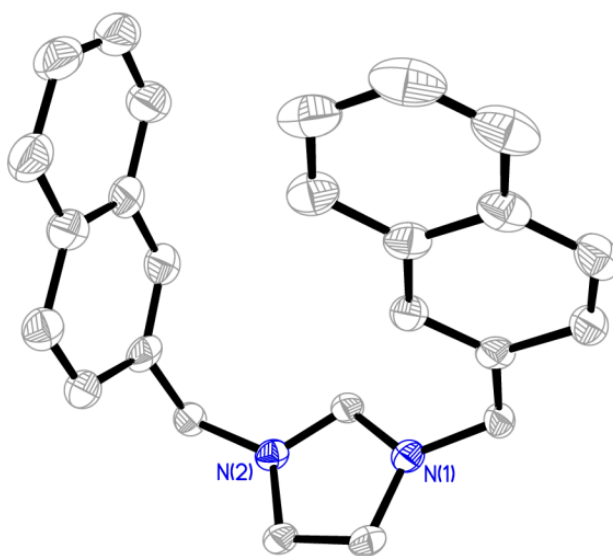


Figure II-2. Thermal ellipsoid plot of the cationic portion of **II 2** with thermal ellipsoids drawn at 50 % probability. Hydrogen atoms, carbon labels and the bromide anion have been removed for clarity

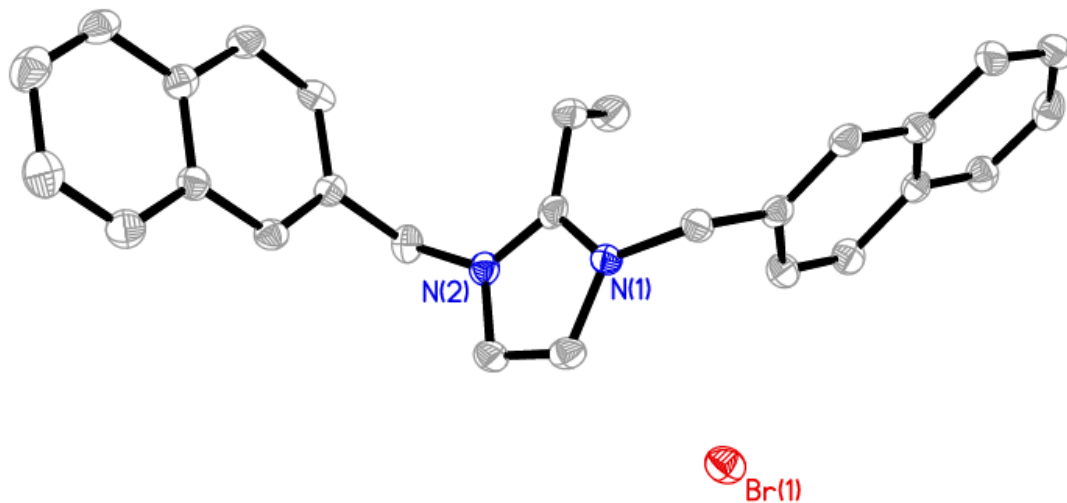


Figure II-3. Thermal ellipsoid plot of **II 3** with thermal ellipsoids drawn at 50% probability. Hydrogen atoms and carbon labels have been removed for clarity.

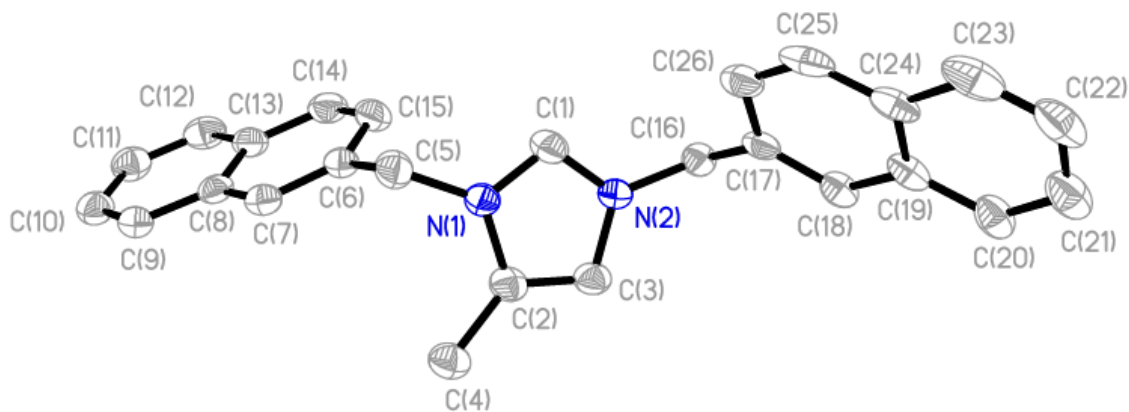


Figure II-4. Thermal ellipsoid plot of **II 5** with thermal ellipsoids drawn at 50% probability. Hydrogen atoms and bromide anion have been removed for clarity.

2.2.2. *In vitro* studies

2.2.2.1. MTT Assay

The anti-cancer activity of compounds **II 1** - **II 5** were evaluated against several NSCLC cell lines (NCI-H460, NCI-H1975, A549, and HCC827). Cells were exposed to compounds **II 1** - **II 5** or cisplatin for 72 hours, at which time the MTT assay was utilized to determine cell viability. The anti-proliferative effects of compounds **II 1** - **II 5** were evaluated by their IC₅₀ values, where the IC₅₀ value denotes the drug concentration at which there was 50% inhibition in cell viability relative to control cells. The major disadvantage of imidazolium salts with naphthylmethyl substituents on both nitrogen atoms is their low water solubility.²⁶ Therefore, solutions of each compound were prepared by first dissolving the compound in DMSO and then diluting with water to a final concentration of 1% DMSO in water. Compounds were further diluted into growth medium with a maximum DMSO concentration of 0.032% that was added to the cells. A solution of cisplatin was prepared by adding the compound to pure water and stirring at room temperature for several hours. Compounds **II 1** - **II 5** had varying degrees of solubility in the 1% DMSO in water solution and to our knowledge there are no approved drugs on the market that are co-formulated with DMSO for the treatment of cancer. Therefore, a different vehicle would be necessary to increase water solubility and allow for systemic administration. Excipients such as 2-hydroxypropyl- β -cyclodextrin (HPCD) have also been included to determine the effect of this excipient on the activity of imidazolium salts. A solution of 10% (w/v)

of HPCD in water was used with the HPCD being weighed and solubilized in water before addition of the solution to the pre-weighed imidazolium salt. The maximum concentration of HPCD in treated wells was 0.008% by weight. The concentration of HPCD in all control wells was 0.008% by weight. Cells treated with fresh medium were also compared to cells treated with HPCD and virtually no toxicity was observed (when considering the four different cell lines tested, cells treated with HPCD grew at rates of 96–106% when compared to cells treated with medium alone).

Table II-1. IC₅₀ values of compounds **II 1** – **II 5** in either 1% DMSO/water or a 10% (w/v) HPCD solution.

Compound (Solubilizing agent)	Cell Line and IC ₅₀ values (μM)			
	NCI-H460	NCI-H1975	A549	HCC827
II 1 (DMSO)	5	5	9	6
II 2 (DMSO)	4	6	10	9
II 3 (DMSO)	1	<1	3	2
II 3 (HPCD)	1	<1	3	2
II 4 (DMSO)	3	1	3	2
II 5 (DMSO)	3	3	ND	4
Cisplatin	3	10	6	5

ND = Not determined

The IC₅₀ values of **II 1** – **II 4** were comparable to those of cisplatin, indicating the great potential of these compounds as anti-proliferative agents against NSCLC. With the low aqueous solubility of these compounds, it is important to note that the IC₅₀ values of **II 3** do not significantly change when comparing the DMSO versus the

HPCD solutions. This shows that at the MTT testing time of 72 hours, there is no difference in efficacy. In previous studies, lipophilicity has been shown to play a very important role in the anti-cancer activity of compounds like imidazolium salts. This is presumed to be due to the fact that lipophilicity is essential for crossing the cell membrane. As more water solubility is imparted from more hydrophilic substituents, activity decreases but water solubility increases. It is therefore extremely important to find a balance between lipophilicity and water solubility. The use of HPCD, an excipient that is generally regarded as safe (GRAS) by the Food and Drug Administration (FDA), is therefore a way to impart solubility without compromising activity.¹⁶⁰ It is also important to note that the presence of electron withdrawing groups, such as the chlorides of **II 1**, and bulky lipophilic groups, such as the phenyl rings of **II 4**, allow for modification of the imidazole core without a decrease in activity. The possibilities of functionalization at all positions of the imidazole core lead to an endless amount of possible compounds that can be made. As more information is gained about how these compounds work, they can be modified accordingly for even better activity.

2.2.2.2. National Cancer Institute Developmental Therapeutics Program

The National Cancer Institute's (NCI) Developmental Therapeutics Program (DTP) tested **II 1** – **II 5** in their 60 human tumor cell line one-dose and five-dose assays. The 60 human tumor cell line panel consists of nine non-small cell lung cancer lines, two of which we also tested in our laboratory, the NCI-H460 and A549 lines. In the one-dose assay, each cell line is exposed to the tested compound at a single dose (10 μ M). Results are given as a growth percentage relative to the initial

number of cells at the beginning of the study. Briefly, cells are plated at a density relative to their doubling rate and incubated overnight. Compounds are exposed to the cells at 10 μ M for 24 h. Growth percentage is calculated by comparing the protein density at the end of the experiment to the protein density of control cells not treated with any drug as related to the number of cells at the beginning of the experiment. Values for growth percent range from -100 (all cells are dead) to 100 (all cells are still alive). For example, a growth percent value of 60 would mean that there was a 40% growth inhibition and a value of -60 would mean 60% lethality and a value of 0 means that there is no overall growth of the cells. Full experimental details can be found on the NCI's DTP webpage (https://dtp.cancer.gov/discovery_development/nci-60/methodology.htm).

Results for the one-dose assay can be found in Table II-2. These results show some general trends. First, it is clear that **II 4** is a lethal compound, with all growth percent values being negative. This demonstrates that adding lipophilicity and steric bulk to the C⁴ and C⁵ positions render derivatives like **II 4** extremely toxic. In fact, compound **II 4** displayed negative growth percentages for all cell lines tested in the study with the exception of the cell line NCI/ADR-RES, an ovarian cancer cell line that is adriamycin (doxorubicin) resistant and has elevated levels of P-glycoprotein, according to the NCI. Another observed trend is that compounds **II 1** – **II 5** all exhibit negative growth percentages for the HOP-92 and NCI-H522 cell lines. It is also important to note that in this 60 human tumor cell line panel, **II 1** – **II 5** also exhibit growth percent values that indicate they are effective against melanoma cell lines.

Table II-2. Growth percent values for NSCLC cell lines treated with **II 1** – **II 5** in the NCI DTP 60 human tumor cell line one-dose assay.

Compound	Cell Line									Average
	A549/ATCC	EKVX	HOP-62	HOP-92	NCI-H226	NCI-H23	NCI-H322M	NCI-H460	NCI-H522	
II 1	52.51	38.66	-27.63	-12.05	44.36	32.77	51.04	26.13	-52.54	17.03
II 2	67.63	51.65	42.12	-13.30	52.09	41.65	62.77	39.60	-11.71	36.94
II 3	28.54	11.92	11.94	-31.42	6.75	-14.57	44.31	5.54	-25.40	4.18
II 4	-81.83	-46.67	-86.12	-83.90	-75.79	-74.86	-20.79	-78.57	-85.76	-70.48
II 5	60.54	38.14	33.16	-20.86	31.78	27.66	65.66	21.86	-17.86	26.68

Compounds **II 1** – **II 5** were selected to be tested in the five-dose assay. In this assay, cells are exposed to compounds at concentrations of 10 nM, 100 nM, 1 μ M, 10 μ M, and 100 μ M. Results for this assay are given as GI₅₀ (growth inhibition of 50% of cell relative to control cells), TGI (total growth inhibition in relation to control cells), and LC₅₀ (lethal concentration for 50% of cells relative to control cells) values. Results are summarized in Table II-3. Of note, the only LC₅₀ value that could be determined for **II 4** was for the HOP-92 cell line at 3.98 μ M, a compound outlined by our MTT assay studies as an effective drug with IC₅₀ values ranging from 1-3 μ M. Results from the 5-dose assay correlate well to our results from the MTT assay, verifying that compounds **II 1** - **II 5** have potent anti-cancer activity.

Table II-3. GI₅₀, TGI, and LC₅₀ values for NSCLC cell lines treated with **II 1** – **II 5** in the NCI DTP 60 human tumor cell line one-dose assay. All values are presented in μM concentrations.

Compound	Value	Cell Line								
		A549/ ATCC	EKVX	HOP- 62	HOP- 92	NCI- H226	NCI- H23	NCI- H322M	NCI- H460	NCI- H522
II 1	GI ₅₀	3.31	1.83	1.26	0.733	1.85	1.35	1.87	1.53	1.12
	TGI	11.7	4.98	2.61	2.14	4.11	3.15	4.46	2.98	2.66
	LC ₅₀	51.1	32.4	5.39	5.11	N/A	7.34	13.1	5.81	6.32
II 2	GI ₅₀	7.97	2.51	3.26	0.160	1.72	0.901	8.40	1.27	0.393
	TGI	22.9	15.5	17.0	1.39	14.3	10.1	21.3	10.4	3.11
	LC ₅₀	55.3	47.5	45.9	15.2	71.9	39.4	47.3	42.0	26.8
II 3	GI ₅₀	2.59	0.766	1.42	0.338	1.08	0.396	2.12	0.724	0.303
	TGI	13.9	5.55	3.65	1.77	3.82	2.02	6.71	2.15	1.44
	LC ₅₀	57.9	35.8	9.36	8.51	51.0	8.35	26.0	5.44	4.94
II 4	GI ₅₀	1.00	0.837	1.41	0.122	1.20	0.445	1.20	0.384	0.325
	TGI	2.48	2.29	2.97	1.26	3.16	1.88	2.50	1.65	1.78
	LC ₅₀	N/A	N/A	N/A	3.98	N/A	N/A	N/A	N/A	N/A
II 5	GI ₅₀	5.05	2.15	1.61	0.448	2.12	1.49	2.87	1.72	1.41
	TGI	18.7	9.71	3.80	2.02	5.87	3.97	10.3	3.65	3.06
	LC ₅₀	53.5	43.8	8.97	6.49	>100	12.5	33.7	7.75	6.63

2.2.2.3. Annexin V Assay

While the MTT assay is a great way to determine whether a compound can inhibit the proliferation of cancer cells, it gives no information on how this occurs. Determining a mechanism of action (MOA) for a compound or group of compounds is extremely important. Not only does the MOA tell you what the compound does, it can also allow you to gain enough information to drive the synthesis of new, more effective therapeutic derivatives. However, determining a compound's MOA is not a simple task. An organized, step-wise approach must be employed in order to tackle this problem in a systematic way. We therefore have decided to first utilize the Annexin V assay in order to distinguish between the processes of apoptosis and necrosis.

In cells that undergo apoptosis, phosphatidylserine (PS) is detected on the outside of the cellular membrane.¹⁶¹ This occurs during the early stages of apoptosis because cell membrane asymmetry and integrity is lost allowing PS to translocate to the outer leaflet of the cell membrane where it can interact with Annexin V, which is conjugated to FITC to give fluorescence detectable by microscopy. In order to fully distinguish apoptosis from necrosis, a secondary stain is necessary. Propidium iodide (PI), which interacts with DNA, is a cell membrane impermeable compound. It only has the ability to enter cells that have compromised membranes, which occurs later in the process of apoptosis.¹⁶¹ The progression in time of cells from having strictly green fluorescence to green and red fluorescence is indicative of apoptosis. On the other hand, necrotic cells would be visualized with both green and red fluorescence even at early time points. Cell morphology is also an important indicator with blebbing being a distinction for cells going through the process of apoptosis.

Compounds **II 1** – **II 5** were tested for mode of cell death using the Annexin V kit. Figure II-5 shows the progression of apoptosis caused by the introduction of compound **II 1** into the growth media at increasing time frames. As a comparison, negative and positive controls were tested alongside the **II 1** treated cells. The negative control consisted of H460 cells grown in media, and H460 cells grown in the presence of cisplatin constituted the positive control, as cisplatin is a known inducer of apoptosis. Treatment of cells with **II 1** for a period of 1 hour revealed cells in the early stage of apoptosis. These results were comparable to the cisplatin positive control images after treatment for 6 hours. Cells treated with **II 1** for a

period of 3 hours showed late stage apoptotic cells based on the visualization of both red and green fluorescence. Blebbing, a common indicator of apoptosis, could be visualized at this time point (Figure II-5 (D) and Figure II-6). After treatment of **II 1** for 6 hours, imaged cells showed both red and green fluorescence. This combined with the absence of blebbing lead to the conclusion that these cells were in the end stage of apoptosis and were no longer viable. These results indicate that treatment of H460 cells with **II 1** induces apoptosis at a faster rate than what is observed with cisplatin.

In a similar experiment, H460 cells were treated with **II 2** (Figure II-7), an analogue of **II 1**, which employs hydrogen in the C⁴ and C⁵ positions rather than chlorine. While cells could be visualized in the early stages of apoptosis, this was not seen until the latest time period at 6 hours. These cells were relatively comparable to the cisplatin treated cells visualized at the same time period. Treatment with **II 2** at 1 hour and 3 hours were similar to the control cells. When comparing these cells to the **II 1** treated cells it is obvious that while **II 2** can cause H460 cells to begin the early stages of apoptosis, it takes a longer time frame to do so than **II 1**. This experiment shows that while there may be a difference in time needed for full effect of naphthalene substituted analogues, they do cause cells to go through the process of apoptosis. In a separate experiment, H460 cells were treated with **II 2** for longer time periods (8-14 hours) in order to determine how long it would take for **II 2** to exert its anti-proliferative effects as demonstrated by the MTT assay (Figure II-8). Red fluorescence as well as blebbing could be visualized at the 12 and 14 h time points (Figure II-9). This progression of fluorescence with the presence of blebbing

indicates that **II 2** is able to induce apoptosis but that more time is needed for this process to occur.

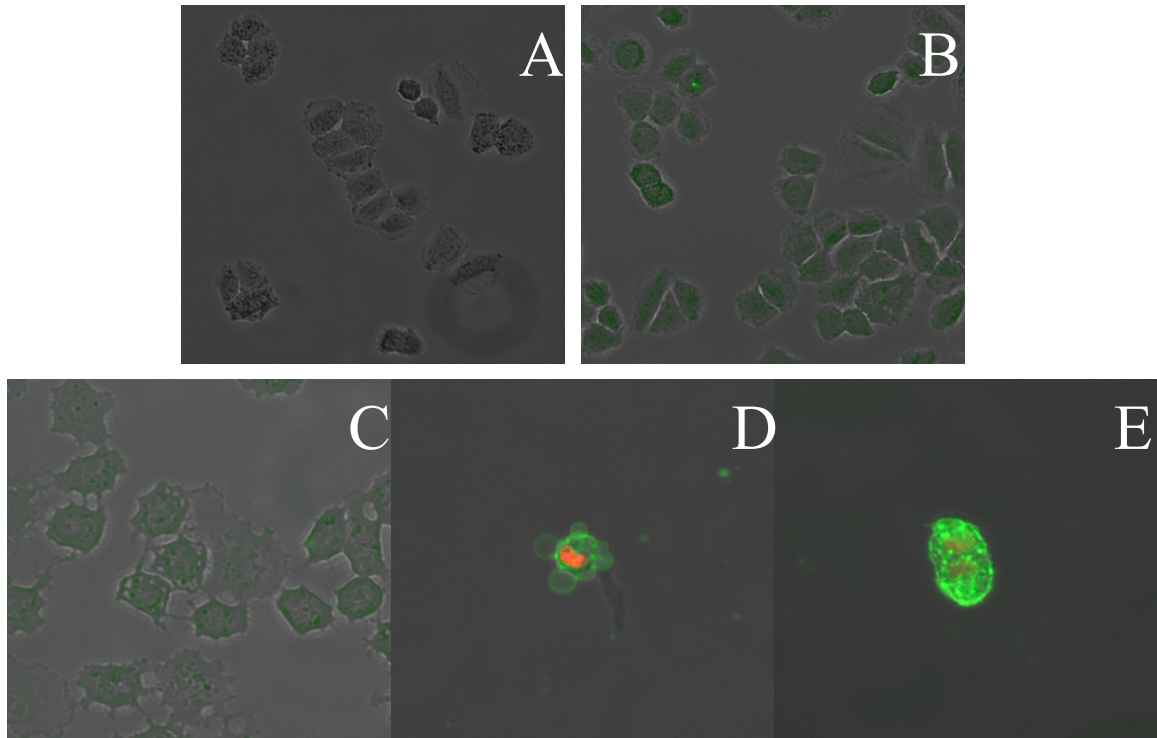


Figure II-5. H460 cells grown in 6-well plates. Merged images of Annexin V (green), propidium iodide (red), and normal transmitted light image. Images captured using an EVOS fl Digital Inverted Microscope with the 10x objective (A and B), and the 20x objective (C-E). A: Control cells grown in the presence of 10% FBS supplemented RPMI-1640 media. B: Cells grown in the presence of 40 μ M cisplatin. Note that the presence of green fluorescence indicates early stage apoptosis. H460 cells grown in the presence of 40 μ M **II 1** for a period of (C) 1 hour, (D) 3 hours, and (E) 6 hours. Note the presence of early stage apoptotic cells comparable to the 6 hour cisplatin treatment at 1 hour, late stage apoptotic cells showing blebbing at 3 hours, and dead, end stage apoptotic cells at 6 hours

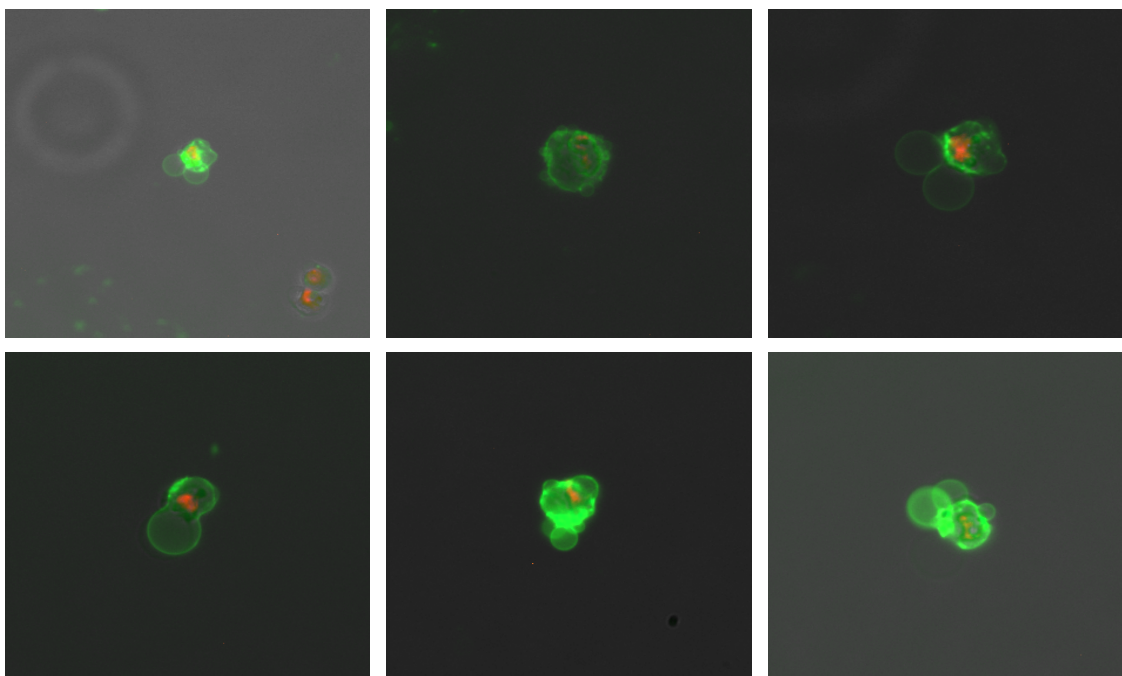


Figure II-6. H460 cells grown in 6-well plates. Merged images of Annexin V (green), propidium iodide (red), and normal transmitted light image. Images captured using an EVOS fl Digital Inverted Microscope with the 20x objective. Blebbing was observed after 3 hour treatment with **II 1** at 40 μ M

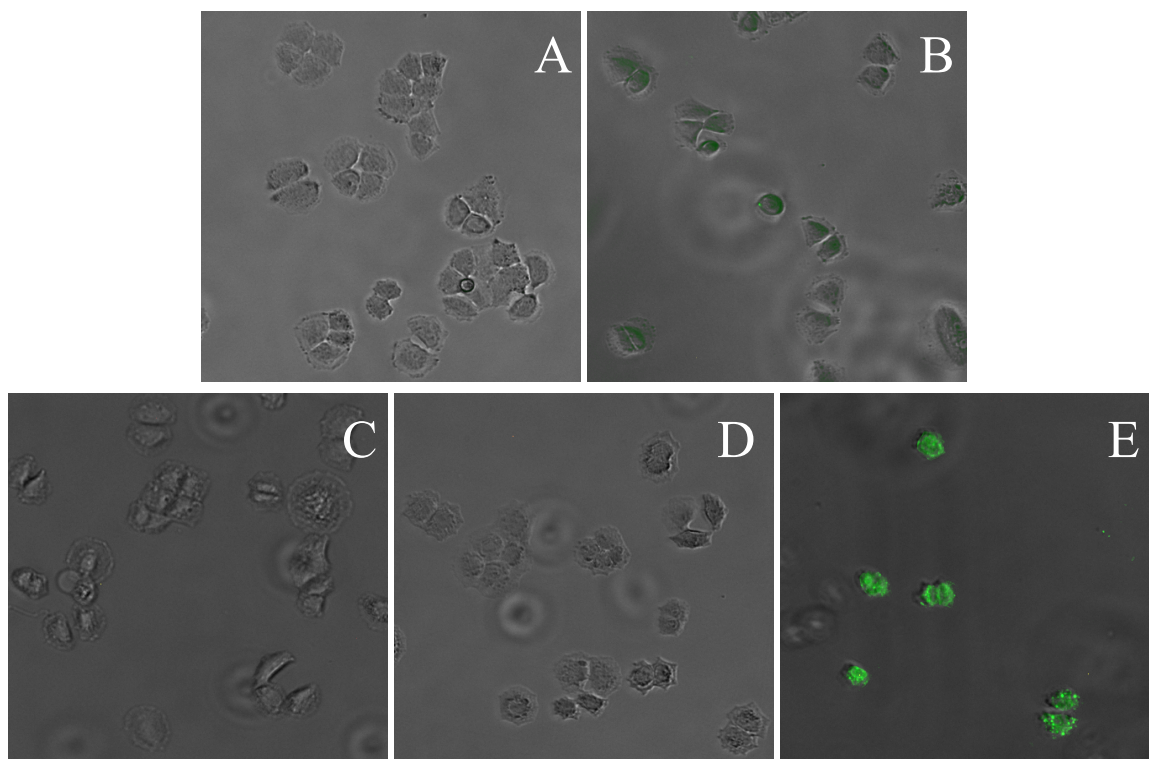


Figure II-7. H460 cells grown in 6-well plates. Merged images of Annexin V (green), propidium iodide (red), and normal transmitted light image. Images captured using an EVOS fl Digital Inverted Microscope with the 10x and the 20x objectives. A: Control cells grown in the presence of 10% FBS supplemented RPMI-1640 media. B: Cells grown in the presence of 40 μ M cisplatin. Note that the presence of green fluorescence indicates early stage apoptosis. H460 cells grown in the presence of 40 μ M **II 2** for a period of (C) 1 hour, (D) 3 hours, and (E) 6 hours. Note the presence of early stage apoptotic cells at 6 hours

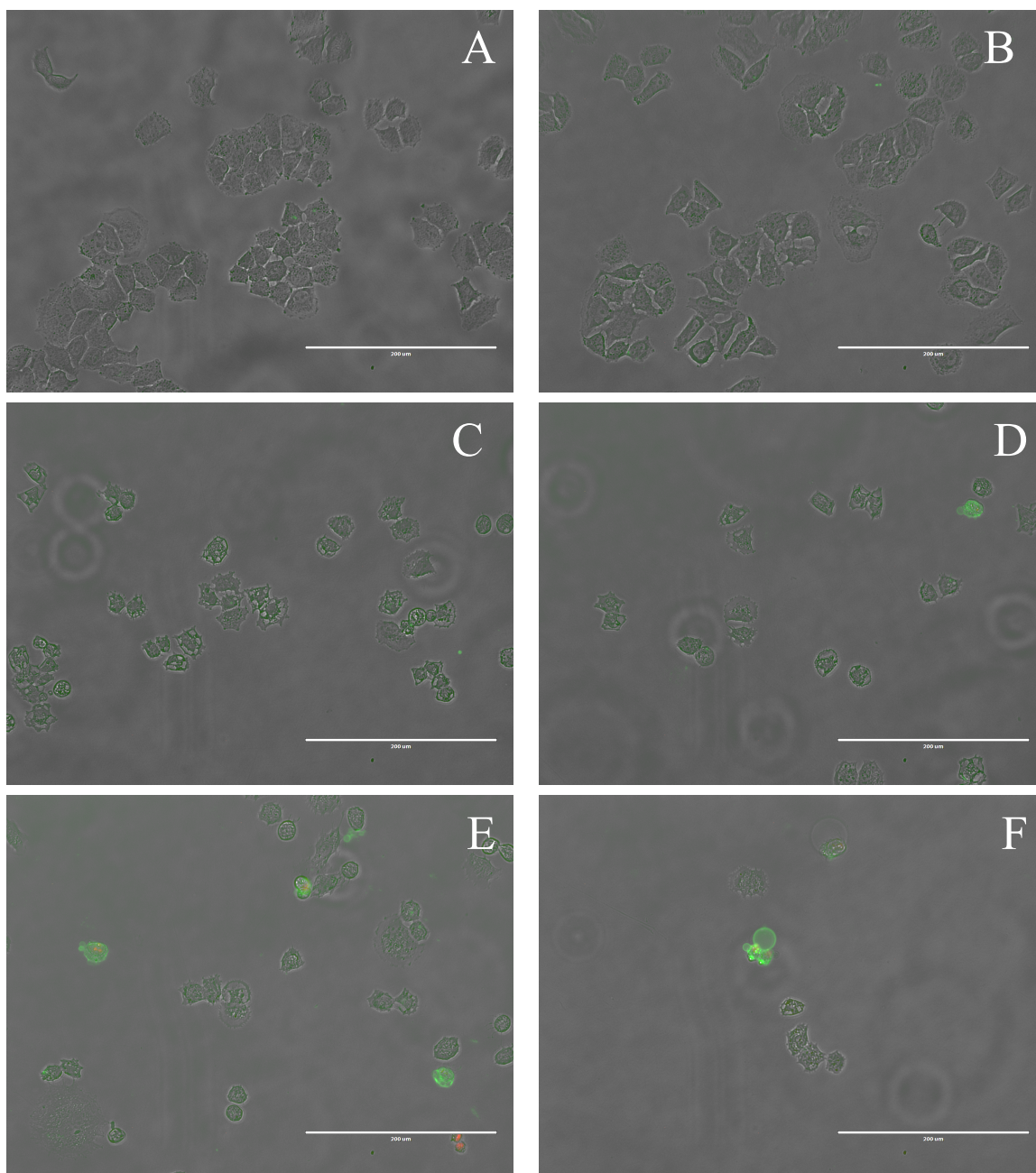


Figure II-8. H460 cells grown in 6-well plates. Merged images of Annexin V (green), propidium iodide (red), and normal transmitted light image. Images captured using an EVOS fl Digital Inverted Microscope. A: DMSO Control cells. B: Cells grown in the presence of 40 μ M cisplatin for 14 h. Note that the presence of green fluorescence indicates early stage apoptosis. H460 cells grown in the presence of 40 μ M **II 2** for a period of (C) 8 hours, (D) 10 hours, (E) 12 hours, and (F) 14 hours.

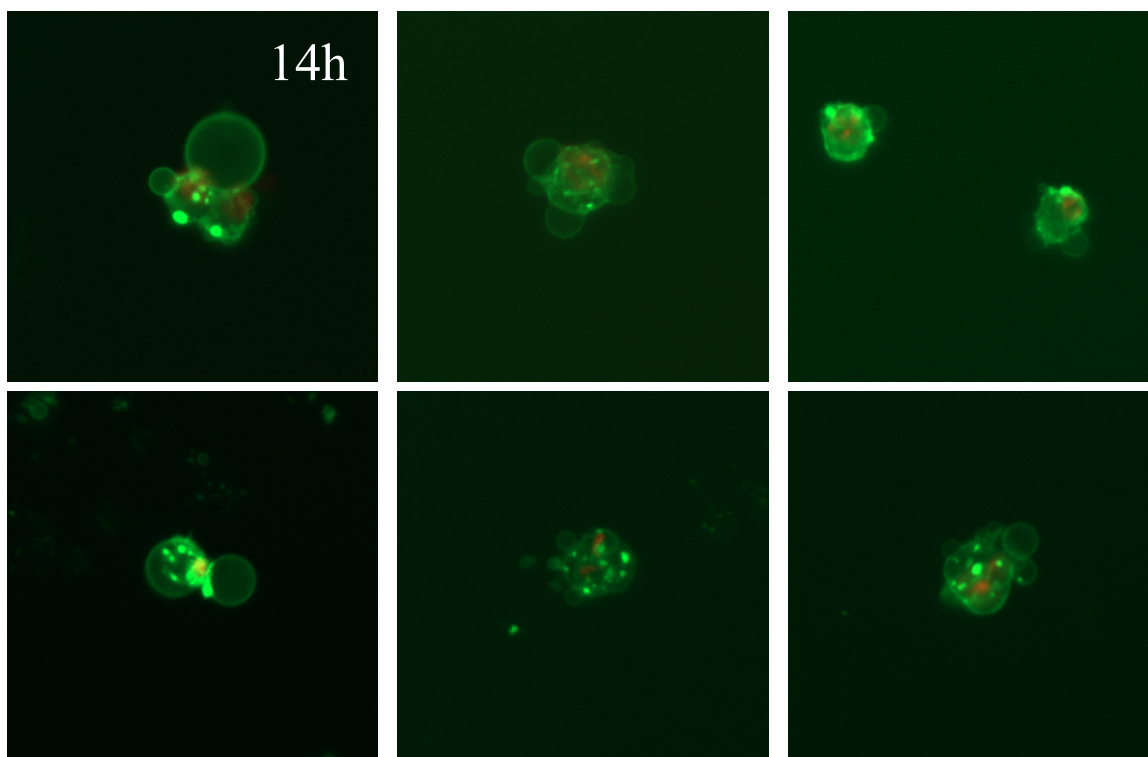


Figure II-9. H460 cells grown in 6-well plates. Merged images of Annexin V (green), propidium iodide (red). Images captured using an EVOS fl Digital Inverted Microscope with the 20x objective. Blebbing was observed after 12 hour treatment with **II 2** at 40 μ M. All images were taken at the 12 hour time point, unless otherwise noted

The Annexin V assay was performed with compound **II 3** to determine if adding an alkyl group to the C² position would influence the initiation of cellular death. The results comparing **II 1** and **II 2** indicate that subtle changes to the imidazole scaffold can have effects on anti-proliferative efficacy. Strong green fluorescence was observed for **II 3** when dissolved in a 1% DMSO/ water solution at time points similar to that of **II 1** (i.e., 1 h). However, when **II 3** was dissolved in the 10% by weight HPCD aqueous solution, strong green fluorescence was not observed until the 12 h time point. Compound **II 3** also caused blebbing when administered with either DMSO or HPCD as the solubilizing vehicle. However, a stark contrast can

be seen in the time frames of when this occurs. When in DMSO, blebbing occurs at 6 h of treatment, whereas blebbing was not seen until 14 h of treatment when **II 3** was dissolved with HPCD (Figures II-11 and II-13). This suggests that **II 3** not only causes apoptosis in two independent Annexin V trials, but that the vehicle used to administer it has an effect on compound availability and timely progression of cell fate. It is known that when compounds are dissolved in cyclodextrin solutions there is equilibrium between the freely dissolved compound and the compound in complex with the cyclodextrin. Therefore, the delay in detecting the early stages of apoptosis visualized in cells treated with **II 3** dissolved in HPCD compared to **II 3** dissolved with DMSO was not surprising and further studies are underway to better understand this interaction.

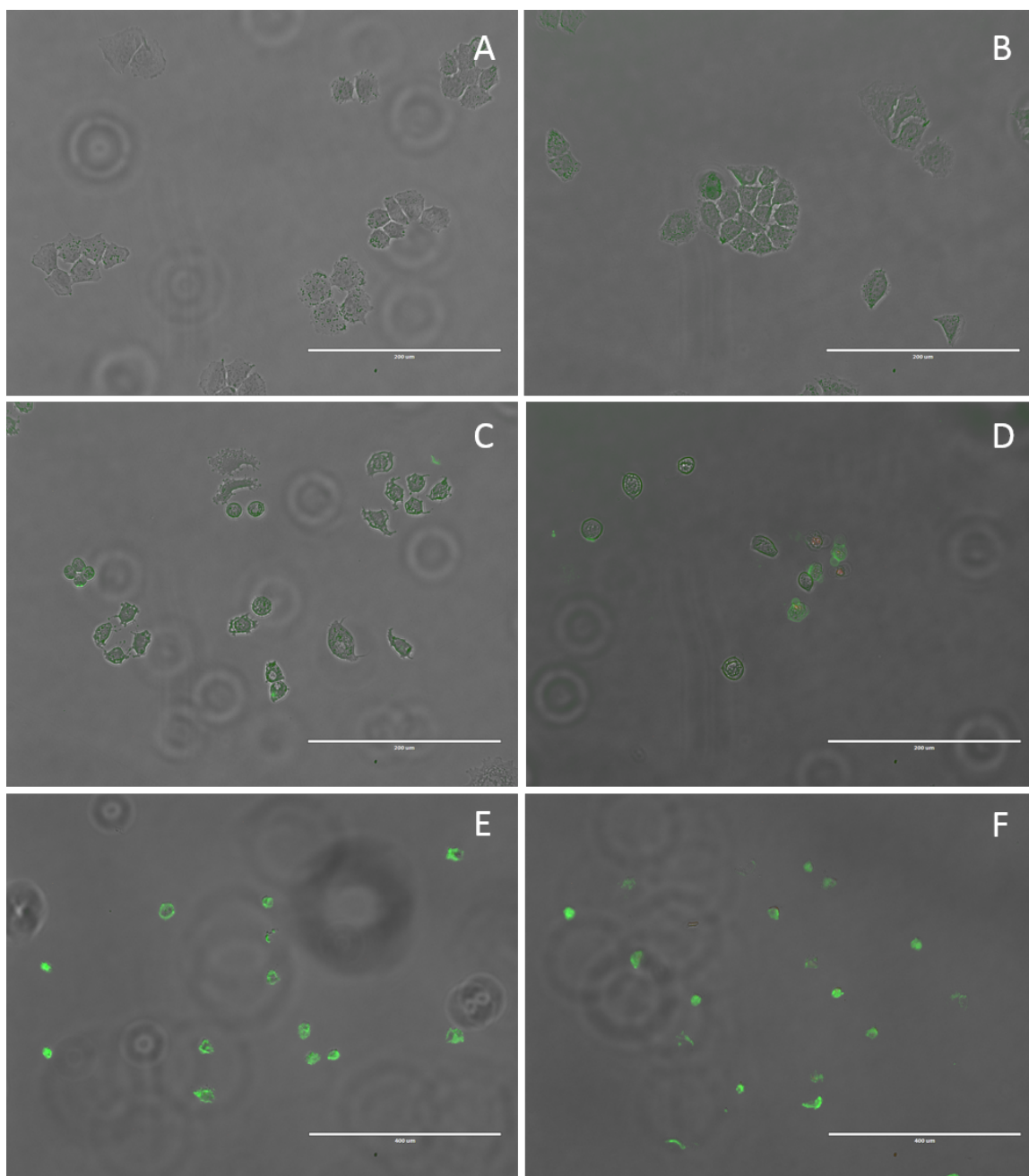


Figure II-10. Images of the Annexin V assay on H460 cells grown in 6-well plates using compound **II 3** in 1% DMSO aqueous solution as the compound treatment. All images taken using a 20x objective unless otherwise stated. Images are presented as a merged image of the normal transmitted light, green fluorescence and red fluorescence figures. (A) DMSO control, 12 hours. (B) Cisplatin control, 12 hours. (C) **II 3**, 1 hour. (D) **II 3**, 3 hours. (E) **II 3**, 6 hours, 10x objective. (F) **II 3**, 12 hours, 10x objective. (A-D) Scale bars equal 200 μm ; (E and F) Scale bars equal 400 μm .

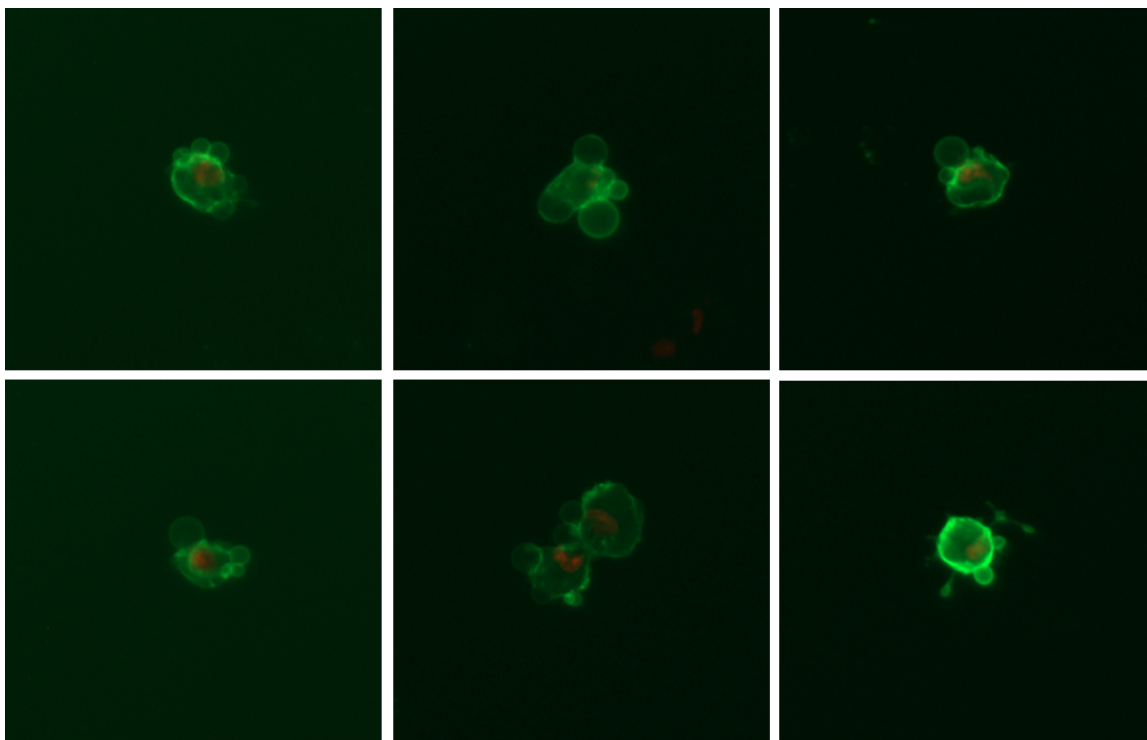


Figure II-11. Images of the Annexin V assay on H460 cells grown in 6-well plates using compound **II 3** in 1% DMSO aqueous solution as the compound treatment. All images taken using a 20x objective. Images are presented as a merged image of the green fluorescence and red fluorescence figures, omitting the normal transmitted light image for blebbing clarity. All images taken at the 3 hour time point.

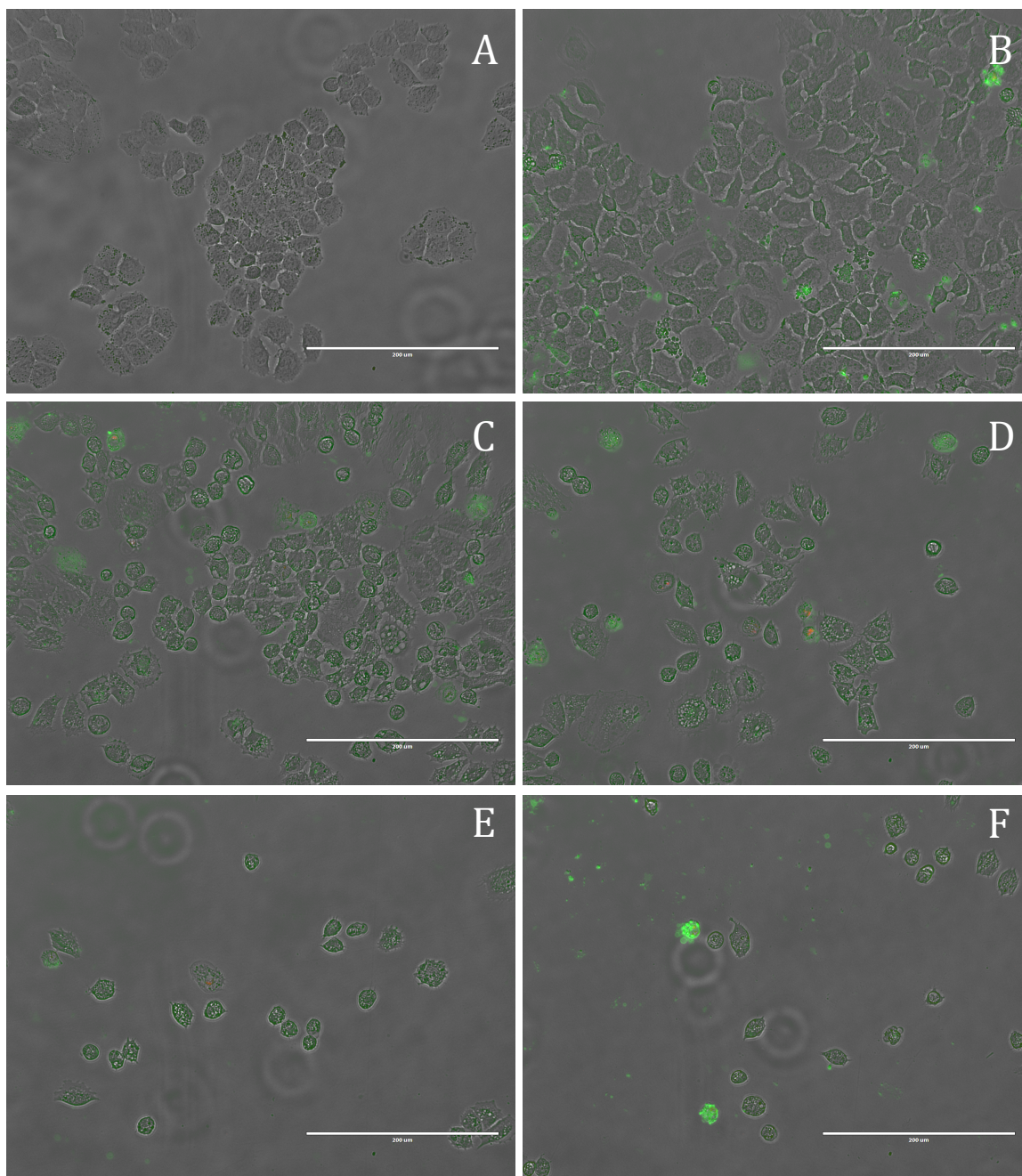


Figure II-12. Images of the Annexin V assay on H460 cells grown in 6-well plates using compound **II 3** in 10% by weight HPCD aqueous solution as the compound treatment. All images taken using a 20x objective. Images are presented as a merged image of the normal transmitted light, green fluorescence and red fluorescence figures. (A) HPCD control, 20 hours. (B) Cisplatin control, 20 hours. (C) **II 3**, 12 hours. (D) **II 3**, 14 hours. (E) **II 3**, 17 hours. (F) **II 3**, 20 hours. Scale bars equal 200 μm .

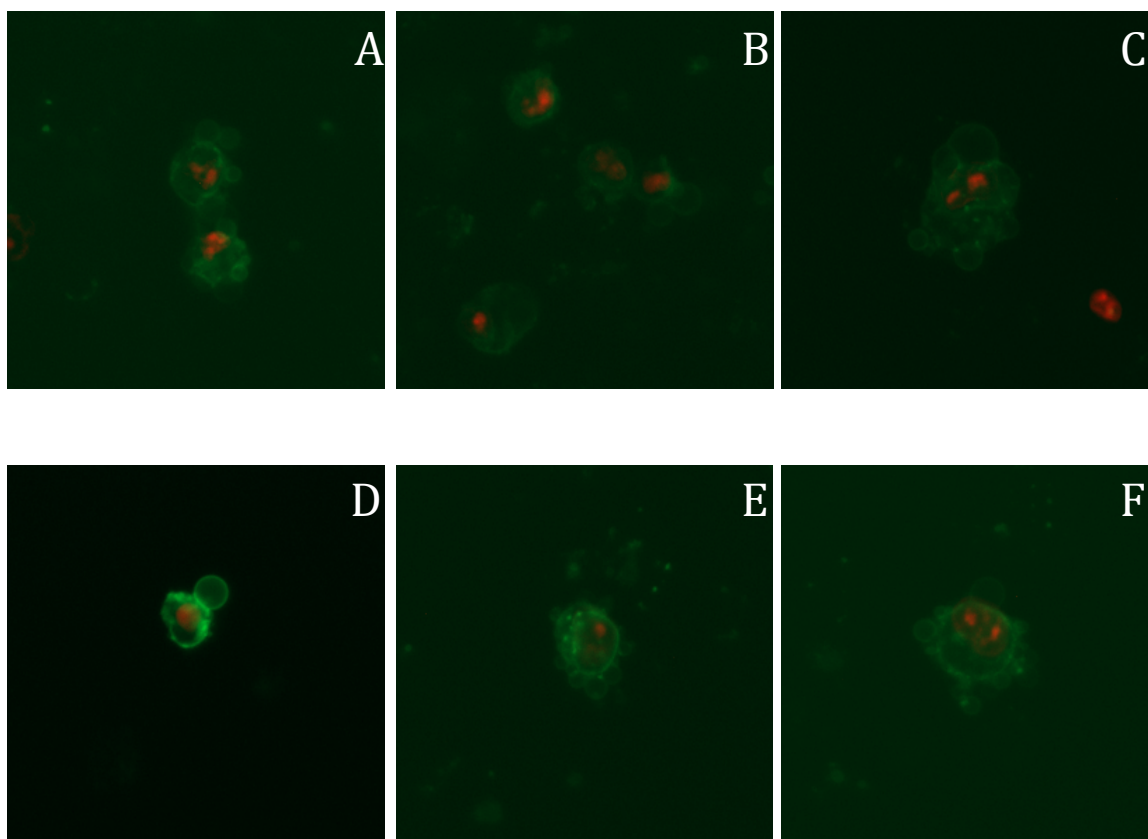


Figure II-13. Images of the Annexin V assay on H460 cells grown in 6-well plates using compound **II 3** in 10% by weight HPCD aqueous solution as the compound treatment. All images taken using a 20x objective. Images are presented as a merged image of the green fluorescence and red fluorescence figures, omitting the normal transmitted light image for blebbing clarity. Images A–C were taken at the 14 hour time point and D–F were taken at the 17 hour time point.

Compounds **II 4** and **II 5** are highly lipophilic compounds with poor solubility in aqueous solutions. *In vitro* MTT assays and the previous Annexin V assays suggest there was no difference in the anti-cancer activity of compounds solubilized by the 1% DMSO solution or by HPCD. Therefore, compounds **II 4** and **II 5** were dissolved in a 20% (w/v) solution of HPCD. However, only **II 5** could be solubilized by the HPCD solution. We propose that the steric bulk of the C⁴ and C⁵ position of **II 4** contributes to its inability to be solubilized by HPCD. The HPCD solution of **II 5** was exposed to cells at a concentration of 40 μ M for 12, 14, 17, and 20-hour time points.

At the end of the treatment periods, the Annexin V apoptosis detection kit was utilized and cells were visualized by fluorescence microscopy (Figure II-14). Images were compared to cells exposed to only the HPCD vehicle solution and cells treated with cisplatin. There was minimal fluorescence from cells treated with the vehicle, which was expected. A significant amount of fluorescence and blebbing was observed from cells treated with cisplatin as this compound is known to induce apoptosis. Signs of apoptosis including green fluorescence of the cell membrane, blebbing, and staining of the nucleus from propidium iodide were observed at all the time points for cells treated with **II 5** (Figure II-15). However, not all cells were in the same stage of cell death as indicated by the progression of fluorescence in individual wells. At the 12 h time point, a fraction of the cells were visualized with green fluorescence only while some had green and red fluorescence together and the rest had no fluorescence. At the 17 and 20 h time points, a significant percentage of the cells were both green and red fluorescent, showing blebbing and thus suggesting apoptosis.

Due to its insolubility in HPCD, compound **II 4** was dissolved in a 1% DMSO solution, and H460 cells were exposed at a concentration of 40 μ M for 1, 3, 6, and 12 hour time points. The vehicle control and cisplatin positive control also contained the same percentage of DMSO as the cells treated with **II 4**. Again, the Annexin V assay detection kit was utilized. Minor green fluorescence was observed with cells treated with vehicle, while early signs of apoptosis were observed in cells treated with cisplatin as would be expected at the 12 hour time point (Figure II-16). Strong green fluorescence was observed as early as the 1 hour time point and continued to

be observed at all of the later time points in cells treated with **II 4**. No blebbing was observed at any of the time points and green fluorescence as well as red fluorescence were observed at all time points (Figure II-17). However, cells treated with **II 4** were abnormal when compared to the controls, especially in that the morphology of the membrane was vastly different. This suggests that **II 4** induces a necrotic cell death pathway versus an apoptotic cell death pathway as observed with **II 1** – **II 3** (Figure II-18).

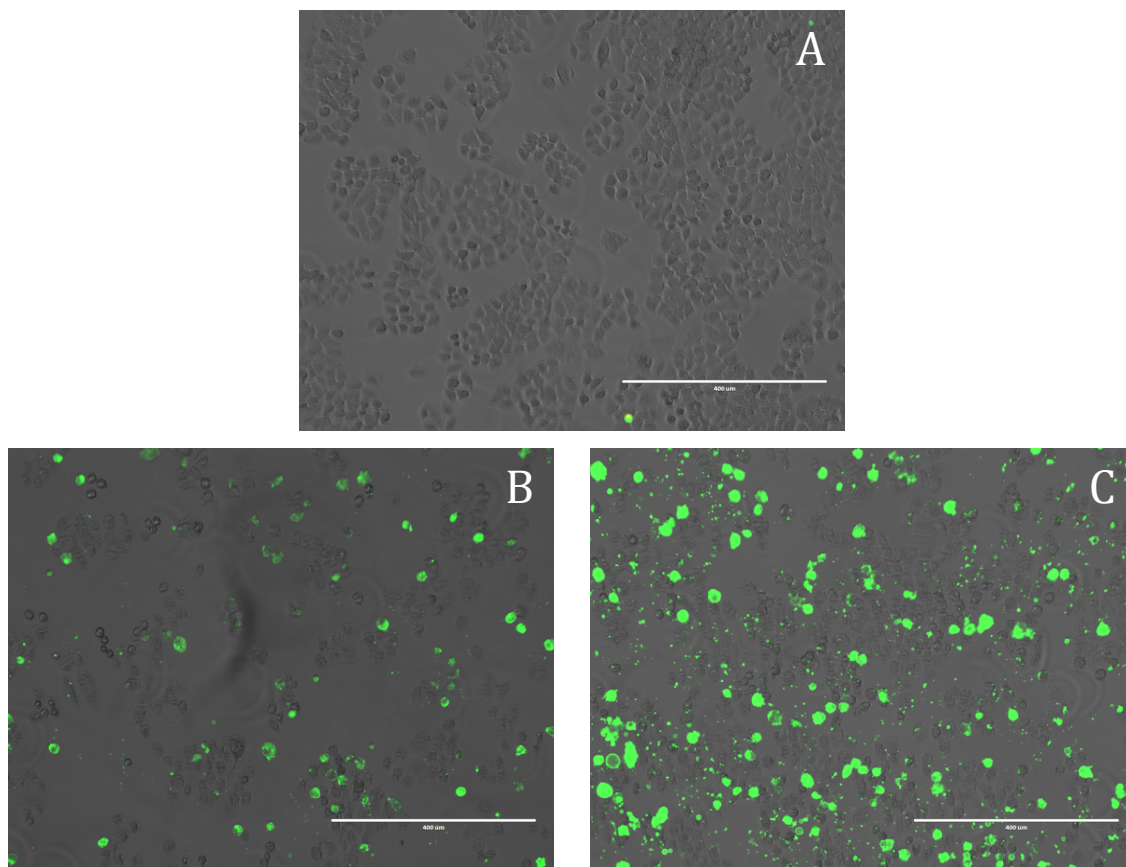


Figure II-14. Images of the Annexin V assay on H460 cells grown in 6-well plates using compound **II 5** in 20% (w/v) HPCD aqueous solution as the compound treatment. All images were taken using a 10x objective. Images are presented as a merged image of the normal transmitted light, green fluorescence and red fluorescence figures. (A) HPCD control, 20 hours. (B) Compound **II 5**, 14 hours. (C) Compound **II 5**, 20 hours. Scale bars equal 400 µm.

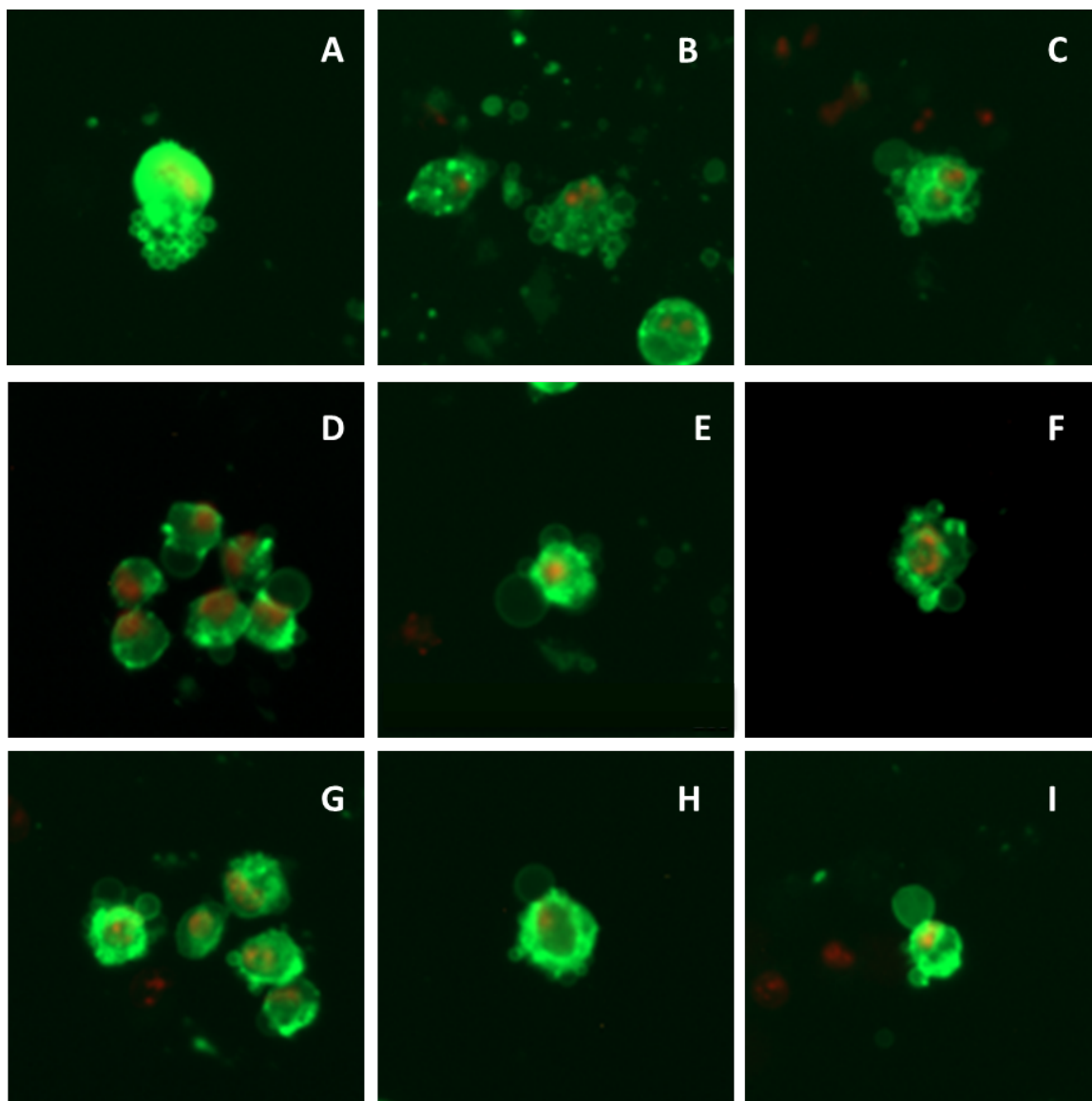


Figure II-15. Images of the Annexin V assay on H460 cells grown in 6-well plates using compound **II 5** in 20% (w/v) HPCD aqueous solution as the compound treatment. All images were taken using a 20x objective. Images are presented as a merged image of the green fluorescence and red fluorescence figures, omitting the normal transmitted light image for blebbing clarity. Images A-C were taken at the 20 hour time point, D-E were taken at the 17 hour time point, F-G were taken at the 14 hour time point, and images H-I were taken at the 12 hour time point.

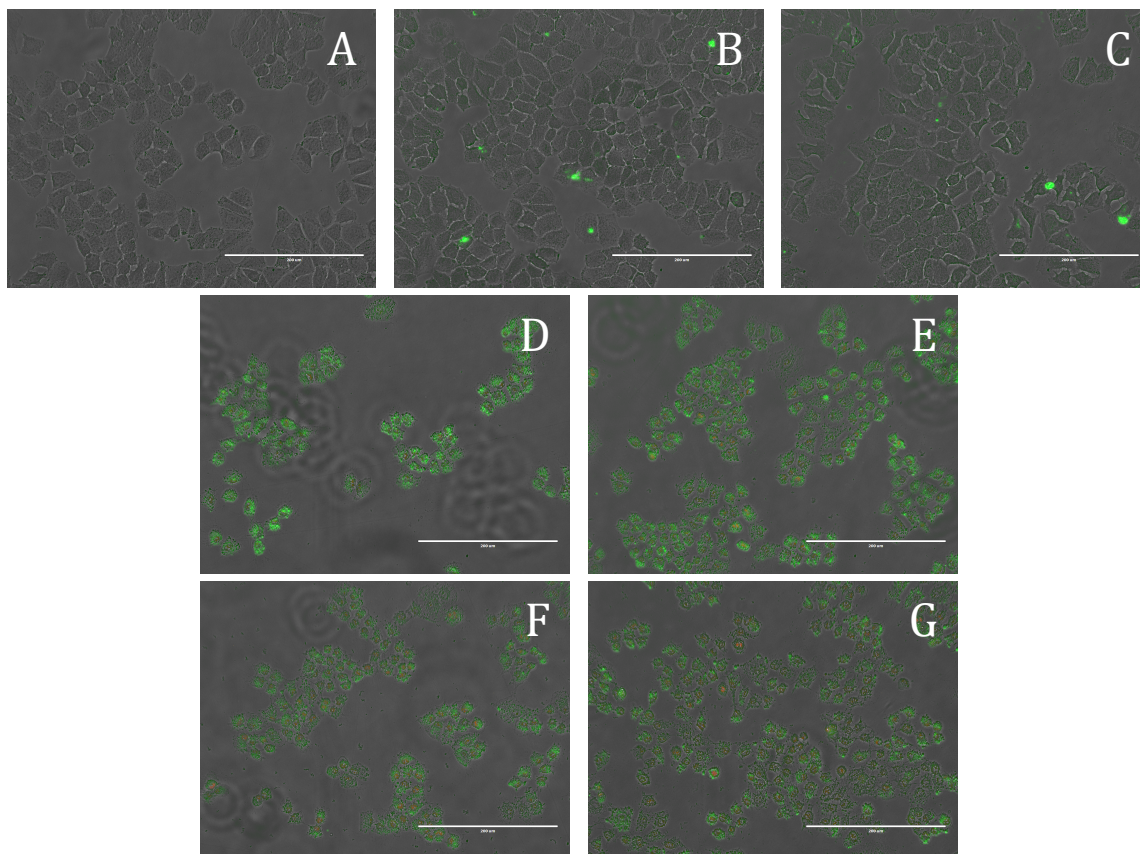


Figure II-16. Images of the Annexin V assay on H460 cells grown in 6-well plates using **II 4** dissolved in a 1% DMSO aqueous solution as the compound treatment. All images were taken using a 20x objective. Images are presented as a merged image of the normal transmitted light, green fluorescence and red fluorescence figures. (A) Media control, 12 hours. (B) DMSO control, 12 hours. (C) Cisplatin control, 12 hours. (D) Compound **II 4**, 1 hour. (E) Compound **II 4**, 3 hours. (F) Compound **II 4**, 6 hours. (G) Compound **II 4**, 12 hours. Scale bars equal 200 μm .

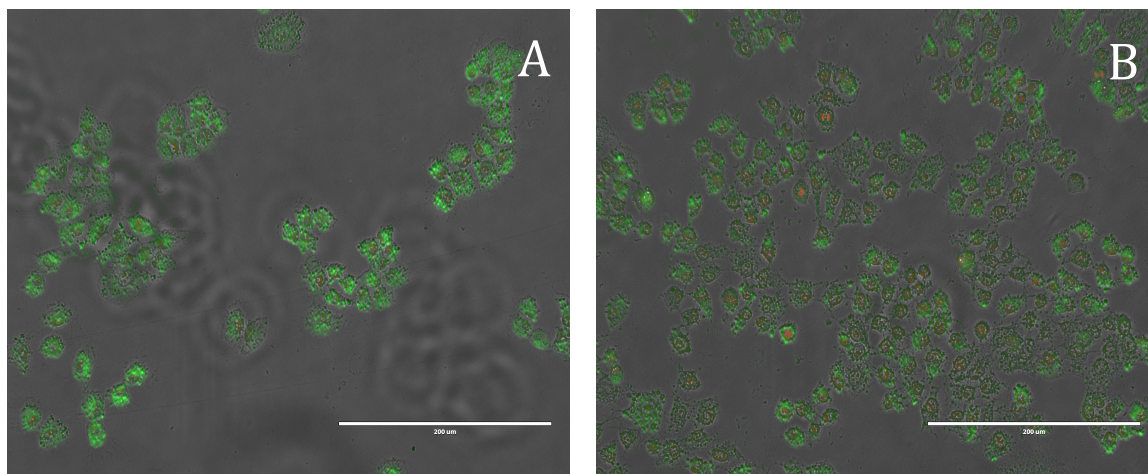


Figure II-17. Images of the Annexin V assay on H460 cells grown in 6-well plates using **II 4** dissolved in a 1% DMSO aqueous solution as the compound treatment. All images were taken using a 20x objective. Images are presented as a merged image of the normal transmitted light, green fluorescence and red fluorescence figures. (A) Compound **II 4**, 1 hour. (B) Compound **II 4**, 12 hours. Scale bars equal 200 μm .

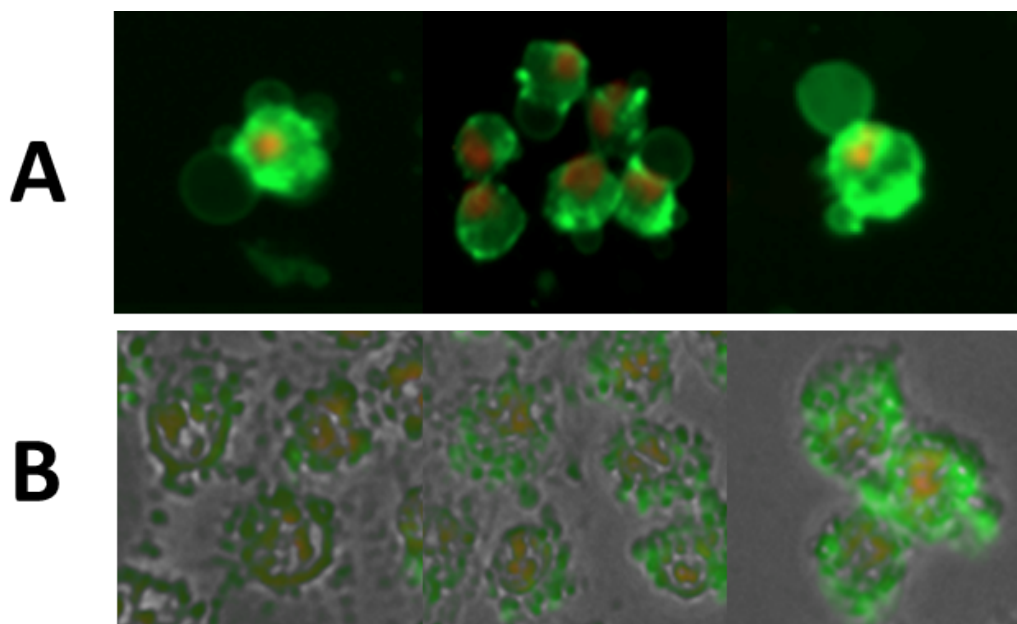


Figure II-18. Image depicting the comparison of compound **II 4** versus compound **II 5** treated cells. (Row A) H460 blebbing cells after treatment with compound **II 5** (normal transmitted light image omitted for blebbing clarity). (Row B) H460 cells after treatment with compound **II 4**.

2.2.2.3. DNA Assays

Imidazolium salts with methylnaphthyl substituents have the potential to interact with cellular DNA. The planar, aromatic nature of the substituents would lend itself well to the intercalation between DNA base pairs due to the pi-pi stacking forces between the base pairs and naphthalene rings. Interaction with DNA was investigated by viscosity and fluorescent intercalator displacement (FID) assays with select imidazolium salts. The viscosity assay is useful for determining if a compound intercalates between DNA base pairs. As intercalation occurs, the base pairs become strained and the backbone of the DNA begins to unwind in order to account for this strain. Unwinding of the normal helix of DNA equates to an increase in viscosity. Utilizing a solution of calf thymus DNA (CT-DNA) and making small additions of the compound in question viscosity can be measured. However, viscosity will only increase if a compound is able to intercalate and therefore does not account for compounds that can interact with DNA as groove-binders. To evaluate potential groove-binders an FID assay can be utilized. This assay begins with CT-DNA that is intercalated with ethidium bromide, which gives a strong fluorescent signal upon interaction with DNA. The compound in question is then titrated into the DNA solution and evaluated for the ability to displace ethidium bromide by monitoring if there is a reduction in fluorescence. This test can determine if a compound is a groove-binder or intercalator that has a strong enough interaction with DNA to displace the ethidium bromide. For comparison, the viscosity measurements utilize ethidium bromide as a positive control and netropsin, a known groove-binder, as a negative control while also testing solvent

controls. Furthermore, the FID study utilizes netropsin as a positive control, as netropsin is known to have the ability to displace ethidium bromide.¹⁶² Results from these assays have suggested that imidazolium salts have no interaction with DNA, proposing that DNA is an unlikely intracellular target. As an example, results from these experiments on compound **II 3** can be seen in Figures II-19 and II-20.

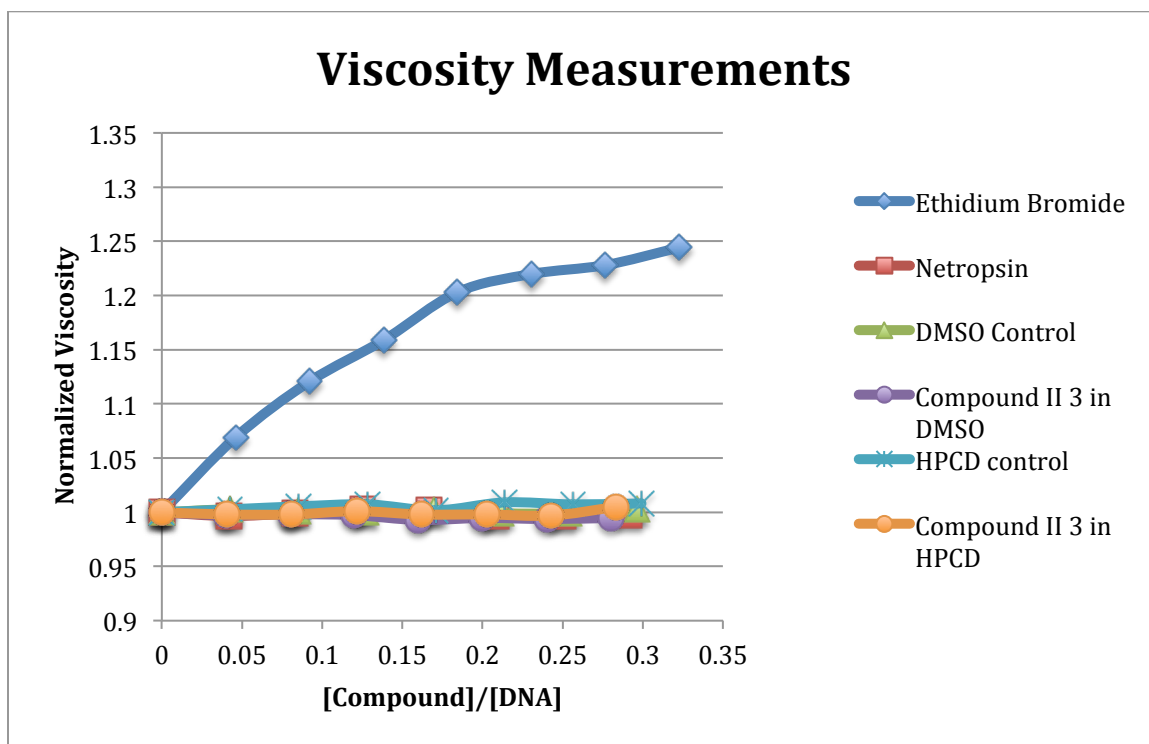


Figure II-19. Viscosity plot of compound **II 3** using CT-DNA relative to controls.

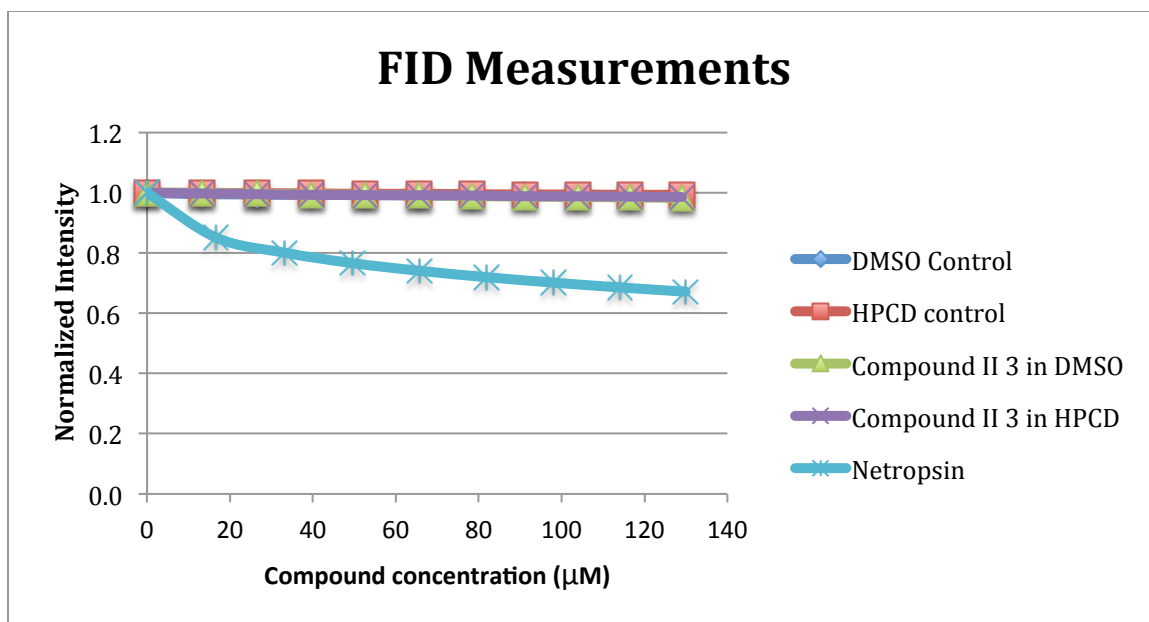


Figure II-20. Plot of FID measurements of compound **II 3** using CT-DNA relative to controls.

2.2.2.4. JC-1 Assay

After determining that DNA was not a viable cellular target for the tested imidazolium salts, the mitochondria was considered as an intracellular target considering it has been previously reported that delocalized lipophilic cations (DLCs) can target the mitochondria of cells.^{49,163} Imidazolium salts containing naphthylmethyl substituents at the N¹ and N³ positions can be classified as DLCs, and thus mitochondria were studied for their potential role in the mechanism of action. The JC-1 assay was utilized to determine if mitochondrial disruption occurred after treatment with **II 1** and **II 3**. JC-1 is a cationic dye that can accumulate in mitochondria with intact membrane potentials (Fig. II-21). This mitochondrial membrane potential, or MMP, is caused by a proton gradient across the inner membrane and is important for the production of ATP by the enzyme ATP synthase.¹⁶⁴ The formation of J-aggregates by a high concentration of JC-1 in the

matrix of mitochondria produces red fluorescence. However, when MMP is disrupted, J-aggregates do not congregate in the matrix and fluorescence is shifted from red to green as the monomer disperses in the cell. Interestingly, the structure of JC-1 shows some similarities to the imidazolium salts presented here (Figure II-21).¹⁶⁵ Healthy cells with intact MMP will display red fluorescence in the mitochondria with green fluorescence in the cytosol, and cells with disrupted MMP will show green fluorescence with a decrease in the amount of red fluorescence or no red fluorescence at all.

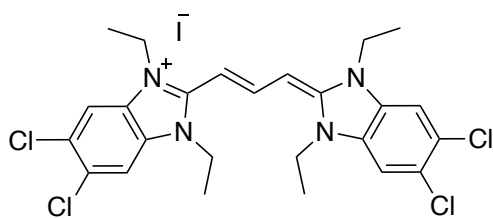


Figure II-21. Structure of JC-1.

The H460 cell line was treated with **II 1** and **II 3** at a concentration of 40 μM (the same as for the Annexin V assay) for 1 h and 2.5 h (Annexin V showed blebbing at 3 h when using DMSO for solubility). There was minimal red fluorescence observed at either time point. However, cells exposed to the media and vehicle control solutions had intact MMP. This suggested that at a concentration of 40 μM , **II 1** and **II 3** had disrupted the MMP of the majority of mitochondria by 1 hour. It was presumed that a shorter time frame was necessary to observe the progression of fluorescence from normal MMP to disrupted MMP. Therefore, the H460 cells were treated with **II 1** and **II 3** at 40 μM for 30 min and 1 h prior to adding JC-1. Unfortunately, the 30 min time point also showed minimal red fluorescence;

whereas, media control cells had red fluorescence suggesting the mitochondria were still intact. Figure II-22 shows a comparison of the 30 min and 1 h treatments.

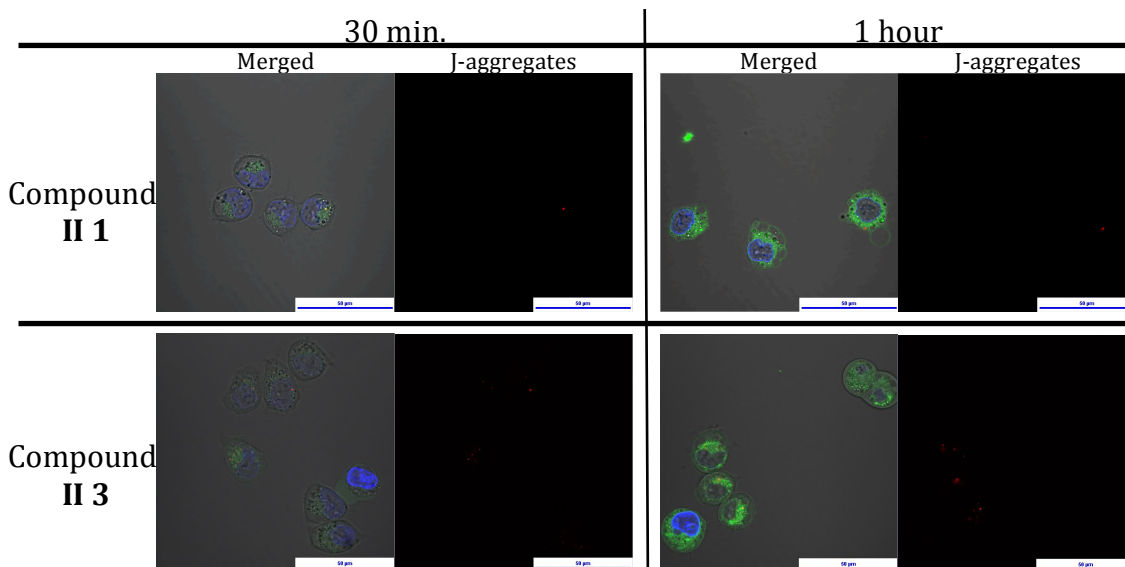


Figure II-22. Images of the JC-1 assay on H460 cells grown in 35 mm glass bottom dishes using compounds **II 1** and **II 3** at 40 μM in a 1% DMSO aqueous solution as the compound treatment. All images were taken using a 100x objective. Images are presented as a merged image of the normal transmitted light, green fluorescence, blue fluorescence, and red fluorescence figures (merged columns) or the red fluorescence alone (J-aggregates columns) at the specified time frames. Scale bars equal 50 μM .

In order to visualize the progression of red fluorescence to the lack of red fluorescence at time points feasible for cellular treatment and imaging, the concentration of **II 3** was decreased from 40 μM to 20 μM . Compound **II 3** was exposed to cells for 15 min and 1 h at this concentration. Red fluorescence was observed at 15 min and the 1 h time point with an apparent decrease in intensity for cells treated with **II 3** for 1 h. A positive control, carbonyl cyanide m-chlorophenyl hydrazone (CCCP), was used to verify the assay. Similarly to the cells treated with **II 3**, mitochondrial potential was decreased compared to the media control cells, as shown by a decrease in the red fluorescence signal. Results of this assay suggest that

II 3 may have disrupted the MMP, visualized by the decrease in observed red fluorescence of cells (Figure II-23). It is important to note that this is a preliminary study, and the JC-1 assay alone is not evidence enough to say that these imidazolium salts can target the mitochondria, as disruption of MMP is a typical step in the process of apoptosis.¹⁶⁶ Therefore, these results, in accordance with the Annexin V assay, are a confirmation of the process of apoptosis.

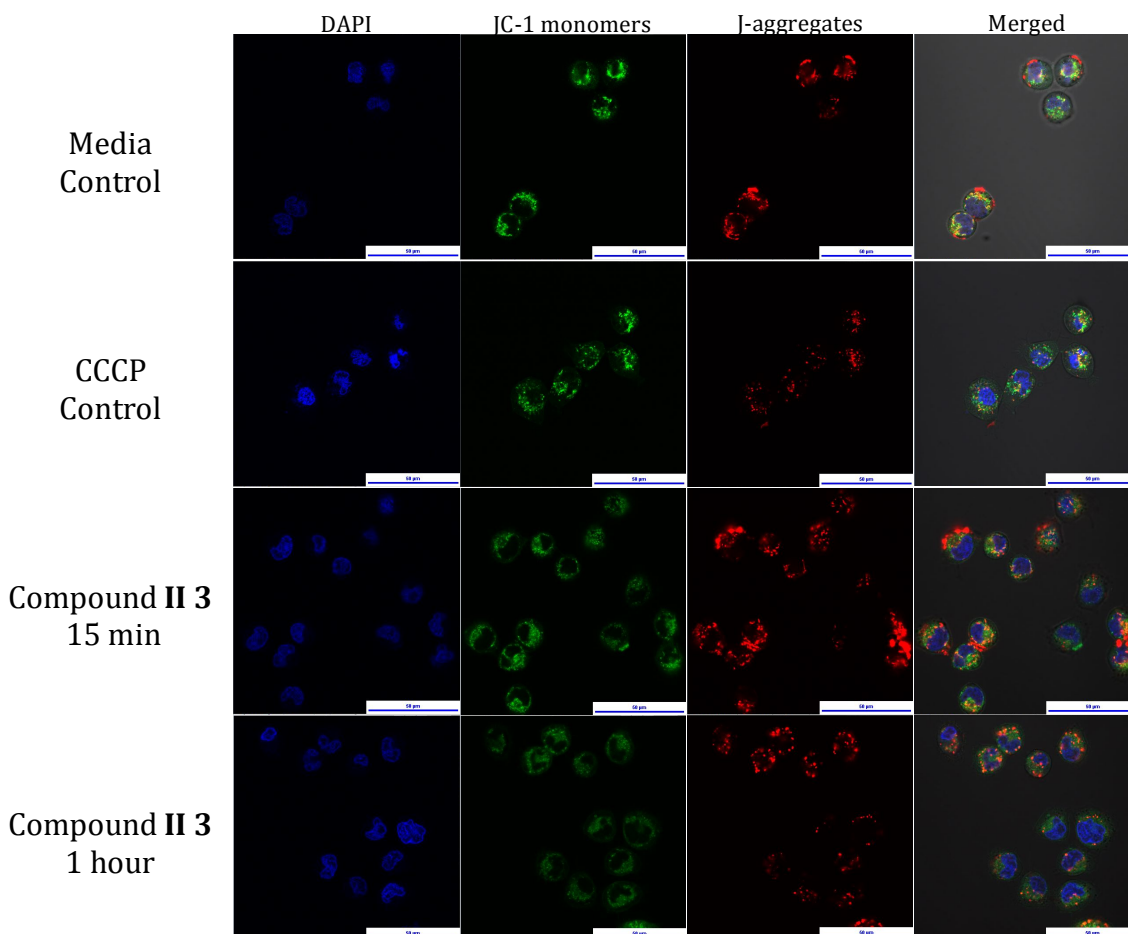


Figure II-23. Images of the JC-1 assay on H460 cells grown in 35 mm glass bottom dishes using compound **II 3** at 20 μM in a 1% DMSO aqueous solution as the compound treatment. All images were taken using a 100x objective. Images are presented as the individual a merged image of the normal transmitted light, green fluorescence, blue fluorescence, and red fluorescence figures (merged columns) or the red fluorescence alone (J-aggregates columns) at the specified time frames. Scale bars equal 50 μM .

2.3. Conclusion and Future Outlook

Overall, the results from the MTT assay suggest that the imidazolium salts presented here have the ability to kill select NSCLC cancer cell lines at values that are comparable to that of cisplatin. However, the limited aqueous solubility limits the potential of these compounds. Use of excipients, such as the FDA approved cyclodextrin, are able to increase the solubility of imidazolium salts while not significantly changing their IC₅₀ values. In accordance with these results, HPCD does not alter the mode of cell death, but rather only increases the time frame that cell death occurs. The NCI DTP 60 cell line screen has also validated our results, suggesting that in both the one-dose and five-dose assays, compounds **II 1** – **II 5** are cytotoxic towards NSCLC cancer cell lines.

Annexin V results showed that compounds **II 1** – **II 3** and **II 5** are able to induce an apoptotic mode of cell death, as indicated by the progression of fluorescence and the visualization of blebbing. Compound **II 4** was found to be the only lead imidazolium salt compound that was found to induce a necrotic cell death pathway, indicated by the fluorescence and observed cellular morphology. It is also interesting to note that **II 4** was found in the NCI DTP 60 cell line screen to have negative growth percentages for 59 out of 60 cancer cell lines tested, identifying this compound to be extremely toxic.

Interaction with DNA was studied, as this was believed to be a potential cellular target for these planar imidazolium salts. However, the viscosity and FID studies did not show any interaction with DNA. Time differences between the effects seen in the JC-1 assay versus the Annexin V assay indicate to us that mitochondria as

a cellular target should be studied further. In the JC-1 assay, cells treated with **II 3** at a concentration of 40 μM were visualized to have completely disrupted MMP by the 30 min time point. Images from the Annexin V assay, at the same concentration of **II 3**, show green fluorescence of cells with normal morphology at double that amount of time with cellular blebbing at 3 h. We therefore believe that for MMP disruption to occur so quickly, the imidazolium salts enter the cells and are attracted to the mitochondria, although, as mentioned previously, other studies are needed to confirm this hypothesis. Further studies include evaluating other lead imidazolium salts compounds by the methods outlined in this chapter as well as quantification of fluorescence from the JC-1 assay, isolation of mitochondria from treated cancer cells that can be evaluated for imidazolium salts by analytical methods, and utilizing other cellular assays to further evaluate mitochondrial viability, such as cytochrome c release and ATP production.

2.4. Acknowledgements

Imidazolium salt synthesis was completed by Dr. M. A. DeBord and Dr. K. S. Taylor. The crystal structures were solved by Dr. P. O. Wagers and Dr. M. A. DeBord with guidance from Dr. M. J. Panzner. Dr. M. A. DeBord and N. K. Robishaw performed the MTT assays and gave importance guidance in teaching me how to perform the MTT assay. Dr. M. C. Konopka and K. T. Whiddon assisted in obtaining the microscopy images with the JC-1 assay. Dr. S. Paruchuri was kind enough to let me use the microscope in her lab for the Annexin V assays. The DTP performed the NCI-60 cell line one-dose and five-dose assays.

2.5. Materials and Methods

2.5.1. General Considerations

All reactions were carried out under aerobic conditions. Carbonyl cyanide *m*-chlorophenylhydrazone, imidazole, 4,5-dichloroimidazole, and 4-methylimidazole were purchased from Alpha Aesar. 2-Ethyl imidazole and DAPI were purchased from Acros Organics. 2-(Bromomethyl)naphthalene was purchased from Waterstone Technologies. 2-Hydroxypropyl- β -cyclodextrin (batch average molecular weight: 1400) was purchased from Tocris Bioscience. The TACS MTT cell proliferation assay kit was purchased from Trevigen. JC-1 was purchased from AdipoGen. Glass bottom dishes coated with poly-D-lysine used in the JC-1 assay (P35GC-1.5-14-C) were purchased from MatTek Corporation. FITC Annexin V Apoptosis Detection Kit was purchased from BD Biosciences. UltraPure™ Calf Thymus DNA Solution, UltraPure™ ethidium bromide, and UltraPure™ DNase/RNase-Free Distilled Water were purchased from Thermo Fisher Scientific. All acids, bases, and solvents were purchased from Fisher Scientific. All reagents were used as received without further purification. Melting points were obtained using a MelTemp apparatus with a calibrated thermometer. ¹H and ¹³C NMR spectra were obtained on a Varian 300 or 500 MHz instrument with all spectra referenced to residual deuterated solvent (DMSO-d₆: ¹H NMR: 2.50 ppm, ¹³C NMR: 39.5 ppm). Mass spectrometry was performed in the University of Akron mass spectrometry laboratory. Elemental analysis was performed by Atlantic Microlab in Norcross,

Georgia, Microanalysis Laboratory at University of Illinois at Urbana-Champaign or by The University of Akron Department of Geology.

The human NSCLC cell lines NCI-H1975 and HCC827 were generously provided by Dr. Lindner from the Cleveland Clinic. The human NSCLC cell lines NCI-H460 and A549 were purchased from ATCC (Manassas, VA, USA). All cell lines were grown at 37 °C with 5% CO₂ in RPMI 1640 medium supplemented with 10% fetal bovine serum and passed every 2-3 days.

2.5.2. X-ray Analysis

Crystals of the compounds were coated in paratone oil, mounted on a CryoLoop and placed on a goniometer under a stream of nitrogen. Crystal structure data sets were collected on either a Bruker SMART APEX I CCD diffractometer with graphite-monochromated Mo K α radiation ($\lambda = 0.71073 \text{ \AA}$) or a Bruker Kappa APEX II Duo CCD system equipped with a Mo ImuS source and a Cu ImuS micro-focus source equipped with QUAZAR optics ($\lambda = 1.54178 \text{ \AA}$). The unit cells were determined by using reflections from three different orientations. Data sets were collected using SMART or APEX II software packages. All data sets were processed using the APEX II software suite.^{167,168} The data sets were integrated using SAINT.¹⁶⁹ An empirical absorption correction and other corrections were applied to the data sets using multi-scan SADABS.¹⁷⁰ Structure solution, refinement, and modelling were accomplished by using the Bruker SHELXTL package.¹⁷¹ The structures were determined by full-matrix least-squares refinement of F² and the selection of the

appropriate atoms from the generated difference map. Hydrogen atom positions were calculated and $U_{\text{iso}}(\text{H})$ values were fixed according to a riding model.

2.5.3. MTT Assay

Cells were grown to confluence and plated in 96-well plates at 5,000-7,000 cells per well, depending on the cell line. Cells were incubated for 24 h prior to adding the compounds. Compounds **II 1** – **II 5** were dissolved in either a 1% DMSO/water solution or a HPCD solution and diluted in fresh medium to the desired concentrations. Cisplatin was dissolved in pure water by stirring for several hours at room temperature and then diluted to the appropriate concentrations. Compounds were added (6 replicates each) and cells were incubated for 72 h, at which time the MTT assay protocol was followed. MTT reagent (10 μL) was added to each well and cells were incubated for 3-4 h, again depending on the cell line. Growth medium was removed by aspiration and DMSO (100 μL) was added to each well. Plates were incubated for 15 min. The optical density was read at 540 nm on a Fisher Scientific Multiskan FC plate reader.

2.5.4. Annexin V assay

The Annexin V assay was conducted using the components of a FITC Annexin V Apoptosis Detection Kit I. The NCI-H460 cell line was grown in 6-well plates at a density of 1×10^5 cells per well. After allowing cells to adhere overnight, they were treated with controls or imidazolium salts at a concentration of 40 μM for the

indicated time points. To prepare medium for treatments, cisplatin was first solubilized in DMSO and diluted to give a 1% DMSO/water solution and was further diluted to a 40 μM concentration in culture medium. For imidazolium salt treatments, the compound was first solubilized in either a 1% DMSO/water solution (solubilizing in the DMSO first before diluting with water) or a 10% by weight aqueous HPCD solution and further diluted to the aforementioned concentration in culture medium. Treatments consisted of aspirating medium from the respective wells and replacing with either DMSO, HPCD, cisplatin, or imidazolium salt supplemented medium (2 wells per treatment type) at time points that allow the treatment times to have the same end point. After treatment, the medium was aspirated, and cells were washed twice with cold PBS. The provided 10X binding buffer was diluted to 1X, and 400 μL was added to each well. Subsequently, 20 μL each of the provided FITC Annexin V and PI was also added to each well. The plates were incubated for 15 min on a platform shaker while covered with aluminum foil at room temperature. After this time, the binding buffer was aspirated from the wells, and 1 mL of the 1X binding buffer was added to each well for imaging. The fluorescence microscope used was an EVOS fl Digital Inverted Microscope with 10X and 20X objectives.

2.5.5. DNA interaction studies

Buffer used for both viscosity and FID studies consisted of a concentration of 5mM Tris and 50mM NaCl regulated to a pH of 7.2 with hydrochloric acid and was made with UltraPure™ DNase/Rnase-Free Distilled Water. DNA solutions for the

experiments were made with UltraPure™ Calf Thymus DNA Solution. Concentration of CT-DNA in solution was determined using a Varian Cary 100 Bio UV-Visible Spectrophotometer at 260nm using a molar extinction coefficient of $6600 \text{ M}^{-1} \text{ cm}^{-1}$ to give mononucleotide concentration.¹⁷² Average CT-DNA concentration for viscosity studies was $235 \mu\text{M}$ and average CT-DNA concentration for FID studies was $150 \mu\text{M}$. UltraPure™ ethidium bromide, 10 mg/mL was used as received.

2.5.6. Viscosity

An Ostwald viscometer was used for the viscosity measurements. The viscometer was submerged in a water bath held at 30°C so that the entire contained sample was temperature regulated. The time it took for the sample to run between the calibrated lines was recorded three times and the average was used for calculation purposes. The flow time of the buffer alone as well as the CT-DNA solution was tested before each new experiment. The compound was titrated in so that each addition made a final solution with a concentration increase of $10 \mu\text{M}$, with the first addition being $10 \mu\text{M}$ and ending with $70 \mu\text{M}$. Compound **II 3** solutions were made by solubilizing the compound in either a 10% DMSO/water solution (solubilizing in the DMSO first before diluting with water) or a 10% by weight HPCD aqueous solution. Calculations to plot data were obtained by following procedures outlined by Fu *et al.*¹⁷³

2.5.7. Fluorescent Intercalator Displacement

Fluorescence measurements were taken on a Horiba Jobin Yvon FluoroMax-4 spectrofluorometer. The excitation wavelength was set at 510 nm and emission data were obtained at 601 nm. After adding the CT-DNA solution to the cuvette, ethidium bromide was added to give a final concentration of 25 μM . Additions of compound **II 3** were added to give a final concentration of roughly 13.3 μM per addition. Compound **II 3** was either solubilized in a 10% DMSO/water (solubilizing in the DMSO first before diluting with water) or a 10% HPCD aqueous solution. Normalized intensities were calculated by dividing the intensity of the CT-DNA solution with ethidium bromide by the intensity of the CT-DNA solution with ethidium bromide plus compound **II 3** and plotted against compound concentration.

2.5.8. JC-1 Assay

The JC-1 assay was completed using JC-1 as the MMP fluorescent dye, carbonyl cyanide *m*-chlorophenylhydrazone as the positive control, and DAPI as the nuclear stain. A 5 mg/mL stock solution of JC-1 was prepared by solubilizing 5 mg of JC-1 in 1 mL of DMSO. The JC-1 stock solution was diluted in medium to a final concentration of 10 $\mu\text{g/mL}$ to use as the working concentration. A 1 mg/mL stock solution of DAPI nuclear stain was prepared by solubilizing 10 mg of DAPI in 10 mL of deionized water. The DAPI stock solution was diluted in PBS to a final concentration of 1 $\mu\text{g/mL}$ to use as the working solution. A 20 mg/mL stock solution of CCCP was prepared by solubilizing 100 mg of CCCP in 5 mL of DMSO. The CCCP

stock solution was diluted in medium to a final concentration of 20 $\mu\text{g}/\text{mL}$ to use as the working solution.

The NCI-H460 cell line was grown in 35-mm glass bottom dishes coated with poly-D-lysine at a cell density of 15,000 cells per well. The cell suspension was added to the glass cover of each well (500 μL) and allowed to adhere for 1 hour before additional medium (2 mL) was added to the plate. Cells were placed in the incubator overnight. Cells were treated with supplemented medium at a concentration of 20-40 μM for compound **II 3**, 40 μM for compound **II 1** and at 20 $\mu\text{g}/\text{mL}$ (98 μM) of CCCP. Media control cells were treated with growth medium, and vehicle control cells were treated with medium supplemented with an equal volume of the 1% DMSO aqueous solution as used for the imidazolium salt treatments. Treatments consisted of aspirating medium from respective plates and replacing with 3 mL of the above specified medium. Treatments were completed so that they all ended at the same time and were thus prepared for imaging together. Imaging preparation began with aspirating the treatment medium and replacing with 1 mL of JC-1 supplemented medium (10 $\mu\text{g}/\text{mL}$). Plates were then placed in the incubator for 15 minutes. The JC-1 supplemented medium was then aspirated and cells were washed with PBS. DAPI-supplemented PBS was then added to each plate (1 mL; 5 $\mu\text{g}/\text{mL}$) and plates were placed in the incubator for 15 minutes. DAPI-supplemented PBS was aspirated and cells were washed twice with PBS. Finally, 1 mL of PBS was placed in each plate for imaging. Cells were imaged using a Nikon A1+ laser scanning confocal microscope using a 100x Plan Apo λ (1.45 NA) objective lens.

Excitation was done by 405 nm (DAPI), 488 nm (JC-1), and 561 nm (JC-1) solid state lasers.

2.5.9. Synthesis of 1,3-bis(naphthalen-2-ylmethyl)imidazolium bromide (**II 2**)

Imidazole (0.68 g, 10 mmol) was dissolved in 10 mL of acetonitrile, potassium hydroxide (0.62 g, 11 mmol) was added, and the mixture was heated at reflux for 0.5 h. (2-Bromomethyl)naphthalene (2.21 g, 10 mmol) was added, and the mixture was refluxed for 2.5 h, during that time a white precipitate was formed. The solid was filtered off, and to the filtrate was added a second equivalent of (2-bromomethyl)naphthalene (2.21 g, 10 mmol). The mixture was returned to reflux for 1 h. Volatiles were removed by rotary evaporation under reduced pressure, yielding a viscous brown oil. Hot water (*90 °C) was added to the oil, stirred, and slowly decanted. This was repeated several times, and the water layers were combined. A white solid, **II 2**, was precipitated from the cooled water layers and was isolated by filtration and air-dried (1.47 g, 35 % yield). Mp: 165–168 °C. Found: C, 67.5; H, 5.0; N, 6.3 Calcd for $C_{25}H_{21}N_2Br_1$: C, 69.9; H, 4.9; N, 6.5 %. 1H NMR (500 MHz, DMSO- d_6) δ = 9.50 (s, 1H, NCHN), 7.95 (m, 10H, Ar), 7.56 (m, 6H, Ar), 5.62 (s, 4H, CH₂). $^{13}C\{^1H\}$ NMR (125 MHz, DMSO- d_6) δ = 136.5 (NCN), 132.7 (Ar), 132.7 (Ar), 132.1 (Ar), 128.8 (Ar), 127.8 (Ar), 127.6 (Ar), 127.6 (Ar), 126.7 (Ar), 126.7 (Ar), 125.7 (Ar), 123.0 (Ar), 52.3 (CH₂). MS: m/z = 348.9, (theor for $M^+ C_{25}H_{21}N_2 = 349.2$).

Crystal data for **II 2**: C₂₅H₂₁N₂ Br, M = 429.35, monoclinic, a = 19.810(6) Å, b = 8.060(2) Å, c = 12.591(4) Å, β = 95.941(5)°, V = 1,999.8(10) Å³, T = 100(2) K, space group P2(1)/c, Z = 4, 15,271 reflections measured, 4,046 independent reflections (R_{int} = 0.0560). The final R₁ values were 0.0467 (I > 2σ(I)). The final wR(F²) values were 0.1225 (I > 2σ(I)). The final R₁ values were 0.0594 (all data). The final wR(F²) values were 0.1313 (all data).

2.5.10. Synthesis of 2-ethyl-1,3-bis(naphthalen-2-ylmethyl)imidazolium bromide (**II 3**)

2-Ethylimidazole (1.01 g, 10.4 mmol) dissolved in acetonitrile (20 mL) was combined with KOH (0.71 g, 12.6 mmol) and 2-(bromomethyl)naphthalene (2.56 g, 11.6 mmol, first addition; 3.01 g, 13.6 mmol, second addition). Compound **II 3** precipitated from addition of diethyl ether and was recrystallized from ethanol (3.00 g, 62% yield). Mp: 220-221 °C. Found C, 70.6; H, 5.7; N, 6.1%. Calculated for C₂₇H₂₅N₂Br: C, 70.9; H, 5.5; N, 6.1%. ¹H NMR (500 MHz, DMSO-*d*₆) δ = 8.00 (1H, s, Ar), 7.99 (1H, s, Ar), 7.91-7.96 (8H, m, Ar), 7.55-7.57 (4H, m, Ar), 7.51 (1H, s, Ar), 7.49 (1H, s, Ar), 5.70 (4H, s, CH₂), 3.23 (2H, q, CH₂, J = 7.4 Hz), 0.86 (3H, t, CH₃, J = 7.5 Hz). ¹³C NMR (125 MHz, DMSO-*d*₆) δ = 148.3 (NCN), 132.7 (Ar), 132.5 (Ar), 132.1 (Ar), 128.7 (Ar), 127.8 (Ar), 127.6 (Ar), 126.7 (Ar), 126.7 (Ar), 126.6 (Ar), 125.2 (Ar), 122.4 (Ar), 50.9 (CH₂), 16.6 (CH₂), 11.1 (CH₃). MS: m/z = 377.3 (theor for M⁺ C₂₇H₂₅N₂⁺ = 377.2).

Crystal data for **II 3**: $C_{27}H_{25}N_2Br$, $M = 457.40$, monoclinic, $a = 13.3523(17)$ Å, $b = 9.8237(11)$ Å, $c = 16.542(2)$ Å, $\beta = 97.385(4)^\circ$, $V = 2151.8(4)$ Å³, $T = 100(2)$ K, space group $P2(1)/n$, $Z = 4$, 15661 reflections measured, 4353 independent reflections ($R_{\text{int}} = 0.0650$). The final R_1 values were 0.0408 ($I > 2\sigma(I)$). The final $wR(F^2)$ values were 0.1057 ($I > 2\sigma(I)$). The final R_1 values were 0.0763 (all data). The final $wR(F^2)$ values were 0.1282 (all data). A single crystal of **II 3** was obtained by slow evaporation of a concentrated solution of **II 3** dissolved in ethanol. Crystallographic information file (CIF) can be found on the Cambridge Crystallographic Data Center website (CCDC # 1044145)

2.5.11. Synthesis of 1,3-bis(naphthalen-2-ylmethyl)-4,5-diphenylimidazolium bromide (**II 4**)

A mixture of 4,5- diphenylimidazole (1.00 g, 4.54 mmol) and potassium hydroxide (0.38 g, 6.77 mmol) in acetonitrile (10 mL) was refluxed for 30 min. 2-(Bromomethyl)naphthalene (1.00 g, 4.52 mmol) was added and the mixture was refluxed overnight. The reaction mixture was filtered hot to remove a white precipitate, presumed to be potassium bromide. The filtrate was stirred with 2-(bromomethyl)naphthalene (1.00 g, 4.52 mmol) and refluxed overnight. The resulting precipitate was collected via vacuum filtration of the hot reaction mixture. The white solid was stirred in a round bottom flask with diethyl ether (20 mL). The product was collected via vacuum filtration, washed with diethyl ether in the funnel and air-dried to yield a white powder **II 4** (1.39 g, 52%). Mp: 199-202 C. ¹H NMR

(500 MHz, DMSO- d_6) δ 9.79 (s, 1H), 7.92 (m, 4H), 7.82 (m, 2H), 7.59 (s, 2H), 7.54 (m, 4H), 7.41 (m, 2H), 7.36 (m, 8H), 7.32 (m, 2H), 5.61 (s, 4H). ^{13}C $\{^1\text{H}\}$ NMR (125 MHz, DMSO- d_6) δ 136.8, 132.54, 132.52, 131.9, 131.4, 130.8, 130.1, 128.7, 128.5, 127.8, 127.6, 127.2, 126.63, 126.59, 125.3, 125.0, 50.7. HRMS (ESI $^+$) calcd for $\text{C}_{37}\text{H}_{29}\text{N}_2$ [M-Br] $^+$ of $m/z = 4501.2331$, found $m/z = 4501.2242$.

2.5.12. Synthesis of 4-methyl-1,3-bis(naphthalen-2-ylmethyl)imidazolium bromide

(II 5)

4-Methylimidazole (1.00 g, 12.2 mmol) was dissolved in acetonitrile (15 mL), potassium hydroxide (0.78 g, 14 mmol) was added, and the mixture was refluxed for 1 h. 2-(Bromomethyl)naphthalene (2.68 g, 12.1 mmol) was added and the mixture was refluxed overnight. The reaction mixture was filtered hot to remove a white solid, presumed to be potassium bromide. 2-(Bromomethyl)naphthalene (3.20 g, 14.5 mmol) was added to the filtrate which was refluxed overnight. The resulting precipitate was collected via vacuum filtration of the hot reaction mixture. The solid in the funnel was washed with diethyl ether, and air-dried to provide a white powder **II 5** (2.66 g, 49%). Mp: 198-200 C. Anal. Calcd for $\text{C}_{26}\text{H}_{23}\text{BrN}_2$: C, 70.43; H, 5.23; N, 6.32%. Found C, 69.71; H, 5.37; N, 6.25%. ^1H NMR (500 MHz, DMSO- d_6) δ 9.57 (s, 1H), 8.04 (s, 1H), 8.01 (s, 1H), 7.99 (s, 1H), 7.94 (m, 5H), 7.71 (s, 1H), 7.57 (m, 5H), 7.51 (m, 1H), 5.65 (s, 4H), 2.22 (s, 3H). ^{13}C $\{^1\text{H}\}$ NMR (125 MHz, DMSO- d_6) δ 136.4, 132.68, 132.67, 132.65, 132.57, 132.1, 131.5, 131.4, 128.8, 128.7, 127.80,

127.77, 127.65, 127.6, 127.0, 126.7, 126.63, 126.60, 125.7, 125.3, 119.8, 52.0, 49.7,

8.9. MS (ESI⁺) calcd for C₂₆H₂₃N₂⁺[M- Br]⁺ of m/z = 4363.2, found m/z = 4363.1.

Crystal data for 4-methyl-1,3-bis(naphthalen-2-ylmethyl)imidazolium bromide (**II 5**): C₂₆H₂₃Br₁N₂, M = 4443.37, monoclinic, a = 410.779(4) Å, b = 417.353(7) Å, c = 411.919(5) Å, α = 90°, β = 111.99(2)°, γ = 90°, V = 42067.2(13) Å³, T = 100(2) K, space group P2(1)/n, Z = 4, 17385 reflections measured, 4200 independent reflections (R_{int} = 0.0747). The final R₁ values were 0.0492 (I > 2σ(I)). The final wR(F²) values were 0.0986 (I > 2σ(I)). The final R₁ values were 0.0949 (all data). The final wR(F²) values were 0.1147 (all data). Crystallographic information file (CIF) can be found on the Cambridge Crystallographic Data Center website (CCDC # 1048512).

CHAPTER III

IN VIVO TOXICITY STUDIES OF SELECT IMIDAZOLIUM SALTS

“Reproduced in part with permission from [DeBord, M. A.; Southerland, M. R.; Wagers, P. O.; Tiemann, K. M.; Robishaw, N. K.; Whiddon, K. T.; Konopka, M. C.; Tessier, C. A.; Shriver, L. P.; Paruchuri, S.; Hunstad, D. A.; Panzner, M. J.; Youngs, W. J. *Bioorganic Med. Chem. Lett.* **2017**, 27 (4), 764–775.]

[Shelton, K. L.; Debord, M. A.; Wagers, P. O.; Southerland, M. R.; Taraboletti, A.; Robishaw, N. K.; Jackson, D. P.; Tosanovic, R.; Kofron, W. G.; Tessier, C. A.; Paruchuri, S.; Shriver, L. P.; Panzner, M. J.; Youngs, W. J. *Tetrahedron* **2016**, 1–15.]”

3.1. Introduction

The *in vitro* evaluation of potential cancer chemotherapeutics, such as imidazolium salts, provides valuable information on their efficacy against cancer cells. In addition, many labs can easily become equipped to perform various *in vitro* studies with a large variety of available cancer cell lines. However, there are limitations to this type of analysis. *In vitro* studies are defined as studies on components of an organism, such as cancer cells, performed outside of their normal environment. For example, cancer cells such as the HeLa cell line originated from a

human patient, in this instance Henrietta Lacks. Tissue biopsies afforded the cells that were cultured and found to be immortal and have been a staple in laboratories all around the world.¹⁷⁴ The limitation becomes the environment that the cancer cells are exposed to. Biological assays completed in a typical laboratory deal with the growth of cells in flasks or petri dishes in medium that is supplemented for optimal cell growth. This type of environment is not able to mimic that of the original host, eliminating potentially important interactions. Although the ease and cost effectiveness of *in vitro* studies is undeniable, it is important to study compounds through *in vivo* methods as well.

Previous work by the Youngs lab has utilized multiple *in vitro* assays to identify lead imidazolium salt compounds that have the ability to act as anti-proliferative agents against non-small cell lung cancer (NSCLC) cell lines.^{26,149-151} The Youngs lab has also utilized the excipient 2-hydroxypropyl- β -cyclodextrin (HPCD) as a way to solubilize lipophilic imidazolium salts without compromising anticancer activity. In order to further evaluate their future as potential chemotherapeutics, lead compounds have been tested for toxicity through *in vivo* methods. This chapter will focus on the study of a select number of imidazolium salts solubility in HPCD and their toxicity by intraperitoneal (IP) injection of C57BL/6 mice by analysis of their weight gain percent, percent survival and overall health and well-being through the course of the study.

3.2. Results and Discussion

3.2.1. Lead Imidazolium Salts

Lead imidazolium salts chosen for the *in vivo* toxicity study can be seen in Figure III-1. Compounds **II 3** and **II 5**, presented previously, have been shown to be effective against NSCLC cell lines and induce an apoptotic mode of cell death according to the Annexin V assay.^{149,151} Full details of their synthesis, characterization and *in vitro* evaluation can be found in chapter II. The synthesis of compounds **III 1** and **III 2** have been reported previously.^{175,176}

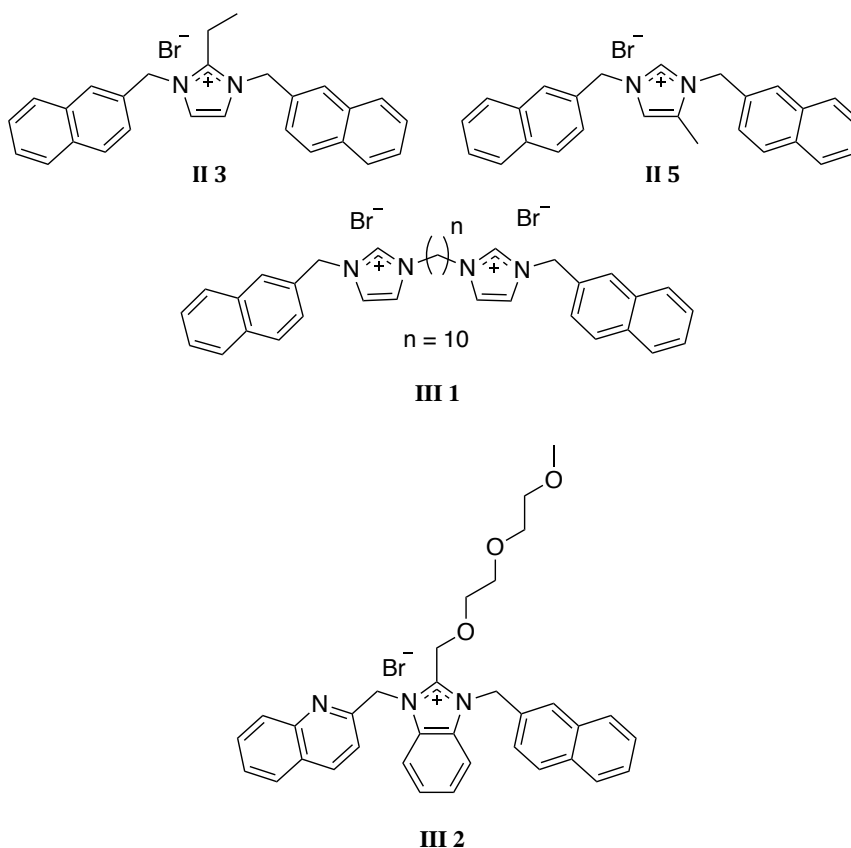


Figure III-1. Structures of lead imidazolium salts, **II 3**, **II 5**, **III 1**, and **III 2**, tested for *in vivo* cytotoxicity. Compounds **II 3** and **II 5** have been previously tested in chapter II.

3.2.2. MTT Assay

Imidazolium salts **II 3**, **II 5**, **III 1**, and **III 2** have all been evaluated by the MTT assay in order to determine their IC₅₀ values, defined as the drug concentration at which there was 50% inhibition in cell viability relative to control cells, against select NSCLC cell lines. These values are outlined in Table III-1. The compounds presented herein have been identified as lead compounds due to their IC₅₀ values being lower or comparable to the numbers obtained for cisplatin.

Table III-1. IC₅₀ values of compounds **II 3**, **II 5**, **III 1**, and **III 2**.

Compound (Solubilizing agent)	Cell Line and IC ₅₀ values (μM)			
	NCI-H460	NCI-H1975	A549	HCC827
II 3 (HPCD)	1	<1	3	2
II 5 (DMSO)	3	3	ND	4
III 1 (DMSO)	<1	2	<1	7
III 2 (DMSO)	3	<1	3	6
Cisplatin	3	10	6	5

3.2.3. Solubilization and Injection Solutions of Imidazolium Salts

Previous reports have shown that imidazolium salts are able to be solubilized in aqueous solutions that are supplemented with HPCD.^{149,151} This type of treatment has been shown to give rise to unchanged IC₅₀ values by the MTT assay and to induce the same mode of cell death, although at different time frames as

compared to the imidazolium salt in a 1% DMSO/water solution.¹⁵¹ To our knowledge, there are no known therapeutics that are administered in a DMSO solution, with the exception of Rimso-50™, which is a 50% DMSO aqueous solution that is FDA approved for the treatment of interstitial cystitis.¹⁷⁷ For biological assays, imidazolium salts had been solubilized in a 1% DMSO/ water solution with only a fraction of imidazolium salts being fully soluble. In order to obtain compounds that are soluble enough for systemic administration, hydrophilic groups can be added to the imidazole core. However, modifying the scaffold of the imidazolium salt to enhance water solubility can have drastic effects on the anti-cancer activity.¹⁴⁹ It is therefore advantageous to solubilize lipophilic derivatives with FDA approved excipients such as HPCD.¹⁶⁰ To make solutions that were suitable for IP injection into C57BL/6 mice, a 20% (w/v) solution of HPCD was made in sterile PBS and added to pre-weighed imidazolium salts. An average weight of 20 g was assumed for the mice throughout the course of the study and solutions were made to account for a concentration of either 15 or 20 mg/kg of each compound with an injection volume of 100 μ L. Control mice were injected with the same volume of the 20% (w/v) solution of HPCD.

3.2.4. *In vivo* Toxicity

After arrival of the mice to the research facility, they were split up into five cages with three mice per cage and allowed to acclimate to the environment for five days. All mice were labeled, weighed, and injected with 100 μ L of the compound to

be tested or HPCD control solution on day 1. All mice were weighed everyday for the duration of the study, as applicable. Standard procedures were used to evaluate the strength and overall health of the mice (i.e. ability and strength to pull on cage lid when lifted, ability to regain footing when placed on their back, etc.) and percent weight loss was monitored closely to determine if injections could be continued. The Kaplan-Meier curve for all tested compounds can be seen in Figure III-2.

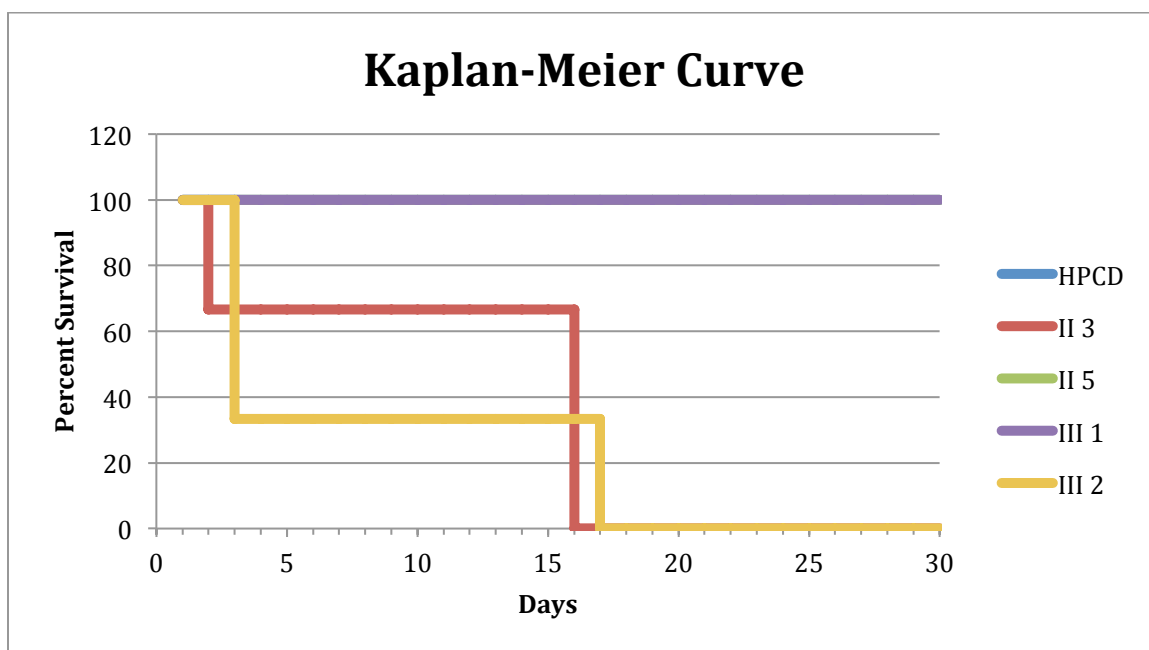


Figure III-2. Kaplan Meier curve of mice treated with imidazolium salts.

3.2.4.1. Mice Injected with Compound II 3

After the first injection of II 3 at 20 mg/kg, it was noted that the mice seemed a bit slower than before the injections (i.e. no normal running or jumping in the cages) and upon observation 30 minutes after injection were still slow, although

techniques to evaluate their well-being were normal. A full day after the first injection, mice were once again evaluated and responded normally to tests while still being observed as slow. At observation on day 3, one mouse was found to be dead. After the remaining two mice were weighed, it was observed that the mice had weight loss percentages ranging from 10-15.75 %. Due to the significant weight loss, the mice could not be injected but they were observed to still have normal strength when responding to wellness tests. The next 11 days showed a continual weight recovery of the mice, with a weight loss percent range from 0.37 – 4.54 %. It was therefore determined that the mice could receive another injection of **II 3** at a concentration of 15 mg/kg on day 15. By day 16, the two remaining mice had weakened and appeared lethargic and were sacrificed on that day. The average weight gain percent graph for the **II 3** treated mice as compared to the HPCD control mice through day 16 can be seen in Figure III-3.

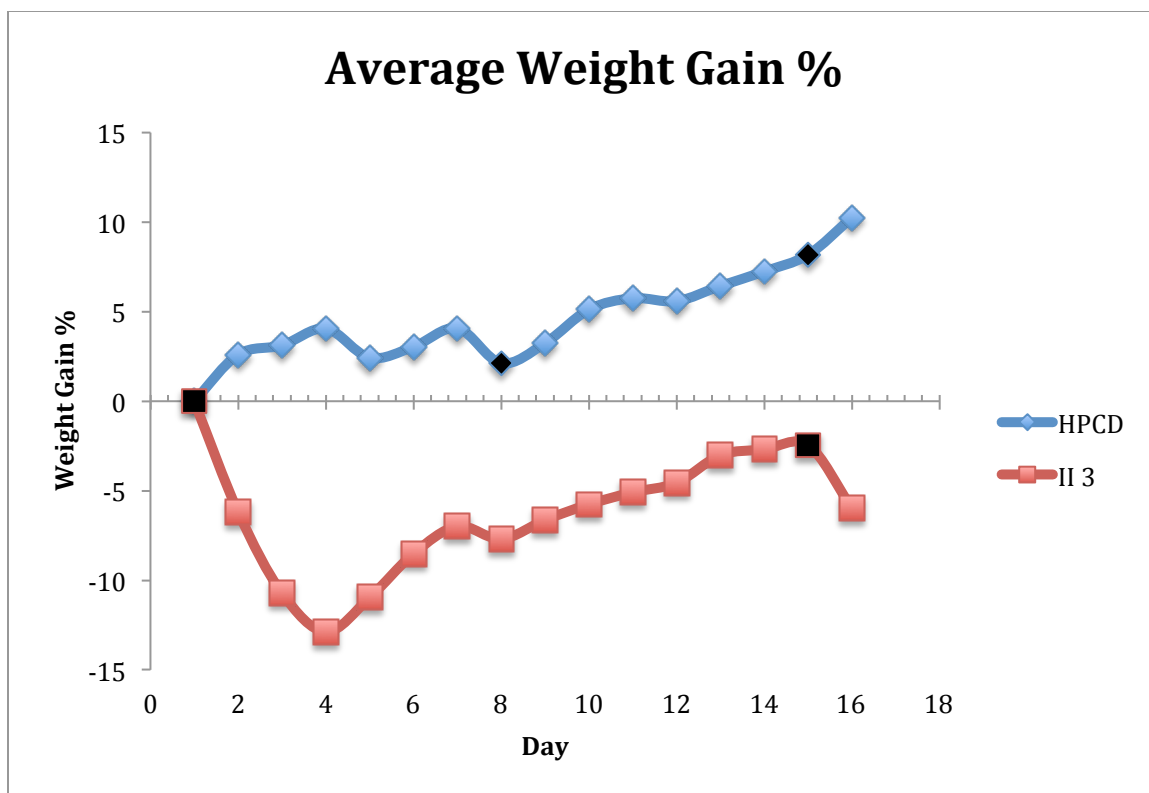


Figure III-3. Graph of the average weight gain percent for mice treated with **II 3** as compared to HPCD control mice. Black data point markers indicate days of injection, with all mice being injected on day 1.

3.2.4.2. Mice Injected with Compound **II 5**

On day 1, mice were injected with **II 5** at a concentration of 20 mg/kg. After injection, all mice seemed rather slow but strength seemed normal by the evaluation techniques. Over the next three days, mice steadily lost weight and reached an average percent weight loss of 7.71% by day 4. This was followed by a steady increase in weight over the next three days to an average percent weight loss of -1.15% on day 7. Mice were injected again on day 8 at 20 mg/kg with no adverse

effects as seen after the first injection. The next two days showed a decrease in weight again, down to an average percent weight loss of 8.23% on day 10, followed by another steady increase in weight to day 14, with a -0.84% weight loss. Mice were injected again on day 15, remaining at the 20 mg/kg dose. The same weight trend was observed, with an average percent weight loss ranging from 6.23% on day 17 to -2.51% on day 22. It was also on day 22 that mice were injected again at 20 mg/kg. Once again, the same weight trend was observed with an average percent weight loss of 6.05% on day 25 and a large jump to -2.15% by day 26. Mice were injected again on day 26 at 20 mg/kg with one mouse seeming a bit lethargic after injection. On day 27, a patch of redness and thinning fur was detected on the **II 5** treated mice, with all other functions being normal. The next day saw a decrease in the redness with still apparent thinness of fur at the injection site. By the end of the study, the average percent weight loss was at 3.44% on day 27 and -3.04% at day 30. Finally, on day 30, mice were injected one last time at 20 mg/kg and were sacrificed one hour later. The average weight gain for mice treated with **II 5** can be seen in Figure III-4. It is interesting to note the rhythmic sequence of weight gain and loss experienced by these mice throughout the study.

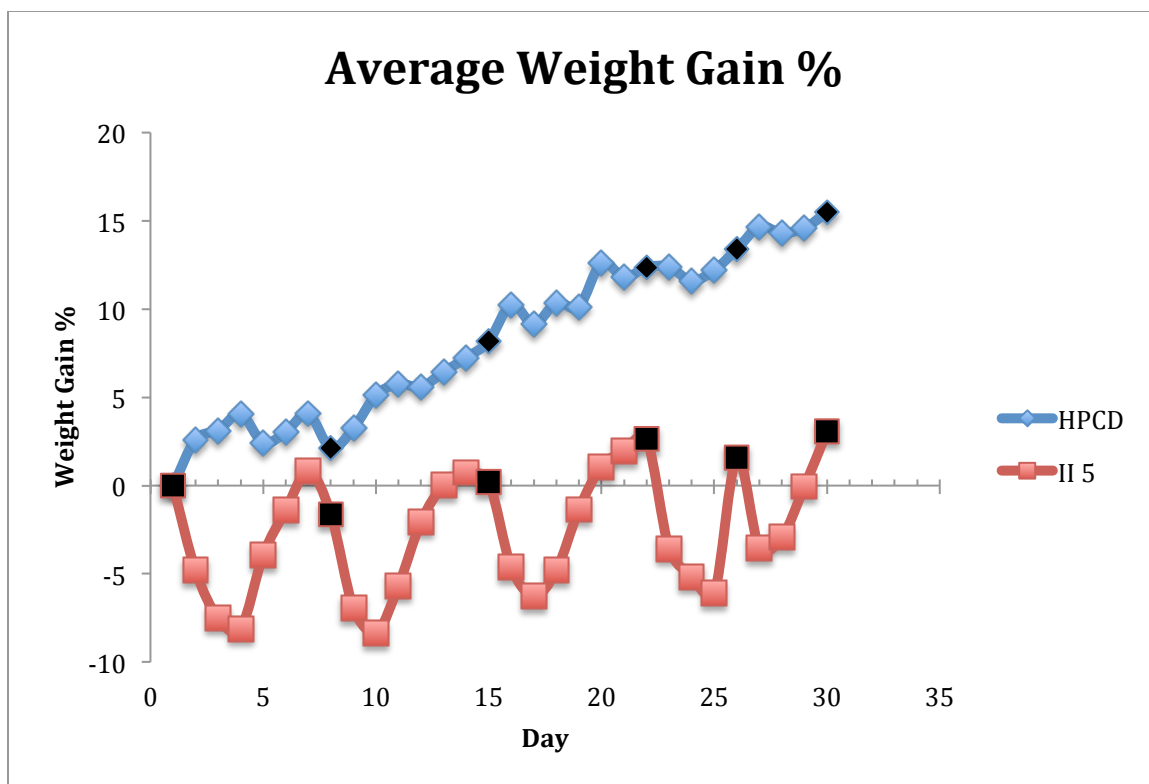


Figure III-4. Graph of the average weight gain percent for mice treated with **II 5** as compared to HPCD control mice. Black data point markers indicate days of injection, with all mice being injected on day 1.

3.2.4.3. Mice Injected with Compound **III 1**

In accordance with the other mice, day 1 consisted of an injection at 20 mg/kg and seemed to have slowed their activity while not losing any strength. The average percent weight loss had a maximal decrease to 10.14% on day 3 with a recovery to 4.09% by day 7. Mice received a second injection of **III 1** at 20 mg/kg on day 8 after which was followed by a decrease to a 6.40% average weight loss on day 9. It was observed that upon injection on day 8, the skin of the mice at the injection site was thin, as the needle penetrated much easier than before. On day 9, the mice

were observed to have a small patch of fur missing at the injection site, which appeared to be getting better by day 10. After healing of the injection site, mice were injected at 20 mg/kg again on day 15 but the missing fur returned with redness at the injection site by the next day. An antibiotic cream was applied once per day at the injection site. By day 22, one mouse had a large scab and missing fur at the injection site while the other two mice only had patches of fur missing. Because of this result, the mice were not injected for the rest of the study until day 30, where they were injected at 20 mg/kg, 1 hour before being sacrificed. Despite the sores at the injection site, the mice recovered well with a final average weight loss percent of -5.81%. The average weight gain for mice treated with **III 1** can be seen in Figure III-5 as compared to HPCD control mice. It is important to note the general trend of weight gain over the course of the experiment.

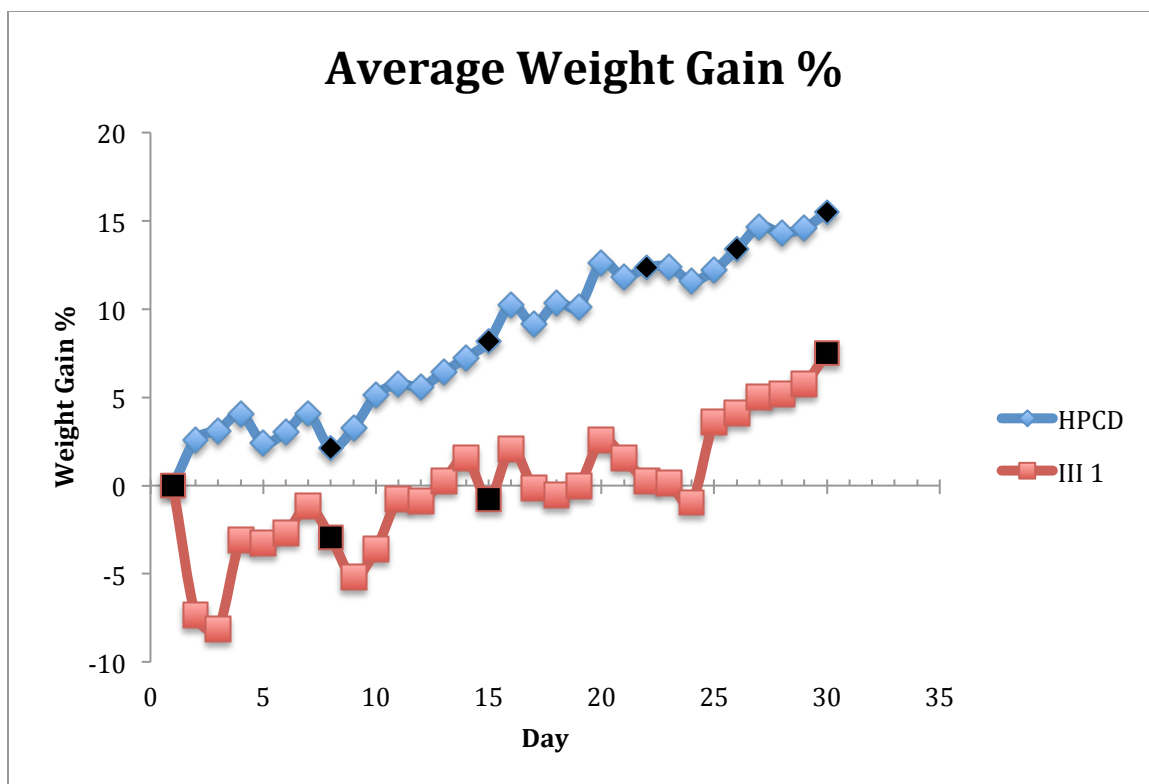


Figure III-5. Graph of the average weight gain percent for mice treated with **III 1** as compared to HPCD control mice. Black data point markers indicate days of injection, with all mice being injected on day 1.

3.2.4.4. Mice Injected with Compound **III 2**

Similar to the other tested compounds, day 1 consisted of injections at 20 mg/kg for the mice treated with **III 2**. Mice were observed to be slow while still having strength as evaluated during normal health exam. However, due to lethargic tendencies, two of the three mice were sacrificed on day 3. These two mice had a percent weight loss of 9.20% and 10.09%. No more injections were made on the remaining mouse for the course of the experiment and steady weight gain was observed. On day 10, a small scratch was observed that was not at the injection site.

It was postulated that this could have been a self-inflicted wound due to the isolation of the remaining mouse. The wound seemed to be healing until a scab was noted on day 16. The remaining mouse was sacrificed on day 17. The average weight gain percent for mice treated with **III 2** can be seen in Figure III-6.

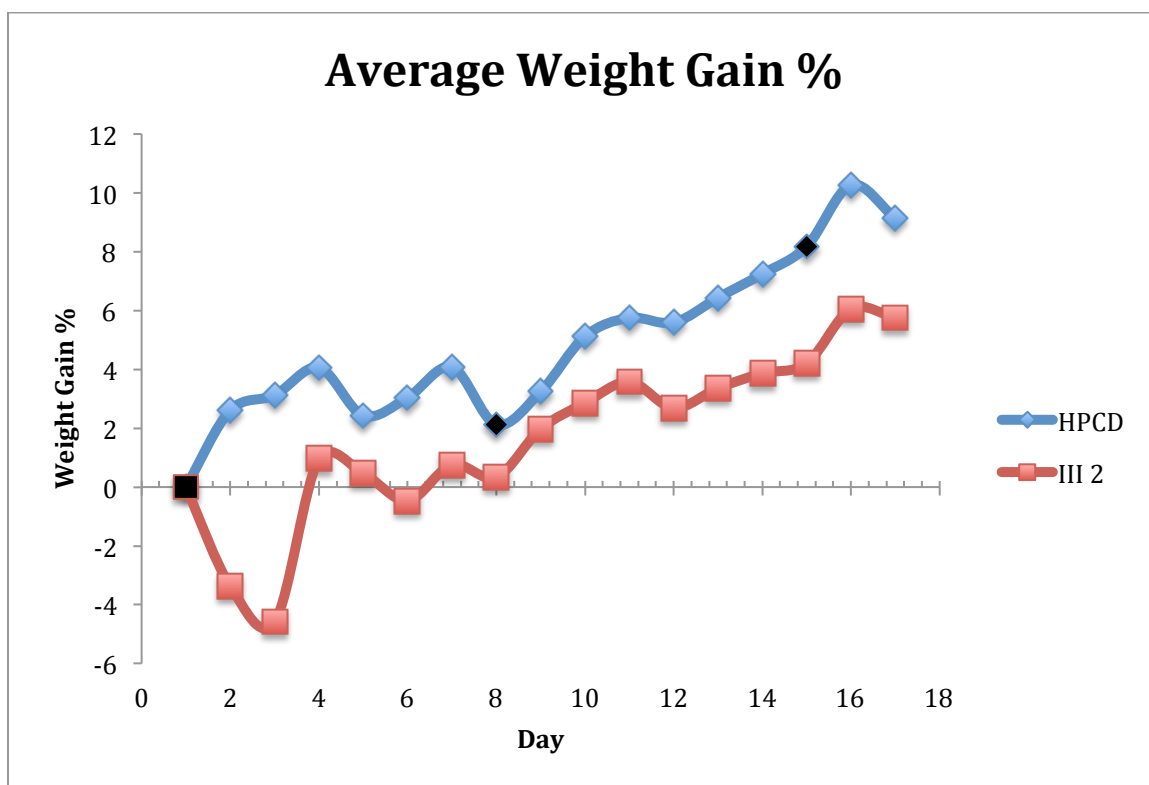


Figure III-6. Graph of the average weight gain percent for mice treated with **III 2** as compared to HPCD control mice. Black data point markers indicate days of injection, with all mice being injected on day 1.

3.2.4.5. Final Results

Injections of HPCD as a control comparison were tolerated well by the mice, as indicated by their health throughout the course of the study and their overall weight gain. Out of all tested compounds, results show that **III 2** was not well

tolerated by the mice, as indicated by the fact that two of the three mice had to be sacrificed on day 3. The remaining mouse did display recovery after the first and only injection, with a weight gain of 6% as compared to the original weight, but it is believed that being alone in the cage contributed to the apparent self-inflicted wounds. This mouse was sacrificed halfway through the study.

Mice treated with **II 3** also did not survive for the entire study. The injections were not well tolerated by the mice as evidenced by the mouse found dead on day 3 and the other two mice that were sacrificed after the second injection. The two mice remaining after the first injection had significant weight recovery but even decreasing the concentration of **II 3** down to 15 mg/kg for the second injection did not prove to be enough to ensure the well-being of the mice.

Both **II 5** and **III 1** were better in regards to the overall health of the mice and all mice survived for the duration of the experiment. Mice treated with **III 1** for a total of four injections at 20 mg/kg over the course of the experiment were observed to be slow after the first injection, but had fully recovered after a couple of days. Although the mice survived for the whole experiment, of concern was the apparent sore at the injection site, where fur was missing. This missing patch of fur appeared after the second injection, but mice recovered well and a third injection was completed. It was after the third injection that the missing patch of fur began to get red. Non-steroidal antibiotic cream was applied to the area each day and injections were stopped so that the area could heal. The mice were able to recover and were injected again on the last day of the study, 1 hour before being sacrificed.

Despite the area of the injection site being sore, mice had an overall weight gain for the course of this study.

The most well tolerated compound in this study was **II 5**. The average weight gain percentage chart (Figure III-4) shows a particularly interesting pattern in the measured weight of the mice that was unique as compared to the other compounds (Figure III-7). The repetition of weight recovery after injections is particularly promising. Despite mice being observed as a bit lethargic after the first injection, the following injections were received relatively well. It was not until the fifth injection that one mouse was found to be lethargic and all three mice were observed to have thinning fur at the injection site while all other functions and strength remained normal. By the end of the study, mice had received six injections (with the last injection being 1 hour before being sacrificed).

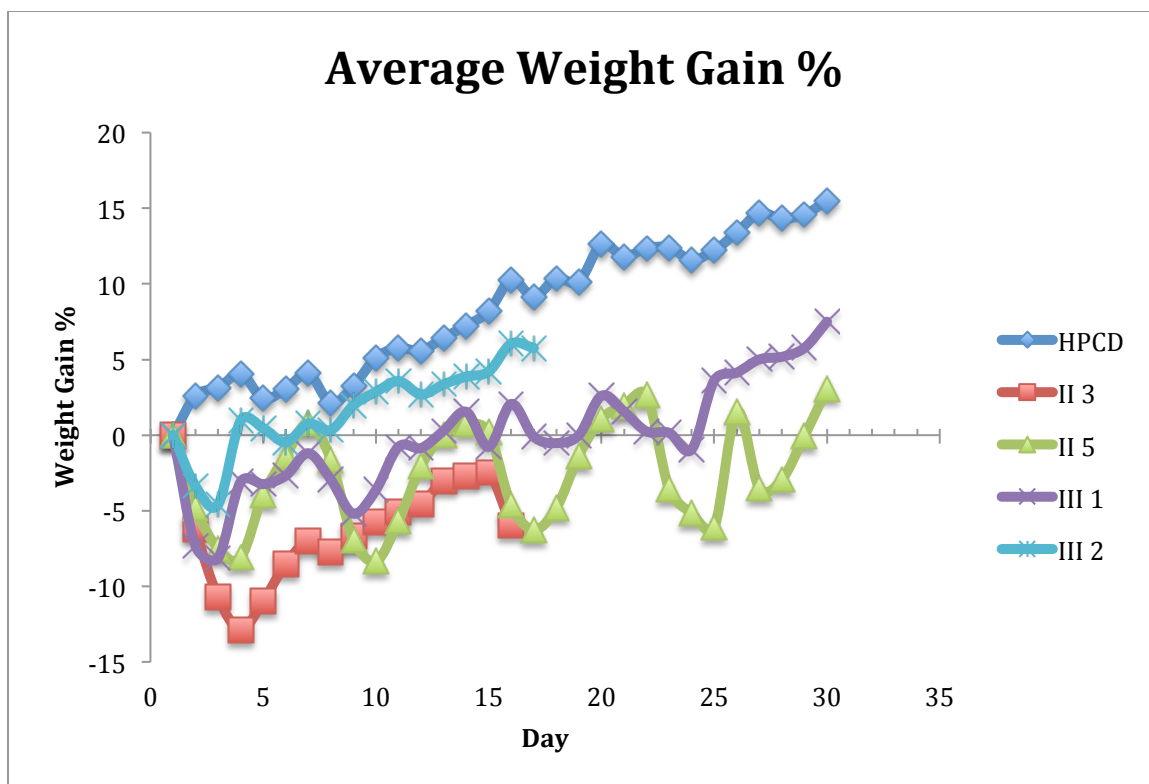


Figure III-7. Comparison of the average weight gain percent of all tested imidazolium salt compounds and controls.

3.3. Conclusion and Future Outlook

The information from this *in vivo* toxicity study has provided important information in regards to the overall toxicity of the presented imidazolium salts. Overall, compounds **II 5** and **III 1** were the most well tolerated compounds in the study with survival rates of 100%. Presence of sores at the injection site of both groups lead to the conclusion that although a concentration of 20 mg/kg did not cause death, a lower concentration may be necessary in order to avoid the irritation observed. Compound **III 2** was determined to be the most toxic, with a survival rate of only 33% after the first and only injection. However, the remaining mouse

remained solitary in a cage, which could have contributed negatively to the overall health and well-being of that mouse for the rest of the study. Compound **II 3**, which was previously studied through various *in vitro* methods also did not seem to be well tolerated by the mice as evidenced by a 66% survival after the first injection and the need to sacrifice mice after the second injection, despite using a lower concentration. Although the weight loss was around 6% after the second injection, the observed lethargy led to the sacrifice of the mice.

While this study has provided invaluable information, it does not mean that studies will not continue with compounds **II 3** and **III 2**. Other applications are still an area of current research, namely the use of **III 2** as a bladder exfoliant for the treatment of chronic bladder infections.¹⁷⁵ In fact, when **III 2** is administered intravesically, (i.e. through a catheter directly into the bladder) it shows potent exfoliation of the epithelial layer with two 15-minute treatments over the course of 16 h. Recovery of the epithelial layer is also apparent after a few days.¹⁷⁵ We therefore conclude that although mice in this study did not receive these compounds well, a lower concentration could be a viable option for further *in vivo* toxicity studies.

It is also important to note the comparison of the *in vitro* and *in vivo* studies. No patterns in the *in vitro* MTT assay could have predicted the outcome of the *in vivo* toxicity study presented here. This gives further importance to the study of compounds through *in vivo* methods, as interaction with the host cannot be predicted.

Future proposed experiments include similar *in vivo* studies with these imidazolium salts at lower concentrations (such as 10 mg/kg). After toxicity is determined, further experiments could also include xenograft models to determine whether or not imidazolium salts have the ability to reduce tumor growth *in vivo*.

3.4. Acknowledgements

Dr. M. A. DeBord has worked to not only synthesize some of these compounds but to also complete the *in vivo* toxicity study and the MTT assays. Dr. K. S. Taylor and Steven Crabtree have synthesized imidazolium salts in this chapter as well. I would also like to thank Dr. L. P. Shriver for her guidance in completing the animal studies.

3.5. Materials and Methods

3.5.1. MTT assay

Cells were grown to confluence and plated in 96-well plates at 5,000-7,000 cells per well, depending on the cell line. Cells were incubated for 24 h prior to adding the compounds. Compounds were dissolved in either a DMSO/water solution or a 2-HP β CD solution and diluted in fresh medium to the desired concentrations. Cisplatin was dissolved in pure water by stirring for several hours at room temperature and then diluted to the appropriate concentrations. Compounds were added (6 replicates each) and cells were incubated for 72 h, at which time the MTT

assay protocol was followed. MTT reagent (10 μ L) was added to each well and cells were incubated for 3-4 h, again depending on the cell line. Growth medium was removed by aspiration and DMSO (100 μ L) was added to each well. Plates were incubated for 15 min. The optical density was read at 540 nm on a Fisher Scientific Multiskan FC plate reader.

3.5.2. *In vivo* Toxicity Study

All animal procedures were reviewed and approved by the Institutional Animal Care and Use Committee at the University of Akron. Eight-week-old male C57BL/6 mice were obtained from Charles River laboratories. Animals were housed in a 12h light/dark cycle, and food and water were provided *ad libitum* (n = 3 animals per cage). Prior to the toxicity testing, animals were allowed to acclimate for 5 days. Vehicle control mice received IP injections on days 1, 8, 15, 22, 26, and 30 of 100 μ L of a 20% (w/v) HPCD sterile PBS solution. One group of experimental mice received IP injections of 100 μ L of \sim 20 mg/kg of **II 3** in 20% (w/v) HPCD on day 1 and 100 μ L of a \sim 15 mg/kg on day 15. A second group of experimental mice received IP injections of 100 μ L of \sim 20 mg/kg of **II 5** in 20% (w/v) HPCD on days 1, 8, 15, 22, 26, and 30. A third group of experimental mice received IP injections of 100 μ L of \sim 20 mg/kg of **III 1** in 20% (w/v) HPCD on days 1, 8, 15, and 30. A fourth group of experimental mice received IP injections of 100 μ L of \sim 20 mg/kg of **III 2** in 20% (w/v) HPCD on day 1. Animals were closely monitored and weighed on a daily basis. For compound **II 3**, one mouse was found dead on day 3 and the remaining

two mice were sacrificed on day 16. For compound **III 1**, two mice were sacrificed on day 3 and the other mouse was sacrificed on day 17.

CHAPTER IV

SYNTHESIS AND *IN VITRO* EVALUATION OF MITOCHONDRIAL TARGETING IMIDAZOLIUM SALTS

4.1. Introduction

Lung cancer is the leading cause of cancer-related deaths in the US, and the second most frequently diagnosed cancer worldwide. The disease is divided into two main categories, small cell lung cancer (SCLC) and non-small cell lung cancer (NSCLC), with the latter accounting for greater than 80% of diagnosed cases. Current treatments depend on the stage of the disease at the time of diagnosis, and can include a combination of surgery, radiation, chemotherapy, and targeted therapy. Despite the variety of treatment options available, the 5-year survival rate (~18% on average) has remained relatively unchanged for decades, and lags far behind that of other leading cancers such as breast and colon cancer.¹⁵⁵ Given these statistics there is an undeniable need for the development of more effective treatments for this disease.

Current chemotherapy regimens include the use of a combination of platinum and organic-based drugs. Cisplatin is the most commonly used platinum-

based drug and is prescribed as a first-line treatment for NSCLC.¹⁷⁸ However, platinum-based drugs can cause severe side effects such as nephrotoxicity.¹⁷⁹ In addition, many NSCLCs are resistant or can become resistant to platinum-based drugs, thus lessening their effectiveness in treating the disease.¹⁵⁷ Therefore, there remains an urgent need to develop a new treatment for NSCLC that can eradicate cancer cells effectively while minimizing toxicity to normal cells.

Today's chemotherapeutic approaches offer numerous methods aimed at stopping the proliferation of cancer cells. Targets can include specific genes and proteins or cellular targets such as DNA and mitochondria. The significance of mitochondria to cell proliferation and maintenance is undeniable. Mitochondria are tasked with producing energy needed by cells as well as controlling important cellular processes such as apoptosis. Rapidly proliferating cancer cells depend on fully functioning mitochondria to keep up with their growth rate. Of even more significance for cancer cells is the fact that mitochondria are able to adapt themselves to the environment around them. One of the most well known examples of this in cancer cell metabolism is the Warburg effect, described by Otto Warburg in 1924. This hypothesis states that cancer cells can maintain energy production via glycolysis even when oxygen is present, defining that mitochondria are important to cancer cell survival.¹⁸⁰ Targeting a cell's production of ATP at the source would lead to irreparable damage. A group of compounds known to accumulate in the mitochondria of cells are known as delocalized lipophilic cations (DLCs). These compounds are specifically attracted to the inner matrix of the mitochondria due to the mitochondrial membrane potential (MMP) across the inner membrane, which is

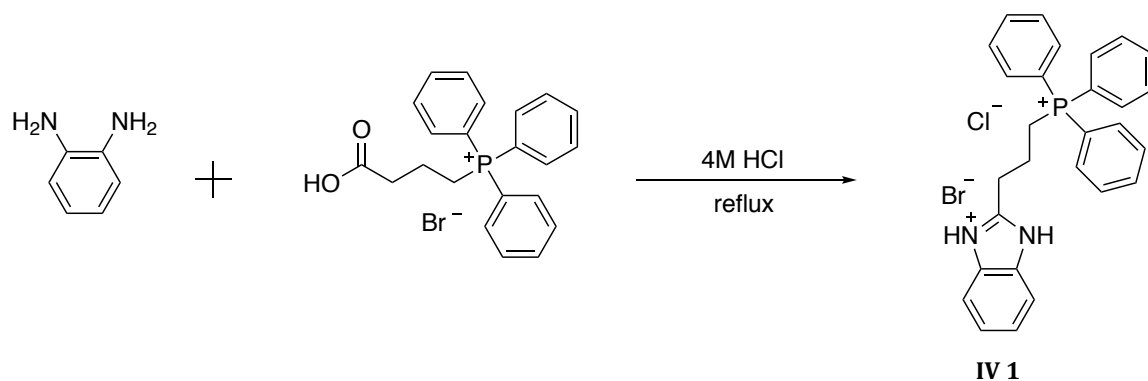
essential for ATP production.¹⁵⁴ Triphenylphosphonium (TPP) is a group classified as a DLC that is known to target mitochondria.¹⁸¹ When incorporated in the structure of doxorubicin, it can actually direct it to the mitochondria and enhance cytotoxicity in doxorubicin resistant cell lines.¹⁸² Imidazolium salts have been of recent interest in literature for their anti-cancer potential.^{26,149-152} In particular, some have been shown to induce apoptosis and disrupt the MMP of lung cancer cells.¹⁵¹ Because imidazolium salts are already DLCs, they may already be targeted to the mitochondria. However, including the TPP group may facilitate even better targeting to the mitochondria. It is therefore proposed that combining the targeting power of the TPP moiety with an imidazolium salt will be an effective treatment against NSCLC cell lines.

This chapter focuses on preliminary results of the synthesis and *in vitro* evaluation of a TPP containing imidazolium salt. Preliminary verification of synthesis has been done by ¹H NMR, ³¹P NMR, X-ray crystallography, and melting point determination. Evaluation of the cytotoxicity has been performed utilizing the MTT assay on a select number of NSCLC cancer cell lines.

4.2. Preliminary Results and Discussion

4.2.1. General Synthesis

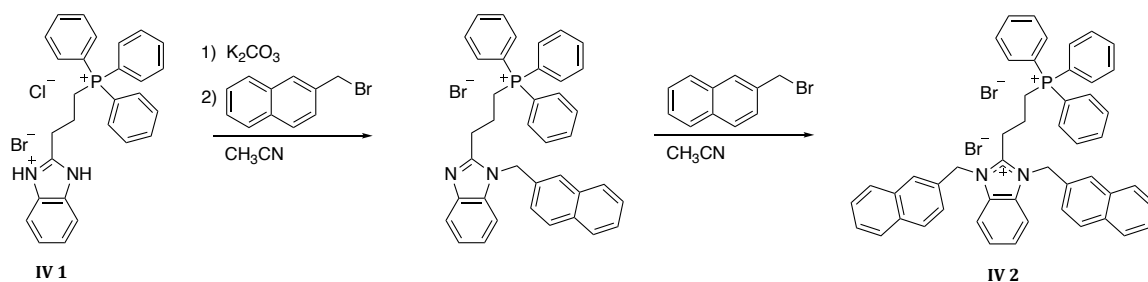
Compound **IV 1** and **IV 2** (Figure IV-1 and Figure IV-2) have been synthesized similar to previously published procedures.¹⁵⁰ The synthetic scheme to produce the benzimidazole core with the TPP group on the C² position of the ring is outlined in Equation IV-1.



Equation IV-1. Synthesis of compound **IV 1**.

Briefly, o-phenylenediamine and (3-carboxypropyl)triphenylphosphonium bromide were stirred at reflux in a solution of 4M HCl for 48 h. When the solution cooled, aqueous ammonium hydroxide was added until the solution was at a pH of 6-7 as indicated by pH paper. The solid was removed by vacuum filtration, yielding an off white solid that was washed with water to afford a yellow, cloudy filtrate. As the filtrate was allowed to sit at room temperature, more white solid had precipitated and was isolated by vacuum filtration to yield **IV 1**.

The substituted imidazolium salt was synthesized by the technique in Equation IV-2. Briefly, **IV 1** was deprotonated with potassium carbonate for 30 minutes in refluxing acetonitrile. 2-(Bromomethyl)naphthalene was added and allowed to stir at reflux for 3.5 h. The reaction mixture was vacuum filtered, isolating a solid product that was assumed to be potassium bromide. To the filtrate, another equivalent of 2(bromomethyl)naphthalene was added and allowed to stir at reflux for 74 hours. Addition of ether followed by vacuum filtration yielded **IV 2**, and a small amount of the single alkylation product.



Equation IV-2. Synthesis of compound **IV 2**.

Compound structures were preliminarily characterized by 1H and ^{31}P NMR spectroscopy and melting point determination. Structures were verified by single-crystal X-ray diffraction. The 1H NMR spectrum of **IV 1** showed peaks for the CH_2 groups at 2.30 ppm (multiplet), 3.44 ppm (triplet) and 3.92 ppm (multiplet) accounting for the protons closest to the phosphorus atom, protons closest to the imidazole core, and the center CH_2 group, respectively. The 1H NMR spectrum of **IV 2** contained peaks at 5.90 ppm and 6.08 ppm from the CH_2 methylene groups that bridge the imidazole core to the naphthalene groups. As seen previously, the bis-naphthalene substituted imidazolium salts have a downfield shifted methylene resonance due to the positive charge of the imidazolium salt. Therefore, the 5.90 ppm singlet resonance can be assigned to the mono-substituted product while the 6.08 ppm singlet can be assigned to the bis-substituted product. While there is a significant increase in intensity of the bis-naphthalene methylene linker, it is apparent that mono-naphthalene is still present (in a 5-10% yield by NMR). The impurities therefore make the 1H NMR spectrum difficult to assign in regards to the CH_2 groups linking the benzimidazole and the TPP group, so assignments cannot be made at this time. However, work is currently being done to isolate **IV 2**, such as

modifying synthetic procedures to ensure full reaction to the bis-substituted product. The ^{31}P NMR spectra show resonances for **IV 1** and **IV 2** at 23.72 ppm and 23.26 ppm.

Structures of **IV 1** and **IV 2** were also confirmed by single-crystal X-ray analysis. Crystals suitable for analysis of **IV 1** (Figure IV-1) were grown from water than had been heated to solubilize the sample of **IV 1** and then slowly cooled to room temperature. Crystals of **IV 2** (Figure IV-2) were grown from the evaporation of ethanol.

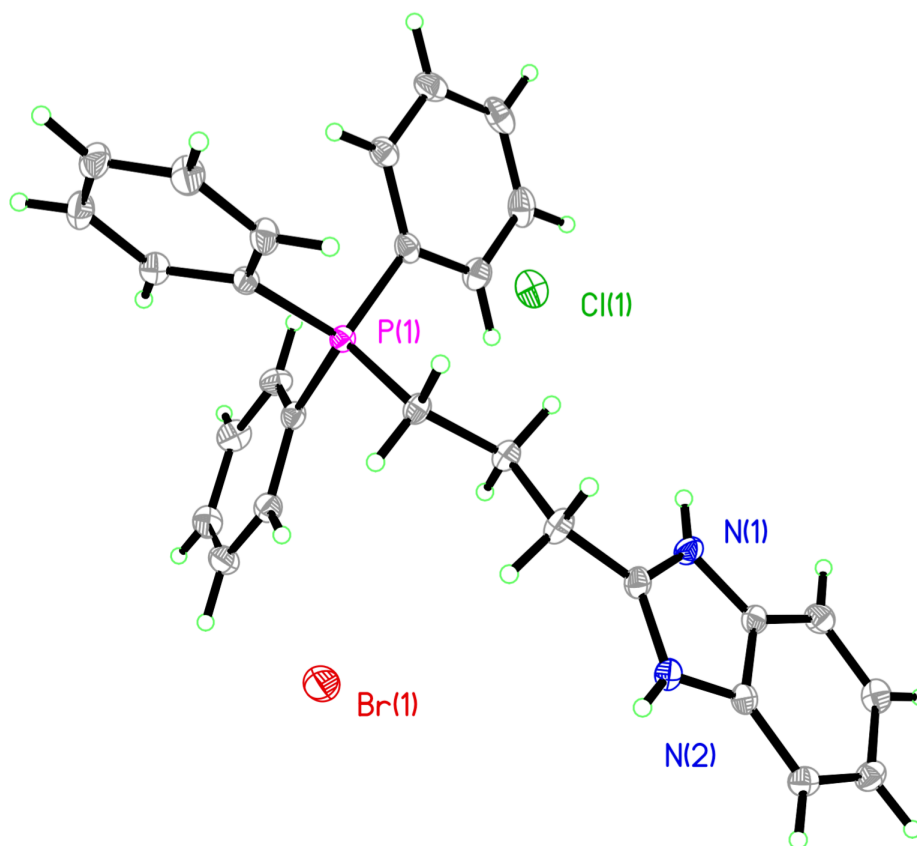


Figure IV-1. Thermal ellipsoid plot of **IV 1** with thermal ellipsoids drawn to 50% probability. Hydrogen and carbons labels and solvent molecules have been removed for clarity.

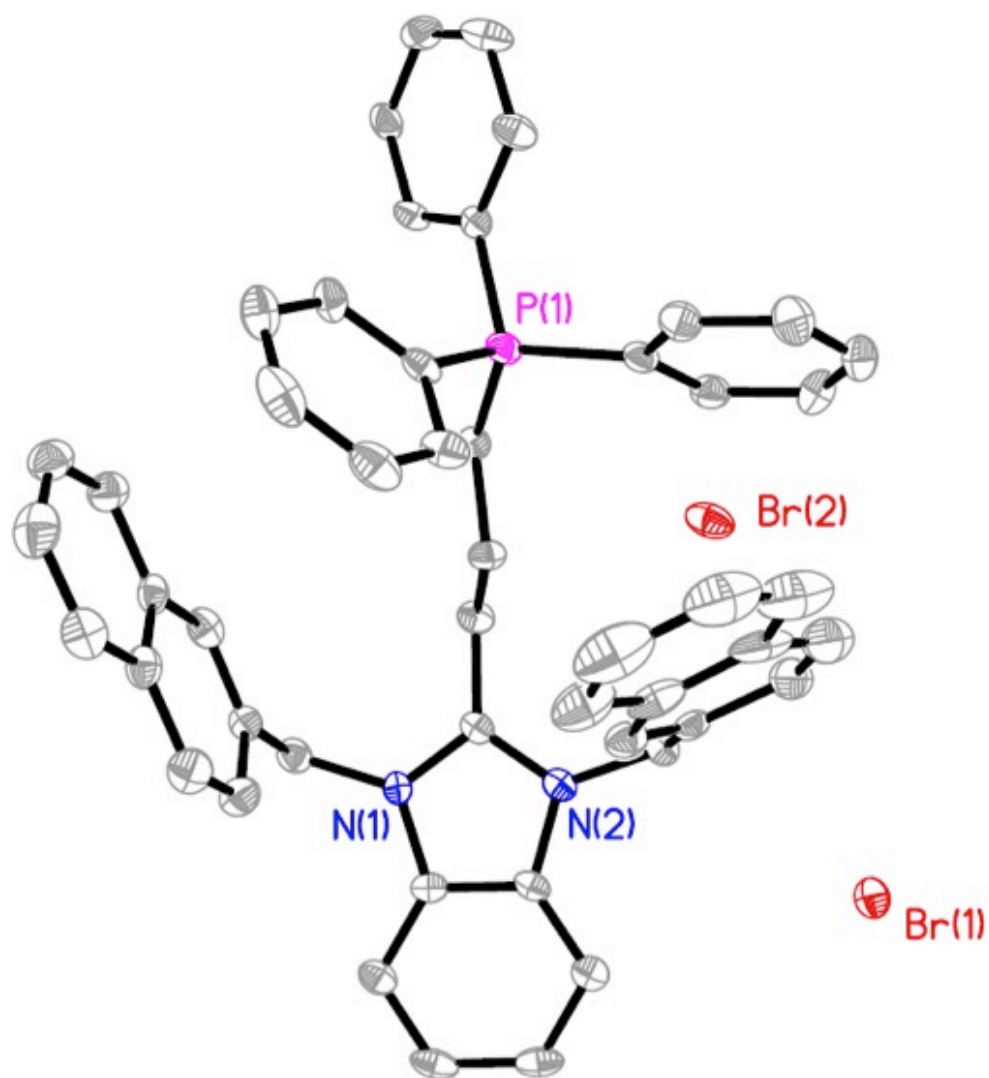


Figure IV-2. Thermal ellipsoid plot of **IV 2** with thermal ellipsoids drawn to 50% probability. Hydrogens, carbon labels and solvent molecules have been removed for clarity.

4.2.2. MTT assay

The anti-cancer activity of compounds **IV 1** and **IV 2** were evaluated on select NSCLC cancer cell lines (NCI-H460, NCI-H1975, A549, and HCC827) using the MTT assay. Briefly, cells were exposed to compounds **IV 1** and the mixed bis- and mono-naphthylated **IV 2** product for 72 hours before the MTT assay was utilized to determine cell viability. Results from the assay are used to calculate each compounds IC₅₀ value, which is the concentration at which the compound in question inhibits 50% of cell growth as compared to untreated control cells. The advantage of the TPP containing benzimidazolium salt **IV 2** is the increased water solubility (7 mg/mL) due to the bis-cationic nature of the compound. Because of this feature, both **IV 1** and the mixed product of **IV 2** were solubilized in a heated water solution before being diluted in cell culture medium to the desired concentrations of 1, 4, 16, and 32 μM (calculations for **IV 2** were done according to the molecular weight of **IV 2**). The tested compounds were compared side-by-side to cisplatin, as that is a first line treatment for NSCLC. While the product of the reaction to make **IV 2** is not completely pure by NMR, the MTT assay was still conducted to determine whether or not this group of compounds would have any anti-cancer activity at all and could warrant the time and effort to go into isolating a pure product. Results of the MTT assay are shown in Table IV-1.

Table IV-1. IC₅₀ values of **IV 1** and **IV 2** solubilized in pure water.

Compound (Solubilizing agent)	Cell Line and IC ₅₀ values (μM)			
	NCI-H460	NCI-H1975	A549	HCC827
IV 1 (water)	23	14	>32	>32
IV 2 (water)	3	2	8	3
Cisplatin	3	10	6	5

With the IC₅₀ values of the mixed product of **IV 2** being comparable to those of cisplatin, it can therefore be concluded that **IV 2** does exhibit anti-cancer activity. In comparison, the TPP containing benzimidazolium core alone, **IV 1**, has IC₅₀ values that are much higher and even has values higher than the tested range for half of the cell lines tested. Of extreme importance is the water solubility of **IV 2** as compared to the IC₅₀ values. Previous structure activity relationships have shown that increasing aqueous solubility was detrimental to anti-cancer activity. However, with a solubility of 7 mg/mL in water, **IV 2** still displays activity by the MTT assay. This type of compound therefore has great potential in future work concerning the treatment of NSCLC. As mentioned previously, work is being done to isolate **IV 2**. When this occurs and the MTT assay is repeated, it is assumed that the IC₅₀ values with pure product could slightly decrease.

4.3. Conclusion and Future Outlook

The conclusion from this study is extremely unique in that this is the first imidazolium salt in our library that has anti-cancer activity while also at the same time being soluble in water (7 mg/mL) without the use of DMSO or an excipient like 2-hydroxypropyl- β -cyclodextrin (HPCD). While these results are promising, there is still work that needs to be completed on this family of compounds. First, other TPP containing imidazolium salts need to be synthesized. This includes making both imidazole and benzimidazole cores containing the TPP group in different positions. Also, changing the alkyl chain length between the TPP group and the imidazole core would give a better understanding of how far apart the two positive charges can be while still imparting water solubility. Second, determining whether these compounds kill through an apoptotic or necrotic cell death would be of interest in order to understand if TPP containing imidazoles cause trauma to cancer cells or if they kill by a more systematic approach. The idea of introducing the TPP group was for the purpose of more strongly targeting imidazolium salts to the mitochondria of cancer cells so it will also be necessary to validate this through other experiments. After treating cells with TPP imidazolium salts, a commercially available mitochondrial isolation kit could be utilized to separate the mitochondria from the other cellular material. By using analytical methods, such as mass spectrometry, the concentration of the TPP imidazolium salt present inside the mitochondria could be evaluated. Finally, fluorescent substituents could be incorporated into the scaffold of an imidazolium salt with a TPP group so that cellular localization could be observed using fluorescence microscopy.

4.4. Acknowledgements

M. L. Stromyer has given invaluable assistance in the acquisition of the NMR spectra for compounds **IV 1** and **IV 2**. Dr. M. A. DeBord, Dr. N. A. Johnson, L. J. McDonald, A. Osinski, Dr. M. J. Panzner, M. L. Stromyer and Dr. C. A. Tessier have been involved in many helpful conversations about the synthesis and characterization of the compounds presented in this chapter. I would also like to thank Dr. M. A. DeBord for teaching me how to do the MTT assays.

4.5. Materials and Methods

4.5.1. General Considerations

All reactions were carried out under aerobic conditions. O-phenylenediamine was purchased from Alfa Aesar. (3-Carboxypropyl)triphenylphosphonium bromide and ammonium hydroxide were purchased from Sigma Aldrich. Potassium carbonate was purchased from Acros Organics. 2-(Bromomethyl)naphthalene was purchased from Waterstone Technologies. The TACS MTT cell proliferation kit was purchased from Trevigen. All other solvents were purchased from Fisher Scientific. All reagents were used as received without further purification. Melting points were obtained using a MelTemp apparatus with a calibrated thermometer. ^1H and ^{31}P NMR spectra were collected on a Varian 300 or 400 MHz instrument with all spectra referenced to residual deuterated solvent (DMSO d_6 : ^1H NMR: 2.50 ppm)

The human NSCLC cell lines NCI-H1975 and HCC827 were generously provided by Dr. Lindner from the Cleveland Clinic. The human NSCLC cell lines NCI-H460 and A549 were purchased from ATCC (Manassas, VA, USA). All cell lines were

grown at 37 °C with 5% CO₂ in RPMI 1640 medium supplemented with 10% fetal bovine serum and passed every 2-3 days.

4.5.2. X-ray Analysis

Crystals of the compounds were coated in paratone oil, mounted on a CryoLoop and placed on a goniometer under a stream of nitrogen. Crystal structure data sets were collected on either a Bruker SMART APEX I CCD diffractometer with graphite-monochromated Mo K α radiation ($\lambda = 0.71073 \text{ \AA}$) or a Bruker Kappa APEX II Duo CCD system equipped with a Mo ImuS source and a Cu ImuS micro-focus source equipped with QUAZAR optics ($\lambda = 1.54178 \text{ \AA}$). The unit cells were determined by using reflections from three different orientations. Data sets were collected using SMART or APEX II software packages. All data sets were processed using the APEX II software suite.^{167,168} The data sets were integrated using SAINT.¹⁶⁹ An empirical absorption correction and other corrections were applied to the data sets using multi-scan SADABS.¹⁷⁰ Structure solution, refinement, and modelling were accomplished by using the Bruker SHELXTL package.¹⁷¹ The structures were determined by full-matrix least-squares refinement of F^2 and the selection of the appropriate atoms from the generated difference map. Hydrogen atom positions were calculated and $U_{\text{iso}}(\text{H})$ values were fixed according to a riding model.

4.5.3. MTT Assay

Cells were grown to confluence and plated in 96-well plates at 5,000-6,000 cells per well, depending on the cell line. Cells were incubated for 24 h prior to adding the compounds. Compounds **IV 1** and **IV 2** were dissolved in water by heating and allowing the solution to cool to room temperature before diluting in medium to the desired concentrations of 1, 4, 16, and 32 μM . Cisplatin was dissolved in pure water by stirring for several hours at room temperature and then diluted to the appropriate concentrations. Compounds were added (6 replicates each) and cells were incubated for 72 h, at which time the MTT assay protocol was followed. MTT reagent (10 μL) was added to each well and cells were incubated for 3-4 h, again depending on the cell line. Growth medium was removed by aspiration and DMSO (100 μL) was added to each well. Plates were incubated for 15 min. The optical density was read at 540 nm on a Fisher Scientific Multiskan FC plate reader.

4.5.4. Synthesis of $\text{C}_{28}\text{H}_{27}\text{BrClN}_2\text{P}$ (**IV 1**)

O-phenylenediamine (1.003 g, 9.278 mmol) and (3-carboxypropyl)triphenylphosphonium bromide (4.370 g, 10.18 mmol) were dissolved in 20 mL of a 4M HCl solution. The reaction mixture was refluxed for 46 h. Aqueous ammonium hydroxide was added dropwise to the reaction mixture until a pH of 6-7 was obtained by pH paper. The solution was vacuum filtered to give an off-white solid, which was washed with water. The resulting filtrate, after washing the precipitate with water, was yellow and cloudy. The filtrate was allowed to sit at

room temperature and the resulting solid was isolated by vacuum filtration (1.080 g, 21.6% yield). Mp: 156 - 159°C.

Crystal data for **IV 1**: C₂₈H₃₁BrClN₂O₂P, M = 573.88, triclinic, a = 9.2965(2) Å, b = 11.2727(2) Å, c = 13.3227(2) Å, α = 99.7910(10)°, β = 103.8923(10)°, γ = 92.0331(12)°, V = 1336.33(4) Å³, T = 100(2) K, space group P-1, Z = 2, 41875 reflections measured, 5419 independent reflections (R_{int} = 0.0273). The final R₁ values were 0.0518 (I > 2σ(I)). The final wR(F²) values were 0.1239 (I > 2σ(I)). The final R₁ values were 0.0548 (all data). The final wR(F²) values were 0.1242 (all data).

4.5.5. Synthesis of C₅₀H₄₃BrN₂P (**IV 2**)

Compound **IV 1** (0.503 g, 0.936 mmol) and potassium carbonate (0.290 g, 2.10 mmol) were dissolved in 5 mL of acetonitrile and heated at reflux for 0.5 h. (2-Bromomethyl)naphthalene (0.310 g, 1.40 mmol) was added and the mixture was refluxed for 3.5 h, during which time a white precipitate formed. The solid, presumed to be potassium chloride and potassium bicarbonate, was removed via vacuum filtration. The volatile components were removed by vacuum and the solid was reconstituted in 5 mL of acetonitrile. (2-Bromomethyl)naphthalene (0.318 g, 1.44 mmol) was added to the reaction mixture which was refluxed for 74 h. The mixture was transferred to a new round bottom flask and addition of 100 mL of

ether afforded a white precipitate, which was isolated by vacuum filtration (0.611 g, 75.7% yield). Mp: Color change from 168 - 175°C, fully melted at 185°C.

Crystal data for **IV 2**: C₅₂H₅₁Br₂N₂O₂P, M = 926.74, monoclinic, a = 10.8583(2) Å, b = 34.0758(6) Å, c = 12.9337(13) Å, α = 90°, β = 112.0353(10)°, γ = 90°, V = 4435.97(13) Å³, T = 100(2) K, space group P2(1)/n, Z = 4, 50384 reflections measured, 9015 independent reflections (R_{int} = 0.1152). The final R₁ values were 0.0502 (I > 2σ(I)). The final wR(F²) values were 0.0869 (I > 2σ(I)). The final R₁ values were 0.1017 (all data). The final wR(F²) values were 0.1055 (all data).

4.5.6. Evaluation of Water Solubility

The solid product containing **IV 2** and a small amount of the mononaphthylated impurity was added to a vial containing 3 mL of deionized water. The vial was heated to solubilize all solid. More solid was added and heated until a saturated solution was achieved. The vial and its contents were allowed to cool to room temperature. A syringe was then used to push 1 mL of the solution through a Whatman 0.45 μm PTFE w/GMF filter into a centrifuge tube. The solution was frozen with liquid nitrogen and lyophilized overnight. The resulting solid was weighed and yielded 0.007 g.

CHAPTER V

SYNTHESIS AND *IN VITRO* EVALUATION OF A FLUORESCENT IMIDAZOLIUM SALT

5.1. Introduction

Imidazolium salts are the precursor ligands to N-heterocyclic carbenes (NHCs). Metal-NHC complexes have a vast array of utility including use as antimicrobial agents. The release of metals such as copper and silver is the main function of these antimicrobial metal-NHC complexes and after degradation an imidazolium salt is left behind. Research has shown that this ligand precursor and eventual metabolic product of an NHC, the imidazolium salt, has the ability to function as a potent anti-cancer therapeutic and a structure activity relationship (SAR) between various functional groups off of the imidazole ring and anti-cancer activity has been established.^{26,149-152} However, gaining more information about the cellular target and mechanism of action of imidazolium salts has proven to be more challenging. One general route to determine the cellular target of non-fluorescent compounds is to add fluorescent tags and use fluorescence microscopy to track the compounds progression. Unfortunately, while this technique offers visual confirmation of cellular localization, it is of a modified compound and not the therapeutic alone. The developed SAR shows that increasing lipophilicity will alter

activity. For larger compounds, this fluorescent tag addition may not make a difference in overall lipophilicity or activity but for smaller, simpler compounds like imidazolium salts, large groups can have a drastic effect on activity. Therefore, the addition of a large, lipophilic fluorescent tag to an imidazolium salt could alter important factors such as cellular uptake or target. One way to combat this issue is to make imidazolium salts that have intrinsic fluorescent properties (i.e. compounds with anti-cancer activity that are also fluorescent without modification) that can be exploited for the dual purpose of an anti-cancer therapeutic that does not have to be modified in order to determine cellular localization.

This chapter will focus on the synthesis and *in vitro* evaluation of a fluorescent imidazolium salt compound **V 1**. Specifically, MTT assay values as well as ability to stain cancer cells through fluorescence microscopy will be discussed.

5.2. Preliminary Results and Discussion

5.2.1. Structure of **V 1**

The structure of **V 1** can be seen in Figure V-1. The structure has been validated through single-crystal X-ray crystallography (Figure V-2). To evaluate the fluorescent properties of **V 1**, a UV-Vis absorbance spectrum was taken to determine that the maximum absorbance value was 456 nm. Next, a fluorescence spectrum was obtained utilizing 456 nm as the excitation wavelength. The resulting fluorescence spectrum can be seen in Figure V-3. Maximum fluorescence was observed at 522 nm. It is therefore presumed that fluorescence of **V 1** will be green,

with some overlap in red as indicated by the broad tail of the spectrum in Figure V-3.

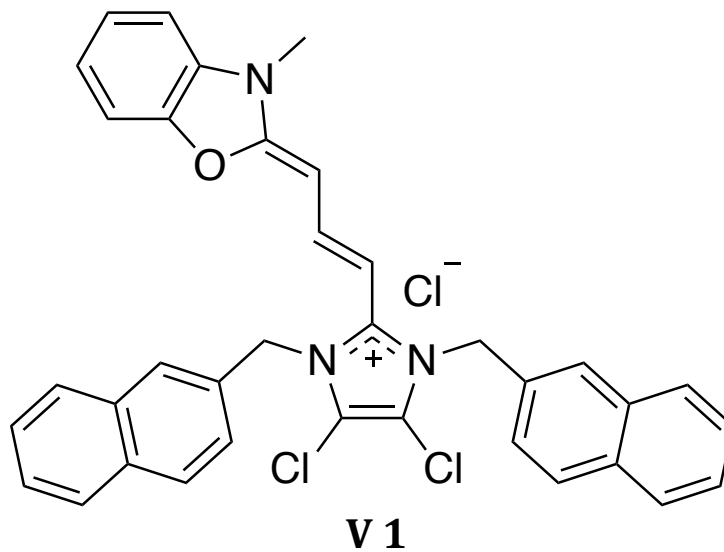


Figure V-1. Structure of V 1.

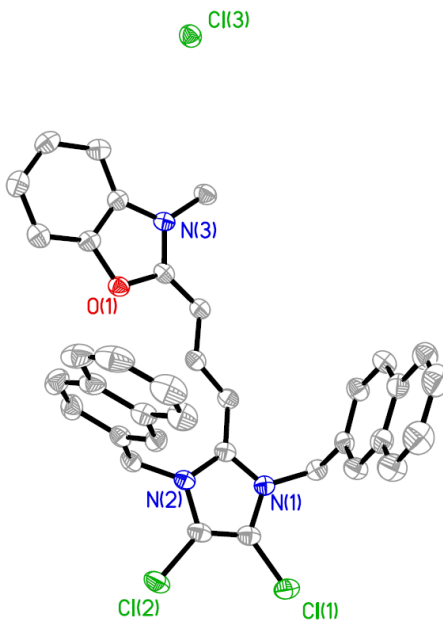


Figure V-2. Thermal ellipsoid plot of IV 2 with thermal ellipsoids drawn to 50% probability. Hydrogens, carbon labels and solvent molecules have been removed for clarity.

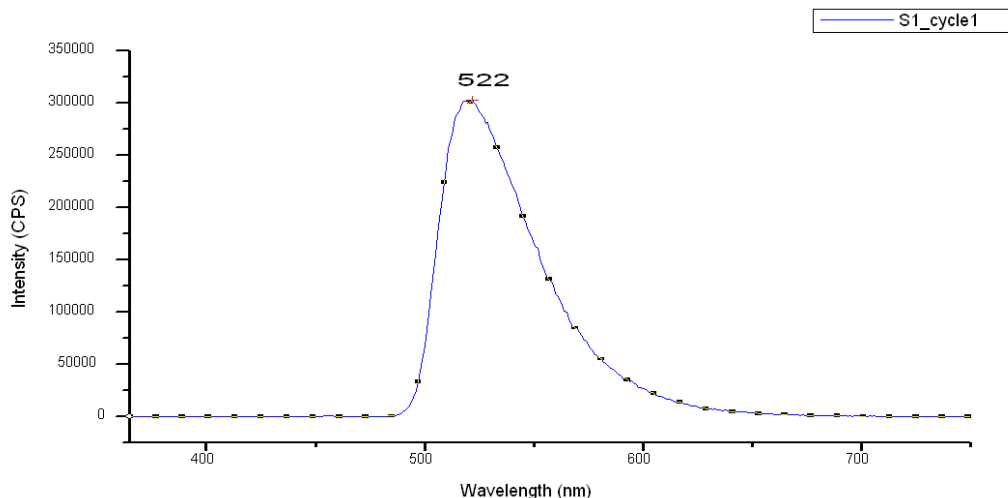


Figure V-3. Fluorescence spectrum of **V 1** (excitation wavelength : 456 nm).

5.2.2. *In vivo* Studies

5.2.2.1. MTT Assay

The MTT assay was used to evaluate the anti-cancer potential of **V 1** against select NSCLC cancer cell lines. All IC_{50} values were in the low micromolar to high nanomolar range showing the potent toxicity of this compound. However, when preparing **V 1** for use in the MTT assay, solubility was extremely poor. To prepare the 1% DMSO aqueous solution, the solid is first dissolved in 100 μ L of DMSO. Subsequently 9.9 mL of water was added. When water is added to the solubilized sample of **V1** in DMSO, the solid instantly precipitates back out of solution. The resulting suspension is vortexed thoroughly and the appropriate amount is aliquoted into medium at the desired concentrations. Results, as shown in Table V-1, are directly compared to cisplatin. The values for **V 1** are all in the low micromolar

to nanomolar range, depicting the high anti-cancer activity of **V 1**. However, it is troublesome that the solubility, even in a 1% DMSO/water solution is so low. Had solubility been better, these IC₅₀ values would most likely be even lower. Compound **V 1** can not be solubilized by 2-hydroxypropyl-β-cyclodextrin (HPCD), presumably due to the size of the molecule. In the future, use of larger cyclodextrin rings, such as γ-cyclodextrin could be utilized to account for the larger size of **V 1**.

Table V-1. IC₅₀ values of compound **V 1** in a 1% DMSO/water solution.

Compound (Solubilizing agent)	Cell Line and IC ₅₀ values (μM)			
	NCI-H460	NCI-H1975	A549	HCC827
V 1 (DMSO)	1	<1	1	1
Cisplatin	3	10	6	5

5.2.2.2. *In vitro* Cell Staining

The overall goal in the synthesis of this compound was to make an imidazolium salt that had potent anti-cancer activity while also being fluorescent. This would eliminate the need to add on bulky, lipophilic fluorescent tags that could potentially change the activity level of the compound in question. To evaluate the fluorescent nature of **V 1**, medium that was supplemented with **V 1** was introduced to cells and images were taken over time. A comparison of the images at 0.5 h and 2 h can be seen in Figure V-4. When comparing the two time points, one major difference is the presence of bright pockets of fluorescence at the 2 h time point,

which could indicate that there is a particular location in the cell where **V 1** is being collected. Cells were also stained with propidium iodide (PI) to determine if there was any disruption of the cellular membrane. However, apparent fluorescence from **V 1**, as presumed from the fluorescence spectrum in Figure V-3, carries over into red as seen in Figure V-5. Therefore, performing co-localization studies with commercially available fluorescent compounds that are known to target specific cellular organelles can still be performed, but only with those that are not fluorescent in the green or red region.

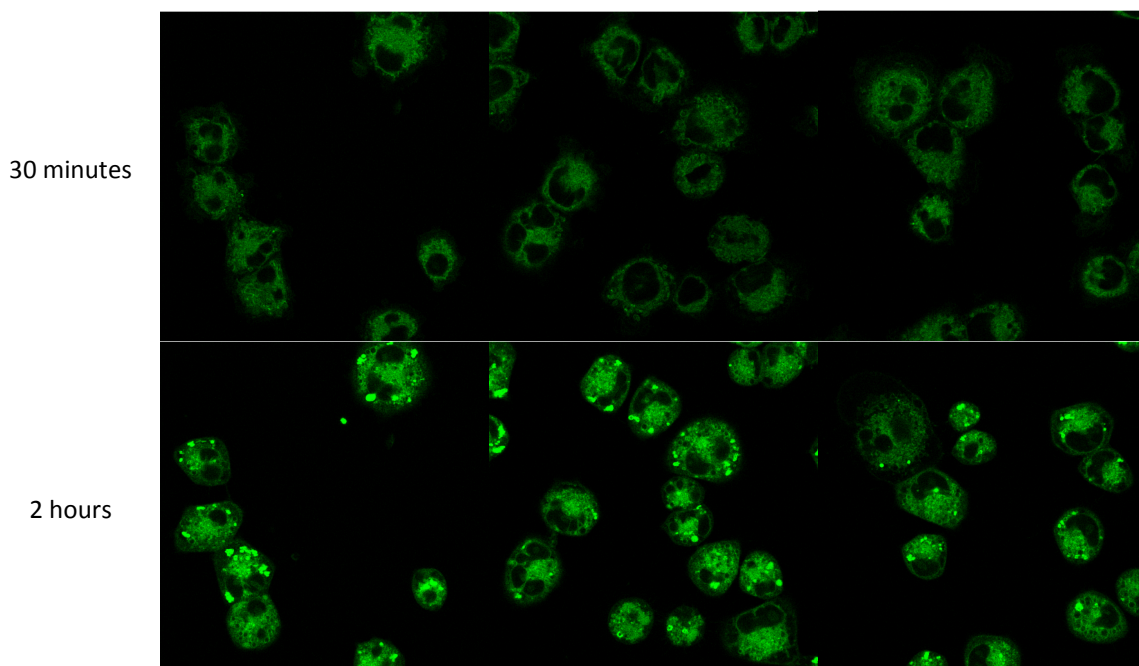


Figure V-4. H460 cells stained with **V 1** and imaged at the 30 minute and 2 hour time point.

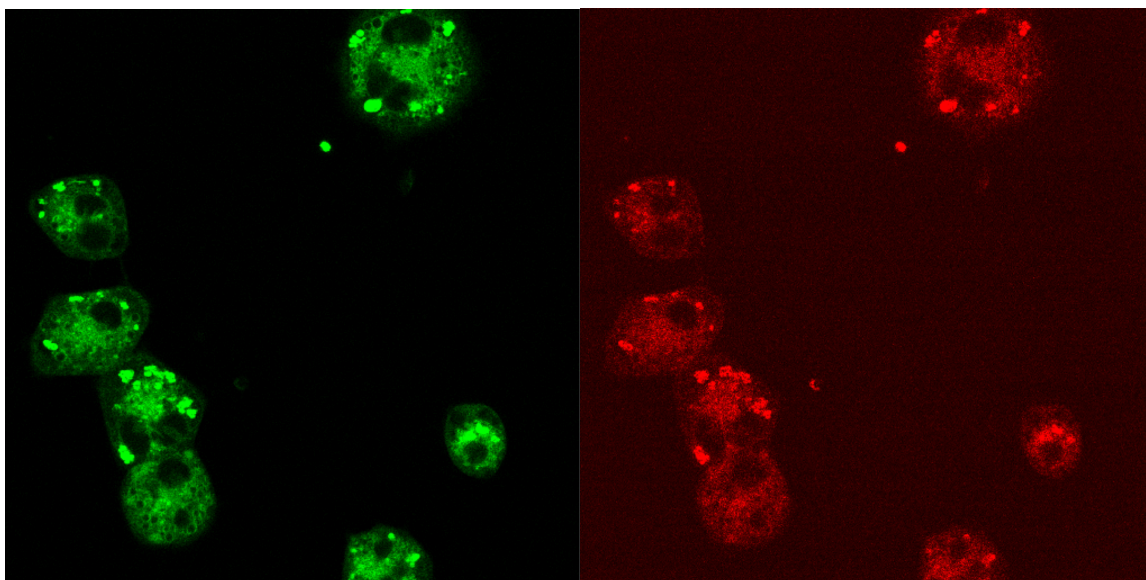


Figure V-5. H460 cells stained with **V 1** at the 2 hour time point. Images depict both the green and red fluorescence of **V 1**.

5.3. Conclusion and Future Outlook

Although further work is needed, compound **V 1** has been proven, according to these preliminary studies, to be a promising new imidazolium salt. With the low IC_{50} values and the ability to stain cells, the ability to determine if **V 1** is targeting a specific cellular location is possible. This would give important information in regards to determining what the mechanism of action of this compound is. However, compound **V 1** is not without its own limitations. First, the solubility needs to be addressed. Being completely insoluble in the 1% DMSO/water solution that is used for *in vitro* assays results in data that is not completely reflective of the overall properties of **V 1** and leads to issues in regards to the clinical relevance of this compound. Future work to increase the solubility includes the use of larger cyclodextrin systems, such as the γ -cyclodextrin system, and inclusion of

hydrophilic groups that would increase water solubility. Other future experiments include the co-localization of **V 1** and commercially available fluorescent compounds that localize to different cellular organelles. This would allow for the determination of where in the cell compound **V 1** is going. With **V 1**, fluorescent dyes that would work well are those that are blue. However, other efforts are being completed to shift the fluorescence of new derivatives of **V 1** so that the fluorescence overlap of green and red does not limit the co-localization studies.

5.4. Acknowledgements

M. L. Stromyer is responsible for synthesizing and characterizing compound **V 1**. Dr. M. C. Konopka, K. Whiddon and L. Ray have given invaluable expertise and hands on assistance in obtaining cell images with **V 1** as well as allowing us to utilize the microscope. I would also like to thank Dr. M. A. DeBord for teaching me how to do the MTT assays.

5.5. Materials and Methods

5.5.1. General Considerations

The TACS MTT cell proliferation kit was purchased from Trevigen. The propidium iodide (PI) solution was included in the FITC Annexin V Apoptosis Detection Kit that was purchased from BD Biosciences. Glass bottom dishes coated with poly-D-lysine used in the fluorescence cell study (P35GC-1.5-14-C) were

purchased from MatTek Corporation. The human NSCLC cell lines NCI-H1975 and HCC827 were generously provided by Dr. Lindner from the Cleveland Clinic. The human NSCLC cell lines NCI- H460 and A549 were purchased from ATCC (Manassas, VA, USA). All cell lines were grown at 37 °C with 5% CO₂ in RPMI 1640 medium supplemented with 10% fetal bovine serum and passed every 2-3 days.

5.5.2. MTT Assay

Cells were grown to confluence and plated in 96-well plates at 5,000-6,000 cells per well, depending on the cell line. Cells were incubated for 24 h prior to adding the compounds. Compounds **V 1** was prepared by solubilizing in 100 µL of DMSO and then adding 9.9 mL of water before diluting in medium to the desired concentrations of 1, 4, 16, and 32 µM. Cisplatin was dissolved in pure water by stirring for several hours at room temperature and then diluted to the appropriate concentrations. Compounds were added (6 replicates each) and cells were incubated for 72 h, at which time the MTT assay protocol was followed. MTT reagent (10 µL) was added to each well and cells were incubated for 3-4 h, again depending on the cell line. Growth medium was removed by aspiration and DMSO (100 µL) was added to each well. Plates were incubated for 15 min. The optical density was read at 540 nm on a Fisher Scientific Multiskan FC plate reader.

5.5.3. *In vitro* fluorescence evaluation

The NCI-H460 cell line was grown in 35-mm glass bottom dishes coated with poly-D-lysine at a cell density of 15,000 cells per well. The cell suspension was added to the glass cover of each well (500 μ L) and allowed to adhere for 1 hour before additional medium (2 mL) was added to the plate. Cells were placed in the incubator overnight. Cells were treated with supplemented medium at a concentration of 40 μ M for compound **V 1** that had been solubilized in 100 μ L of DMSO with the subsequent addition of 9.9 mL of water. Treatment consisted of aspirating medium from plates and replacing with 3 mL of the above specified medium that was also supplemented with 20 μ L of a 50 μ g/mL solution of PI. Cells were imaged using a Nikon A1+ laser scanning confocal microscope using a 100x Plan Apo λ (1.45 NA) objective lens. Excitation was done by 488 nm, and 561 nm solid state lasers.

5.5.4. X-ray Analysis

Crystals of the compounds were coated in paratone oil, mounted on a CryoLoop and placed on a goniometer under a stream of nitrogen. Crystal structure data sets were collected on either a Bruker SMART APEX I CCD diffractometer with graphite-monochromated Mo $K\alpha$ radiation ($\lambda = 0.71073 \text{ \AA}$) or a Bruker Kappa APEX II Duo CCD system equipped with a Mo ImuS source and a Cu ImuS micro-focus source equipped with QUAZAR optics ($\lambda = 1.54178 \text{ \AA}$). The unit cells were determined by using reflections from three different orientations. Data sets were collected using SMART or APEX II software packages. All data sets were processed

using the APEX II software suite.^{167,168} The data sets were integrated using SAINT.¹⁶⁹ An empirical absorption correction and other corrections were applied to the data sets using multi-scan SADABS.¹⁷⁰ Structure solution, refinement, and modelling were accomplished by using the Bruker SHELXTL package.¹⁷¹ The structures were determined by full-matrix least-squares refinement of F^2 and the selection of the appropriate atoms from the generated difference map. Hydrogen atom positions were calculated and $U_{\text{iso}}(\text{H})$ values were fixed according to a riding model.

5.5.5. Crystal Structure Data

Crystal data for **V 1**: $\text{C}_{36}\text{H}_{30}\text{Cl}_3\text{N}_3\text{O}_2$, $M = 642.98$, triclinic, $a = 10.1036(3) \text{ \AA}$, $b = 10.2309(3) \text{ \AA}$, $c = 16.2459(4) \text{ \AA}$, $\alpha = 99.954(2)^\circ$, $\beta = 98.123(2)^\circ$, $\gamma = 107.477(2)^\circ$, $V = 1543.96(7) \text{ \AA}^3$, $T = 100(2) \text{ K}$, space group P-1, $Z = 2$, 16037 reflections measured, 4782 independent reflections ($R_{\text{int}} = 0.0399$). The final R_1 values were 0.0372 ($I > 2\sigma(I)$). The final $wR(F^2)$ values were 0.0849 ($I > 2\sigma(I)$). The final R_1 values were 0.0527 (all data). The final $wR(F^2)$ values were 0.0920 (all data).

CHAPTER VI

CONCLUDING REMARKS

Imidazolium salts are a promising family of compounds that have potent anti-cancer activity. Originally finding use in other areas of research, such as the precursor ligands for N-heterocyclic carbene complexes, the application of imidazolium salts in medicinal chemistry has proven to be of great importance. Structure activity relationships by utilizing the MTT assay have established that increasing lipophilicity will lead to an enhancement of anti-cancer activity. However, increasing lipophilicity leads to a decrease in aqueous solubility and leads to issues of systemic administration. Use of excipients, like the FDA approved cyclodextrin that is generally regarded as safe (GRAS), is able to increase the water solubility of certain imidazolium salts. Some derivatives with bulky substituents cannot be solubilized with the β -cyclodextrin, but further studies are being done to determine whether larger cyclodextrin systems are able to combat this issue.

Knowledge of how imidazolium salts kill cancer cells has still been rather limited in current literature, and a specific mechanism of action has not yet been confirmed. In order to learn more about this process, the Annexin V assay was utilized to distinguish between the process of programmed cell death or cell death

caused by trauma. Interestingly, not all imidazolium salts kill cancer cells in the same way, as seen with **II 4**, which was the only lead compound tested that was determined to cause cell death by necrosis. The other lead imidazolium salts appeared to kill cancer cells by apoptosis, but at different time frames, dependent on the substituents off of the imidazole core. To validate these findings, the JC-1 assay was employed to evaluate the mitochondrial membrane potential (MMP) of cells that were treated with certain imidazolium salts. It was found that cancer cells treated with **II 1** and **II 3** had complete loss of MMP at very early time points. Both concentration and the treatment time had to be decreased in order to observe the fluorescent progression of the JC-1 reagent in the mitochondria of treated cells. Even though this cannot confirm that imidazolium salts target the mitochondria of cancer cells, it has led to the further study of mitochondria as a possible cellular target.

While imidazolium salts have proven to be effective *in vitro*, they have also been tested for toxicity in animal models. At injections of 20 mg/kg, it was determined that **II 5** and **III 1** were tolerated well by C57BL/6 mice. Further studies include toxicity testing of **II 3** and **III 2** at lower concentrations to determine if that could alleviate issues observed at the 20 mg/kg dose.

With the knowledge that imidazolium salts do not interact with DNA and that mitochondria should be further studied as a cellular target, a new family of imidazolium salts was developed. Delocalized lipophilic cations (DLCs), such as imidazolium salts, are known to target the mitochondria of cells, giving even further confirmation that mitochondria may be an important part of their mechanism of

action. The triphenylphosphonium (TPP) group is a DLC that can be used to target compounds to mitochondria and can be incorporated into the structure of imidazolium salts to facilitate their localization to the mitochondria of cancer cells. Preliminary work has been completed on this new family of compounds and has shown compounds like **IV 2** to possess both aqueous solubility (7 mg/mL) and anti-cancer properties (IC_{50} values ranging from 2 – 8 μ M). Compound **IV 2** is the first of its kind in our library to have both activity and solubility, enough that MTT assays could be completed with a solution of **IV 2** in pure water. The work completed thus far is in preliminary stages, as issues with purity need to be addressed and corrected before further studies can be completed. However, this preliminary work validates that this family of imidazolium salts has great potential and warrants the time and effort needed to establish these compounds further. Future work also includes utilizing *in vitro* assays to learn more about how TPP containing imidazolium salts kill cancer cells and by isolating mitochondria to determine if they can in fact collect in the mitochondria as they have been designed to do.

Finally, preliminary work has also been completed on an imidazolium salt, **V1**, that has intrinsic fluorescent properties, eliminating the need to attach bulky, lipophilic fluorescent tags that could alter both cellular localization and anti-cancer activity of imidazolium salt derivatives. The anti-cancer activity as determined by the MTT assay shows that these unique compounds have potent anti-cancer activity, with all IC_{50} values being 1 μ M or below. Compound **V 1** also introduces a new property, intrinsic fluorescence, that allows for the study of these compounds through fluorescence microscopy. Co-localization cell staining can be employed in

the future to elucidate that specific cellular target of **V 1** as well as derivatives that will be made in the future. The limitation of this group of compounds is the aqueous solubility. 2-Hydroxypropyl- β -cyclodextrin (HPCD) was not able to assist in the solubility of **V 1**, but inclusion of groups that are more hydrophilic, use of larger cyclodextrins, and synthesis of fluorescent imidazolium salts containing the TPP group are all areas of future study.

Of all the future work that should be completed on further developing imidazolium salts and anti-cancer chemotherapeutics, the most important study that needs to be done is evaluating toxicity of these lead compounds to normal epithelial cells, such as the 16 HBE cell line (human bronchial epithelial cells). This study is of extreme importance because it will determine if imidazolium salts have any selectivity for cancer cells over non-cancerous cells. At this time, we predict that our imidazolium salts will display selectivity for cancer cells, a property that is also observed for other delocalized lipophilic cations, such as rhodamine 123, due to the increased mitochondrial membrane potential of cancer cells.^{183,184} Completing the MTT assay on the 16 HBE cell line will be able to confirm or deny this hypothesis.

Furthermore, knowledge of the previously presented imidazolium salts combined with information about DLCs direct us to the idea that mitochondria are the cellular target of these compounds. While the JC-1 assay presented cannot confirm this idea, it has given us an interesting starting point to begin thinking about this possibility. Our results show complete depolarization at the 30-minute time frame when cells are treated with the same concentration of compound as for

the Annexin V assay, leading us to believe that this could be what causes apoptosis to occur.

In order to more fully understand the cell death processes undertaken as a result of imidazolium salts, we propose to begin studying an extremely important player in the regulation of apoptosis, cytochrome c. Cytochrome c is an important part of the electron transport chain in mitochondria and functions in transferring electrons between complex III and complex IV. When cytochrome c is released, it interacts with apoptotic protease activating factors (Apaf) and begins the cascade of caspase activation. This change can lead to the generation of superoxide.¹⁸⁵ Fortunately, the release of cytochrome c can be studied by western blot analysis using commercially available monoclonal antibodies after isolating mitochondria from treated cells.

Furthermore, we hypothesize that an important inner mitochondrial membrane phospholipid, cardiolipin, is another area of research to begin studying. Cardiolipin is known to interact with cytochrome c. This interaction can be disrupted through the oxidation of cardiolipin from reactive oxygen species and leads to the release of cytochrome c into the cytosol, thus beginning the cell death pathway.^{186,187} If imidazolium salts are able to generate reactive oxygen species, which can also be studied through *in vitro* experiments, this could result in the oxidation of cardiolipin and thus cause cytochrome c release and cell death. However, generation of superoxide could either be caused by imidazolium salts directly or by the inhibition of superoxide dismutase (SOD) or through other

downstream events that involve regulation of the generated hydrogen peroxide. SOD is an enzyme whose function is to convert the superoxide radical to oxygen and hydrogen peroxide.¹⁸⁸ Therefore, we also propose to study the function of manganese SOD through commercially available assay kits to determine if imidazolium salts have the ability to interact with this fundamental mitochondrial enzyme. Finally, other areas that can be studied include the Bcl-2 family of proteins and other factors that can induce permeability of the mitochondria through the permeability transition pore that would lead to membrane depolarization.¹⁸⁹

Overall, the studies presented herein and the proposed future studies shed light on what we currently know about imidazolium salts and how their effect on cancer cell survival can be studied in the future. Understanding how imidazolium salts kill cancer cells is important for the purpose of being able to create new derivatives that have increased anti-cancer activity. With the potent anti-cancer activity of current imidazolium salts, it is clear that they have a future in cancer research and elucidating their mechanism of action is an important step towards the overarching goal of developing clinically relevant imidazolium salt chemotherapeutics.

REFERENCES

- (1) Wanzlick, H. -W; Schönherr, H. -J. *Angew. Chemie Int. Ed. English* **1968**, 7 (2), 141–142.
- (2) Öfele, K. *J. Organomet. Chem.* **1979**, 12, 42–43.
- (3) Igau, A.; Grutzmacher, H.; Baceiredo, A.; Bertrand, G. *J. Am. Chem. Soc.* **1988**, 110 (19), 6463–6466.
- (4) Arduengo, III, A. J.; Harlow, R. L.; Kline, M. *J. Am. Chem. Soc.* **1991**, 113 (1), 361–363.
- (5) Hopkinson, M. N.; Richter, C.; Schedler, M.; Glorius, F. *Nature* **2014**, 510 (7506), 485–496.
- (6) Herrmann, W. A.; Köcher, C. *Angew. Chemie Int. Ed. English* **1997**, 36 (20), 2162–2187.
- (7) Cetinkaya, B.; Cetinkaya, E.; Küçükbay, H.; Durmaz, R. *Arzneimittel-forsch. Drug Res.* **1996**, 46 (8), 821–823.
- (8) Egorova, K. S.; Ananikov, V. P. *Organometallics* **2017**, 36 (21), 4071–4090.
- (9) Dizaj, S. M.; Lotfipour, F.; Barzegar-Jalali, M.; Zarrintan, M. H.; Adibkia, K. *Mater. Sci. Eng. C* **2014**, 44, 278–284.
- (10) Rosenberg, B. *Platin. Met. Rev.* **1971**, 15 (2), 42–51.
- (11) Rosenberg, B.; VanCamp, L.; Trosko, J. E.; Mansour, V. H. *Nature* **1969**, 222, 385–386.
- (12) Rosenberg, B.; VanCamp, L. *Cancer Res.* **1970**, 30 (6), 1799–1802.
- (13) Cleare, M. J. *Coord. Chem. Rev.* **1974**, 12, 349–405.
- (14) Haiduc, I.; Silvestru, C. *Coord. Chem. Rev.* **1990**, 99, 253–296.
- (15) Romero-Canelón, I.; Sadler, P. J. *Inorg. Chem.* **2013**, 52 (21), 12276–12291.
- (16) Medvetz, D. A.; Hindi, K. M.; Panzner, M. J.; Ditto, A. J.; Yun, Y. H.; Youngs, W. J. *Met. Based. Drugs* **2008**, 2008, 1–7.
- (17) Youngs, W. J.; Knapp, A. R.; Wagers, P. O.; Tessier, C. A. *Dalton Trans.* **2012**, 41 (2), 327.
- (18) Deblock, M. C.; Panzner, M. J.; Tessier, C. A.; Cannon, C. L.; Youngs, W. J. In *N-Heterocyclic Carbenes: From Laboratory Curiosities to Efficient Synthetic Tools*; Diez-Gonzalez, S., Ed.; Royal Society of Chemistry: Cambridge, 2011; pp 119–133.
- (19) Siciliano, T. J.; Deblock, M. C.; Hindi, K. M.; Durmus, S.; Panzner, M. J.; Tessier, C. A.; Youngs, W. J. *J. Organomet. Chem.* **2011**, 696 (5), 1066–1071.

- (20) Aweda, T. A.; Ikotun, O.; Mastren, T.; Cannon, C. L.; Wright, B.; Youngs, W. J.; Cutler, C.; Guthrie, J.; Lapi, S. E. *Med Chem Comm* **2013**, *4* (6), 1015.
- (21) Garrison, J. C.; Youngs, W. J. *Chem. Rev.* **2005**, *105*, 3978–4008.
- (22) Hindi, K. M.; Panzner, M. J.; Tessier, C. A.; Cannon, C. L.; Youngs, W. J. *Chem. Rev.* **2009**, *109*, 3859–3884.
- (23) Kopple, J. D.; Swendseid, M. E. *J. Clin. Invest.* **1975**, *55* (5), 881–891.
- (24) Philippu, A.; Prast, H. *Behav. Brain Res.* **2001**, *124* (2), 151–159.
- (25) Youngs, W. J.; Panzner, M. J.; Deblock, M. C.; Tessier, C. A.; Wright, B. D.; Wagers, P. O.; Robishaw, N. K. Azolium and purinium salt anticancer and antimicrobial agents, June 2015.
- (26) Wright, B. D.; Deblock, M. C.; Wagers, P. O.; Duah, E.; Robishaw, N. K.; Shelton, K. L.; Southerland, M. R.; DeBord, M. A.; Kersten, K. M.; McDonald, L. J.; Stiel, J. a.; Panzner, M. J.; Tessier, C. A.; Paruchuri, S.; Youngs, W. J. *Med. Chem. Res.* **2015**, *24* (7), 2838–2861.
- (27) Glushkov, V. A.; Zhiguleva, M. A.; Maiorova, O. A.; Gorbunov, A. A. *Russ. J. Org. Chem.* **2012**, *48* (5), 699–704.
- (28) Zhou, B.; Liu, L.-X.; Deng, G.-G.; Chen, W.; Li, M.-Y.; Yang, L.-J.; Li, Y.; Yang, X.-D.; Zhang, H.-B. *Org. Biomol. Chem.* **2016**, *14*, 9423–9430.
- (29) Arduengo, A. J.; Krafczyk, R.; Schmutzler, R.; Craig, H. a.; Goerlich, J. R.; Marshall, W. J.; Unverzagt, M. *Tetrahedron* **1999**, *55* (51), 14523–14534.
- (30) Ding, J.; Armstrong, D. W. *Chirality* **2005**, *17* (5), 281–292.
- (31) Kascatan-Nebioglu, A.; Panzner, M. J.; Garrison, J. C.; Tessier, C. A.; Youngs, W. J. *Organometallics* **2004**, *23* (8), 1928–1931.
- (32) Kascatan-Nebioglu, A.; Melaiye, A.; Hindi, K.; Durmus, S.; Panzner, M. J.; Hogue, L. A.; Mallett, R. J.; Hovis, C. E.; Coughenour, M.; Crosby, S. D.; Milsted, A.; Ely, D. L.; Tessier, C. A.; Cannon, C. L.; Youngs, W. J. *J. Med. Chem.* **2006**, *49* (23), 6811–6818.
- (33) Kascatan-Nebioglu, A.; Panzner, M. J.; Tessier, C. A.; Cannon, C. L.; Youngs, W. J. *Coord. Chem. Rev.* **2007**, *251* (5–6), 884–895.
- (34) Anderson, E. B.; Long, T. E. *Polymer (Guildf)*. **2010**, *51* (12), 2447–2454.
- (35) Egorova, K. S.; Gordeev, E. G.; Ananikov, V. P. *Chem. Rev.* **2017**, *117* (10), 7132–7189.
- (36) Lin, J. C. Y.; Huang, R. T. W.; Lee, C. S.; Bhattacharyya, A.; Hwang, W. S.; Lin, I. J. B. *Chem. Rev.* **2009**, *109* (8), 3561–3598.
- (37) Mercks, L.; Albrecht, M. *Chem. Soc. Rev.* **2010**, *39* (6), 1903.

- (38) Oehninger, L.; Rubbiani, R.; Ott, I. *Dalton Trans.* **2013**, 42 (10), 3269–3284.
- (39) Johnson, N. A.; Southerland, M. R.; Youngs, W. J. *Molecules* **2017**, 22 (8), 1–20.
- (40) Zhao, W.; Ferro, V.; Baker, M. V. *Coord. Chem. Rev.* **2017**, 339, 1–16.
- (41) Jahnke, M. C.; Hahn, F. E. In *N-Heterocyclic Carbenes: From Laboratory Curiosities to Efficient Synthetic Tools*; Diez-Gonzalez, S., Ed.; Royal Society of Chemistry: Cambridge, 2017; pp 1–45.
- (42) De Frémont, P.; Marion, N.; Nolan, S. P. *Coord. Chem. Rev.* **2009**, 253, 862–892.
- (43) Balouiri, M.; Sadiki, M.; Ibsouda, S. K. *J. Pharm. Anal.* **2016**, 6 (2), 71–79.
- (44) Berridge, M. V.; Herst, P. M.; Tan, A. S. In *Biotechnology Annual Review*; 2005; Vol. 11, pp 127–152.
- (45) Stacey Ricci, M.; Zong, W. *Oncologist* **2006**, 11 (4), 342–357.
- (46) Voet, D.; Voet, J. G.; Pratt, C. W. *Fundamentals of Biochemistry*, 4th ed.; John Wiley & Sons, Ltd.: Hoboken, NJ, 2013.
- (47) Korytowski, W.; Basova, L. V.; Pilat, A.; Kernstock, R. M.; Girotti, A. W. *J. Biol. Chem.* **2011**, 286 (30), 26334–26343.
- (48) Pinton, P.; Giorgi, C.; Siviero, R.; Zecchini, E.; Rizzuto, R. *Oncogene* **2008**, 27 (50), 6407–6418.
- (49) Kurtoglu, M.; Lampidis, T. J. *Mol. Nutr. Food Res.* **2009**, 53 (1), 68–75.
- (50) Pelli, M.; Gandin, V.; Marinelli, M.; Marzano, C.; Yousufuddin, M.; Dias, H. V. R.; Santini, C. *Inorg. Chem.* **2012**, 51 (18), 9873–9882.
- (51) Almalioti, F.; MacDougall, J.; Hughes, S.; Hasson, M. M.; Jenkins, R. L.; Ward, B. D.; Tizzard, G. J.; Coles, S. J.; Williams, D. W.; Bamford, S.; Fallis, I. A.; Dervisi, A. *Dalton Trans.* **2013**, 42 (34), 12370–12380.
- (52) Monticelli, M.; Bellemin-Laponnaz, S.; Tubaro, C.; Rancan, M. *Eur. J. Inorg. Chem.* **2017**, 2017 (18), 2488–2495.
- (53) Messori, L.; Marchetti, L.; Massai, L.; Scaletti, F.; Guerri, A.; Landini, I.; Nobili, S.; Perrone, G.; Mini, E.; Leoni, P.; Pasquali, M.; Gabbiani, C. *Inorg. Chem.* **2014**, 53 (5), 2396–2403.
- (54) Bertrand, B.; De Almeida, A.; Van Der Burgt, E. P. M.; Picquet, M.; Citta, A.; Folda, A.; Rigobello, M. P.; Le Gendre, P.; Bodio, E.; Casini, A. *Eur. J. Inorg. Chem.* **2014**, 2014 (27), 4532–4536.
- (55) Mui, Y. F.; Fernández-Gallardo, J.; Elie, B. T.; Gubran, A.; Maluenda, I.; Sanaú, M.; Navarro, O.; Contel, M. *Organometallics* **2016**, 35 (9), 1218–1227.
- (56) Rodrigues, M.; Russo, L.; Aguiló, E.; Rodríguez, L.; Ott, I.; Pérez-García, L. *RSC Adv.* **2016**, 6 (3), 2202–2209.

- (57) Schmidt, C.; Karge, B.; Misgeld, R.; Prokop, A.; Franke, R.; Brönstrup, M.; Ott, I. *Chem. - A Eur. J.* **2017**, *23* (8), 1869–1880.
- (58) Chen, C.; Ni, S.; Zheng, Q.; Yu, M.; Wang, H. *Eur. J. Inorg. Chem.* **2017**, *2017* (3), 616–622.
- (59) Hackenberg, F.; Müller-Bunz, H.; Smith, R.; Streciwilk, W.; Zhu, X.; Tacke, M. *Organometallics* **2013**, *32* (19), 5551–5560.
- (60) Hackenberg, F.; Lally, G.; Müller-Bunz, H.; Paradisi, F.; Quaglia, D.; Streciwilk, W.; Tacke, M. *Inorganica Chim. Acta* **2013**, *395*, 135–144.
- (61) Streciwilk, W.; Cassidy, J.; Hackenberg, F.; Müller-Bunz, H.; Paradisi, F.; Tacke, M. *J. Organomet. Chem.* **2014**, *749*, 88–99.
- (62) Streciwilk, W.; Hackenberg, F.; Müller-Bunz, H.; Tacke, M. *Polyhedron* **2014**, *80*, 3–9.
- (63) Dada, O.; Curran, D.; O'Beirne, C.; Müller-Bunz, H.; Zhu, X.; Tacke, M. *J. Organomet. Chem.* **2017**, *840*, 30–37.
- (64) Zou, T.; Lok, C.-N.; Fung, Y. M. E.; Che, C.-M. *Chem. Commun.* **2013**, *49* (47), 5423–5425.
- (65) Li, K.; Zou, T.; Chen, Y.; Guan, X.; Che, C. M. *Chem. - A Eur. J.* **2015**, *21* (20), 7441–7453.
- (66) Betzer, J. F.; Nuter, F.; Chtchigrovsky, M.; Hamon, F.; Kellermann, G.; Ali, S.; Calmèjane, M. A.; Roque, S.; Poupon, J.; Cresteil, T.; Teulade-Fichou, M. P.; Marinetti, A.; Bombard, S. *Bioconjug. Chem.* **2016**, *27* (6), 1456–1470.
- (67) Chekkat, N.; Dahm, G.; Chardon, E.; Wantz, M.; Sitz, J.; Decossas, M.; Lambert, O.; Frisch, B.; Rubbiani, R.; Gasser, G.; Guichard, G.; Fournel, S.; Bellemin-Laponnaz, S. *Bioconjug. Chem.* **2016**, *27* (8), 1942–1948.
- (68) Bouché, M.; Dahm, G.; Wantz, M.; Fournel, S.; Achard, T.; Bellemin-Laponnaz, S. *Dalton Trans.* **2016**, *45* (28), 11362–11368.
- (69) Borré, E.; Dahm, G.; Guichard, G.; Bellemin-Laponnaz, S. *New J. Chem.* **2016**, *40* (4), 3164–3171.
- (70) Haque, R. A.; Nasri, S. F.; Iqbal, M. A.; Al-Rawi, S. S.; Jafari, S. F.; Ahamed, M. B. K.; Abdul Majid, A. M. S. *J. Chem.* **2013**, *2013*, 1–11.
- (71) Sakamoto, R.; Morozumi, S.; Yanagawa, Y.; Toyama, M.; Takayama, A.; Kasuga, N. C.; Nomiya, K. *J. Inorg. Biochem.* **2016**, *163*, 110–117.
- (72) Rieb, J.; Dominelli, B.; Mayer, D.; Jandl, C.; Drechsel, J.; Heydenreuter, W.; Sieber, S. A.; Kühn, F. E. *Dalton Trans.* **2017**, *46* (8), 2722–2735.
- (73) Roymahapatra, G.; Mandal, S. M.; Porto, W. F.; Samanta, T.; Giri, S.; Dinda, J.; Franco, O. L.; Chattaraj, P. K. *Curr. Med. Chem.* **2012**, *19* (August 2014), 4184–

4193.

- (74) Samanta, T.; Roymahapatra, G.; Porto, W. F.; Seth, S.; Ghorai, S.; Saha, S.; Sengupta, J.; Franco, O. L.; Dinda, J.; Mandal, S. M. *PLoS One* **2013**, *8* (3), e58346.
- (75) Wright, B. D.; Shah, P. N.; McDonald, L. J.; Shaeffer, M. L.; Wagers, P. O.; Panzner, M. J.; Smolen, J.; Tagaev, J.; Tessier, C. A.; Cannon, C. L.; Youngs, W. J. *Dalton Trans.* **2012**, *41* (21), 6500–6506.
- (76) Günel, S.; Kaloğlu, N.; Özdemir, İ.; Demir, S.; Özdemir, İ. *Inorg. Chem. Commun.* **2012**, *21*, 142–146.
- (77) Kaloğlu, N.; Özdemir, İ.; Günel, S.; Özdemir, İ. *Appl. Organomet. Chem.* **2017**, *31* (11), e3803.
- (78) Gök, Y.; Sari, Y.; Akkoç, S.; Özdemir, İ.; Günel, S. *Int. J. Inorg. Chem.* **2014**, *2014* (I), 1–6.
- (79) Gök, Y.; Akkoç, S.; Erdoğan, H.; Albayrak, S. *J. Enzyme Inhib. Med. Chem.* **2016**, *31* (6), 1322–1327.
- (80) Gök, Y.; Akkoç, S.; Çelikal, Ö. Ö.; Özdemir, İ.; Günel, S.; Sayin, E. *Turkish J. Chem.* **2013**, *37*, 1007–1013.
- (81) Gök, Y.; Akkoç, S.; Çelikal, Ö. Ö.; Özdemir, İ.; Günel, S. *Arab. J. Chem.* **2015**.
- (82) Sari, Y.; Akkoç, S.; Gök, Y.; Sifniotis, V.; Özdemir, İ.; Günel, S.; Kayser, V. *J. Enzyme Inhib. Med. Chem.* **2016**, *31* (6), 1527–1530.
- (83) Karataş, M. O.; Olgundeniz, B.; Günel, S.; Özdemir, İ.; Alıcı, B.; Çetinkaya, E. *Bioorg. Med. Chem.* **2016**, *24* (4), 643–650.
- (84) Haque, R. A.; Yü Choo, S.; Budagumpi, S.; Adnan Iqbal, M.; Al-Ashraf Abdullah, A. *Eur. J. Med. Chem.* **2015**, *90*, 82–92.
- (85) Haque, R. A.; Haziz, U. F. M.; Abdullah, A. A. A.; Shaheeda, N.; Razali, M. R. *Polyhedron* **2016**, *109*, 208–217.
- (86) Doğan, Ö.; Kaloğlu, N.; Demir, S.; Özdemir, İ.; Günel, S.; Özdemir, İ. *Monatshefte für Chemie - Chem. Mon.* **2013**, *144* (3), 313–319.
- (87) Akkoç, S.; Kayser, V.; İlhan, İ. Ö.; Hibbs, D. E.; Gök, Y.; Williams, P. A.; Hawkins, B.; Lai, F. *J. Organomet. Chem.* **2017**, *839*, 98–107.
- (88) Iqbal, M. A.; Haque, R. A.; Nasri, S. F.; Majid, A. A.; Ahamed, M. B. K.; Farsi, E.; Fatima, T. *Chem. Cent. J.* **2013**, *7* (1), 27.
- (89) Asif, M.; Iqbal, M. A.; Hussein, M. A.; Oon, C. E.; Haque, R. A.; Khadeer Ahamed, M. B.; Abdul Majid, A. S.; Abdul Majid, A. M. S. *Eur. J. Med. Chem.* **2016**, *108*, 177–187.
- (90) Dinda, J.; Kumar Rana, B.; Nandy, A.; Bertolasi, V.; Das Saha, K.; Bielawski, C. W.

RSC Adv. **2014**, *4* (105), 60776–60784.

- (91) Roymahapatra, G.; Dinda, J.; Mishra, A.; Mahapatra, A.; Hwang, W.-S.; Mandal, S. M. *J. Cancer Res. Ther.* **2015**, *11* (1), 105–113.
- (92) Zhang, J.-J.; Che, C.-M.; Ott, I. *J. Organomet. Chem.* **2015**, *782*, 37–41.
- (93) McCall, R.; Miles, M.; Lascuna, P.; Burney, B.; Patel, Z.; Sidoran, K. J.; Sittaramane, V.; Kocerha, J.; Grossie, D. A.; Sessler, J. L.; Arumugam, K.; Arambula, J. F. *Chem. Sci.* **2017**, *8* (9), 5918–5929.
- (94) Longevial, J. F.; El Cheikh, K.; Aggad, D.; Lebrun, A.; van der Lee, A.; Tielens, F.; Clément, S.; Morère, A.; Garcia, M.; Gary-Bobo, M.; Richeter, S. *Chem. - A Eur. J.* **2017**, *23* (56), 14017–14026.
- (95) Pellei, M.; Gandin, V.; Marinelli, M.; Orsetti, A.; Del Bello, F.; Santini, C.; Marzano, C. *Dalton Trans.* **2015**, *44* (48), 21041–21052.
- (96) Serebryanskaya, T. V.; Zolotarev, A. A.; Ott, I. *Med. Chem. Commun.* **2015**, *6* (6), 1186–1189.
- (97) Turek, J.; Panov, I.; Švec, P.; Růžicková, Z.; Růžicka, A. *Dalton Trans.* **2014**, *43*, 15465–15474.
- (98) Turek, J.; Růžicková, Z.; Tloušťová, E.; Mertlíková-Kaiserová, H.; Günterová, J.; Rulíšek, L.; Růžicka, A. *Appl. Organomet. Chem.* **2016**, *30* (5), 318–322.
- (99) He, F.; Danopoulos, A. A.; Braunstein, P. *Organometallics* **2016**, *35*, 198–206.
- (100) Furstner, A. *Science* **2013**, *341*, 1229713-1-1229713-7.
- (101) Arduengo III, A. J.; Harlow, R. L.; Kline, M. *J. Am. Chem. Soc.* **1991**, *113*, 361–363.
- (102) Guncheva, M.; Paunova, K.; Ossowicz, P.; Rozwadowski, Z.; Janus, E.; Idakieva, K.; Todinova, S.; Raynova, Y.; Uzunova, V.; Apostolova, S.; Tzoneva, R.; Yancheva, D. *Int. J. Biol. Macromol.* **2016**, *82*, 798–805.
- (103) Demberelnyamba, D.; Kim, K. S.; Choi, S.; Park, S. Y.; Lee, H.; Kim, C. J.; Yoo, I. D. *Bioorganic Med. Chem.* **2004**, *12* (5), 853–857.
- (104) Vik, A.; Hedner, E.; Charnock, C.; Tangen, L. W.; Samuelsen, Ø.; Larsson, R.; Bohlin, L.; Gundersen, L. L. *Bioorganic Med. Chem.* **2007**, *15* (12), 4016–4037.
- (105) Zhao, L.; Zhang, C.; Zhuo, L.; Zhang, Y.; Ying, J. Y. *J. Am. Chem. Soc.* **2008**, *130* (38), 12586–12587.
- (106) Cui, B.; Zheng, B. L.; He, K.; Zheng, Q. Y. *J. Nat. Prod.* **2003**, *66* (8), 1101–1103.
- (107) Nakahara, T.; Takeuchi, M.; Kinoyama, I.; Minematsu, T.; Shirasuna, K.; Matsuhisa, A.; Kita, A.; Tominaga, F.; Yamanaka, K.; Kudoh, M.; Sasamata, M. *Cancer Res.* **2007**, *67* (17), 8014–8021.

- (108) O'Connor, D. S.; Grossman, D.; Plescia, J.; Li, F.; Zhang, H.; Villa, a; Tognin, S.; Marchisio, P. C.; Altieri, D. C. *Proc. Natl. Acad. Sci. U. S. A.* **2000**, *97* (24), 13103–13107.
- (109) Tolcher, A. W.; Mita, A.; Lewis, L. D.; Garrett, C. R.; Till, E.; Daud, A. I.; Patnaik, A.; Papadopoulos, K.; Takimoto, C.; Bartels, P.; Keating, A.; Antonia, S. *J. Clin. Oncol.* **2008**, *26* (32), 5198–5203.
- (110) Jong, Y. de; Oosterwijk, J. G. van; Kruisselbrink, A. B.; Bruijn, I. H. B.; Agrogiannis, G.; Baranski, Z.; Cleven, A. H. G.; Cleton-Jansen, A.-M.; Water, B. Van de; Danen, E. H. J.; Bovée, J. V. M. G. *Oncogenesis* **2016**, *5*, 1–9.
- (111) Barresi, V.; Bonaccorso, C.; Consiglio, G.; Goracci, L.; Musso, N.; Musumarra, G.; Satriano, C.; Fortuna, C. G. *Mol. Biosyst.* **2013**, *9*, 2426–2429.
- (112) Yang, X.; Zeng, X.; Zhang, Y.; Qing, C.; Song, W.; Li, L.; Zhang, H. *Bioorg. Med. Chem. Lett.* **2009**, *19*, 1892–1895.
- (113) Zeng, X.; Yang, X.; Zhang, Y.; Qing, C.; Zhang, H. *Bioorganic Med. Chem. Lett.* **2010**, *20* (6), 1844–1847.
- (114) Chen, W.; Yang, X.-D.; Li, Y.; Yang, L.-J.; Wang, X.-Q.; Zhang, G.-L.; Zhang, H.-B. *Org. Biomol. Chem.* **2011**, *9*, 4250–4255.
- (115) Song, W.-J.; Yang, X.-D.; Zeng, X.-H.; Xu, X.-L.; Zhang, G.-L.; Zhang, H.-B. *RSC Adv.* **2012**, *2* (11), 4612–4615.
- (116) Yang, X.-D.; Wan, W.-C.; Deng, X.-Y.; Li, Y.; Yang, L.-J.; Li, L.; Zhang, H.-B. *Bioorganic Med. Chem. Lett.* **2012**, *22*, 2726–2729.
- (117) Liu, L.; Wang, X.; Yan, J.; Li, Y.; Sun, C.; Chen, W.; Zhou, B.; Zhang, H.; Yang, X. *Eur. J. Med. Chem.* **2013**, *66*, 423–437.
- (118) Wang, X.-Q.; Liu, L.-X.; Li, Y.; Sun, C.-J.; Chen, W.; Li, L.; Zhang, H.-B.; Yang, X.-D. *Eur. J. Med. Chem.* **2013**, *62*, 111–121.
- (119) Chen, W.; Deng, X.-Y.; Li, Y.; Yang, L.-J.; Wan, W.-C.; Wang, X.-Q.; Zhang, H.-B.; Yang, X.-D. *Bioorg. Med. Chem. Lett.* **2013**, *23*, 4297–4302.
- (120) Sun, C.-J.; Chen, W.; Li, Y.; Liu, L.-X.; Wang, X.-Q.; Li, L.-J.; Zhang, H.-B.; Yang, X.-D. *RSC Adv.* **2014**, *4* (31), 16312.
- (121) Xu, X.; Wang, J.; Yu, C.; Chen, W.; Li, Y.; Li, Y.; Zhang, H.; Yang, X. *Bioorg. Med. Chem. Lett.* **2014**, *24*, 4926–4930.
- (122) Wan, W.-C.; Chen, W.; Liu, L.-X.; Li, Y.; Yang, L.-J.; Deng, X.-Y.; Zhang, H.-B.; Yang, X.-D. *Med. Chem. Res.* **2014**, *23*, 1599–1611.
- (123) Xu, X.; Yu, C.; Chen, W.; Li, Y.; Yang, L.-J.; Li, Y.; Zhang, H.-B.; Yang, X.-D. *Org. Biomol. Chem.* **2015**, *13*, 1550–1557.
- (124) Liu, L. X.; Wang, X. Q.; Zhou, B.; Yang, L. J.; Li, Y.; Zhang, H. B.; Yang, X. D. *Sci.*

- Rep.* **2015**, *5*, 13101.
- (125) Liu, J. M.; Wang, M.; Zhou, Y. J.; Yan, J. M.; Yang, L. J.; Li, Y.; Zhang, H. B.; Yang, X. D. *RSC Adv.* **2015**, *5*, 63936–63944.
- (126) Dominianni, S. J.; Yen, T. T. *J. Med. Chem.* **1989**, *32*, 2301–2306.
- (127) Chivikas, C. J.; Hodges, J. C. *J. Org. Chem.* **1987**, *52* (16), 3591–3594.
- (128) Nguyen, T. D.; Jin, X.; Lee, K.; Hong, Y. S.; Young, H. K.; Jung, J. L. *J. Nat. Prod.* **2009**, *72*, 39–43.
- (129) Katsanou, E. S.; Halabalaki, M.; Aligiannis, N.; Mitakou, S.; Skaltsounis, A. L.; Alexi, X.; Pratsinis, H.; Alexis, M. N. *J. Steroid Biochem. Mol. Biol.* **2007**, *104*, 228–236.
- (130) Halabalaki, M.; Alexi, X.; Aligiannis, N.; Alexis, M. N.; Skaltsounis, A. L. *J. Nat. Prod.* **2008**, *71*, 1934–1937.
- (131) Livingstone, M.; Larsson, O.; Sukarieh, R.; Pelletier, J.; Sonenberg, N. *Chem. Biol.* **2009**, *16*, 1240–1249.
- (132) Hayakawa, I.; Shioya, R.; Agatsuma, T.; Furukawa, H.; Naruto, S.; Sugano, Y. *Bioorganic Med. Chem. Lett.* **2004**, *14*, 4383–4387.
- (133) Zhang, G. N.; Zhong, L. Y.; Bligh, S. W. A.; Guo, Y. L.; Zhang, C. F.; Zhang, M.; Wang, Z. T.; Xu, L. S. *Phytochemistry* **2005**, *66*, 1113–1120.
- (134) Cai, S.; Sun, S.; Zhou, H.; Kong, X.; Zhu, T.; Li, D.; Gu, Q. *J. Nat. Prod.* **2011**, *74*, 1106–1110.
- (135) Ito, T.; Endo, H.; Shinohara, H.; Oyama, M.; Akao, Y.; Iinuma, M. *Fitoterapia* **2012**, *83*, 1420–1429.
- (136) Capon, R. J.; Peng, C.; Dooms, C. *Org. Biomol. Chem.* **2008**, *6*, 2765–2771.
- (137) Zhang, Y.; Au, Q.; Zhang, M.; Barber, J. R.; Ng, S. C.; Zhang, B. *Biochem. Biophys. Res. Commun.* **2009**, *386*, 729–733.
- (138) Kwak, J. H.; Kim, Y.; Park, H.; Jang, J. Y.; Lee, K. K.; Yi, W.; Kwak, J. A.; Park, S. G.; Kim, H.; Lee, K.; Kang, J. S.; Han, S. B.; Hwang, B. Y.; Hong, J. T.; Jung, J. K.; Kim, Y.; Cho, J.; Lee, H. *Bioorganic Med. Chem. Lett.* **2010**, *20*, 4620–4623.
- (139) Lee, C. L.; Liao, Y. C.; Hwang, T. L.; Wu, C. C.; Chang, F. R.; Wu, Y. C. *Bioorganic Med. Chem. Lett.* **2010**, *20*, 7354–7357.
- (140) Kemnitzer, W.; Sirisoma, N.; Jiang, S.; Kasibhatla, S.; Crogan-Grundy, C.; Tseng, B.; Drewe, J.; Cai, S. X. *Bioorganic Med. Chem. Lett.* **2010**, *20*, 1288–1292.
- (141) Songsiang, U.; Thongthoom, T.; Boonyarat, C.; Yenjai, C. *J. Nat. Prod.* **2011**, *74*, 208–212.
- (142) Laine, A. E.; Lood, C.; Koskinen, A. M. P. *Molecules* **2014**, *19*, 1544–1567.

- (143) Garrison, J. C.; Youngs, W. J. *Chem. Rev.* **2005**, *105*, 3978–4008.
- (144) Hindi, K. M.; Siciliano, T. J.; Durmus, S.; Panzner, M. J.; Medvetz, D. A.; Reddy, D. V.; Hogue, L. A.; Hovis, C. E.; Hilliard, J. K.; Mallet, R. J.; Tessier, C. A.; Cannon, C. L.; Youngs, W. J. *J. Med. Chem.* **2008**, *51*, 1577–1583.
- (145) Medvetz, D. a; Hindi, K. M.; Panzner, M. J.; Ditto, A. J.; Yun, Y. H.; Youngs, W. J. *Met. Based. Drugs* **2008**, *2008*, 384010.
- (146) Ornelas-Megiatto, C.; Shah, P. N.; Wich, P. R.; Cohen, J. L.; Tagaev, J. a; Smolen, J. a.; Wright, B. D.; Panzner, M. J.; Youngs, W. J.; Fréchet, J. M. J.; Cannon, C. L. *Mol. Pharm.* **2012**, *9* (11), 3012–3022.
- (147) Wright, B. D.; Shah, P. N.; Mcdonald, L. J.; Shaeffer, M. L.; Wagers, P. O.; Panzner, M. J.; Smolen, J.; Tagaev, J.; Tessier, C. A.; Cannon, L.; Youngs, W. J. *Dalton Trans.* **2012**, *41*, 6500–6506.
- (148) Malhotra, S. V.; Kumar, V. *Bioorganic Med. Chem. Lett.* **2010**, *20* (2), 581–585.
- (149) Shelton, K. L.; Debord, M. A.; Wagers, P. O.; Southerland, M. R.; Taraboletti, A.; Robishaw, N. K.; Jackson, D. P.; Tosanovic, R.; Kofron, W. G.; Tessier, C. A.; Paruchuri, S.; Shriver, L. P.; Panzner, M. J.; Youngs, W. J. *Tetrahedron* **2016**, 1–15.
- (150) Shelton, K. L.; Debord, M. A.; Wagers, P. O.; Southerland, M. R.; Williams, T. M.; Robishaw, N. K.; Shriver, L. P.; Tessier, C. A.; Panzner, M. J.; Youngs, W. J.; Williams, T. M.; Robishaw, N. K.; Shriver, L. P.; Tessier, C. A.; Panzner, M. J.; Youngs, W. J. *Bioorg. Med. Chem.* **2016**.
- (151) DeBord, M. A.; Southerland, M. R.; Wagers, P. O.; Tiemann, K. M.; Robishaw, N. K.; Whiddon, K. T.; Konopka, M. C.; Tessier, C. A.; Shriver, L. P.; Paruchuri, S.; Hunstad, D. A.; Panzner, M. J.; Youngs, W. J. *Bioorganic Med. Chem. Lett.* **2017**, *27* (4), 764–775.
- (152) DeBord, M. A.; Wagers, P. O.; Crabtree, S. R.; Tessier, C. A.; Panzner, M. J.; Youngs, W. J. *Bioorganic Med. Chem. Lett.* **2017**, *27* (2), 196–202.
- (153) Volkova, M.; Russell, R. *Curr. Cardiol. Rev.* **2011**, *7* (4), 214–220.
- (154) Modica-Napolitano, J. S.; Aprille, J. R. *Adv. Drug Deliv. Rev.* **2001**, *49* (1–2), 63–70.
- (155) American Cancer Society. Cancer Facts and Figures 2018. **2018**.
- (156) Hopper-Borge, W.-T. and. *J Can Res Updat.* **2014**, *2* (4), 265–282.
- (157) Katano, K.; Kondo, A.; Safaei, R.; Holzer, A.; Samimi, G.; Mishima, M.; Kuo, Y. M.; Rochdi, M.; Howell, S. B. *Cancer Res.* **2002**, *62* (22), 6559–6565.
- (158) Barabas, K.; Milner, R.; Lurie, D.; Adin, C. *Vet. Comp. Oncol.* **2008**, *6* (1), 1–18.
- (159) Ornelas-Megiatto, C.; Shah, P. N.; Wich, P. R.; Cohen, J. L.; Tagaev, J. A.; Smolen,

- J. A.; Wright, B. D.; Panzner, M. J.; Youngs, W. J.; Fréchet, J. M. J.; Cannon, C. L. *Mol. Pharm.* **2012**, *9* (11), 3012–3022.
- (160) Brewster, M. E.; Loftsson, T. *Adv. Drug Deliv. Rev.* **2007**, *59* (7), 645–666.
- (161) Van Engeland, M.; Nieland, L. J. W.; Ramaekers, F. C. S.; Schutte, B.; Reutelingsperger, C. P. M. *Cytometry* **1998**, *31*, 1–9.
- (162) Boger, D. L.; Fink, B. E.; Brunette, S. R.; Tse, W. C.; Hedrick, M. P. *J. Am. Chem. Soc.* **2001**, *123* (25), 5878–5891.
- (163) Kelley, S. O.; Stewart, K. M.; Mourtada, R. *Pharm. Res.* **2011**, *28* (11), 2808–2819.
- (164) Wadia, J. S.; Chalmers-Redman, R. M.; Ju, W. J.; Carlile, G. W.; Phillips, J. L.; Fraser, A. D.; Tatton, W. G. *J. Neurosci.* **1998**, *18* (3), 932–947.
- (165) Smiley, S. T.; Reers, M.; Mottola-Hartshorn, C.; Lin, M.; Chen, A.; Smith, T. W.; Steele, G. D.; Chen, L. B. *Proc. Natl. Acad. Sci. U. S. A.* **1991**, *88* (9), 3671–3675.
- (166) Ly, J. D.; Grubb, D. R.; Lawen, A. *Apoptosis* **2003**, *8* (2), 115–128.
- (167) Bruker. SMART (Version 5.625). Madison, Wisconsin, USA: Bruker AXS Inc.; **2012**.
- (168) Bruker. APEX II. Madison, Wisconsin, USA: Bruker AXS Inc.; **2012**.
- (169) Bruker. SAINT. Madison, Wisconsin, USA: Bruker AXS Inc.; **2012**.
- (170) Bruker. SADABS. Madison, Wisconsin, USA: Bruker AXS Inc.; **2012**.
- (171) Sheldrick, G. M. *Acta Crystallogr. Sect. C Struct. Chem.* **2015**, *71* (Md), 3–8.
- (172) Dhar, S.; Nethaji, M.; Chakravarty, A. R. *Inorg. Chem.* **2006**, *45* (26), 11043–11050.
- (173) Fu, X.-B.; Zhang, J.-J.; Liu, D.-D.; Gan, Q.; Gao, H.-W.; Mao, Z.-W.; Le, X.-Y. *J. Inorg. Biochem.* **2014**, *143*, 77–87.
- (174) Lucey, B. P.; Nelson-Rees, W. A.; Hutchins, G. M. *Arch Pathol Lab Med* **2009**, *133* (9), 1463–1467.
- (175) Wagers, P. O.; Tiemann, K. M.; Shelton, K. L.; Kofron, W. G.; Panzner, M. J.; Wooley, K. L.; Youngs, W. J.; Hunstad, D. A. *Antimicrob. Agents Chemother.* **2015**, *59* (9), 5494–5502.
- (176) DeBord, M. A. Synthesis, characterization, and anti-cancer structure-activity relationship studies of imidazolium salts, 2017.
- (177) Parkin, J.; Shea, C.; Sant, G. R. *Urology* **1997**, *49*, 105–107.
- (178) Wangari-Talbot, J.; Hopper-Borge, E. *J Can Res Updat.* **2014**, *2* (4), 265–282.
- (179) Yao, X.; Panichpisal, K.; Kurtzman, N.; Nugent, K. *Am. J. Med. Sci.* **2007**, *334* (2),

115–124.

- (180) Kim, J. W.; Dang, C. V. *Cancer Res.* **2006**, *66* (18), 8927–8930.
- (181) Zielonka, J.; Joseph, J.; Sikora, A.; Hardy, M.; Ouari, O.; Vasquez-Vivar, J.; Cheng, G.; Lopez, M.; Kalyanaraman, B. *Chem. Rev.* **2017**, *117* (15), 10043–10120.
- (182) Han, M.; Vakili, M. R.; Soleymani Abyaneh, H.; Molavi, O.; Lai, R.; Lavasanifar, A. *Mol. Pharm.* **2014**, *11* (8), 2640–2649.
- (183) Chen, L. B. *Annu. Rev. Cell Biol.* **1988**, *4* (1), 155–181.
- (184) Zhang, E.; Zhang, C.; Su, Y.; Cheng, T.; Shi, C. *Drug Discov. Today* **2011**, *16* (3–4), 140–146.
- (185) Cai, J.; Yang, J.; Jones, D. *Biochim. Biophys. Acta - Bioenerg.* **1998**, *1366* (1), 139–149.
- (186) Kiebish, M. A.; Han, X.; Cheng, H.; Chuang, J. H.; Seyfried, T. N. *J. Lipid Res.* **2008**, *49* (12), 2545–2556.
- (187) Dong, L.-F.; Neuzil, J. In *Mitochondria: The Anti-cancer Target for the Third Millennium*; Neuzil, J., Pervaiz, S., Fulda, S., Eds.; Springer Netherlands: Dordrecht, 2014; pp 151–181.
- (188) Oberley, L. W.; Buettner, G. R. *Cancer Res.* **1979**, *52242* (April), 1141–1149.
- (189) Harris, M. H.; Thompson, C. B. *Cell Death Differ* **2000**, *7* (12), 1182–1191.

APPENDICES

APPENDIX A

APPROVAL FOR ANIMAL USE



May 15, 2015

Dr. Shriver
The University of Akron
Akron, OH 44325

Dear Dr. Shriver,

On May 15, 2015 the Institutional Animal Care and Use Committee approved your protocol titled: "Evaluation of Novel Chemotherapeutic Agents for Glioblastoma Multiforme" by Designated Member Review.

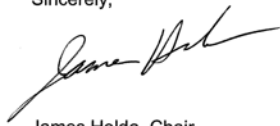
IACUC number 15-05-8-SME

Your project has received final approval on May 15, 2015.

You must notify the committee concerning modifications to the approved protocol. In addition, yearly updates regarding the status of this project are required. IACUC must also be notified of serious or adverse reactions that occur during the course of this project. Please use the IACUC number when submitting this information to the committee.

Please be aware that approval of your protocol does not guarantee space in the animal facility.

Sincerely,



James Holda, Chair

Office of Research Services and Sponsored Programs
Akron, OH 44325-2102
330-972-7666 • 330-972-6281 Fax

The University of Akron is an Equal Education and Employment Institution

APPENDIX B

ABBREVIATIONS AND ACRONYMS

Å	angstrom
α	crystallographic uni-cell angle between axes <i>b</i> and <i>c</i>
β	crystallographic uni-cell angle between axes <i>a</i> and <i>c</i>
°C	degrees Celcius
μL	microliter
μM	micromolar
λ	crystallographic uni-cell angle between axes <i>a</i> and <i>b</i>
δ	scale (nmr) ppm
HPCD	2-hydroxypropyl- β -cyclodextrin
<i>a</i>	crystallographic unit cell axis <i>a</i>
AA	amino acid
ACS	6-methyl-4-oxo-4H-1,2,3-oxathiazin-3-ide 2,2-dioxide
AMP	ampicillin
<i>b</i>	crystallographic unit cell axis <i>b</i>
BF ₄	tetrafluoroborate
<i>c</i>	crystallographic unit cell axis <i>c</i>
Calcd.	calculated
CT-DNA	calf thymus DNA
d	doublet
DLC	delocalized lipophilic cation

DMF	dimethylformamide
DMSO	dimethylsulfoxide
DNA	deoxyribonucleic acid
DTP	Developmental Therapeutics Program
EB	ethidium bromide
EC ₅₀	concentration to induce 50% response
F _c	calculated structure factor
F _o	observed Structure factor
FDA	Food and Drug Administration
FeCl ₄	tetrachloroferrate(III)
FID	fluorescent intercalator displacement
F(000)	scaling coefficient for structure factors
GI ₅₀	growth inhibition of 50% of cells relative to control cells
GRAS	generally regarded as safe
h	hour
IC ₅₀	inhibitory concentration 50%
IP	intraperitoneal
J	nuclear spin-spin coupling constant
K	kelvin
<i>M</i>	molecular weight
LD ₅₀	lethal dose of 50% of a population
m	multiplet
mHz	megahertz
mL	milliliter
mmol	millimole
Mp	melting point
mTOR	mammalian target of rapamycin

MTT	3-(4,5-dimethylthiazol-2-yl)-2,5-diphenyltetrazolium bromide
m/z	mass-to-charge ratio
NCI	National Cancer Institute
NHC	N-heterocyclic carbene
nm	nanometer
NMR	nuclear magnetic resonance
NSCLC	non-small cell lung cancer
pEC ₅₀	negative logarithm of the EC ₅₀ value
PF ₆	hexafluorophosphate
PI	propidium iodide
ppm	parts per million
PS	phosphatidylserine
R	residual factor or reliability factor
ROS	reactive oxygen species
RT	room temperature
s	singlet
SAR	structure-activity relationship
T	temperature
t	triplet
THF	tetrahydrofuran
U	temperature factor
V	volume
wR ₂	weighted residual based on
YM155	1-(2-methoxyethyl)-2-methyl-4,9-dioxo-3-(pyrazin-2-ylmethyl)-4,9-dihydro-1H-3H-naphtho[2,3-d]imidazolium bromide
Z	the number of formula units related by symmetry